Molecular investigations into the effects of the insulin secretagogue dextrorphan on pancreatic islet cell function and viability

Inaugural-Dissertation

zur Erlangung des Doktorgrades
der Mathematisch-Naturwissenschaftlichen Fakultät
der Heinrich-Heine-Universität Düsseldorf

vorgelegt von

Jessica Mrugala
aus Mülheim an der Ruhr

Düsseldorf, Januar 2020

aus dem Institut für Vaskular- und Inselzellbiologie
des Deutschen Diabetes-Zentrums (DDZ)

und

aus dem Institut für Stoffwechselphysiologie
der Heinrich-Heine-Universität Düsseldorf

Gedruckt mit der Genehmigung der
Mathematisch-Naturwissenschaftlichen Fakultät der
Heinrich-Heine-Universität Düsseldorf

Berichterstatter:

1. Prof. Dr. Eckhard Lammert

2. Prof. Dr. Thomas Meissner

Tag der mündlichen Prüfung: 08.05.2020

Table of Contents

1 Summary

One characteristic feature leading to diabetes mellitus is the progressive loss of functional β-cell mass. Currently, many drugs are available on the market to treat diabetes mellitus type 2. Insulin secretagogues are one class of antidiabetic drugs, acting directly on the β-cells to enhance the secretion of insulin. These agents harbor the risk to exhaust β-cells, leading to β-cells dysfunction in treated patients. One recently discovered new insulin secretagogue is dextrorphan (DXO) acting as an antagonist of the N-methyl-D-aspartate (NMDA) receptors on β-cells. During my PhD thesis, I focused on the effects of DXO on islet cell function as well as viability and give first evidence about the molecular mechanism which could lead to β-cell dysfunction induced by an insulin secretagogue.

As inflammation plays a key role in the pathogenesis of type 2 diabetes, we analyzed the effect of DXO on mouse pancreatic islets during treatment with cytokines. We figured out that DXO is beneficial for islet survival because it protects islet cells from cytokine-induced apoptosis. Additionally, *in vitro* experiments with isolated islets of NMDA receptor-deficient mice revealed that the protective effect of DXO is not exclusively mediated by NMDA receptor blockade, but rather additional pathways have to participate in the protective effect.

To investigate the long-term effect of the insulin secretagogue DXO on islet cell function, we incubated mouse islets for 24 - 48 hours with DXO under continuous glucose stimulation. After incubation, we recognized impaired glucose-stimulated insulin secretion (GSIS). To reveal the underlying mechanism, we analyzed the transcriptome via RNA sequencing and found out that besides genes, responsible for islet dedifferentiation, genes coding for core enzymes of the mitochondrial one-carbon metabolism are differentially expressed compared to control. The mitochondrial localized enzyme aldehyde dehydrogenase 1 family member L2 (ALDH1L2) was shown to be upregulated on mRNA and protein level in mouse and human pancreatic islets upon treatment with DXO. Functional characterization revealed that adenoviral ALDH1L2 overexpression of this enzyme reduced GSIS, while genetic deletion of *Aldh1l2* enhanced GSIS. Glucose homeostasis was investigated during *in vivo* experiments. *Aldh1l2* genetic deletion in mice increased plasma insulin concentrations and glucose tolerance when compared to control mice. In contrast, neither overexpression of *ALDH1L2* nor deletion of *Aldh1l2* affected cytokine-induced islet cell death. Furthermore, we observed that lower concentrations of DXO did not show deleterious effects on β-cell function, consistent with lesser upregulation of *Aldh1l2*.

Our results indicate that excessive insulin secretion is accompanied by an up-regulation of the core enzymes of the mitochondrial one-carbon metabolism, in particular,

the enzyme ALDH1L2, a critical regulator which attenuates GSIS and lowers glucose tolerance.

2 Zusammenfassung

Ein charakteristisches Merkmal, welches zu Diabetes mellitus führt, ist der stetige Verlust funktioneller β-Zellen. Zurzeit sind viele Medikamente zur Behandlung von Diabetes mellitus Typ 2 auf dem Markt erhältlich. Eine Klasse von Antidiabetika bilden die Insulinsekretagoga, die direkt auf die β-Zellen wirken und die Insulinsekretion fördern. Diese Wirkstoffe bergen jedoch das Risiko, die Funktion der β-Zellen zu erschöpfen, was bei den behandelten Patienten zu Funktionsstörungen der β-Zellen führen kann. Dextrorphan (DXO) ist ein kürzlich entdecktes Insulin-Sekretagogum, welches als Antagonist des N-Methyl-D-Aspartat (NMDA)-Rezeptors auf β-Zellen wirkt. Während meiner Promotion habe ich mich auf die Funktion und den schützenden Effekt von DXO auf Inselzellen konzentriert. Ich konnte erste Hinweise auf den molekularen Mechanismus sammeln, der zur β-Zell-Fehlfunktion durch das Insulin-Sekretagogum DXO führen könnte. Da entzündliche Prozesse eine Schlüsselrolle in der Pathogenese des Typ 2 Diabetes spielen, analysierten wir die Wirkung von DXO auf Pankreasinseln während der Behandlung mit Zytokinen. Wir fanden heraus, dass DXO die Inselzellen vor Zytokin-induzierter Apoptose schützt. Darüber hinaus zeigten *in vitro* Experimente mit isolierten Inseln von NMDA-Rezeptor-defizienten Mäusen, dass die protektive Wirkung von DXO nicht ausschließlich durch eine NMDA-Rezeptorblockade vermittelt wird, sondern zusätzliche Signalwege am Schutz durch DXO beteiligt sein müssen.

Um die Langzeitwirkung des Insulin-Sekretagogums DXO auf die Funktion der Inselzellen zu untersuchen, inkubierten wir pankreatische Inseln von Mäusen für 24 - 48 Stunden unter kontinuierlicher Glukosestimulation mit DXO. Nach der Behandlung war die Glukose-stimulierte Insulinsekretion (GSIS) in den Inseln gestört. Um den zugrundeliegenden Mechanismus aufzudecken, analysierten wir das Transkriptom mittels RNA-Sequenzierung und fanden heraus, dass neben Genen, die für die Dedifferenzierung verantwortlich sind, auch Gene differentiell exprimiert wurden, die für Kernenzyme des mitochondrialen Ein-Kohlenstoff-Metabolismus kodieren. Das mitochondrial lokalisierte Enzym Aldehyd-Dehydrogenase 1 Familienmitglied L2 (ALDH1L2) wurde auf mRNA- und Proteinebene in Pankreasinseln von Mäusen und menschlichen Spendern unter Stimulation mit DXO hochreguliert. Funktionelle Untersuchungen zeigten, dass die adenovirale ALDH1L2-Überexpression dieses Enzyms die GSIS reduziert, während die genetische Deletion von *Aldh1l2* die GSIS erhöht. Die Glukosehomöostase wurde in *in vivo* Experimenten untersucht. Die genetische Deletion von *Aldh1l2* in Mäusen erhöhte die Insulinkonzentration im Plasma und die Glukosetoleranz im Vergleich zu Kontrollmäusen. Im Gegensatz dazu beeinflusst weder die Überexpression von ALDH1L2 noch die Deletion von *Aldh1l2* den Zytokin-induzierten Inselzelltod. Des Weiteren beobachteten wir, dass eine niedrigere DXO-Konzentration nach längerer Inkubationszeit keine schädliche Auswirkung

auf die Insulinsekretion der β-Zelle hat. Unter diesen Bedingungen ist *Aldh1l2* ebenfalls hochreguliert, jedoch zu einem geringeren Maß.

Unsere Ergebnisse weisen darauf hin, dass eine übermäßige Insulinsekretion mit einer verstärkten Expression der Kernenzyme des mitochondrialen Ein-Kohlenstoff-Metabolismus einhergeht. Insbesondere das Enzyms ALDH1L2 ist ein kritischer Regulator, der die GSIS verringert und die Glukosetoleranz senkt.

3 Introduction

3.1 The pancreas and the islets of Langerhans

The pancreas gland is the key organ known to play an important role in the development of diabetes based on the regulation and secretion of hormones into the bloodstream. The pancreas is a secretory organ that consists of endocrine and exocrine cells. The exocrine part of the pancreas is responsible for the secretion of digestive enzymes into the duodenum. The region of endocrine cells within the pancreas is called the islets of Langerhans [1]. 150 years ago Paul Langerhans described the presence of islet structures in the pancreas in his thesis "Contributions to the microscopic anatomy of the pancreas" for the first time [2, 3]. Only 2% of the adult human pancreas consists of the islets of Langerhans, this reaches 500,000-1 million islets with a size range of 50-250 µm in diameter [3, 4]. The islets are arranged by mixed populations of endocrine cells, each of them producing a specific hormone which is released into the blood stream. These micro-organs consist of at least five different cell types: β-cells (secret insulin), α-cells (secret glucagon), δ-cells (secret somatostatin), PP-cells (secret pancreatic polypeptide) and ε-cells (secret ghrelin) [5].

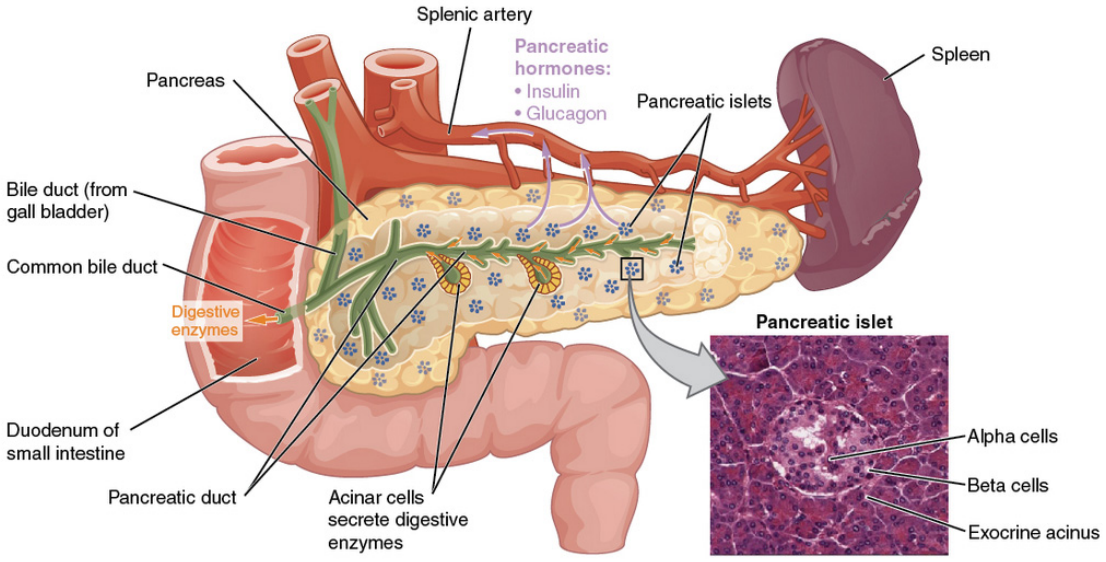

Figure 1: Pancreas with islets of Langerhans (Illustration reprinted from Betts *et.al.*, Anatomy and Physiology 2013, an OpenStax College resource) [6] [1]. The pancreas consists of an exocrine and an endocrine part. The islets of Langerhans form the endocrine part of the pancreas, secreting among others the hormones insulin and glucagon to regulate glucose homeostasis within the body. The micrograph shows pancreatic islets. (Micrograph provided by the Regents of University of Michigan Medical School © 2012).

The proportion and arrangement of the cells within the islet varies between species. In humans, 50-70% of all endocrine cells within the islet are β-cells, whereas 20-40% are α-cells. In mice, the proportion of the cell types differs: β-cells make up 60-80% and α-cells contribute to 10-20% [5]. Mouse islets have a higher percentage of total β-cells within the islets and a smaller amount of α-cells compared to human islets. However, the other cell types only have a small proportion in the whole islet [5]. Although the architecture of the islets is quite important for the correct signaling and release of hormones, it also differs between species. While mouse islets have a core of insulin-secreting β-cells surrounded by a mantle of α-cells, human islets show a more complex architecture [5]. For the efficient release of hormones, islets are connected to blood vessels. To form a dense capillary network each islet is entered by 1-5 arterioles so that the endocrine cells are highly vascularized to measure the glucose concentration in the body and secrete hormones if needed [5]. To regulate glucose homeostasis, the capillary network is responsible for the transport of blood glucose to the β-cells, and as a consequence insulin from the β-cells to the target tissues [7]. Besides the high vascularization, islets are highly innervated. The tight connection between nerve cells, endothelial cells, and endocrine cells is essential for optimal control of blood glucose levels [8].

Insulin and its opponent glucagon are the main players for the glucose homeostasis in the body, trying to preserve the blood glucose concentrations within the body at a very narrow range of 3.5-5.5 mM [9]. At low blood glucose concentrations, also called hypoglycemia, glucagon is released into the bloodstream to stimulate hepatic glycogenolysis and gluconeogenesis [1, 10]. In contrast to the catabolic hormone glucagon, the anabolic hormone insulin is released at high blood glucose levels, also called hyperglycemia, and signals at insulin-responsive tissues like fat, liver, and muscle to trigger the uptake and metabolization of glucose [1]

3.2 Regulation of insulin secretion and blood glucose homeostasis

Removing exogenous glucose from the bloodstream by the uptake in various tissues is one of the key processes to maintain glucose homeostasis. Elevated glucose concentrations, for example following a meal, trigger the release of insulin from endocrine cells into the blood. Insulin is transported via the bloodstream through the body and binds on its receptors located on the cell surface of the target tissue [1]. The insulin receptor is a tyrosine kinase comprising two α-subunits and two β-subunits forming a heterotetramer [11]. Binding of insulin to the receptor initiates the insulin-dependent glucose uptake into the tissue to lower blood glucose levels [1].

The secretion of the peptide hormone insulin from β-cells is a tightly regulated process. The underlying molecular mechanism which translates the stimulus of elevated glucose concentrations into the release of hormones is very complex [1]. Glucose molecules cannot pass the membrane of β-cells simply by diffusion, therefore glucose transporters in the membrane are needed [12]. Uptake of glucose can be performed by two types of transporters: via the sodium-glucose linked transporters (SGLTs) and the facilitative diffusion glucose transporters (GLUTs). Both types of transporters can be divided into many subclasses [12]. The GLUT family of membrane proteins consists of three subclasses containing 14 isoforms (GLUT1-GLUT14) [13]. The transmembrane carrier GLUT2 (SLC2A2) is predominantly expressed in the membrane of rodent β-cells and is required for glucose-stimulated insulin secretion (GSIS) [14]. Without energy-input and with low affinity for glucose, the transporter allows a fast equilibration of extracellular and intracellular glucose (high K_m for glucose and high transport capacity). Glucose enters the cell and is metabolized by glucokinase, the enzyme that catalyzes the rate-controlling step in GSIS [14]. In human β-cells besides GLUT2, GLUT1 and GLUT3 are expressed at a higher level [14]. It is proposed that GLUT2 is not the predominant glucose transporter in human pancreatic β-cells [15].

Transported into the cell, glucose is immediately phosphorylated by glucokinase to glucose 6-phosphate. This step is irreversible and traps glucose inside the cell [16]. Both glucokinase and GLUT2 (in rodents) act as a cellular sensor for glucose [16]. Glucose 6-phosphate is the first substrate in glycolysis. The terminal product of the glycolysis is pyruvate which enters the mitochondrion for further metabolism [17]. Pyruvate is decarboxylated to acetyl-coenzyme A (acetyl-CoA) and enters the tricarboxylic acid cycle (TCA) to generate reduced nicotinamide adenine dinucleotide (NADH) and flavin adenine dinucleotide ($FADH_2$) [17]. These reducing equivalents are utilized in the respiratory chain to enable adenosine triphosphate (ATP) production [17]. As a consequence of the increase in the ATP concentration and the rise in ATP/adenosine diphosphate (ADP) levels within the cell the ATP sensitive potassium (K_{ATP}) channels close [16]. Under non-stimulated conditions, K_{ATP} channels are open and transport positively charged K^+-ions out of the cell [1]. Upon closure, K^+-ions cannot leave the cells according to their concentration gradient resulting in a less negative charge inside the cell referred to as depolarization [16]. This depolarization leads to the opening of voltage-dependent Ca^+-channels (VDCCs) [1]. It is proposed that the rise in intracellular calcium levels triggers exocytosis of insulin-containing granules, leading to the release of insulin into the bloodstream [1]. To guarantee that insulin is directly available for secretion, insulin granules are stored in large dense-core vesicles in close proximity to the plasma membrane [1]. Mouse β-cells contain 9,000 – 13,000 dense-core secretory vesicles, but only a small proportion (about 7%) is directly docked at the

plasma membrane [18]. Besides insulin, the vesicles are also packed with other molecules such as C-peptides, amylin, Zn^{2+}, ATP and γ-aminobutyric acid (GABA), which plays important roles in modulating various homeostatic effects [16].

In vitro and *in vivo* studies in animals and humans demonstrate that, like other hormones, the release of insulin has pulsatile fashion [16, 19]. Compared to the continuous delivery of insulin, the delivery of insulin in pulses has a greater hypoglycemic effect and is proposed to prevent the desensitization of insulin receptors on the target tissues [20]. Studies with isolated islets demonstrate that pulsatility is intrinsic to pancreatic islets modulated by exogenous triggers [21]. Measurements in human islets show that glucose stimulates pulsatile insulin secretion by amplifying the mass of insulin released per burst without altering pulse interval [22]. Furthermore, insulin secretion is a biphasic process consisting of the first-phase and second-phase of release. The transient first-phase of insulin secretion peaks a few minutes after glucose stimulation, followed by the sustained, slow and continued second-phase where the remaining insulin is released [1]. While the first phase lasts about 3-10 minutes, the second phases reached its plateau within 1-3 hours [16]. The underlying mechanism leading to the heterogeneous release of insulin is still under investigation [23]. It is assumed that the first phase of secretion is based on a limited amount of readily releasable insulin granules that are directly secreted and subsequently refilled with new granules, which are mobilized in the second phase [23].

3.3 Diabetes – A global epidemic problem

Diabetes is a growing health issue affecting millions of people worldwide. For the year 2019 it was estimated that about 465 million people (adults 20-75 years) worldwide suffered from diabetes and although the incidence has decreased in some high-income countries the International Diabetes Federation estimates that until 2045 the number will increase by about 50% (700 million people) [24, 25]. It was suggested that 4.2 million people between the age of 20 and 79 years will die as a result of diabetes and its long-term complications in 2019 [25]. In Europe, 59.3 million people suffer from diabetes and another 36.6 million people already show impaired glucose tolerance [24]. About 8.5% of all deaths are related to diabetes [25]. With 9.5 million diabetics, Germany has the highest number of diabetes patients in Europe [25]. Furthermore, medical costs increase dramatically. It is to mention that the total healthcare expenditure on diabetes (adults aged 20-79) will reach USD 760 billion, whereas Europe spends 21% of these costs [25]. Due to the high prevalence of diabetes through all nations associated with serious life-threatening health problems, increasing medical care costs and lowering quality of life, there is an urgent need to discover new therapeutic targets and anti-diabetic drugs for the treatment of diabetes.

The World Health Organization describes diabetes mellitus as a chronic metabolic disorder “characterized by chronic hyperglycemia with disturbances of carbohydrate, fat and protein metabolism resulting from defects in insulin secretion, action, or both” [26]. These defects in insulin sensitivity and secretion lead to high blood glucose levels. Three main types of diabetes can be classified: type 1 diabetes mellitus (T1DM), type 2 diabetes mellitus (T2DM) and gestational diabetes, whereas some less common types of diabetes also exist [27]. In high-income countries, T2DM is the most prevalent type of diabetes with 87% to 91%, whereas 7% to 12% of patients suffer from T1DM. Only 1% to 3% of all patients suffer from other types of diabetes [27].

3.4 Type 1 Diabetes mellitus (T1DM)

T1DM and T2DM vary in their origin and progression. T1DM, also called insulin-dependent or juvenile diabetes, commonly occurs in childhood or adolescence [28]. Globally, the number of children and young adults (<20 years) with T1DM increases every year [25]. T1DM is an autoimmune disease, typically caused by an autoimmune assault targeting pancreatic β-cells, with an important genetic component [29]. The polygenic disease is based on different gene variants affecting [30], for example, the function of the immune system [31] or the β-cell itself [32]. Besides genes that are responsible for insulin production or β-cell function, the human leukocyte antigen (HLA) locus is the genetic region that is most strongly associated with T1DM [29]. This area is located on chromosome 6 and some genes in this region encode for products responsible for the immune response [33]. Whereas HLA class I molecules present endogenous antigens, class II molecules present exogenous antigens to T-cells to initiate an immune response [33]. HLA class II genes, which are expressed in antigen-presenting cells (APCs), such as dendritic cells (DCs), macrophages and thymus epithelium, are mostly associated with T1DM [29].

Crucial for the development and manifestation of T1DM is the combined effect of environmental and genetic predisposition [30]. Studies of monozygotic twins with identical genomes show different health fades due to the exposure to different environmental factors, indicating that environmental factors have a high influence on the onset of T1DM [30]. Various factors like viral infections [34] and altered intestinal microbiome compositions [35], as well as a low serum concentration of vitamin D, are associated with the onset of the multifactorial disease [34]. The interplay between these factors triggers an autoimmune reaction resulting in the infiltration of immune cells into the pancreatic islets causing progressive β-cell destruction leading to insulin deficiency [36]. Insulin deficiency manifests and is clinically diagnosed when the β-cell mass is already reduced by about 80% [37]. It is widely accepted that the selective β-cell destruction induced by massive insulitis (local

pancreatic islet inflammation) is a result of the infiltration of immune cells into the islets. Especially the presence of $CD8^+$ cytotoxic T-cells dominates during insulitis [38], while $CD4^+$ lymphocytes, macrophages ($CD68^+$) and B-cells ($CH20^+$) are also present, although in fewer numbers [38]. The infiltration of immune cells in the islets of Langerhans initiates the secretion of key proinflammatory cytokines such as interleukin (IL-) 1β, interferon- γ (IFN-γ), and tumor necrosis factor-α (TNF-α) at high concentrations in close proximity to pancreatic β-cells [39]. These cytokines are the central mediators for inflammation in T1DM, acting in together to induce cytotoxicity by activating multiple signaling networks [39-41]. Long-term exposure of IL-1β, TNF-α and IFN-γ to human islets and purified β-cells leads to β-cell dysfunction and death [42].

The onset of T1DM is not a sudden phenomenon, it is a chronic autoimmune process that already exists years before hyperglycemia manifests [43]. In this long latency of T1DM autoimmune events occur, which can be measured by the presence of autoantibodies in the blood circulation [44, 45]. T1DM is associated with five autoantibodies directed against pancreatic β-cells, particularly antibodies against insulin (IAA) [46], glutamic acid decarboxylase (GAD) [47], islet tyrosine phosphatase 2 (IA-2) [48], as well as islet cell cytoplasmic antibodies (ICA) [49] and zinc transporter-8 antibodies (ZnT8A) [50]. Patients who carry more than one autoantibody have a higher prevalence to develop diabetes, and the risk of developing T1DM even rises if autoantibodies are present in combination with high-risk HLA genes [45]. Based on that new therapeutic target systems have to be developed that focus on the immune system or β-cell protection itself.

3.4.1 Loss of functional β-cell mass in T1DM

As already mentioned, patients with T1DM, suffer from insulin deficiency and hyperglycemia induced by β-cell destruction. The loss of self-tolerance activates the immune system, which attacks insulin-producing β-cells [51]. In the asymptomatic prediabetic period, at the beginning of the disease, the immunological tolerance to the β-cell is already lost [44]. This period is characterized by prolonged, gradual, and functional impairment of β-cell function, rather than death [51]. Plasma insulin levels are already altered during this period, indicating that cell function is already decreased a long time before clinical diagnosis [52]. A large population cohort study of children confirmed that early in the progress of the disease, the insulin secretory capacity of β-cells is already compromised. Particularly, 4-6 years before the diagnosis of T1DM a decrease in β-cell function was measured [52]. Furthermore, pancreatic sections from autoantibody-positive donors give evidence that insulin area and β-cell mass are maintained before the onset of diabetes [53]. It is assumed that cell death increases right before diabetes onset and further exceeded during the clinical phase [51].

β-cell loss continues due to autoimmune infiltration but extends by the continuous increase in β-cell workload, which leads to stress and cellular exhaustion as a consequence, inducing cell death and the onset of hyperglycemia [51]. Interestingly, pancreatic samples, surgically removed from living individuals with recent-onset of T1DM, showed a significant reduction in the number of insulin-containing islets [53]. Apoptosis is supposed to be the underlying mechanism of β-cell demise in T1DM [54]. Post mortem analysis of the pancreas from recent-onset T1DM patients, which died of diabetic ketoacidosis, showed a decrease of β-cell mass by 90% (mean), which is also accompanied by increased apoptosis in patients compared to control [54]. It is considered that glucose-intolerance and hyperglycemia manifest if the functional β-cell mass decrease under the critical threshold of 20-30% of normal [55]. Shortly after being diagnosed and start of the insulin therapy, some patients show reduced insulin requirements because of increased production of insulin from the remaining β-cells. This period is referred to as “honeymoon phase” and is induced by the application of exogenous insulin, which leads to a moderate reduction in β-cell workload and antigenicity. The duration of this phase is quite variable between patients. Ongoing autoimmunity and elevated workload proceed the onset of diabetes [51, 56].

3.5 Type 2 Diabetes mellitus (T2DM)

With 90% of all diabetes cases, T2DM is the most common type [25]. Age and lifestyle factors, like physical inactivity and obesity, are the major triggers of T2DM, but the disease also has a strong hereditary component [57]. T2DM is characterized by the inability of the body to use insulin combined with the failure of β-cells to compensate the body`s increased demand of insulin that is needed [58]. The reduced ability of the target cells to appropriately respond to insulin is termed “insulin resistance” and affects the key insulin-sensitive organs liver, muscle and white adipose tissue [58]. The major environmental factors preventing the onset of T2DM are a healthy and balanced diet combined with physical activity [59].

Obesity is the major risk factor associated with the development of insulin resistance [60]. The accumulation of ectopic fat deposition in liver and skeletal muscle triggers the development of insulin resistance [30]. If the mass of adipose tissue increases, adipocytes secrete factors, namely adipokines, which negatively affect insulin sensitivity, β-cell function as well as survival [58]. Acting as an endocrine organ, adipose tissue releases several bioactive proteins, such as hormones (adiponectin and leptin) and various cytokines like resistin, IL-6, TNF-α, monocyte chemotactic protein-1 (MCP-1), and IL-1β [61]. Lean adipose tissue contains a population of resident inflammatory cells, whereas obese adipose tissue is populated by a higher number of immune cells [62]. Adipocytes are the major cell

type in the adipose tissue producing adiponectin and leptin. The expression of adipokines is altered in obesity, and plays an important role in the pathophysiology [62]. In insulin-resistant obesity, adipose tissue releases proinflammatory molecules (for example TNF-α, IL-1β, IL-6) that block the action of insulin and induce systemic inflammation. Under these conditions the secretion of adiponectin, a molecule that promotes insulin-sensitivity, is decreased [63]. Interestingly, although adiponectin is secreted from adipocytes, the plasma concentration is significantly lower in obese subjects compared to non-obese subjects [64]. Otherwise, the concentrations of the proinflammatory cytokines TNF-α and IL-1β in sera samples are elevated in overweight individuals, as well as in patients with T2DM, compared to non-overweight individuals [65]. Furthermore, insulin resistance is associated with increased release of non-esterified fatty acids (NEFAs) and glycerol due to enhanced adipocyte lipolysis [58, 60]. Under physiological conditions the increased plasma levels of insulin inhibit lipolysis [66], whereas during obesity, adipose tissue themselves gets resistant to the action of insulin, which results in increased lipolysis [67]. Increased circulating levels of NEFAs and glycerol aggravate insulin resistance in insulin-sensitive target tissues and modulate β-cell function and viability, in a process called lipotoxicity [58, 67].

Although insulin resistance is a major trigger in the pathogenisis of T2DM, insulin resistance alone is not sufficient to develop diabetes. In individuals, suffering from insulin resistance, β-cells function is increased to overcome the reduced efficiency of insulin action to maintain normoglycemia. This process is termed β-cell compensation [68]. Despite the strong variation of β-cell mass between humans [69], several studies reveal an increase in β-cell mass by about 20-50% in overweight or obese subjects [51, 70, 71]. The mechanism of β-cell compensation is not fully understood, but the expansion of β-cell mass, increased insulin biosynthesis, and enhanced function seems to play a role [68]. However, it comes to a critical point if β-cells fail to produce and secrete the sufficient amount of insulin which is needed to overcome insulin resistance. β-cell dysfunction results in impaired glucose tolerance, ultimately fasting hyperglycemia and manifests in diabetes [72]. Although many therories exist, the molecular mechanisms of β-cell failure and demise are still under debate [71, 73].

3.5.1 Loss of functional β-cell mass in T2DM

Loss of functional β-cell mass, which includes β-cell demise as well as dysfunction plays a central role in the pathophysiology of T2DM [51]. When β-cell compensation fails, the decline of β-cell mass, indicated by high fasting blood glucose levels, leads to the development of diabetes [58, 68]. Many studies agree that the β-cell mass in T2DM patients

is decreased. Various studies measured a reduction in β-cell mass between 30 to 60% [70, 71, 74-76]. The underlying mechanism leading to the loss of β-cells in T2DM patients is a critical point and still under debate. There is evidence that the underlying mechanism of β-cell loss is based on massive cell death, particularly by increased rates of apoptosis [71]. This was evaluated by post mortem analysis of whole pancreas sections, as well as isolated islets of T2DM patients compared to nondiabetic controls [71, 77]. Nevertheless, it has to be considered that diabetic and non-diabetic populations show an extraordinarily wide range of β-cell mass with a major overlap between both populations [70, 78]. This raised the question if the exclusive reduction of β-cells is responsible for the development of hyperglycemia in T2DM [70, 78].

Besides the theory of β-cell mass reduction by apoptosis, it is proposed that T2DM is developed upon β-cell dysfunction. It is under debate that the reduction of β-cell mass by 24-65% alone is not sufficient to cause hyperglycemia and T2DM [51]. The β-cell exhaustion theory could be one explanation. β-cell exhaustion is proposed to be a phenomenon based on the physical depletion of insulin stores, induced by prolonged, chronic stimulation with glucose or other insulin secretagogues [79]. It is proposed that the cells become increasingly exhausted due to high production demands [79]. To restore normoglycemia, the compensating β-cells increase the biosynthesis of proinsulin, which results in endoplasmic reticulum (ER) stress [68]. The ER is responsible for the proper folding and modification of proteins. Insulin composes approximately half of the protein production in the β-cell, making the ER an important cellular component within the β-cell [80]. Challenging the β-cell with a high glucose concentration during insulin resistance increase the need for insulin biosynthesis. If nutrient overload exceeded the ER folding capacity, the accumulation of misfolded or unfolded proteins takes place in the ER lumen [81]. To restore ER homeostasis, the unfolded protein response (UPR) is activated to alleviate this situation. The UPR signaling is initiated by the three stress sensors PERK (Protein kinase RNA-like endoplasmic reticulum kinase), IRE1 (inositol-requiring enzym), and ATF6 (activating transcription factor 6) which are located in the membrane of the ER [81]. UPR activation leads to the global attenuation of translation to decrease ER workload, whereas the translation of the transcription factor ATF4 (activating transcription factor 4) is increased due to PERK activation [82]. As a secondary effector, ATF4 is responsible for the transcription of many genes that have beneficial as well as deleterious effects in cell fate during ER stress [82, 83]. The imbalance in ER homeostasis decreases GSIS [80, 84]. β-cells investigated in pancreatic sections from T2DM patients show increased expression of ER stress marker, providing direct evidence that ER stress is responsible for the pathogenesis of T2DM [85, 86].

Furthermore, β-cell dysfunction can occur upon improper glucose metabolism resulting in chronic oxidative stress. Studies suggest that the increase in insulin secretion initiated by a higher presence of glucose induces oxidative stress [87]. β-cells are vulnerable to oxidative stress, because of their low level of antioxidant enzymes (superoxide dismutase, catalase and, glutathione peroxidase) [87]. Reactive oxygen species (ROS) for example are produced in the mitochondrial metabolism, which is central during GSIS [72]. At low levels, ROS acts as a signalling molecule, whereas excessive amounts of ROS, due to persistent high glucose metabolism, impair the mitochondrial activity and cause deleterious effects that lead to β-cell dysfunction [72].

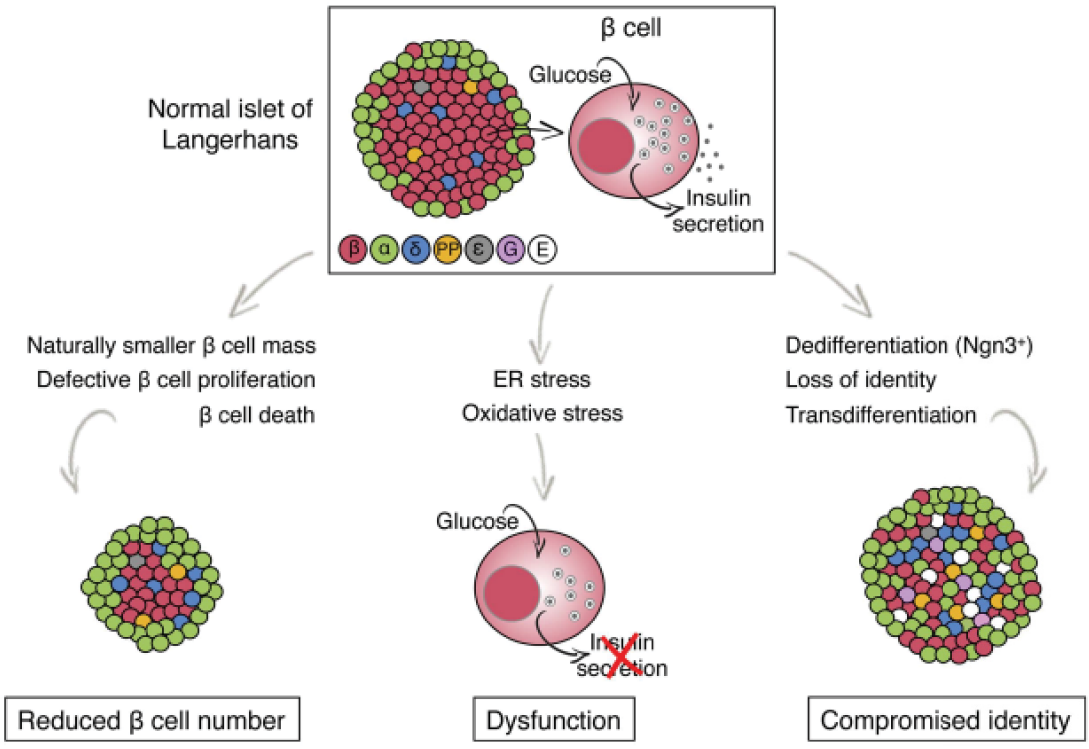

Figure 2: Proposed models for functional β-cell loss in T2DM. (Illustration reprinted from Swisa, A. *et.al.*, Front Genet 2017; 8: 21) [72]. Figure illustrates the alternative mechanisms of functional β-cell demise. Normal pancreatic islets consist of different types of endocrine cells. Insulin is secreted from β-cells. It is still under debate, if the pancreatic islet loses the functional β-cell mass during the progression of T2DM by reduced β-cell number, due to death, β-cells dysfunction leading to impaired insulin secretion, and/or loss of β-cell identity. Different cell types within the β-cell are indicated by different colors. G, gastrin; E, endocrine cell with empty granules (no hormone production).

Furthermore, some animal as well as human studies point to the possibility that β-cell demise is based on insulin-negative silent β-cells rather than dead cells [73, 88, 89]. It is proposed that β-cell dedifferentiation is responsible for β-cell failure [73]. The dedifferentiation of mature β-cells to progenitor-like cells and conversion into other endocrine cells was investigated [73]. High metabolic load alters the activity of the key β-

cell transcription factors including pancreatic and duodenal homeobox 1 (Pdx1), NK6 homeobox 1 (Nkx6.1), MAF BZIP transcription factor A (MafA), and neurogenin 3 (Neurog3), inducing loss of β-cell identity, by silencing β-cell genes and activating alternative islet cell genes that were repressed. In this case, the cell is no longer able to regulate glucose homeostasis [72, 73]. Interestingly, this process seems to be party reversible under normoglycemia conditions [89].

It is proposed that the progression of T2DM, especially the demise of functional β-cell mass, underlies three different mechanisms that are not mutually exclusive. Functional β-cell mass can demise as a consequence of functional exhaustion and β-cell dysfunction, due to oxidative and endoplasmic stress, β-cell death and dedifferentiation.

3.6 Current medications, therapeutic strategies, and limitations in the treatment of diabetes

Based on the increasing number of people suffering from diabetes and its long-term effects, it is of vital importance to design new therapeutic options to stop the progression of the disease. Due to the various origins and clinical course of T1DM and T2DM, patients are treated with different therapeutic approaches. Since 2009, glycated hemoglobin (HbA_{1c}) has been recommended to be a reliable diagnostic marker for glycemic control and to diagnose diabetes [90]. It represents the average blood glucose levels of patients over the last 4 months [58]. Diabetes is diagnosed at an HbA_{1c} level of ≥6.5%, whereas levels between 6% and 6.5% indicate a very high risk of developing diabetes [90]. During the use of anti-diabetic medications, HbA_{1c} is used to monitor the efficiency of the drug [91].

Diabetes is a chronic disease in which the quality of life significantly deteriorates. Without careful management, high levels of blood glucose induce deleterious side effects throughout the whole body [25]. Daily application of insulin is the mainstay of therapy for individuals with T1DM [92], while the additional combination with pramlintide, an amylin analogue, has already been approved by the Food and Drug Administration (FDA) for the use in adults with T1DM. All oral antidiabetic drugs are contraindicated in T1DM [92].

However, several medications are accessible on the market to treat the symptoms of T2DM [93]. Multiple medications can achieve and maintain normoglycemia, but the glucose control of most oral antidiabetic agents gradually diminishes because they fail to prevent functional β-cell mass over the time of medication [94, 95]. Intensive lifestyle changes including diet, increased physical activity, and weight loss are the first intervention to improve insulin sensitivity and glycemic control [93]. In obese patients, weight loss effectively improves glycemic control and delays the onset of T2DM [96, 97]. However, even if lifestyle interventions are successfully implemented, the majority of patients will

require pharmacological therapy to further maintain metabolic control and to be protected from diabetic long-term complications [93, 95]. The insulin-sensitizing agent metformin is recommended as the first pharmacological agent to treat T2DM [92] by lowering plasma glucose levels due to the suppression of hepatic glucose production and improvement of insulin sensitivity [98], but it is well documented that the strong anti-diabetic effect of the oral monotherapy declines over time [58, 99, 100]. The UK Prospective Diabetes Study reported that 3 years after diagnosis of diabetes and start of the metformin monotherapy in overweight T2DM patients, 56% of the patients need an additional therapeutic agent to restore an HbA_{1c} of <7%, whereas after 9 years approximately 87% of the patients will need multiple therapies [100]. Therefore, additionally to monotherapy, many patients require stepwise treatment intensification over time with further anti-diabetic medication on top of metformin to maintain normoglycemia and avoid long-term complications [92, 101, 102]. Tight glycemic control can be achieved by additional oral and injectable treatments. Several drugs are on the market to control blood glucose levels classified into agents based on their different mechanisms of action [92]. Insulin secretagogues (sulfonylureas, meglitinides, incretin mimetics), insulin sensitizers (biguanides, thiazolidinediones) or glucourics (SGTL2 inhibitors) are the most common anti-diabetic drugs [95]. Promising effects could be obtained if metformin is additionally administrated with an insulin secretagogue as second-line medication [102-105]. Insulin secretagogues are agents that increase the workload in pancreatic β-cells by inducing prolonged insulin secretion [106]. Incretin mimetics, or glucagon-like peptide-1 (GLP-1) analogs, are insulin secretagogues that were frequently used for the treatment of T2DM [107]. Incretin peptides are gastrointestinal hormones secreted from the intestine to maintain prandial euglycemia. One physiological incretin is GLP-1 which is secreted after nutrition intake into the circulation inducing the decrease of blood glucose levels and promote weight loss [108]. GLP-1 has a very short half-life because it is inactivated very fast by the proteolytic enzyme dipeptidyl peptidase-4 (DPP-4) [108]. Degradation-resistant agonists of the GLP-1 receptor (e.g., Exendin-4 and Liraglutide), as well as DPP-4 inhibitors, are designed to treat T2DM patients [108]. GLP-1 acts on various tissues, but besides the extrapancreatic effects, GLP-1 receptor agonists improve β-cell function and survival via binding to the GLP-1 receptor located on pancreatic islet cells [108]. Interestingly, it is under debate, that insulin secretagogues promote β-cell exhaustion and as a consequence pancreatic islet dysfunction [107]. β-cell exhaustion could be induced by chronic stimulation to glucose as well as non-glucose secretagogues [79]. The insulin secretagogue Liraglutide (GLP-1 analogue) for example has beneficial effects on human islets upon short-term administration, whereas long-term treatment (injections for more than 250 days) has deleterious effects on islet function leading to a compromised hormone release from human islets [107]. Abdulreda *et al.* hypothesize that

the already-overworked β-cells in T2DM undergo metabolic exhaustion during the long-term treatment with incretin mimetics, and subsequently fail to maintain normoglycemia [107]. Clinical studies in T2DM patients with the sulfonylurea glibenclamide showed similar effects [99]. Whereas in the first 6 months glibenclamide showed beneficial effects on fasting blood glucose and HbA_{1c} levels, after 5-years follow up the monotherapy with glibenclamide failed in 34% of the patients [99, 109].

The newest anti-diabetic drug on the market is the SGLT2 inhibitor. Instead of directly acting on β-cells, it provides the glucose lowering effect by blocking glucose reabsorption in the proximal renal tubule by inhibiting SGLT2 [110]. This drug reduces HbA_{1c} by 0.5%-1% and provides modest weight loss. Additionally, it reduces blood pressure and arterial stiffness, has favorable effects on lipid profile and improve endothelial function [110]. Most importantly, cardioprotective effects were achieved in T2DM patients [111, 112]. Unfortunately, it seems that SGLT2 inhibitors do not have the ability to prevent diabetes progression over a longer time of medication because T2DM patients receiving an SGLT2 inhibitor as an add-on therapy to metformin showed increased HbA_{1c} levels over the follow-up of 4 years [113].

Based on the numerous requirements it is very challenging for future investigators to develop efficient anti-diabetic drugs. Medications that can be easily applied have to be designed. The mechanism of action of these medications needs to increase β-cell function without inducing β-cell exhaustion. Additionally, β-cell mass decline has to be prevented or β-cell mass has to be even increased to stop the progression of the disease. Furthermore, new therapies have to avoid any side effects by additionally managing diabetic complications resulting from high concentrations of glucose in the body. Recently, dextromethorphan (DXM) and its active metabolite dextrorphan was identified as a new insulin secretagogue acting on the N-methyl-D-aspartate (NMDA) receptor on pancreatic islets [114].

3.7 N-methyl-D-aspartate (NMDA) receptor as a new therapeutic target

As highlighted before, the major problem of the current diabetes therapies is the failure to preserve functional β-cell mass as well as the induction of `β-cell exhaustion` upon treatment with insulin secretagogue. Because of the high relevance of new therapeutic strategies to treat diabetes, several groups have intensively studied the role of the NMDA receptor in pancreatic islet cells during the last few years [114-117].

The NMDA receptor belongs to the family of ionotropic glutamate receptors and is, besides the α-amino-3-hydroxy-5-methylisoxazole-4-propionic acid (AMPA) and kainate receptors, part of the glutamate signalling system [114, 118]. NMDA receptors are

heteromeric protein complexes, which are composed of tetramers to build a channel [118]. The subunits building the ion channel are NR1, NR2, and NR3, while the NR1 (encoded by the *GRIN1* gene) subunit is obligatory for the assessment of a functional NMDA receptor [118, 119]. At resting membrane potential the ion flow of the channel is blocked due to the binding of Mg^{2+} within the channel pore [118]. NMDA receptors are ligand- and voltage-gated ion channels, meaning that for the opening of the channel the simultaneous binding of the ligand glutamate in combination with glycine or D-serine and the depolarization of the membrane is required [118]. Depolarization of the membrane releases the Mg^{2+} block and allows monovalent (Na^+, K^+) as well as divalent cations such as Ca^{2+} to pass the channel [118].

In the central nervous system, glutamate is not only responsible for the binding on NMDA receptors, it acts also as an excitatory neurotransmitter that modulates the function and viability of neurons as well. Glutamate is the major excitatory neurotransmitter in the mammalian central nervous system acting on ionotropic and metabotropic glutamate receptors [118, 120]. The prolonged exposure of glutamate to neurons triggers the overactivation of glutamate receptors which leads to increased intracellular Ca^{2+} accumulation and finally to cell death. This process is known as excitotoxicity [121]. Neurotoxicity induced by excessive activation of NMDA receptors was investigated in hippocampal slices [122]. Many studies already show that blocking the NMDA receptor has beneficial effects on the physiology of many cell types and therefore the neuronal receptor already acts as a drug target for the treatment of various diseases. Non-productive cough, pseudobulbar affect (PBA), nonketotic hyperglycinemia, Parkinson's disease, and Alzheimer's disease are known disorders that are treated by targeting the NMDA receptor [121]. Several antagonists of the NMDA receptor have been well investigated and already used as a drug to target the NMDA receptor in patients [123]. As therapeutics for the management of pain ketamine, memantine, Mg^{2+}, and dextromethorphan (DXM) have already been used [123]. Known to have a high safety profile in humans [124], the morphinan DXM is an active ingredient in many over-the-counter cough medications [125] and has therapeutic potential for the treatment of neurological disorders including cerebral ischemia, epilepsy and acute brain injury [126]. Only 2-2.5 hours after oral drug administration, DXM reaches the highest concentration in the blood [123]. Besides the NMDA receptor, DXM interacts with non-opioid sites like the serotonin transporters, noradrenaline transporters and $\alpha 3\beta 4$ nicotinic acetylcholine receptors [123]. Additionally, it acts as an agonist for the sigma-1 receptor, which is localized at the membrane of the ER [121].

Transported via the blood flow to the liver, DXM undergoes hepatic metabolism. In the liver, DXM is converted to its active metabolite dextrorphan (DXO) by cytochrome P450

[121]. As a noncompetitive antagonist of the NMDA receptor [127], it can block the channel pore of the receptor in its closed and open conformation [121, 128]. In the central nervous system, NMDA receptors are widely expressed and investigated but they have been discovered in non-neuronal tissues and cells, including the kidney, lung, stomach, ovaries, skeletal muscle, lymphocytes, and pancreatic β-cells only recently [114, 129].

3.7.1 Protective properties of antagonizing the NMDA receptor

Blocking the NMDA receptor has pathophysiological significance supported by many reports. Our research group gives the first evidence that blocking the NMDA receptor has antidiabetic properties and beneficial effects on pancreatic islets and β-cells [114]. Antagonizing the pancreatic NMDA receptor *in vitro* and *in vivo* predominantly increases GSIS without inducing hypoglycemia. It additionally enhances islet cell survival, and improves islet function under diabetogenic conditions *in vivo* [114]. In detail, blocking the NMDA receptor pharmacologically with DXO as well as genetically by the deletion of *Grin1* leads to the increase of GSIS in mice and in human islets. *In vivo* experiments in *db*/*db* mice, an animal model for T2DM, points to the possibility that the treatment with DXM delays the onset of the disease. After 8 weeks of treatment with DXM, a significant increase in glucose tolerance was measured without causing hypoglycemia [114]. The protective effect is supported by post mortem analysis of the pancreas which shows a decrease in apoptotic islet cells in the pancreas of mice receiving a higher dosage of DXM [114]. Furthermore, *in vitro* experiments with NMDA receptor antagonists support the cell-protective properties against inflammation and glucotoxicity [114, 115]. It is hypothesized that the prolonged activation of the NMDA receptor for example during hyperglycemia, activates K^+ channels, including the Ca^{2+}-activated K^+-channel 4 (SK4 channel) as well as the K_{ATP} channel. This activity could lead to the repolarization of the depolarized cell resulting in a reduced GSIS [121]. Memantine, another antagonist of the NMDA receptor, improves the function of β-cells in diabetic mice, supporting the role of the NMDA receptor in the progression of T2DM [115]. In the streptozotocin (STZ)-induced diabetic mouse model, the treatment with memantine shows improved glucose tolerance and lower expression of cleaved caspase-3, a marker for cell death, in islets of treated mice compared to control mice. Additionally, memantine treated mice expressed higher levels of *Insulin*, *Pdx-1* and *Mafa* mRNA, markers of β-cell function. Simultaneously it lowered levels of *Tnf-α* and *Il-1β* mRNA [115]. All these effects could be beneficial for the prevention or onset delay of diabetes. These preclinical studies could already be transferred into clinical studies. T2DM patients receiving DXM in an oral glucose tolerance test (OGTT) have improved blood glucose-lowering effects and higher insulin concentrations during the first phase of the OGTT compared with placebo treatment [114]. In another clinical trial, DXM was investigated in combination with

sitagliptin. Compared to sitagliptin monotherapy, the combination with DXM improves the blood glucose lowering effect and increase the serum insulin concentrations in the first phase of the OGTT in patients with T2DM [130].

Taken together, these results support the hypothesis that NMDA receptors are required to limit GSIS, whereas the sustained activation of these receptors is harmful to the cells. Based on the enhanced insulin secretion and the protective effect of DXM on pancreatic islets, the treatment of patients with DXM represents a valuable adjunct therapy for current diabetes treatments.

3.8 Aim of the study

The discovery of new antidiabetic targets as well as the development of new antidiabetic drugs is the main goal for many researchers. The recently discovered insulin secretagogue DXM, and its active metabolite DXO, seems to be one possible new therapeutic agent. To our knowledge, until now nothing has been reported about the long-term effects of DXO on pancreatic islets as well as the influence on the molecular level. The major aim of this study was to investigate the effect of DXO on islet cell viability as well as analyze its long-term effects on islet cell function. We address the question, whether high concentrations of the insulin secretagogue DXO (like other insulin secretagogues) induce β-cell exhaustion *in vitro,* and additionally reveal parts of the underlying molecular mechanism.

First, we explored the protective effect of DXO on pancreatic islets during inflammation and intensively investigated the protective effect upon NMDA receptor deletion. Therefore, we performed *in vitro* studies with isolated pancreatic islets of wild-type mice, as well as GluN1-KO mice, lacking the functional NMDA receptor. Secondly, we explored the effect of a high dosage of DXO on islet cell function after long-term treatment under high glucose concentrations. To get insight into the molecular mechanism we, thirdly, analyzed the changes in the whole transcriptome of pancreatic islets upon long-term exposure to DXO. Fourthly, we focus on the candidate gene *Aldh1l2* (Aldehyde dehydrogenase 1 family, member L2) that was highly upregulated upon DXO treatment. We performed gain-of-function, as well as loss-of-function experiments to examine the role of this enzyme in islet cell function and viability. Finally, experiments with lower concentrations of DXO as well as *in vivo* experiments in *db*/*db* mice were performed.

With this work, I wish to significantly contribute to the knowledge about the role of the insulin secretagogue DXO on pancreatic islet viability as well as function and additionally identify new genes involved in regulating GSIS and glucose tolerance.

4 Experimental Procedure

Parts of the following section will be used for a publication in a scientific journal.

4.1 Mouse Work

4.1.1 Mouse Models

For the various experimental questions in this thesis, different mouse models were used. For *in vitro* wild-type studies male C57BL/6J mice at the age above 9 weeks were purchased from Janvier or alternatively from Taconic Biosciences. To investigate the impact of NMDA receptors on islet cell death, GluN1-KO (*Pdx1*-Cre x *Grin1*$^{loxP/loxP}$) male mice were used carrying the genetic deletion of *GluN1* specific in pancreatic cells. GluN1-KO was previously described in Marquard *et al.*, 2015 [114]. *Pdx1*-Cre mice were used as control [131]. For *in vivo* studies, 3-4 weeks old male BKS.Cg-*Dock7m* +/+ *Lepr*^{db}/J mice were purchased from Jackson Laboratory (Stock No: 000642). In the following chapters this leptin receptor-deficient mice are referred to as *db*/*db*. The role of *Aldh1l2* was studied using constitutive *Aldh1l2*$^{-/-}$ (*Aldh1l2*-KO) mice, which were kindly provided by S. Krupenko from the UNC Nutrition Research Institute in Kannapolis. ALDH1L2-WT (*Aldh1l2*$^{+/+}$) mice were used as controls. All animal experiments were performed at the Heinrich Heine University Düsseldorf or at the German Diabetes Center in Düsseldorf. All experiments were permitted by the local Animal Ethics Committee of the Landesamt für Natur, Umwelt und Verbraucherschutz Nordrhein-Westfalen (LANUV North Rhine-Westphalia) and conducted according to the German Animal Protection Laws. All mice were kept in rooms with controlled temperature (22°C), humidity (55%) and 12:12 hour light/dark cycle with lights on at 6 a.m. Mice had unlimited access to standard laboratory chow and water.

4.1.2 Genotyping

4.1.2.1 Tissue Lysis and DNA Extraction

Tails or ear clips were used to determine the genotype of the mice. For genomic DNA extraction, tissue pieces were digested in lysis buffer (0.1 M Tris pH 8.0, 0.2 M NaCl, 5 mM EDTA, 0.4% SDS) containing 0.2 mg/ml Proteinase K (20 mg/ml, AppliChem) for at least 1 hour at 56°C and 300 rpm. Thereafter, isopropanol precipitation was performed and the pellet was washed with 75% ethanol. After centrifugation for 15 minutes at full speed and at 4°C, supernatant was discarded and pellet dried at room temperature. The dry pellet,

containing the genomic DNA, was diluted with 100 µl ddH_2O and amplified directly via polymerase chain reaction (PCR) or stored at –20°C.

4.1.2.2 Polymerase Chain Reaction

To amplify specific regions of the DNA, PCR was performed. For each piece of tissue, the following master mix was used:

Master Mix Components	**Volume**
Go Tag® G2 Hot Start Green Master Mix (Promega)	10 µl
Nuclease Free Water	7 µl
Primer forward (10 µM)	0.5 µl
Primer reverse (10 µM)	0.5 µl
DNA-Lysate	2 µl

All PCRs were carried out in a Professional Trio Thermocycler (Biometra). For the different mouse lines specific primer and PCR programs were used:

Aldh1l2		Primer	Product Size
Wild-Type	Forward	5´-AAT TGG TGG TTC TCT CAA GTC TG	338 bp
	Reverse	5´-GCA CCC ATA AAG GGG CTC AAG	
Mutant	Forward	5´-CAC ACC TCC CCC TGA ACC TGA AA	598 bp
	Reverse	5´-GAC ATA TAC TGA CCT CTG AGG GTG GC	

Aldh1l2 PCR Program	
Wild-Type	**Mutant**
95°C for 10 minutes	95°C for 10 minutes
40 x 95°C for 30 seconds	40 x 95°C for 30 seconds
58°C for 20 seconds	60°C for 20 seconds
72°C for 30 seconds – Go to Step 2	72°C for 30 seconds – Go to Step 2
72°C for 3 minutes	72°C for 3 minutes
4°C for ∞	4°C for ∞

GluN1		Primer	Product Size
Wild-Type	Forward	5´-GTG AGC TGC ACT TCC AGA AG	180 bp
	Reverse	5´-GAC TTT CGG CAT GTG AAA TG	

Mutant	Forward	5´-CTT GGG TGG AGA GGC TAT TC	280 bp
	Reverse	5´-AGG TGA GAT GAC AGG AGA TC	

***GluN1* PCR Program**
Wild-Type and Mutant
94°C for 3 minutes
35 x 94°C for 30 seconds
61°C for 60 seconds
72°C for 60 seconds – Go to Step 2
72°C for 60 seconds
4°C for ∞

Pdx1-Cre		Primer	Product Size
Cre-positive	Forward	5´-CTG GAC TAC ATC TTG AGT TGC	280 bp
	Reverse	5´-GGT GTA CGG TCA GTA AAT TTG	

***Pdx1-Cre* PCR Program**
94°C for 3 minutes
30 x 94°C for 60 seconds
57°C for 60 seconds
72°C for 60 seconds – Go to Step 2
72°C for 3 minutes
10°C for ∞

To separate the PCR products according to their size, a 1-2% agarose gel was used. To visualize the DNA fragments 3% SYBR® Safe DNA Gel Stain (10,000x, Invitrogen) were added to the gel. Gel electrophoresis was performed with a Power PAC™ 1000, 3000 or HC System (Bio-Rad) for 20-30 minutes at 120 V. Visualization and imaging of the DNA fragments were performed by using the ChemiDoc™ XRS Imaging System or ChemiDoc™ MP Imaging System (Bio-Rad).

4.1.3 Glucose tolerance test (GTT) and plasma insulin measurement

To measure glucose metabolism in mice, a glucose tolerance test (GTT) was performed. To measure fasting blood glucose levels, mice fasted overnight for 16 hours. Mice were weighed and 1.5 mg/g body weight glucose were injected intraperitoneally. Blood samples

were collected at the tip of the tail. Blood glucose concentrations were measured at the tail vein before injection and 15, 30, 60, 90 and 120 minutes after injection using a Monometer® Futura glucometer (Cardimac GmbH) with the corresponding test strips (Cardimac GmbH). Measurement was performed twice at every time point. For the measurement of plasma insulin before and 30 minutes after injection, blood was collected in EDTA coated microvette® CB 300 tubes (Sarstedt). Blood samples were centrifuged at 2.000 g for 10 minutes and at 4°C. Plasma was transferred into a new tube and stored at -80°C for further analysis. To measure plasma insulin level, the ultrasensitive rat insulin ELISA (CrystalChem) was used according to manufacturer's instructions. Absorbance was measured using the Infinite M200 NanoQuant reader (Tecan). After the final *in vivo* experiment, mice were killed for islet isolation. Just islets of mice with a strong phenotype during GTT were used for further *in vitro* analysis.

4.1.4 Long-term DXM treatment of *db*/*db* mice

To check the protective effect of DXM on pancreatic islets *in vivo*, four-weeks-old *db*/*db* mice were treated with DXM (Sigma-Aldrich) via the drinking water. Therefore, drinking water was supplemented with DXM in two different concentrations and administered to *db*/*db* mice for two weeks. The low-dose group got 1 mg/ml DXM, whereas the high-dose group got 3 mg/ml DXM. To control the effect of DXM in mice, fasting blood glucose level and body weight were measured weekly. For fasting, mice were kept for 6 hours without food but with unlimited excess to drinking water containing DXM. Fasting blood glucose concentrations were measured at the tip of the tail vein using the GlucoSmart® Swing2 glucometer (MSP Bodmann GmbH) with the corresponding test strips (MSP Bodmann GmbH). Additionally, blood was collected in EDTA coated microvette® CB 300 tubes (Sarstedt) to measure the amount of DXM in the plasma. Therefore, blood samples were centrifuged at 2.000 g for 10 minutes and 4°C. Plasma was transferred into a new tube and stored at -80°C for further analysis. After two weeks of treatment, islets were isolated as described in 4.2.1 and directly used for RNA-isolation with the RNeasy Mini Kit (Qiagen) (4.4.1). Extracted RNA was stored at -80°C until delivery to ETH Zurich for RNA sequencing (4.5.1). For a better comparison of the two groups, one mouse of the control group (1 mg/ml) was excluded, because the mouse had a blood glucose concentration by around 150 mg/dl and did not develop diabetes. Additionally, a hypoglycemic DXM mouse with a blood glucose concentration by around 50 mg/dl was excluded from the treatment group.

4.2 *In vitro* Methods

4.2.1 Isolation of mouse pancreatic islets

For *in vitro* experiments mouse pancreatic islets were isolated. Isolation was performed using Liberase TL Research Grade (Roche) as reported by the protocol published by Yesil *et al.*, 2009 with few minor changes [132]. Enzymatic digestion was performed for up to 17.5 minutes at 37°C and stopped with Dulbecco's Modified Eagle's Medium + GlutaMAX (1 g/ml glucose) (DMEM, Gibco® by Life Technologies) containing 15% heat-inactivated Fetal Bovine Serum (FBS, Gibco® by Life Technologies). Following digestion, the tissue was washed and filtered. To separate the islets from the exocrine tissue, gradient centrifugation was performed at 1,200 *g* for 25 minutes. Islets were collected from the interphase between Histopaque-1077 (Sigma-Aldrich) and DMEM. Isolated islets were washed twice with islet medium containing Connaught Medical Research Laboratories medium 1066 (CMRL, Gibco® by Life Technologies) supplemented with 15% heat-inactivated FBS, 100 U/ml penicillin (Gibco® by Life Technologies), 100 µg/ml streptomycin (Gibco® by Life Technologies), 50 µM β-mercaptoethanol (Gibco® by Life Technologies), 0.15% $NaHCO_3$ (Gibco® by Life Technologies), and 10 mM glucose (Sigma-Aldrich). To recover from the isolation procedure, islets were cultured in islet medium at 37°C and 5% CO_2 overnight. All functional assays were performed after overnight culture.

4.2.2 Human pancreatic islets

Human pancreatic islets were provided by the NIDDK-funded Integrated Islet Distribution Program (IIDP) at City of Hope, NIH Grant # 2UC4DK098085. All experiments were performed according to the respective ethics committees (ethics committee of the Medical Faculty, Heinrich Heine University Düsseldorf, study number 3921; and ethics committees of the IIDP centers). The requirements for ordering human islets include an islet preparation with a purity >80% and viability of 95-98%. After arrival, human islets were washed up to three times and cultured in islet medium as indicated previously. Islets were cultured at 37°C and 5% CO_2 overnight before functional assays were performed.

4.2.3 Treatment of mouse and human islets *in vitro*

To induce cell death, islets were cultured in islet medium as described above supplemented with a mixture of cytokines. According to the experimental conditions, islets were treated with or without DXO (Sigma-Aldrich) to investigate the protective effect of the compound. Thus, islets were pretreated for 1 hour with or without DXO before starting the treatment with cytokines. Mouse islets were treated with a cytokine mix consisting of 1,000 U/ml

recombinant mouse TNF-α, (R&D Systems), 1,000 U/ml recombinant mouse IFN-γ, (eBioscience or Thermo Scientific) and 50 U/ml recombinant mouse IL-1β (R&D Systems) with or without DXO for 24 hours. Human islets were treated with a cytokine mix consisting of 1,000 U/ml recombinant human TNF-α (R&D Systems), 1,000 U/ml recombinant human IFN-γ (PeproTech) and 2 ng/ml recombinant human IL-1β-(R&D Systems) with or without DXO for 42 hours. All incubation steps were performed at 37°C and 5% CO_2.

4.2.4 Insulin secretion from pancreatic islets and pseudo-islets

To investigate various effects on insulin secretion isolated islets as well as pseudo-islets (4.6.2) were used. Before islets were stimulated with low and high glucose concentrations, islets were starved for 1 hour in Krebs Ringer HEPES (KRH) buffer containing 15 mM HEPES (Gibco® by Life Technologies), 5 mM KCl (Chemsolute, Th.Geyer), 120 mM NaCl (Carl Roth), 2 mM $CaCl_2$ (Sigma-Aldrich), 10 µM glycine (Sigma-Aldrich), 24 mM $NaHCO_3$ (Sigma-Aldrich) supplemented with 0.1% bovine serum albumin (BSA, Sigma-Aldrich) and 2 mM glucose (Sigma-Aldrich) ± compounds. The compounds glibenclamide (Glib, Sigma-Aldrich) and DXO were tested in insulin secretion assays. Glib was solved in dimethyl sulfoxide (DMSO, Sigma-Aldrich) and DXO was solved in water. All incubation steps were performed for 1 hour in a humidified incubator at 37°C and 5% CO_2. To measure basal insulin secretion KRH buffer was replaced with pre-warmed KRH buffer ± compounds supplemented with 2 mM glucose. After incubation, supernatant was collected and centrifuged for 5 minutes at 500 *g* and 4°C. The supernatant was collected and stored at - 20°C. To check insulin secretion at high glucose concentrations, the same islets were treated with KRH buffer ± compounds supplemented with 20 mM glucose. After incubation, supernatant was collected and samples were treated as previously described. To normalize insulin secretion, total insulin content had to be determined. Therefore, islets were lysed with radioimmunoprecipitation assay (RIPA) buffer containing 50 mM Tris-HCl (pH 7.4) (Sigma-Aldrich), 150 mM NaCl, 1% IGEPAL (Sigma-Aldrich), 0.25% Na-deoxycholate (AppliChem), and 1 mM EDTA (Ambion) and placed on the cell disrupter (Scientific Industries, Inc) for 10 minutes at 4°C. To remove cell debris, cells were centrifuged for 10 minutes at full speed and 4°C. Afterwards, all supernatants were stored at -20°C until measurement. To measure insulin secretion and content the ultrasensitive rat insulin ELISA (CrystalChem) was used according to manufacturer's instructions. Absorbance was measured using the Infinite M200 NanoQuant reader (Tecan).

4.3 Imaging Analysis

4.3.1 Determination of apoptosis by TUNEL staining

To detect apoptotic cell death on a single cell level TUNEL (TdT-mediated dUTP-X nick end labeling) staining was performed. TUNEL staining is based on the labeling of DNA strand breaks with a red fluorescent dye. Therefore, the In Situ Cell Detection Kit, TMR (Roche) was used to detect apoptotic cells in pancreatic mouse islets after treatment with cytokines in combination with or without 10 µM DXO. Treatment was performed as described in 4.2.3. After treatment, islets were washed in pre-warmed KRH buffer prepared as described above containing 0.1% BSA and 5.5 mM glucose. For fixation, islets were incubated in Bouin`s solution (Sigma-Aldrich) for 15 minutes at room temperature (RT) on a 360° sample rotor (VWR International GmbH). Fixed cells were centrifuged for 1 minute at 1,000 *g* and washed up to four times with Dulbecco's phosphate-buffered saline (DPBS, Gibco® by Life Technologies) under rotation. The supernatant was discarded after each centrifugation. For cryo-sectioning, islets were embedded into embedding molds (Tissue-Tek® Cryomold®, Sakura Finetek) and filled up with Tissue-Tek® O.C.T. embedding media (Sakura Finetek). For slow freezing, molds were stored at -80°C. Using the microtome HM 560 (Thermo Fisher Scientific), embedded islets were sliced into 12 µm thick cryo-sections and transferred to Superfrost® plus microscope slides (Thermo Scientific). For TUNEL and antibody staining, slides were washed three times for 5 minutes at RT with PBS^{++} (5.4 mM KCl, 0.27 M NaCl, 3 mM KH_2PO_4, 1.3 mM Na_2HPO_4, 5 mM $MgCl_2$, 9 mM $CaCl_2$ in H_2O) followed by the treatment with 40 µg/ml Proteinase K (AppliChem) diluted in 10 mM Tris-HCL for 10 minutes at 37°C in a humidified atmosphere. After three additional washing steps with PBS^{++} slides were treated with permeabilization solution (0.1% Triton X-100/0.1% Sodium citrate, pH 7.5, AppliChem, Sigma-Aldrich) for 2 minutes at 4°C. For TUNEL staining, solutions were used according to the manufacturer's instructions. Slides were incubated with TUNEL staining solution for 1 hour at 37°C in a humidified atmosphere in the dark. Antibody staining was performed immediately afterward. All the following steps were performed in the dark. Slides were washed three times with washing buffer (PBS^{++} supplemented with 0.2% Triton X-100, AppliChem) for 5 minutes, followed by fixation with paraformaldehyde (PFA, Alfa Aesar) for 15 minutes at RT in the dark. To avoid background staining, slides were incubated for 5 minutes in 50 mM ammonium chloride (Merk) diluted in washing buffer. Before blocking, slides were washed three times in washing buffer. For blocking, slides were incubated with PBS^{++} containing 5% normal donkey serum (NDS, Jackson ImmunoResearch), 5% normal goat serum (NGS, Jackson ImmunoResearch), 2% BSA (AppliChem) and 0.2% Triton X-100 (AppliChem) for 1 hour in a humidified chamber. Afterward, slides were stained overnight at 4°C in a moist chamber with the primary

antibody polyclonal guinea pig anti-insulin (DAKO, #A0564) diluted 1:300 in blocking solution. After incubation, slides were washed three times with washing buffer before treatment with the secondary antibody goat anti-guinea pig conjugated with Alexa 488 (A11073, Invitrogen) diluted 1:200 in blocking solution. Staining was performed 45 minutes at RT in a humidified atmosphere. Additionally, cell nuclei were visualized by staining with DAPI (1:1000, Sigma-Aldrich). Afterward, slides were washed three times for 5 minutes with PBS^{++} before mounting the slides with Fluorshield™ (Sigma-Aldrich) for the following imaging. Imaging and quantification were performed blinded.

4.3.2 Determination of cell viability using live-cell imaging

To measure cell viability of isolated mouse or human pancreatic islets LIVE-DEAD Viability-Cytotoxicity Kit (Thermo Fisher Scientific) was used. For the visualization of viable and dead cells, whole islets were co-stained with 2 µM calcein AM, 4 µM ethidium homodimer-1 and Hoechst (1:1000, Thermo Fisher Scientific) in KRH buffer prepared as described above supplemented with 0.1% BSA and 10 mM glucose. Co-staining was performed for 1 hour in the dark at 37°C and 5% CO_2. Following staining, images of every single islet were recorded as described in 4.3.3.

4.3.3 Imaging and imaging analysis

All images were obtained using a Zeiss Laser Scan Microscope (LSM) 710 coupled to an Axio Observer.Z1 microscope (Carl Zeiss MicroImaging GmbH). Fiji (ImageJ) image analysis software was used to analyze the images.

Images of whole islets for the measurement of cell viability (4.3.2) were acquired by maximum intensity projections of Z-stacks under 20x magnification. For quantification, the area of dead cells, ethidium homodimer-1–positive area (as determined by thresholding with a fixed value) was determined and normalized to the Hoechst–positive area (as determined by Otsu thresholding).

For the determination of apoptotic islet cells by TUNEL staining (4.3.1), images were also acquired as Z-stacks under 40x magnification. Before analysis, maximum intensity projections were performed for all images. TUNEL positive cells were counted manually, whereas TUNEL positive cells were only counted if the TUNEL staining was co-localized with DAPI. For quantification, TUNEL positive cells were normalized to the total islet area. Imaging and quantification were performed blinded.

4.4 Molecular biological methods

4.4.1 RNA extraction from mouse islets

For the isolation and purification of total RNA from mouse islets, RNeasy Mini Kit (Qiagen) was used. Cultured islets were transferred into ice-cold DPBS (Gibco® by Life Technologies) and centrifuged for 5 minutes at 2,000 *g* and 4°C. After centrifugation, supernatant was discarded and replaced by 350 µl RLT lysis buffer. For homogenization, islets were placed for 10 minutes on the cell disrupter. RNA extraction was either performed directly after homogenization or samples were stored at -80°C until further procedure. In the following step, 350 µl of 70% Ethanol was added to the cell suspension and extraction was performed according to the manufacturer's instructions. To eliminate genomic DNA contamination, on-column DNAse digestion was performed using the RNase-Free DNase Set (Qiagen). The RNA concentration and quality were measured using BioMate™ 3 (Thermo Fisher Scientific).

4.4.2 RNA extraction from human islets

Isolation of human RNA was performed using the single-step acid guanidinium thiocyanate-phenol-chloroform extraction method [133]. Before extraction, islets were washed with ice-cold DPBS. After 2 minutes centrifugation at 2,000 *g*, the supernatant was discarded and replaced by 1 ml peqGOLD TriFast™ (VWR International GmbH) and incubated for 15 minutes on a horizontal shaker at RT. For RNA separation from other cellular components, chloroform was added to the mixture, shaken for 15 seconds and incubated for 5 minutes at RT before the sample was centrifuged at maximal speed for 15 minutes at 4°C. The upper, aqueous phase, containing the RNA, was transferred into a new tube and mixed with GlycoBlue™ (Ambion® by life technologies™) to visualize the RNA pellet. For the precipitation of RNA, isopropanol was added, shaken for 15 seconds and incubated for 15 minutes at RT before the sample was centrifuged at full speed for 15 minutes at 4°C. The pellet was washed twice with 70% ethanol and dried afterward for 5 minutes at 60°C or at RT. Pellet was dissolved in RNase free water before RNA concentration and quality were measured using BioMate™ 3 (Thermo Fisher Scientific).

4.4.3 Quantitative real-time PCR

To measure the mRNA level, quantitative real-time PCR was performed. 0.3 µg – 1 µg RNA was transcribed into complementary DNA (cDNA) by using SuperScript® II Reverse Transcriptase (Invitrogen by Thermo Fisher Scientific) according to the manufacturer's instructions. The cDNA was stored at -20°C or directly used for quantitative PCR.

Quantitative PCR was performed using the reaction mix FastStart Essential Green Master (Roche).

The reaction solution was mixed per sample as follows:

5 µl FastStart Essential DNA Green Master (Mix I)

2 µl Primer-Mix (reverse Primer and forward primer, conc. 0.3 µM each)

1-2 µl cDNA (prediluted 1:5 or undiluted)

ad 10 µl H_2O (PCR Grade, Mix II)

Primers were manufactured by Eurogentec (Belgium) if not indicated otherwise. The following primer pairs were used:

Gene	Species	Primer sequence
Hprt	Mouse	Forward 5´-GCT GGT GAA AAG GAC CTC T Reverse 5´-CAC AGG ACT AGA ACA CCT GC
Aldh1l2	Mouse	Forward 5´-ACC AGC CGG GTT TAT TTC AAA Reverse 5´-ACT CCC ACT ACT CGG TGG C
HPRT	Human	Forward 5´-TGA CAC TGG CAA AAC AAT GCA Reverse 5´-GGT CCT TTT CAC CAG CAA GCT
B2M (Eurofins)	Human	Forward 5´-GAG GCT ATC CAG CGT ACT CCA Reverse 5´-CGG CAG GCA TAC TCA TCT TTT
ALDH1L2	Human	Forward 5´-GCT CAT CTG GAA AAG CTG CT Reverse 5´-CTC TTT GGC GAG GTA CAT GT

Quantitative PCR was performed utilizing the LightCycler® Nano Device (Roche) with the LightCycler® Nano software 1.1 and the following program:

Program	
Pre-Incubation	95°C for 600 seconds
3-Step Amplification	45 cycles of 95°C to 60°C to 72°C
Melting	65°C to 95°C at 0.1°C/second

Triplicates were done for every sample. For relative quantification, one or two reference genes were used as standard. Calculation of $2^{-\Delta CT}$ was performed by the comparative C_T method, in which ΔC_T is defined as C_T gene of interest $-C_T$ reference gene. Values are shown normalized to the treatment control [134, 135].

4.4.4 Western blot

Protein quantification in human and murine pancreatic islets was performed by Western blot technique. To have a nearly equal amount of protein in each sample, for every experiment

the same number of islets were used in each condition. Islets were washed in ice-cold PBS and centrifuged at 2,000 *g* for 5 minutes at 4°C. Supernatant was discarded and islets were lysed in lysis buffer containing the following components:

1x Laemmli sample buffer (4x, Bio-Rad)
1x cocktail of protease inhibitors (25x, Roche)
10 mM NaF (Sigma-Aldrich)
1% 2-Mercaptoethanol (Roth)
in dH_2O

For cell lysis, lysates were placed on the cell disrupter for 10 minutes at 4°C. Thereafter, lysates were heated for 5 minutes at 95°C and directly placed on ice for further procedure or stored at -80°C and heated up again before starting the WB. To remove cell debris, lysates were centrifuged at full speed for 10 minutes at 4°C and supernatant was transferred into a new tube. Polypeptides were separated according to their molecular weight using the Mini-PROTEAN® Tetra Electrophoresis System (Bio-Rad). Samples were separated using the 4–15% Mini Protean TGX Stain-free Protein Gels (Bio-Rad). Molecular weight was indicated via the Precision Plus Protein™ Dual Color Standards (Bio-Rad) containing ten pre-stained recombinant proteins with defined molecular weight. Separation was done at 160-210 V for 30-60 minutes in 1x Tris/Glycine running buffer (10x, Bio-Rad) using the Power PAC Basic System (Bio-Rad). Thereafter polypeptides were transferred to a PVDF membrane using the Trans-Blot Turbo Transfer System (Bio-Rad). Western Blotting was performed for 7 minutes with the mixed molecular weight program. To block unspecific bindings, membranes were incubated with a blocking solution containing 5% BSA (AppliChem) or 5% non-fat dried milk (Roth) diluted in PBS + 0.1% Tween-20 (PBS-T, AppliChem) for 60 minutes at RT. Incubation of the primary antibody was performed overnight at 4°C diluted in blocking solution. Membranes were washed three times for 15 minutes in PBS-T and incubated with the appropriate secondary antibody conjugated with horseradish peroxidase (HRP) for 60 minutes at RT. The secondary antibody was also diluted in blocking solution. For an equal treatment of the membranes, all incubation steps were performed under agitation. After three additional washing steps in PBS-T, chemiluminescence detection was performed using Clarity™ Western ECL substrate (Bio-Rad) according to the manufacturer's instructions and imaged by ChemiDoc™ XRS (BioRad) or ChemiDoc™ MP Imaging System (Bio-Rad). Quantification of protein bands was done using Fiji (ImageJ) image analysis software.

Primary Antibody	Dilution
Rabbit anti-ALDH1L2 ThermoFisher Scientific #PA5-48161	1:1,000
Rabbit anti-COX IV Cell Signaling #4844	1:1,000
Mouse anti- β–Actin Sigma-Aldrich #A5441	1:20,000

Secondary Antibody	Dilution
Donkey anti-rabbit HRP Jackson ImmunoResearch #711-035-152	1:5,000
Donkey anti-mouse HRP Jackson ImmunoResearch #715-035-150	1:5,000

4.4.5 Separation of mitochondrial and cytosolic fraction

To study the localization of proteins within the cell, mitochondria were isolated from the cytosolic fraction. Therefore, islets were transferred into ice-cold PBS and centrifuged for 5 minutes at 2,000 *g*. The supernatant was discarded and isolation of cytosolic and mitochondrial fraction was performed using the Mitochondrial/Cytosol Fractionation Kit (Abcam). Separation was carried out according to the manufacturer's instructions. Lysates were stored at -80°C or directly used for Western blot (4.4.4).

4.5 Next-Generation Sequencing

4.5.1 RNA sequencing

To investigate downstream target genes of DXO in pancreatic islets, whole transcriptome analysis was performed via RNA sequencing at the Functional Genomics Center Zurich (FGCZ, ETH in Zurich, Switzerland). Following the treatment of pancreatic islets, total RNA was isolated (4.4.1) and stored at -80°C until further procedure. RNA was sent to the Functional Genomics Center Zurich (FGCZ, ETH in Zurich, Switzerland) were quality control and transcriptome analysis was performed. The quality of the RNA was determined with a Qubit® (2.0) Fluorometer (Life Technologies, California, USA) and a TapeStation 4200 RNA Screen Tape (Agilent, Waldbronn, Germany). With RIN values > 9.1 a Poly-A enrichment strategy for generating sequencing libraries could be accomplished. For the succeeding steps, the TruSeq mRNA Stranded Library Prep Kit (Illumina, Inc, California,

USA) was used. After Poly-A selection using Oligo-dT beads, the mRNA was reverse-transcribed into cDNA. The cDNA samples were fragmented, end-repaired and polyadenylated before ligation of TruSeq UD Indices (IDT, Coralville, Iowa, USA). Fragments were selectively amplified with PCR. The quality and quantity of the enriched libraries were validated using Qubit® (1.0) Fluorometer and TapeStation 4200 D1000 Screen Tape (Agilent, Waldbronn, Germany). For cluster generation, the TruSeq SR Cluster Kit HS4000 (Illumina, Inc, California, USA) was used. Therefore, 10 pM of pooled normalized libraries were used on the cBOT System. The library sequencing was performed on the HiSeq4000 with 125 cycles single-read using the TruSeq SBS Kit HS4000 (Illumina, Inc, California, USA). RNA sequencing reads were aligned to the mouse GRCm38 reference genome using the STAR aligner [136]. Gene expression values were computed with the function featureCounts from the R package Rsubread [137]. Differential expression was computed using the generalized linear model implemented in the Bioconductor package edgeR [138]. Expression values were indicated as the metric “fragments per kilobase of transcript per million mapped reads” (FPKM). The Sushi framework was used to run the data analyses [139]. Genes were only considered expressed if the FPKM value was above > 1. For further analysis, the cutoff for the log2 Fold Change (log2 FC) was set above 1 or below -1. False discovery rate (FDR) less than 0.05 was considered significant.

4.6 Manipulation of primary islet cells

4.6.1 Generation of adenovirus carrying the *hALDH1L2* construct

For efficient overexpression of ALDH1L2 in primary islet cells, cells had to be infected with adenoviruses. Adenoviruses were purchased from ViraQuest Inc. (North Liberty, Iowa, USA). This replication-incompetent adenovirus carries the reporter gene in the E3 region of the backbone. Therefore, the coding sequence of human *ALDH1L2* (*hALDH1L2*) was generated and supplied by Integrated DNA Technologies, Inc (IDT, Coralville, Iowa, USA). The cDNA sequence was dissolved according to the manufacturer's instructions and cloned into the shuttle vector VQAd5CMVK-NpA provided by ViraQuest Inc. Therefore, the shuttle vector was linearized using *EcoRV-HF* (New England Biolabs®, #R3195) followed by the dephosphorylation of the vector to prevent recirculation. Dephosphorylation was performed using shrimp alkaline phosphatase (New England BioLabs®). To check the linearization, gel electrophoresis was performed and the linearized vector was isolated by gel purification using the GenElute™ Extraction Kit (Sigma-Aldrich) according to the manufacturer's instructions. To create the new DNA construct, ligation of *hALDH1L2* cDNA and purified

linearized VQAd5CMVK-NpA shuttle vector was carried out using the Quick Ligation™ Kit (New England BioLabs®) with the following mix:

Quick T4 Ligase	3.5 µl
Quick Ligation Buffer	35 µl
Linear dephos. pUC57 vector	50 ng
cDNA hALDH1L2	153.45 ng
dH_2O	ad 70µl

The reaction mix was gently pipetted up and down and incubated for 25 minutes at RT. Following ligation, the hALDH1L2-VQAd5CMVK-NpA construct was subcloned into DH5α competent cells (Invitrogen). 5 ng of the ligation mix was used for the transformation, which was carried out according to the manufacturer's instructions. To check if a colony carries the hALDH1L2-VQAd5CMVK-NpA construct, colony-PCR was performed. Therefore, the following PCR mix was used:

Master Mix Components	**Volume**
JumpStart™ REDTaq® ReadyMix™ Reaction Mix (Sigma-Aldrich)	175 µl
Nuclease Free Water	172.2 µl
Primer forward (100 µM)	1.4 µl
Primer reverse (100 µM)	1.4 µl

The PCRs were carried out in a Professional Trio Thermocycler (Biometra). For the construct specific primers and a specific PCR program were used:

hALDH1L2-VQAd5CMVK-NpA		Primer	Product Size
	Forward	5´-AGC TCG TTT AGT GAA CCG TCA	728 bp
	Reverse	5´-TCT GGC TGG GGT ATA CGA GG	

hALDH1L2- VQAd5CMVK-NpA Program
94°C for 2 minutes
35 x 94°C for 30 seconds
54.5°C for 30 seconds
72°C for 2 minutes
72°C for 5 minutes
4°C for ∞

PCR products were separated according to their size as described in 4.1.2.2.
Colonies carrying the hALDH1L2-pUC57 construct were used for overnight cultures and plasmid DNA was isolated for adenovirus production using the NZYMaxiprep (NZYtech) performed according to the manufacturer's instructions. For further procedure, the plasmid DNA of the hALDH1L2-VQAd5CMVK-NpA construct was confirmed by sanger sequencing at the Biologisch-Medizinisches Forschungszentrum at the Heinrich Heine University, Duesseldorf. The purified shuttle-vector ligated with the hALDH1L2 cDNA was sent to ViraQuest Inc (North Liberty, Iowa, USA) were virus particles were generated and titrated commercially as previously described [140]. Additionally, a control adenovirus was purchased from ViraQuest Inc (North Liberty, Iowa, USA) with an empty backbone. The viral construct allows strong protein overexpression as well as detection of infected cells, due to an upstream cytomegalovirus (CMV) promoter and an eGFP (enhanced green fluorescent protein) reporter gene. The eGFP encoding gene is under control of the RSV (Robus Sarcoma Virus)-promoter. In the control adenovirus, the eGFP encoding gene is under the control of the CMV promoter. Particle concentration was about 1.1×10^{12} particles/ml.

4.6.2 Formation of pseudo-islets by hanging drop technology

Infection of murine pancreatic islets and formation of pseudo-islets were performed in the S2 laboratory at the German Diabetes Center in Duesseldorf. For efficient overexpression of ALDH1L2 in pancreatic islets, single islet cells had to be infected by adenoviruses followed by the formation of pseudo-islets. Hanging drop technology, which was reported by Cavallari *et al.* 2007 was performed for the generation of pseudo-islets with few changes [141]. One day after isolation, mouse pancreatic islets were used for transduction. Therefore, islets were transferred into 10 ml pre-warmed DPBS and centrifuged for 3 minutes at 900 rpm. The supernatant was discarded and islets were washed again two times with 5 ml DPBS to remove islet medium and ensure an efficient single-cell preparation. Islets were dispensed in single cells with 0.05% Trypsin-EDTA (Gibco® by Life Technologies) for 8 minutes at 37°C and 5% CO_2. After 3, 5, and 8 minutes islets were pipetted up and down to ensure a homogeneous single-cell suspension. To stop trypsinization, 2 ml islet medium was added to the suspension and centrifuged for 6 minutes at 900 rpm. Pellet was resuspended in 2-4 ml islet medium and cells were counted using the Fast-Read 102® Counting chambers (Biosigma). Cell viability was assessed using Trypan Blue Solution (0.4%, Gibco® by Life Technologies). For transduction, single-cell suspension was incubated with adenovirus at indicated concentrations for 6 hours in a humidified incubator at 37°C and 5% CO_2. After transduction, single cells were centrifuged at 900 rpm for 6 minutes and supernatant, containing the virus particles, was discarded. For

pseudo-islet generation, islet medium was added to the single cells at the density of 1500 cells/30 µl islet medium. 30 µl drops were placed on the lid of a petri dish, inverted and placed on the petri dish, which was filled with 25 ml DPBS. For pseudo-islet aggregate formation, hanging drop cultures were incubated for 3 days in a humidified incubator at 37°C and 5% CO_2. The formation of pseudoislets as well as the efficiency of transduction were checked using the Zoe™ fluorescent cell imager (Bio-Rad). Pseudo-islets were picked into fresh islet medium and washed up to 6 times in fresh islet medium to remove remaining adenovirus in the medium. To perform functional assays out of the S2 area, medium was checked for remaining adenovirus. Therefore, PCR was performed with the medium of the islets as described in 4.1.2.2 For the PCR specific primers and a specific PCR program were used:

Adenovirus Backbone	Primer	Product Size
Forward	5´-CGA AGA CGG CGT AGT TTC GC	ca. 500 bp
Reverse	5´-GTA TCC CTG CCG CAT GGC	

Adenovirus Backbone Program
94°C for 3 minutes
35 x 94°C for 30 seconds
61°C for 60 seconds
72°C for 60 seconds
72°C for 60 seconds
4°C for ∞

PCR products were separated according to their size as described in 4.1.2.2.
If no adenovirus were detected, functional assays were performed on the same day or on the next day. To guarantee excess of substrate for viability assay, culture medium was supplemented with 10 mM folic acid (Sigma-Aldrich). KRH buffer during insulin secretion assay was supplemented with 1 mM serine (SERVA).

4.7 Liquid chromatography-tandem mass spectrometry (LC-MS/MS)

Mice plasma samples including the stable labelled deuterated internal standards d3-dextromethorphan (d3-DXM) and d3-dextrorphan (d3-DXO) (Cerilliant Corporation, Sigma-Aldrich) were analyzed by ultra-pressure liquid chromatography coupled to tandem mass spectrometry (UPLC-MS/MS). The UPLC-I Class and the tandem mass spectrometer Xevo-TQS (Waters) were used for the analysis. Both compounds, DXM as well as DXO, were

separated on an Aquity UPLC BEH C18 column (1.7µm, 100mm×2.1mm, Waters). The column oven temperature was 40°C, the flow rate 0.4 ml/min and the injection volume was 2 µl. The first mobile phase A consists of 5 mM ammonium acetate including 0.05% formic acid while the second mobile phase B consists of acetonitrile. An isocratic elution mode (A:B, 65:35) was applied. Tandem mass spectrometric analysis was performed in positive electrospray ionization mode. Multiple reaction monitoring (MRM) mode with following mass transitions were applied *m/z*: 272 > 171 (DXM), 275 > 171 (d3-DXM), 258 > 157 (DXO) and 261 > 157 (d3-DXO). Collision energy of 40 V and 30 V were used for fragmentation of DXM/d3-DXM and DXO/d3-DXO. The software MassLynx V4.1 (Waters) was used for the acquisition and processing of data. Quantification was performed by the software TargetLynx (Waters).

4.8 Statistical Analysis

Statistical significance was evaluated for all data using Prism 6 software (GraphPad) or Excel (Microsoft Corporation). According to the number of conditions within one experiment, different statistical tests were performed. *P* values were determined as indicated in the figure legends. Differences with *P* values < 0.05 were considered as significant. To highlight only the relevant effects in insulin secretion assays, statistical significance was not indicated between 2 mM and 20 mM conditions. Note that all effects between high (20 mM) and low (2 mM) glucose conditions in insulin secretion assays within this thesis are significant, if not indicated otherwise in the figure legends. Data were presented as mean ± standard error of the mean (SEM) in most cases, with the exception of the glucose tolerance test in which data were presented as mean ± standard deviation (SD). Normal distribution was not tested. Within the viability assays, single values were excluded from the analysis if determined as a significant outlier (*P* value = 0.05) by Grubbs' test for outliers.

4.9 Personal contributions

J. Mrugala performed and designed most of the experiments. J. Mrugala was supervised by E. Lammert.

J. Marquardt, A. Welters and S. Otter started the research on the NMDA receptor as well as DXO. A. Welters and S. Otter have handed over the project to J. Mrugala.

D. Gebel designed and cloned the ALDH1L2 vector for adenoviral overexpression. J. Mrugala established the overexpression experiments with pseudo-islet generation.

J. Mrugala and A. Pelligra performed the adenoviral overexpression experiments at the German Diabetes Center in Düsseldorf. A. Pelligra started her PhD in 2018 to further evaluate the function of ALDH1L2 and performed in this regard some insulin secretion assays (as indicated in the figure legends).

O. Scholz performed the GTT with the help of J. Mrugala.

Within the collaboration, D. Herebian (Department of General Pediatrics, Neonatology and Pediatric Cardiology, University Children's Hospital Düsseldorf, Düsseldorf, Germany) measured the DXM concentrations in the plasma samples of *db*/*db* mice and wrote the experimental procedure part "Liquid chromatography-tandem mass spectrometry (LC-MS/MS)".

The Functional Genomics Center in Zurich (FGCZ, ETH in Zurich, Switzerland) performed the RNA sequencing, made the statistical analysis and wrote the experimental procedure part "RNA sequencing". Parts of the protocol were already published [142].

Y.Koh created the illustrations. The ideas and the design were given by J. Mrugala and A. Pelligra.

5 Results

5.1 Role of DXO in pancreatic islet cell survival

Previous data from our lab, published by Marquard et al. (2015), provided the first evidence that the clinically relevant over-the-counter drug DXM and its active metabolite DXO protect against pancreatic islet cell death *in vitro* and *in vivo* [114]. In *db*/*db* mice, a rodent model for T2DM, a slower progression of hyperglycemia was measured after the administration of DXM via the drinking water. Additionally, the same mice showed reduced apoptosis in islet cells, indicating a protective effect of DXM under diabetogenic conditions [114]. Furthermore, *in vitro* studies showed that the treatment of mouse and human isolated islets with 10 µM DXO protects against cytokine-induced cell death [114]. Based on those findings, our aim was to further examine the protective effect and reveal the underlying molecular mechanisms and side effects of DXM/DXO on pancreatic islets.

5.1.1 DXO protects pancreatic islets from cytokine-induced DNA damage

In order to validate the protective effect of DXO on pancreatic islets during inflammation, additional *in vitro* studies were performed. Therefore, isolated mouse islets were treated with a mixture of cytokines (TNF-α, IFN-γ, and IL-1β) in combination with or without 10 µM DXO (Fig. 3). Detection of DNA strand breaks, which are characteristic of apoptotic cells, by TUNEL-staining showed a significant increase of cell death when islets were treated for 24 hours with cytokines compared to control ($p < 0.0007$). Strikingly, a reduction of DNA strand breaks was detected when cytokine treatment was combined with 10 µM DXO compared to cytokine treatment alone ($p < 0.0110$). These results strongly indicate that DXO protects pancreatic islets against cytokine-induced DNA fragmentation.

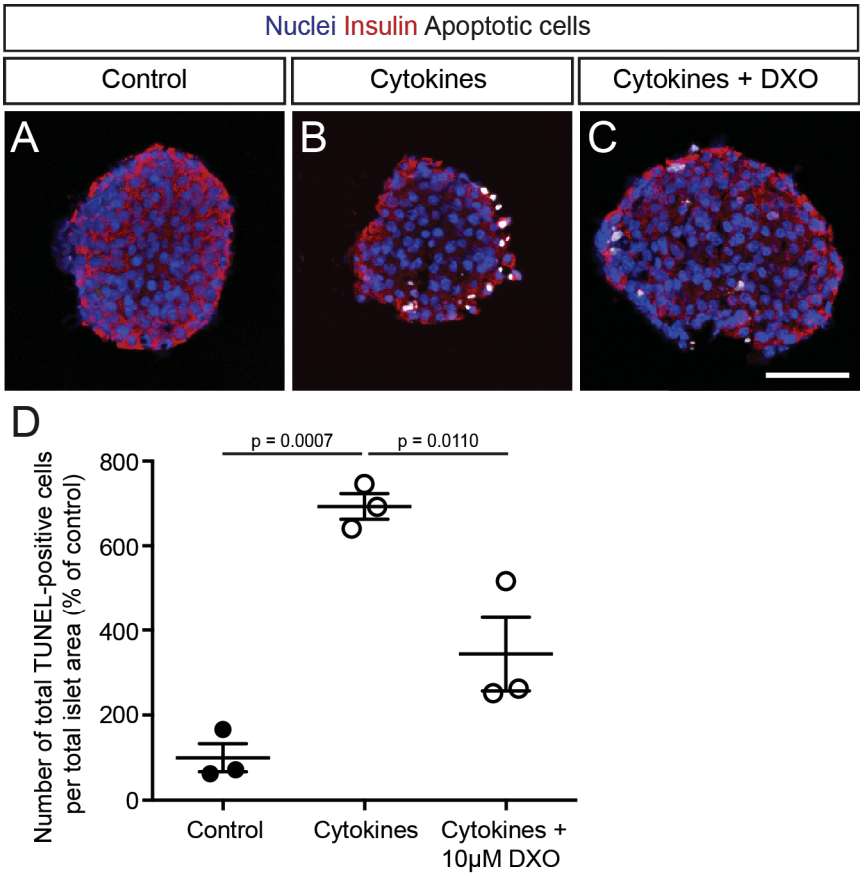

Figure 3: DXO protects pancreatic islet cells from DNA damage induced by proinflammatory cytokines. **A-C**, Representative LSM images of mouse islets either untreated or treated with a mixture of cytokines in combination with or without 10 µM DXO. Scale bar: 50 µm. **D**, Quantification of apoptosis was performed by counting the number of TUNEL-positive cells normalized to total islet area (n = 3 with n ≥ 47 islets in total). Data are shown as mean ± SEM and calculated as percentage of control. Statistical significance was determined using one-way ANOVA followed by Tukey's multiple comparison test.

5.1.2 Lower concentration of DXO even protects pancreatic islet cells from cytokine-induced cell death

To avoid any side effects based on a high concentration of DXO, we addressed the question whether a low concentration of DXO already protects pancreatic islets against inflammation. Therefore, we performed live-cell imaging experiments to examine whether 1 µM DXO (Fig. 4 A-C) and 5 µM DXO (Fig. 4 D-F) protects mouse and human pancreatic islet cells against inflammation. Our analysis revealed that lower concentrations of DXO already protect mouse (Fig. 4 G) and human (Fig. 4 H) pancreatic islet cells from cytokine-mediated cell death.

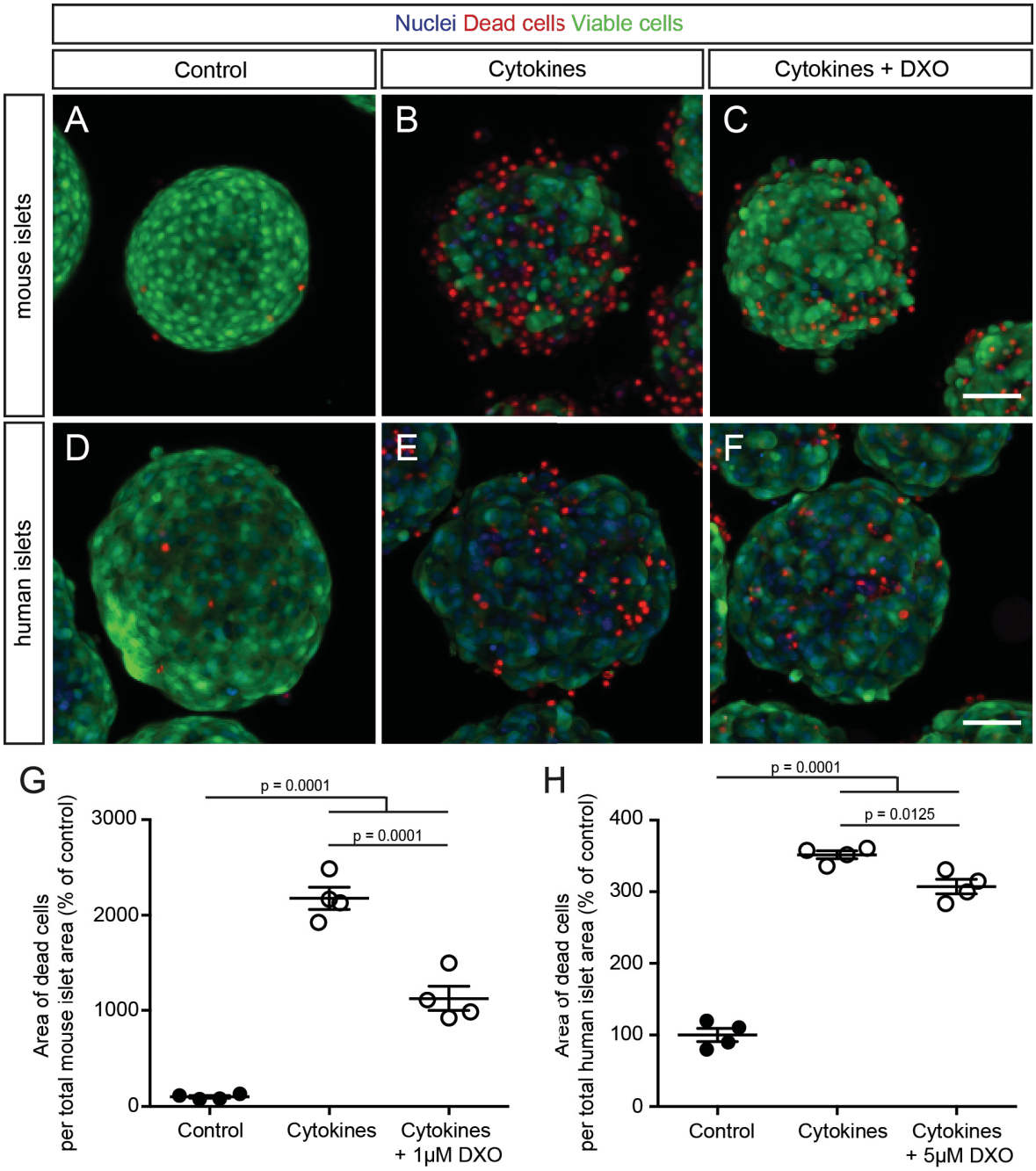

Figure 4: Treatment of mouse and human islets with lower concentrations of DXO protects islets from cytokine-induced cell death *in vitro*. A-C, Representative LSM images of mouse islets either untreated or treated with a mixture of cytokines in combination with or without 1 µM DXO. Scale bar: 50 µm. **D-F**, Representative LSM images of human pancreatic islets either untreated or treated with a mixture of cytokines in combination with or without 5 µM DXO. Scale bar: 50 µm. **G**, Calculation of cell death in mouse pancreatic islets. Calculated area of dead cells normalized to total nuclei area (n = 4 with n ≥ 56 islets in total). **H**, Calculation of cell death in human pancreatic islets. Calculated area of dead cells normalized to total nuclei area (n = 4 with n ≥ 57 islets in total). Human islet donor: 66-year-old male; BMI, 27.2 kg/m². Both quantifications are shown as percentage of control. Data are shown as mean ± SEM and statistical significance was determined using one-way ANOVA followed by Tukey's multiple comparison test.

5.1.3 Genetic deletion of the NMDA receptor is not sufficient but required for the protective effect of DXO

Various studies have shown that DXO is a potent antagonist of the NMDA-receptor [123, 143]. Additionally, it could be shown that antagonizing the NMDA receptor pharmacologically has protective effects against glucotoxicity and inflammatory factors [114, 115]. Furthermore, studies in MIN6 cells indicate that the sustained activation of the NMDA receptor is a mediator for apoptotic signaling via the mitochondrial apoptotic pathway [117]. Therefore, we aimed to investigate whether the deletion of the NMDA-receptor protects islets from cytokine-induced cell death.

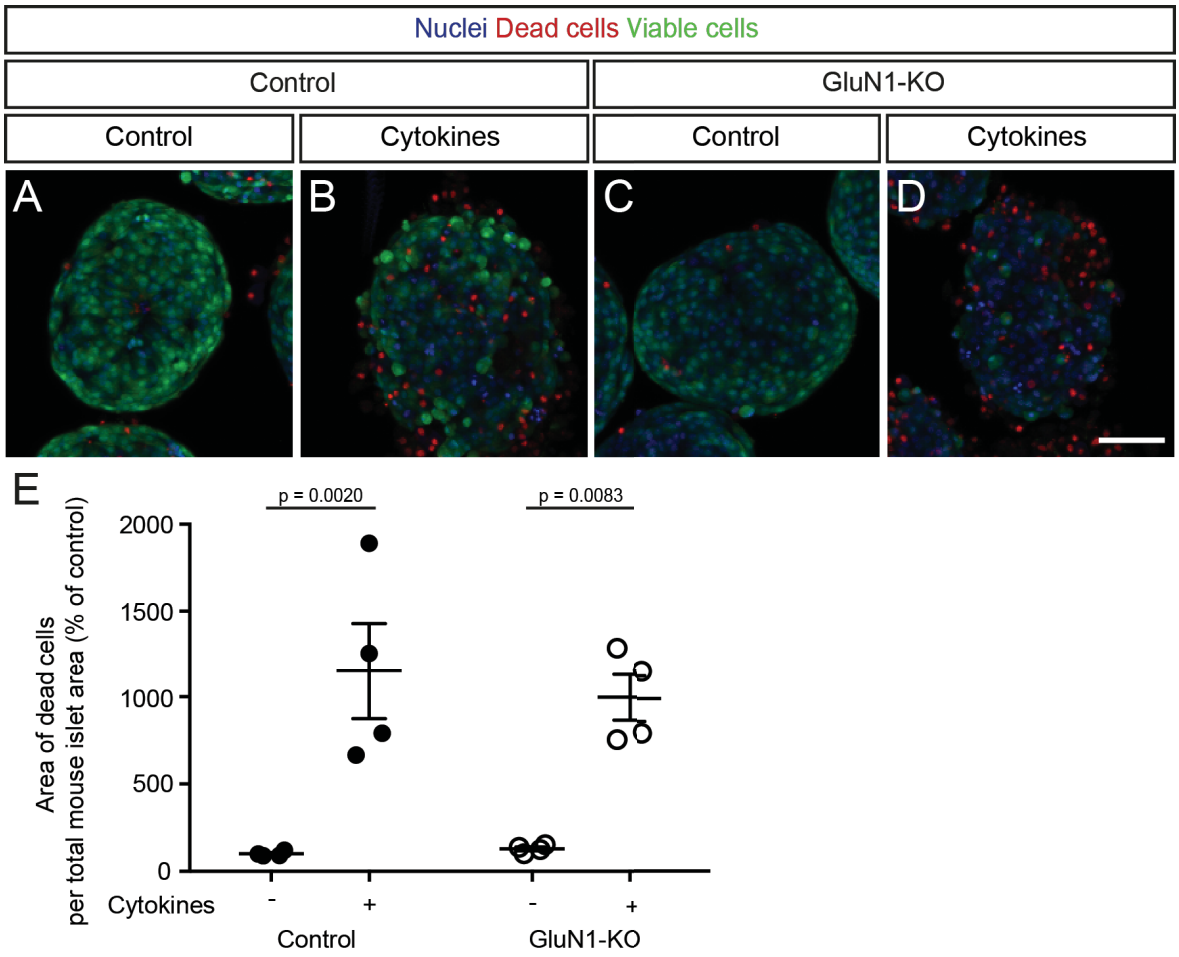

Figure 5: Deletion of the functional NMDA receptor is not sufficient to protect islets from cytokine-induced cell death. A-D, Representative LSM images of isolated mouse islets from GluN1-KO mice and control mice treated with (B, D) or without (A, C) a combination of cytokines. Scale bar: 50 µm. **E**, Calculation of cell death in pancreatic islets. Calculated area of dead cells normalized to total nuclei area (n = 4 with n ≥ 53 islets in total). Quantification is shown as percentage of control. Data are shown as mean ± SEM and the statistical difference was determined using two-way ANOVA followed by Tukey's multiple comparison test.

To examine this hypothesis, we treated pancreatic islets from GluN1-KO (*Pdx1*-Cre x *Grin1*$^{loxP/loxP}$) and control (*Pdx1*-Cre) mice with and without a mixture of cytokines to

see if the deletion of the functional NMDA receptor has beneficial effects (Fig. 5). Upon treatment, no difference in cell death was detected, which indicates that the exclusive deletion of the NMDA-receptor subunit *GluN1* is not sufficient to protect islets from cytokine-induced cell death.

We further determined if DXO implements the protective effect independent of the NMDA receptor. Therefore, *GluN1*-deficient islets were incubated with cytokines in combination with DXO (Fig. 6). Interestingly, in contrast to wild-type islets (Fig. 4 G), the treatment of GluN1-KO islets with cytokines in combination with 1 µM DXO do not protect islets against cytokines, indicating that the NMDA receptor is required for the protective effect. We conclude that the NMDA receptor is not sufficient for the protection of pancreatic islets against cytokines but the receptor is required for the protective effect of DXO.

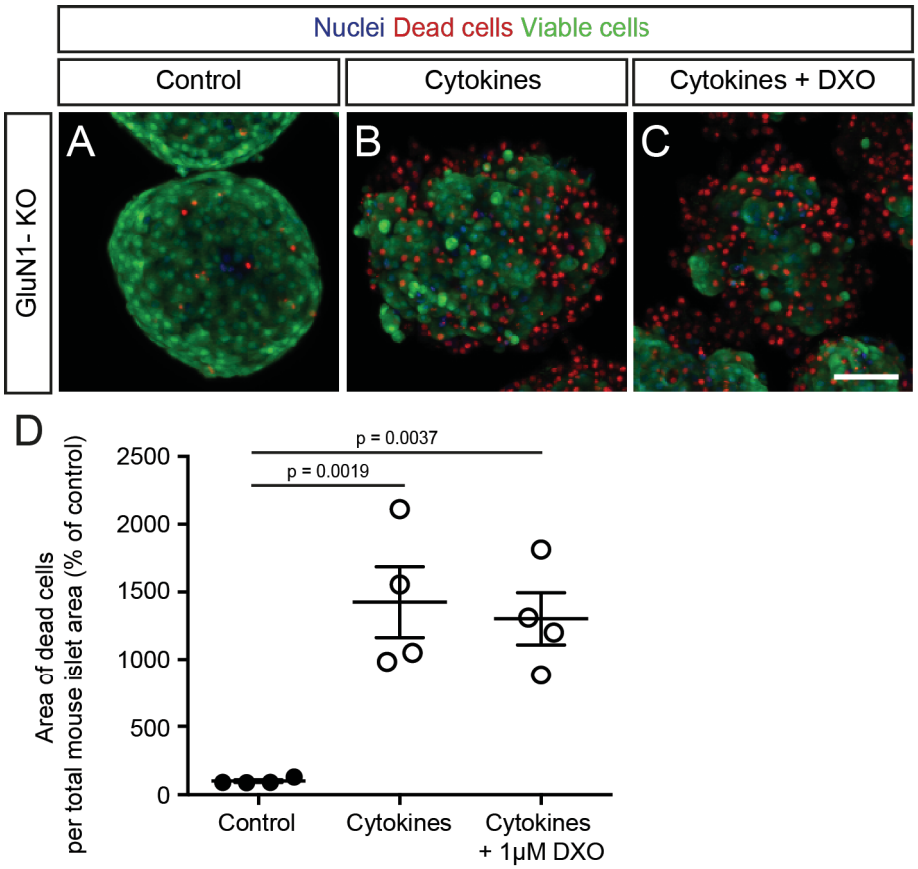

Figure 6: The NMDA receptor is required for the protective effect of DXO. A-C, Representative LSM images of isolated mouse islets from GluN1-KO mice either untreated or treated with a mixture of cytokines together with or without 1 µM DXO. Scale bar: 50 µm. **D**, Calculation of cell death in GluN1-KO pancreatic islets. Calculated area of dead cells normalized to total nuclei area (n = 4 with n ≥ 46 islets in total). Quantification is shown as percentage of control. Data are shown as mean ± SEM and statistical significance was determined using one-way ANOVA followed by Tukey's multiple comparison test.

5.2 Effects of the insulin secretagogue DXO on islet function after long-term pre-treatment

Previous experiments from our lab showed that the clinically relevant agent DXO acts as an insulin secretagogue directly on β-cells to modulate β-cell function [114]. It was speculated that insulin secretagogues initially improve pancreatic function, whereas prolonged daily treatment results in metabolic exhaustion [79, 107]. This argues for the use of alternative drugs that protect β-cells from exhaustion. With this study, we aimed to answer the question whether prolonged incubation of pancreatic islets with high concentrations of the insulin secretagogue DXO could have deleterious effects on islet function. Furthermore, we are giving first evidence about a possible underlying molecular mechanism for the induction of β-cell dysfunction by an insulin secretagogue (that is, DXO).

5.2.1 Long-term pre-treatment of mouse islets with a high concentration of DXO induces islet cell dysfunction *in vitro*

Based on the proposed deleterious effect of excessively stimulating insulin release from islets, we addressed the question if long-term treatment of islets with high concentrations of DXO influence islet function and insulin content. Therefore, we cultured mouse islets for 48 hours with or without either 1 µM glibenclamide (Glib) or 10 µM DXO at a stimulatory glucose concentration of 10 mM *in vitro*. To check insulin content and secretory function we performed an insulin secretion assay. The results showed that long-term incubation with the insulin secretagogues Glib as well as DXO induces islet cell dysfunction, indicated by a statistically significant decrease in the release of insulin during GSIS (Fig. 7 A, C). Furthermore, both secretagogues decreased insulin content (Fig. 7 B, D).

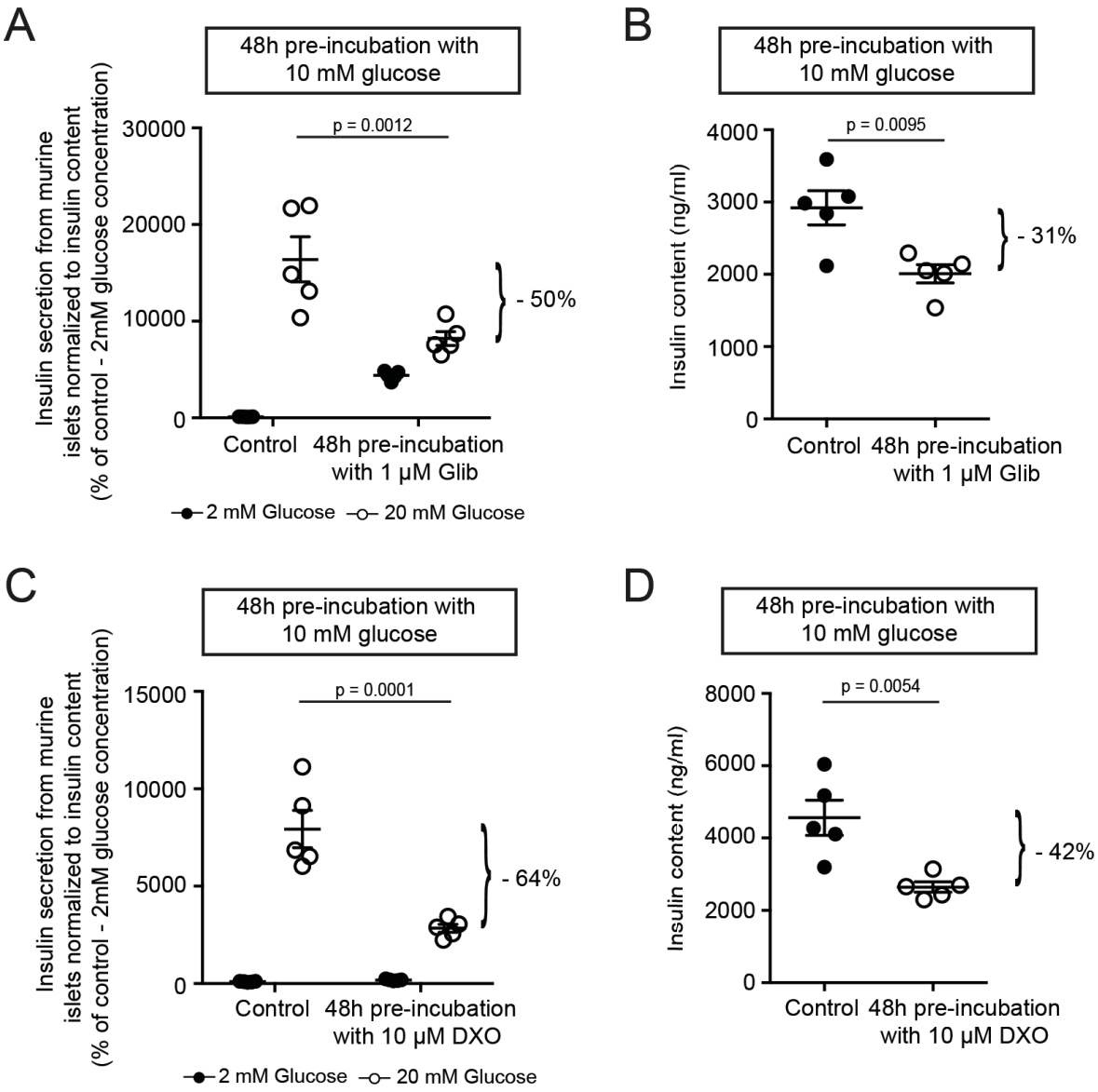

Figure 7: *In vitro* exposure of pancreatic islets to 1 µM glibenclamide (Glib) and 10 µM DXO induce islet dysfunction under continuous glucose stimulation. A, Insulin secretion was measured after 48 hours pre-incubation with 1 µM Glib and 10 mM glucose compared to glucose supplemented with the same amount of the Glib solvent DMSO (control). Insulin secretion was measured at 2 mM and 20 mM glucose (n = 5 islet batches per condition with 8 islets each). Islets pre-treated with Glib did not show a significant increase in insulin secretion between 2 mM and 20 mM glucose. **B**, Insulin content of pancreatic islets shown in A. **C**, Insulin secretion was measured after 48 hours pre-incubation with 10 µM DXO and 10 mM glucose compared to glucose alone (control). Insulin secretion was measured at 2 mM and 20 mM glucose (n = 5 islet batches per condition with 8 islets each). **D**, Insulin content of pancreatic islets shown in C. All Data are shown as mean ± SEM. *P* values in A and C were determined by two-way ANOVA followed by Tukey's multiple comparison test. Statistical differences in B and D were determined by Student's *t*-test. Angela Pelligra performed the represented experiments in panels A and B.

5.3 Long-term treatment with DXO increases the expression of genes encoding core enzymes of the mitochondrial one-carbon metabolism

To identify new candidate genes and provide insight into the underlying molecular mechanism upon DXO treatment, next-generation sequencing was performed. Using RNA sequencing we analyzed changes in transcriptional activity of pancreatic islets after stimulation with DXO. Therefore, murine pancreatic islets were treated with 10 mM glucose in combination with or without 10 µM DXO for 24 hours. A total of 22,880 genes were investigated. A comparison of gene expression levels revealed that under certain criteria (fragments per kilobase of transcript per million mapped reads (FPKM) > 1 and log2 Fold Change (log2 FC) > 1 or < -1) 698 genes (3.1% of all mapped genes) were differentially expressed (Fig. 8 A). 387 genes were downregulated, while 311 genes were upregulated after DXO treatment compared to untreated control islets. Interestingly, among these 387 downregulated genes, genes were detected which are responsible for the differentiated state of pancreatic β-cells. Particularly, β-cell marker like *Mafa* (log2 FC = -4.26), *Slc2a2* (log2 FC = -3.23), *Insulin 1* (*Ins1*, log2 FC = -3.22), and *Insulin 2* (*Ins2,* log2 FC = -2.34) were downregulated upon treatment with 10 µM DXO (Fig. 8 A).

Surprisingly, within the upregulated genes, we identified genes which code for core enzymes of the mitochondrial one-carbon metabolism. Enzymes, such as *aldehyde dehydrogenase 1 family member L2* (*Aldh1l2*, log2 FC = 3.19), *methylenetetrahydrofolate dehydrogenase (NADP$^+$ dependent) 2, methenyltetrahydrofolate cyclohydrolase* (*Mthfd2,* log2 FC = 1.58), and *serine hydroxymethyltransferase 2* (*Shmt2,* log2 FC = 1.49) were highly upregulated compared to control. In contrast, the corresponding cytosolic enzymes, such as *aldehyde dehydrogenase 1 family member L1* (*Aldh1l1,* log2 FC = 0.62), *methylenetetrahydrofolate dehydrogenase, cyclohydrolase and formyltetrahydrofolate synthetase 1* (*Mthfd1*, log2 FC = -0.72) and *serine hydroxymethyltransferase 1* (*Shmt1,* log2 FC = -0.58), did not show a strong change in their expression levels upon DXO treatment (Fig. 8 B).

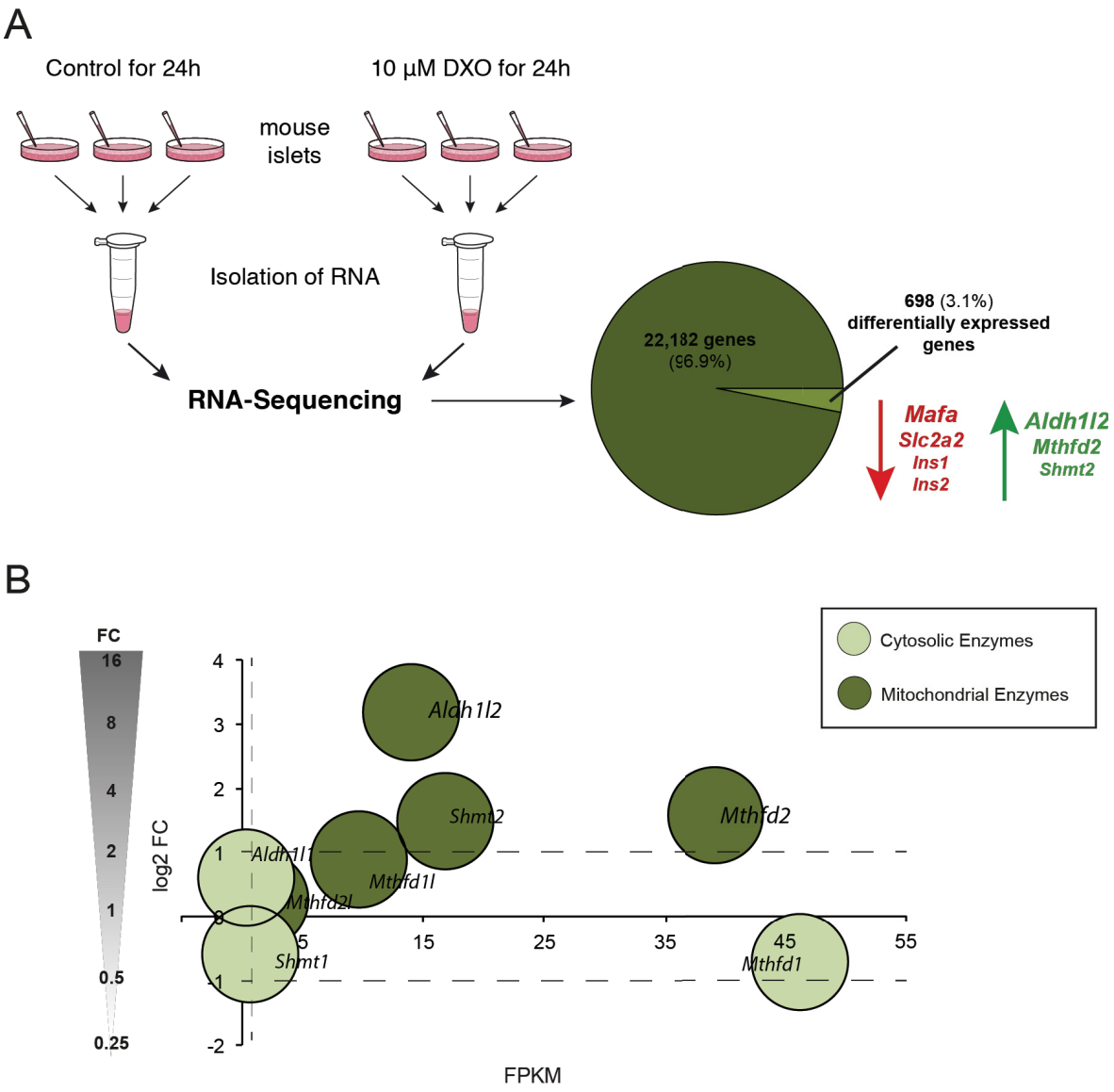

Figure 8: Genome-wide analysis reveals genes of the mitochondrial one-carbon metabolism to be differentially expressed in murine pancreatic islets upon long-term exposure to the insulin secretagogue DXO. A, Illustration of RNA sequencing setup. Differentially expressed genes were defined by log2 Fold Change (log2 FC) > 1 or < -1 and fragments per kilobase of transcript per million mapped reads (FPKM) > 1. **B**. Analysis of eight genes coding for core enzymes involved in the folate-mediated one-carbon metabolism. Horizontal axes denote FPKM value and vertical axes denote log2 FC. Dashed lines indicate the restriction criteria of the log2 FC and the FPKM. Grey arrow indicates the fold change (FC).

5.3.1 DXO does not change the expression of genes coding for enzymes of the one-carbon metabolism after short-term exposure

Previously published data showed that the short-term exposure of pancreatic islets to DXO increases GSIS [114]. To check if the short-term exposure of DXO to pancreatic islets already has deleterious effects, islets were incubated with 10 mM glucose in combination with or without 10 µM DXO for 1 hour. After incubation, GSIS and insulin content were measured. After short-term exposure to DXO, neither GSIS (Fig. 9 A) nor insulin content

(Fig. 9 B) was changed, indicating that short incubation with DXO does not induce islet cell dysfunction.

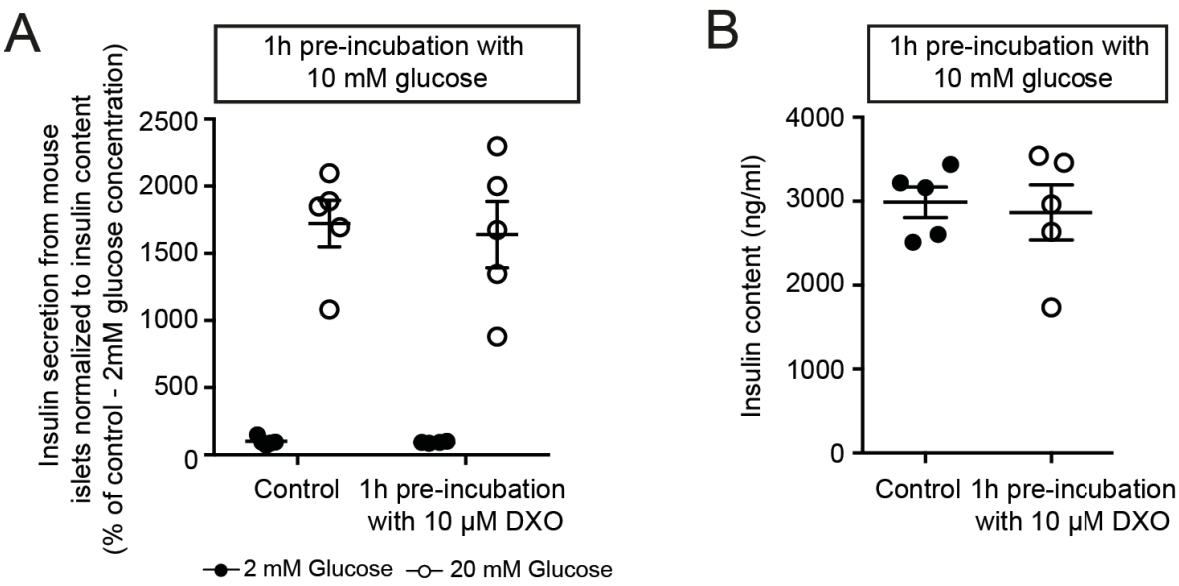

Figure 9: Short-term exposure of pancreatic islet to the insulin secretagogues DXO does not change GSIS and insulin content. A, Insulin secretion was measured after 1 hour pre-incubation with 10 mM glucose combined with or without 10 µM DXO. Insulin secretion was measured at 2 mM and 20 mM glucose (n = 4-5 islet batches per condition with 8 islets each). **B**, Insulin content of pancreatic islets shown in A. Data in A and B are shown as mean ± SEM. Statistical significance in A was determined by two-way ANOVA followed by Tukey's multiple comparison test. Statistical significance in B was determined by Student's *t*-test.

Next, we addressed the question whether genes, coding for enzymes of the folate-mediated one-carbon metabolism, are differentially expressed upon short-term exposure. Therefore, we performed an additional transcriptome analysis. RNA sequencing revealed that only 0.5% of all analyzed genes were differentially expressed (105 genes of 22,880 genes in total; FPKM > 1 and log2 FC > 1 or < -1) after 1 hour DXO treatment compared to control (Fig. 10 A). Interestingly, none of the genes, coding for the core enzymes of the folate-mediated one-carbon metabolism, were affected upon short-term exposure of DXO (Fig. 10 D).

Therefore, we addressed the question if the mitochondrial one-carbon metabolism is responsible for β-cell dysfunction that develops after long-term exposure of islets to DXO under continuous glucose stimulation. To further analyze the biological relevance of this pathway, we focused during the further study on the mitochondrial localized enzyme ALDH1L2, because this gene showed the strongest increase upon DXO long-term treatment compared to control.

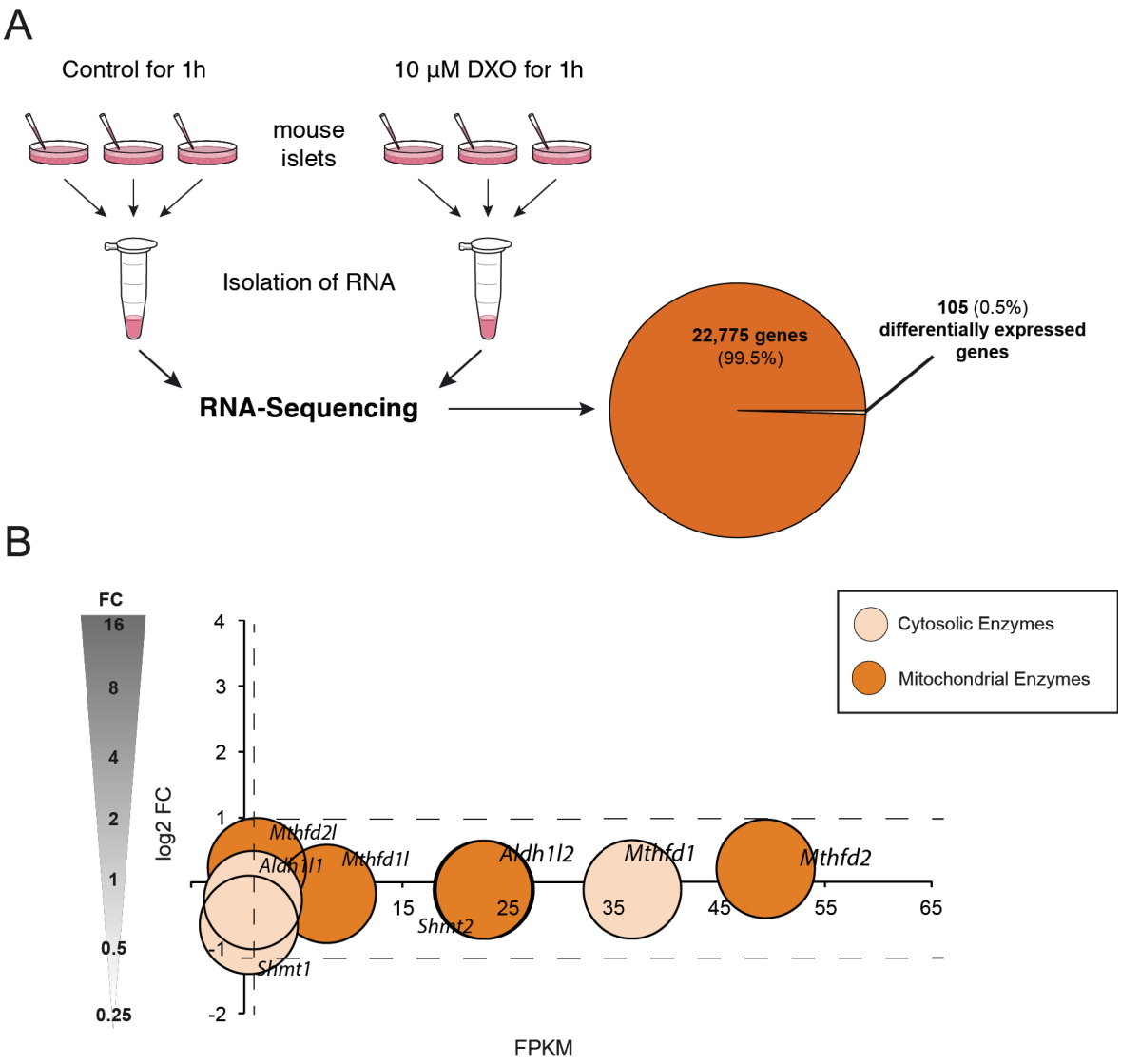

Figure 10: Short-term exposure of pancreatic islet to the insulin secretagogue DXO does not change the expression of core enzymes of the mitochondrial one-carbon metabolism. A, Illustration of RNA sequencing setup. Differentially expressed genes were defined by log2 FC > 1 or < -1 and FPKM > 1. **B**. Analysis of eight genes coding for core enzymes involved in the folate-mediated one-carbon metabolism. Horizontal axes denote FPKM value and vertical axes denote log2 FC. Dashed lines indicate the restriction criteria of the log2 FC and the FPKM. Grey arrow indicates the FC.

5.3.2 DXO increases mRNA and protein level of ALDH1L2 in mouse and human pancreatic islets *in vitro*

To confirm the RNA sequencing results, we measured mRNA and protein levels in murine and human pancreatic islets. Therefore, islets were isolated and cultured in medium containing 10 mM glucose combined with or without 10 µM DXO. In mouse pancreatic islets we verified that *Aldh1l2* mRNA expression is significantly increased ($p = 0.0015$) by around 994% after stimulation of islets with 10 µM DXO for 24 hours (Fig. 11 A). Those observations were supported by measuring the protein level of ALDH1L2, showing a statistically significant increase ($p = 0.0157$) by 74% after DXO treatment (Fig. 11 B).

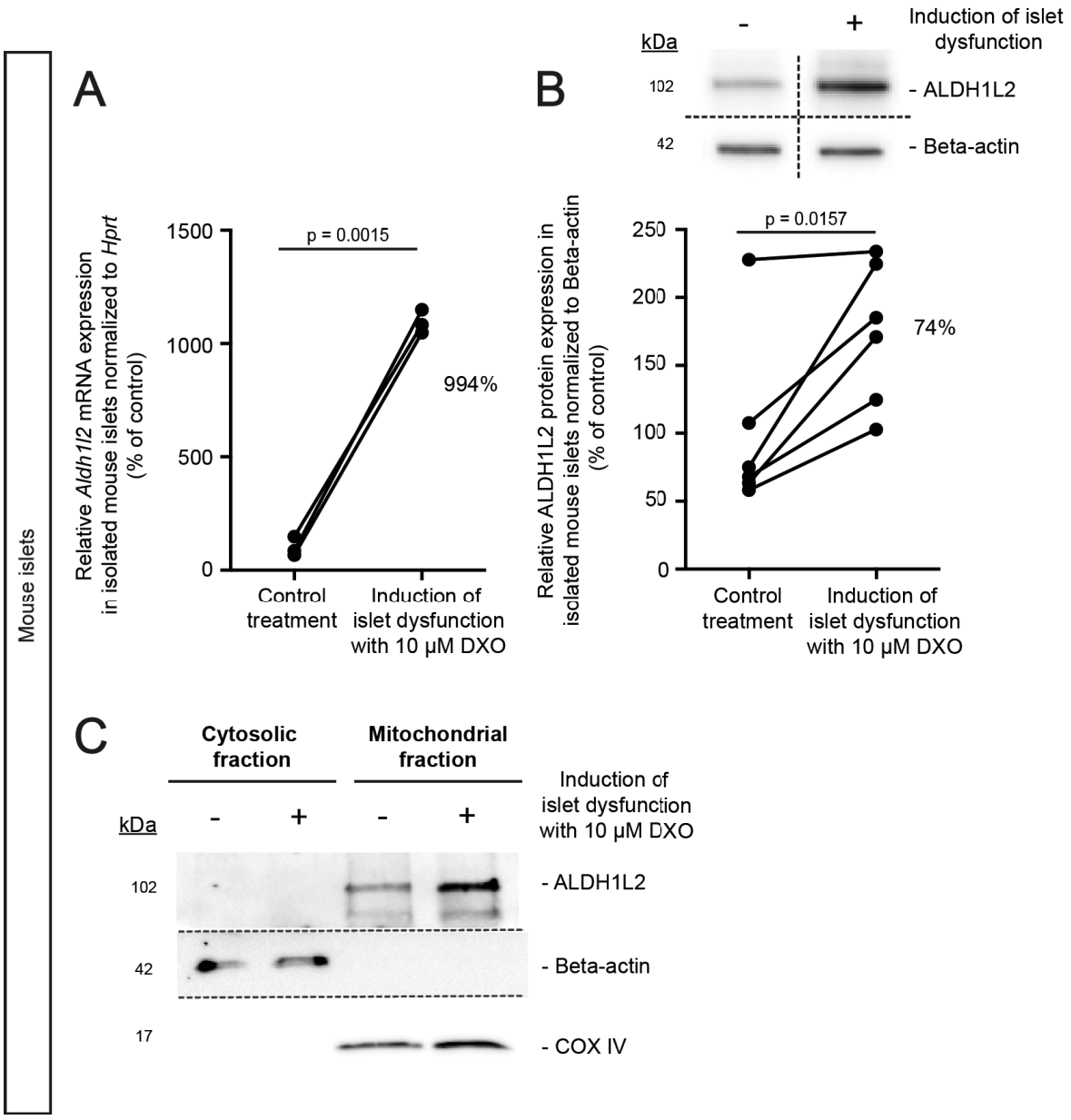

Figure 11: *In vitro* treatment of mouse pancreatic islets with 10 µM DXO increases the mitochondrial localized enzyme ALDH1L2 on mRNA and protein level. A, Quantification of relative *Aldh1l2* mRNA levels in mouse pancreatic islets treated with or without 10 µM DXO, normalized to *hypoxanthine-guanine phosphoribosyltransferase* (*Hprt*). n = 3 independent experiments. **B**, Representative Western blot image from lysates of isolated pancreatic mouse islets treated with 10 µM DXO for 24 hours to induce islet cell dysfunction and detected for ALDH1L2 and Beta-actin. Quantification shows ALDH1L2 expression levels normalized to Beta-actin. n = 6 independent experiments. **C**, Western blot image of mouse pancreatic islets detected for ALDH1L2, Beta-actin and COX IV. Islets were treated with or without 10 µM DXO for 24 hours, followed by the separation in the mitochondrial and cytosolic fraction. Quantifications are shown as percentage of untreated islets and statistical significance was determined by two-tailed paired Student's *t*-test.

To our knowledge nothing is known about the presence of ALDH1L2 in pancreatic islet cells. Therefore, we checked if ALDH1L2 is localized within the mitochondria, as indicated in other cell types [144, 145]. Therefore, islet cells were separated into their cytosolic and mitochondrial fractions (Fig. 11 C). Cytochrome c oxidase (COX) IV (localized in the

mitochondria) and Beta-actin (localized in the cytosol) were used as marker proteins. The results confirmed that ALDH1L2 is exclusively localized within the mitochondrial fraction in pancreatic islets.

Since results from rodent animal models are not always predictive for the situations in humans, we checked the effect of DXO on ALDH1L2 regulation in islets from human donors. We treated islets from three human donors with 10 µM DXO for 24 hours and measured mRNA and protein levels. *ALDH1L2* was upregulated by 554% on mRNA (p = 0.0951) and twice on protein level (p = 0.0384) after stimulation with 10 µM DXO (Fig. 12). Interestingly, one of the three human donors was diagnosed with T2DM for over 10 years, still showing an increase in ALDH1I2 mRNA and protein level after stimulation.

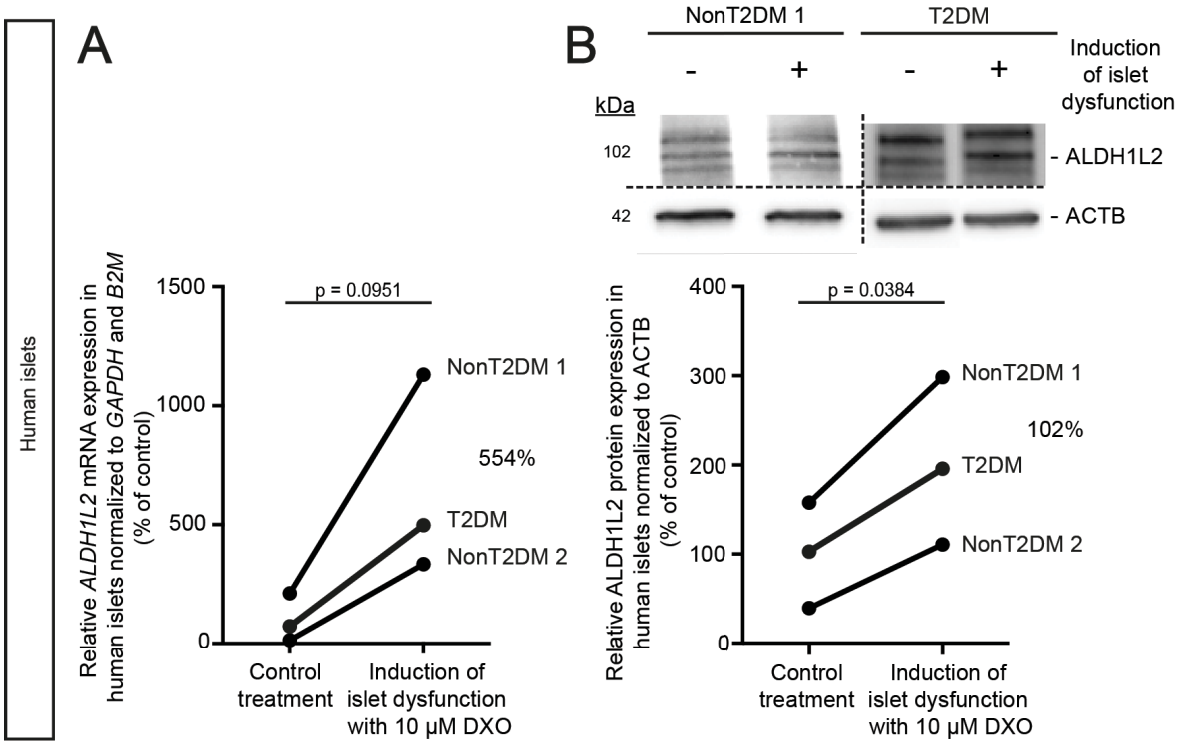

Figure 12: Treatment of human pancreatic islets with 10 µM DXO increases ALDH1L2 expression on mRNA and protein level. A, Quantification of relative *ALDH1L2* mRNA levels in human pancreatic islets treated with or without 10 µM DXO, normalized to *glyceraldehyde 3-phosphate dehydrogenase* (*GAPDH*) and *Beta-2 microtubulin* (*B2M*). n = 2 non-diabetic donors (NonT2DM) and n = 1 T2DM donor. **B**, Representative Western blot image of human islet lysates from NonT2DM and T2DM donors treated with 10 µM DXO for 24 hours and detected for ALDH1L2 and ACTB. Quantification shows ALDH1L2 protein amount normalized to Beta-Actin (ACTB). All quantifications are shown as percentage of untreated islets and statistical significance was determined by two-tailed paired Student's *t*-test. Islet donors: NonT2DM 1: 25-year-old male; BMI, 31.0 kg/m^2; NonT2DM 2: 66-year-old male; BMI, 27.2 kg/m^2. T2DM: 50-year-old female; BMI, 35.4 kg/m^2, T2DM > 10 years.

5.3.3 ALDH1L2 overexpression decreases GSIS

To further analyze the biological relevance of one-carbon metabolism and especially ALDH1L2, we performed gain-of-function experiments. To reveal the effect of ALDH1L2 in

primary pancreatic islet cells, adenovirus-mediated overexpression of ALDH1L2 was induced. Therefore, we cloned the human *ALDH1L2* gene into the adenovirus (Ad-*ALDH1L2*) under control of the CMV (Cytomegalovirus)-promoter. To check the transduction efficiency in pancreatic islet cells, the vector additionally encoded *GFP* (green fluorescent protein) under control of the RSV (Robus Sarcoma Virus)-promoter. For control transduction, a *GFP* carrying adenovirus was used (Ad-*GFP*) (Fig. 13 A). To perform the transduction, islets of C57Bl/6J mice were isolated, separated into a single-cell solution and infected for 6 hours with adenoviruses at a defined multiplicity of infection (MOI) at culture conditions (Fig 13 B). MOI is commonly defined as the ratio of infectious viral particles to the cells in culture [146]. After infection, pseudo-islets were formed using the hanging-drop technology. The efficiency of transduction was visualized by fluorescent microscopy following the quantification of induction by Western blot.

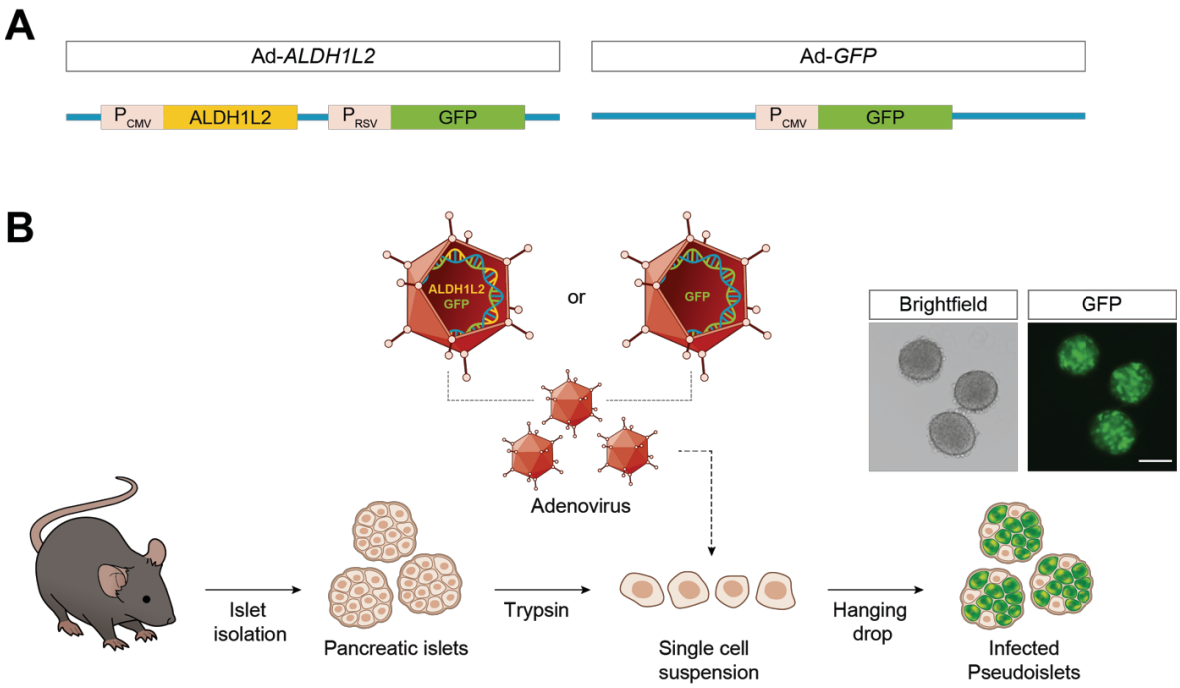

Figure 13: Experimental setup of adenovirus transduction in murine pancreatic pseudo-islets. A, Illustration of vector maps. Ad-*ALDH1L2* carries CMV-*ALDH1L2* and RSV-*GFP*. Control virus (Ad-*GFP*) carries CMV-*GFP*. **B**, Experimental setup shows adenoviral transduction of mouse islet cells and generation of pseudo-islets. Representative image of pseudo-islets transfected with Ad-*GFP* taken with Zoe^{TM} fluorescent cell imager. Scale Bar: 100 µM. The design and generation of the vectors were performed by Dominik Gebel.

After transduction, we checked if the infection of islet cells was successful and ALDH1L2 was overexpressed as well as translocated into the mitochondria. The results showed that the ALDH1L2 protein is strongly upregulated in mitochondria upon transfection with Ad-*ALDH1L2* compared to the control transfection with Ad-*GFP* (Fig. 14 A).

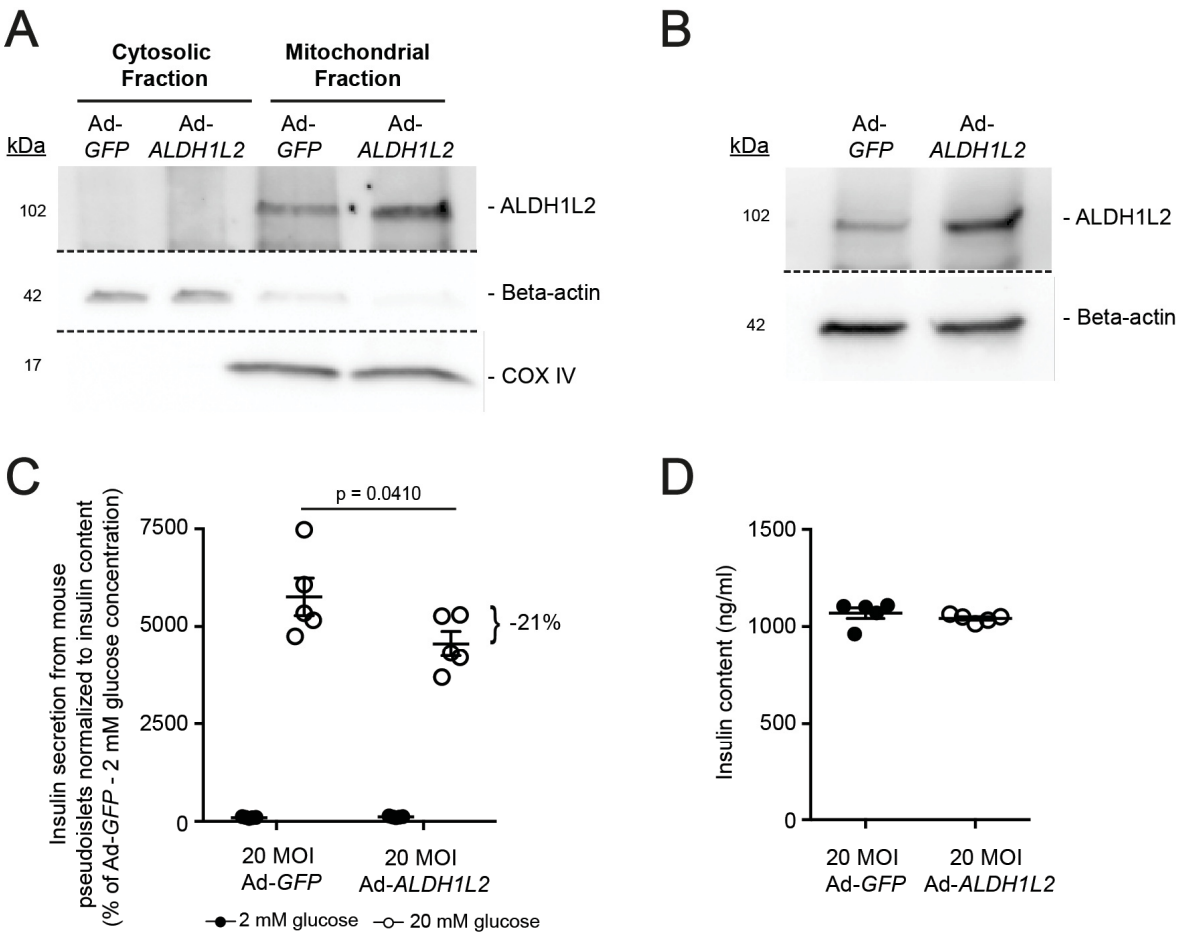

Figure 14: The mitochondrial localized enzyme ALDH1L2 reduces GSIS. A, Western blot image of lysates from murine pseudo-islets infected with Ad-*ALDH1L2* or Ad-*GFP* as control. Lysates were separated into a cytosolic and mitochondrial fraction. Western blot was detected for ALDH1L2, Beta-actin and COX IV. **B**, Western blot image of lysates from murine pseudo-islets infected with Ad-*ALDH1L2* or Ad-*GFP* as control. Lysates of pseudo-islets from the same transduction like pseudo-islets used in panel C and D. Western blot was detected for ALDH1L2 and Beta-actin. ALDH1L2 was about 3.3-fold increased after adenoviral infection. **C**, Insulin secretion from pseudo-islets infected either with 20 MOI Ad-*ALDH1L2* or Ad-*GFP* (n = 5 islet batches per condition with 8 islets each). Insulin secretion was measured at 2 mM and 20 mM glucose. Data are shown as mean ± SEM and *P* values were determined using two-way ANOVA followed by Tukey's multiple comparison test. **D**, Insulin content of pancreatic pseudo-islets shown in C. Data are shown as mean ± SEM. Statistical significance was determined by Student's *t*-test. Represented experiments in B – D were performed by Angela Pelligra.

To analyze the role of ALDH1L2 in the secretion mechanism of insulin, we performed an insulin secretion assay in pseudo-islets overexpressing ALDH1L2. During infection we wanted to be sure that ALDH1L2 was not overexpressed to a non-physiological extent, therefore we always performed a corresponding Western blot with islets from the same infection. Overexpression was increased around 3-fold compared to Ad-*GFP* control (Fig. 14 B). Under low glucose conditions (2 mM), no difference in insulin secretion was detected between both conditions. In contrast, GSIS was significantly decreased (p = 0.0410) in pancreatic pseudo-islets compared to control (Fig. 14 C). Notably, insulin content was not

affected (Fig. 14 D). These results point to the possibility that the mitochondrial localized enzyme ALDH1L2 plays a key role in limiting the amount of released insulin during GSIS.

5.3.4 Increased expression of ALDH1L2 did not protect pancreatic islet cells from cytokine-mediated cell death

To investigate whether the increased expression of ALDH1L2 protects islet cells during inflammatory conditions, live-cell imaging was performed with pseudo-islets overexpressing ALDH1L2. Notably, at standard culture conditions, the adenovirus-mediated overexpression of ALDH1L2 did not affect islet cell viability. Next, to examine the influence of ALDH1L2 during inflammatory conditions, we performed a viability assay upon cytokine treatment (Mix of TNF-α, IFN-γ and IL-1β) for 24 hours. Live-cell imaging revealed that a higher protein level of ALDH1L2 does not protect cells from cytokine-induced cell death (Fig. 15).

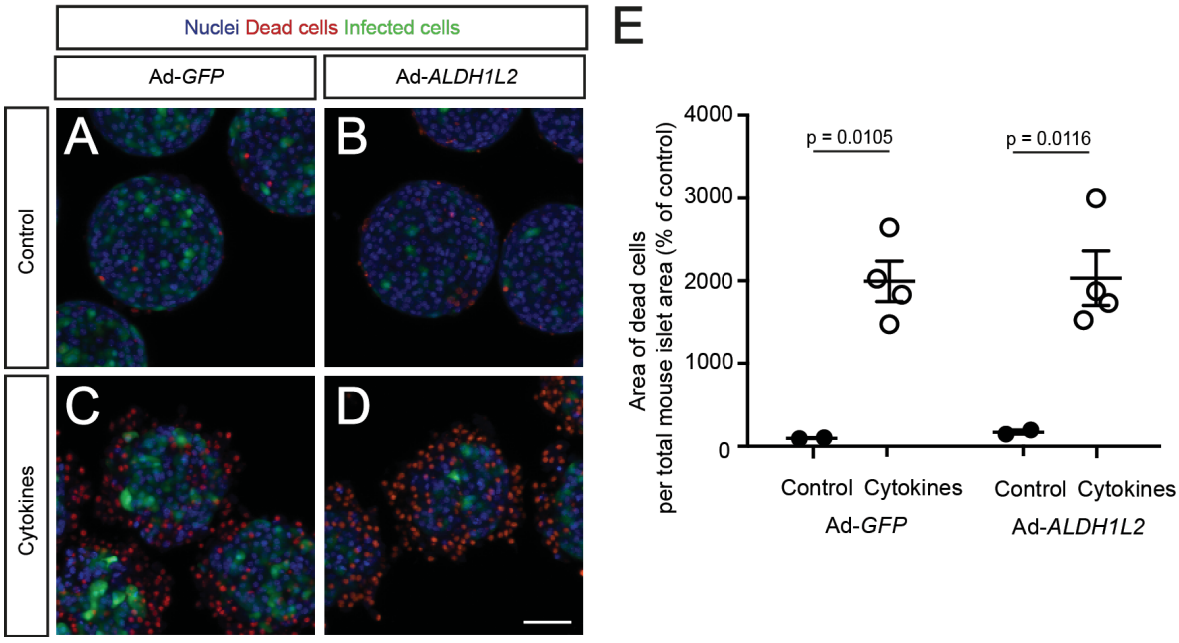

Figure 15: Overexpression of the mitochondrial localized protein ALDH1L2 does not protect pseudo-islets from cytokine-induced cell death. A-D, Representative LSM images of adenoviral infected pseudo-islets treated with or without a combination of cytokines. Scale bar: 50 µm. **E**, Calculation of cell death after cytokine treatment in murine pseudo-islets. Calculated area of dead cells is normalized to total nuclei area (control: n = 2 with n ≥ 25 islets in total, cytokines: n = 4 with n ≥ 59 islets in total). Quantification is shown as percentage of control. Data are shown as mean ± SEM and statistical significance was determined using two-way ANOVA followed by Tukey's multiple comparison test.

5.3.5 ALDH1L2 deficiency improves GSIS and glucose tolerance

For *in vivo* studies adult mice with a whole-body genetic deletion of *Aldh1l2* (ALDH1L2-KO) were used. The absence of ALDH1L2 was confirmed via Western blot of isolated islets from

male ALDH1L2-KO mice (Fig. 16 A). To investigate the influence of ALDH1L2 on islet function, we next isolated islets from ALDH1L2-KO male mice as well as control mice and performed an insulin secretion assay. Strikingly, at stimulatory glucose concentrations, a significant increase (p = 0.0019) of insulin release in *Aldh1l2*-deficient islets compared to control islets was measured (Fig. 16 B).

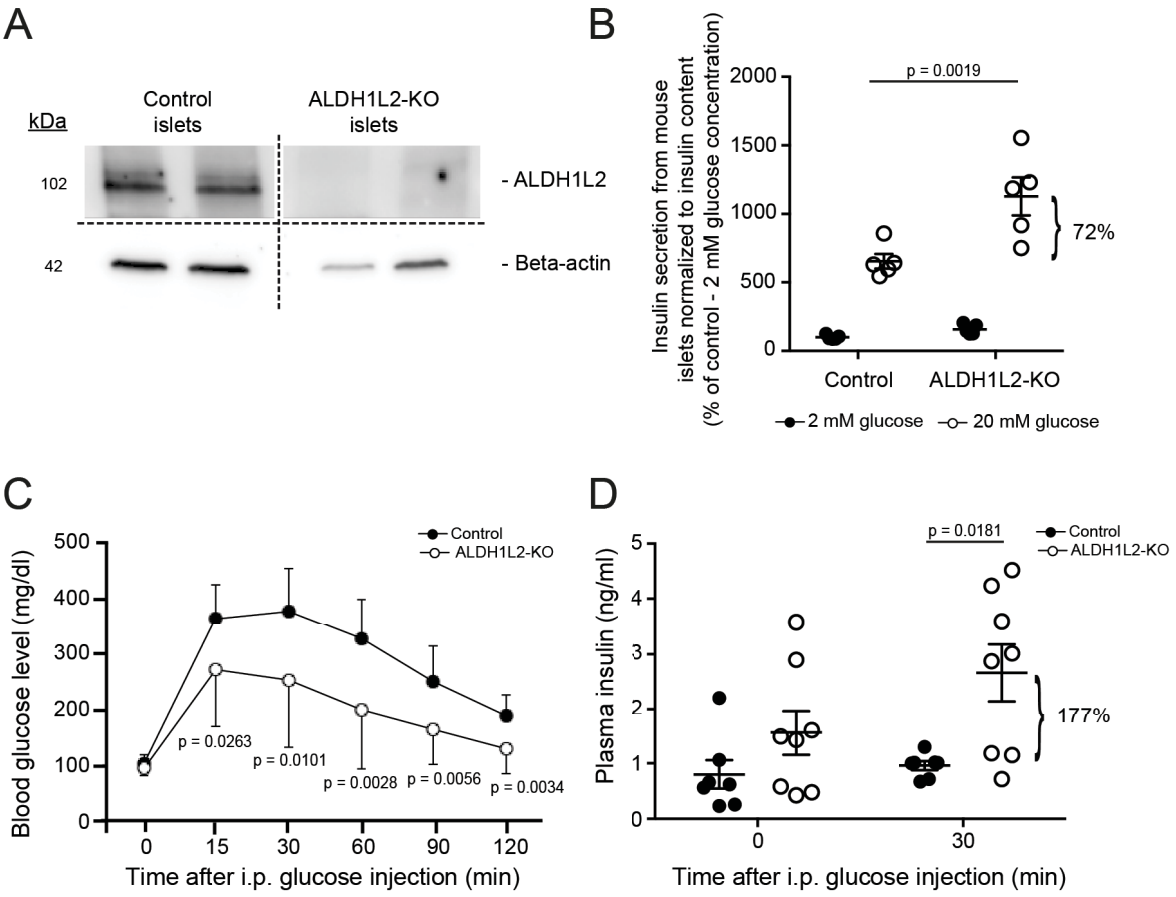

Figure 16: Genetic deletion of *Aldh1l2* results in enhanced glucose tolerance and increased insulin secretion in male mice. A, Western blot image shows knockout efficiency of ALDH1L2 in ALDH1L2-KO islets compared to wild-type islets (control) **B,** Insulin secretion from ALDH1L2-KO and control islets (n = 5 islet batches per condition with 8 islets per batch). Quantifications are shown as percentage of unstimulated control. Data are shown as mean ± SEM and *P* values were determined by two-way ANOVA followed by Tukey's multiple comparison test. **C**, Blood glucose concentrations of male control and ALDH1L2-KO mice during ipGTT (n = 7 for control, n = 8 for ALDH1L2-KO). Data are shown as mean ± SD and *P* values were determined by Student's *t*-test followed by Holm–Bonferroni correction. **D,** Plasma insulin concentrations before and 30 minutes after the start of the ipGTT in ALDH1L2-KO mice and control mice. Data are shown as mean ± SEM and statistical significance was determined by two-way ANOVA followed by Tukey's multiple comparison test.

Besides the *in vitro* experiments, we additionally performed *in vivo* experiments to confirm our results. Therefore, an intraperitoneal glucose tolerance test (ipGTT) was administrated in mice deficient for *Aldh1l2* compared to control mice (wild-type mice). Under fasting conditions, blood glucose concentrations were unchanged, whereas ALDH1L2-KO

mice showed significantly improved glucose tolerance compared to control mice (e.g. p = 0.0263 at 15 minutes and p = 0.0034 at 120 minutes) after glucose administration (Fig. 16 C). Surprisingly, three out of eight ALDH1L2-KO mice did not show an improved glucose tolerance. In addition, we measured insulin concentrations in the plasma at the beginning, and 30 minutes after glucose injection. In accordance with the findings, we detected a significant increase (p = 0.0181) of plasma insulin concentrations 30 minutes after glucose injection in *Aldh1l2*-KO mice compared to control mice (Fig. 16 D). In contrast, fasting plasma insulin concentrations were only slightly increased.

A recently published review points out that glucose homeostasis and prediabetic syndromes are differentially regulated in males and females [147]. To exclude any gender effects, experiments were additionally obtained in a female cohort of ALDH1L2-KO mice. Strikingly, glucose tolerance and insulin secretion were reproduced in the female cohort (Fig. 17 A, B). *Aldh1l2*-deficient islets of female mice showed increased secretion of insulin during glucose stimulation to a significant extent (p = 0.0236) (Fig. 17 A). Additionally, *Aldh1l2*-deficient female mice responded in the same way during the ipGTT like male mice (Fig. 17 B). Under fasting conditions, glucose concentrations were unchanged, whereas ALDH1L2-KO mice showed an enhanced glucose tolerance compared to control (wild-type) mice (e.g. p = 0.0137 at 15 minutes and p = 0.0173 at 120 minutes). In contrast, we did not recognize any difference in the plasma insulin concentration at the beginning and 30 minutes after glucose injection (Fig. 17 C).

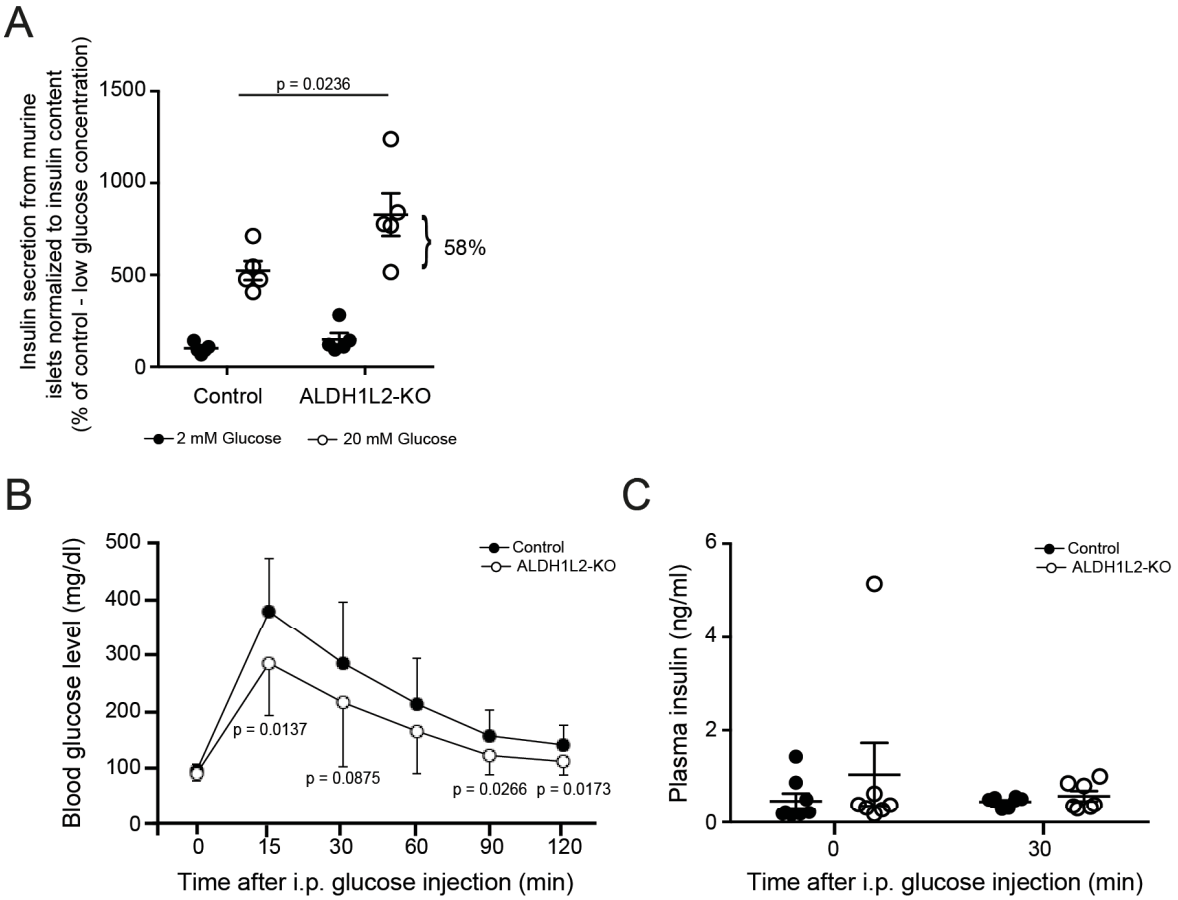

Figure 17: Genetic deletion of *Aldh1l2* in female mice results in enhanced glucose tolerance and increased insulin secretion. A, Insulin secretion from female ALDH1L2-KO and control (wild-type) islets (n = 5 islet batches per condition with 8 islets per batch). Quantifications are shown as percentage of control. Data are shown as mean ± SEM and *P* values were determined by two-way ANOVA followed by Tukey's multiple comparison test. **B,** Blood glucose concentrations of female control and ALDH1L2-KO mice during an ipGTT (n = 8 for control, n = 7 for ALDH1L2-KO). Data are shown as mean ± SD and *P* values were determined by Student's *t*-test followed by Holm–Bonferroni correction. **C,** Plasma insulin concentrations before and 30 minutes after the start of the ipGTT in ALDH1L2-KO mice compared to control mice. Data are shown as mean ± SEM and statistical significance was determined by two-way ANOVA followed by Tukey's multiple comparison test.

These results support the hypothesis that the mitochondrial localized enzyme ALDH1L2 is involved in glucose metabolism by regulating GSIS in pancreatic islet cells.

5.3.6 Lack of ALDH1L2 does not affect cytokine-induced cell death in islet cells

To check if the deletion of ALDH1L2 has an influence on cell viability, live-cell imaging experiments were performed. *Aldh1l2*-deficient islets, cultured under standard conditions, did not show any change in islet cell death compared to islets isolated from wild-type mice (Fig. 18 A, B). Next, we stimulated the islets with a mixture of cytokines (Mix of TNF-α, IFN-γ and IL-1β) for 24 hours to induce cell death. In islets deficient for ALDH1L2, cell death

was induced to the same extent, as in control islets, indicating that the deletion of ALDH1L2 does not influence cytokine-mediated cell death.

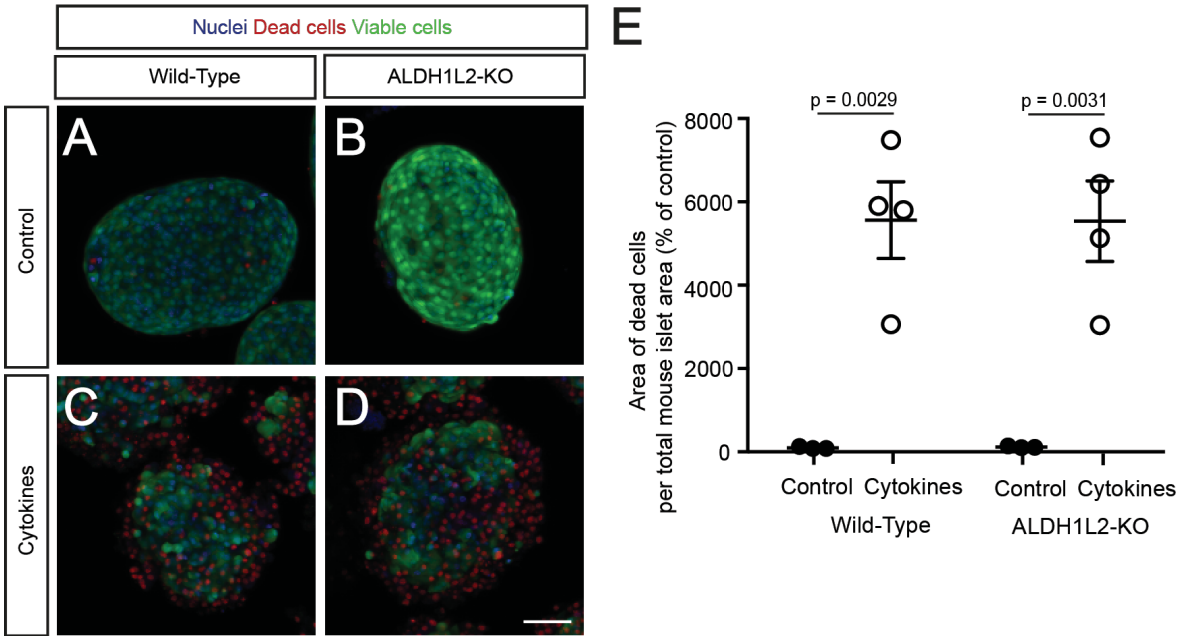

Figure 18: Genetic deletion of *Aldh1l2* does not protect islet cells from cytokine-induced cell death. A-D, Representative LSM images of ALDH1L2-KO and wild-type islets treated with or without a mixture of cytokines. Scale bar: 50 µm. **E**, Calculation of cell death after cytokine treatment in islets. Calculated area of dead cells is normalized to total nuclei area (control: n = 3 with n ≥ 43 islets in total, cytokines: n = 4 with n ≥ 57 islets in total). Quantification is shown as percentage of the untreated wild-type control. Data are shown as mean ± SEM and statistical significance was determined using two-way ANOVA followed by Tukey's multiple comparison test.

5.4 Long-term treatment of pancreatic islets with 1 µM DXO does not induce islet cell dysfunction

From previous experiments we could conclude that a concentration of DXO as low as 1 µM already protects mouse islets from cytokine-induced cell death. Therefore, we asked the question whether lower concentrations of DXO already have negative effects on islet cell function. Therefore, we investigated the effect of 1 µM DXO on islet cell function by performing an insulin secretion assay after 48 hours of incubation. Incubating islets with 1 µM DXO decreased insulin content by about 36% (Fig. 19 B), whereas insulin secretion was not affected (Fig. 19 A).

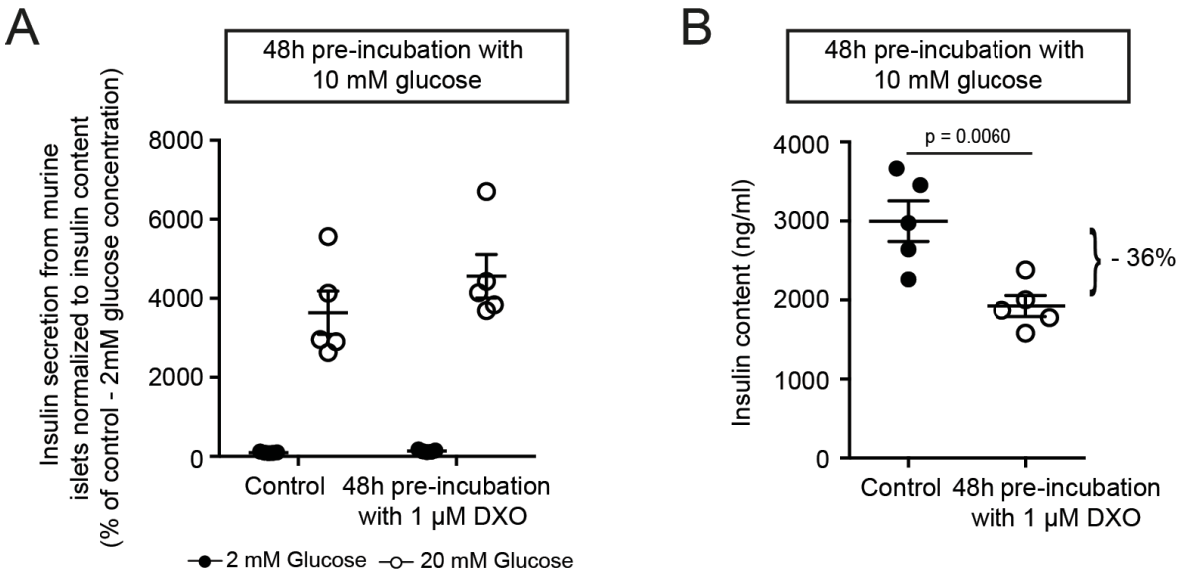

Figure 19: *In vitro* exposure of pancreatic islet to 1 µM DXO under continuous glucose stimulation does not induce islet dysfunction based on insulin secretion. A, Insulin secretion was measured after 48 hours pre-incubation with 1 µM DXO and 10 mM glucose compared to glucose alone (control). Insulin secretion was measured at 2 mM and 20 mM glucose (n = 5 islet batches per condition with 8 islets each). **B**, Insulin content of pancreatic islets shown in A. Data in A and B are shown as mean ± SEM. Statistical significance in A was determined by two-way ANOVA followed by Tukey's multiple comparison test. Statistical significance in B was determined by Student's *t*-test. Angela Pelligra performed the presented experiment.

In the next step, we analyzed the transcriptome of pancreatic islet cells after 24 hours of exposure to 1 µM DXO. RNA sequencing revealed that 327 genes (1.3% of all analyzed genes) were alternatively expressed after DXO treatment compared to control (Fig. 20 A). Consistently to the expression changes measured after treatment with 10 µM DXO, key genes for β-cell differentiation (*Mafa*, log2 FC = -1.40; *Slc2a2*, log2 FC = -1.67; *Ins1*, log2 FC = -1.73; *Ins2*, log2 FC = -1.00) were downregulated, whereas genes coding for core enzymes of the mitochondrial one-carbon metabolism (*Aldh1l2*, log2 FC = 2.58; *Mthfd2*, log2 FC = 1.34; *Shmt2*, log2 FC = 1.26) were upregulated (Fig. 20 B). Notably, after exposure of the islets to 1 µM DXO, the expression of *Aldh1l2* on mRNA level was increased about 6-fold, whereas 10 µM DXO increased the expression 9-fold compared to control.

We conclude that DXO acts concentration-dependent and hypothesize that *Aldh1l2*, as well as the other enzymes of the mitochondrial one-carbon pathway must exceed a certain expression value to induce insulin secretion defects.

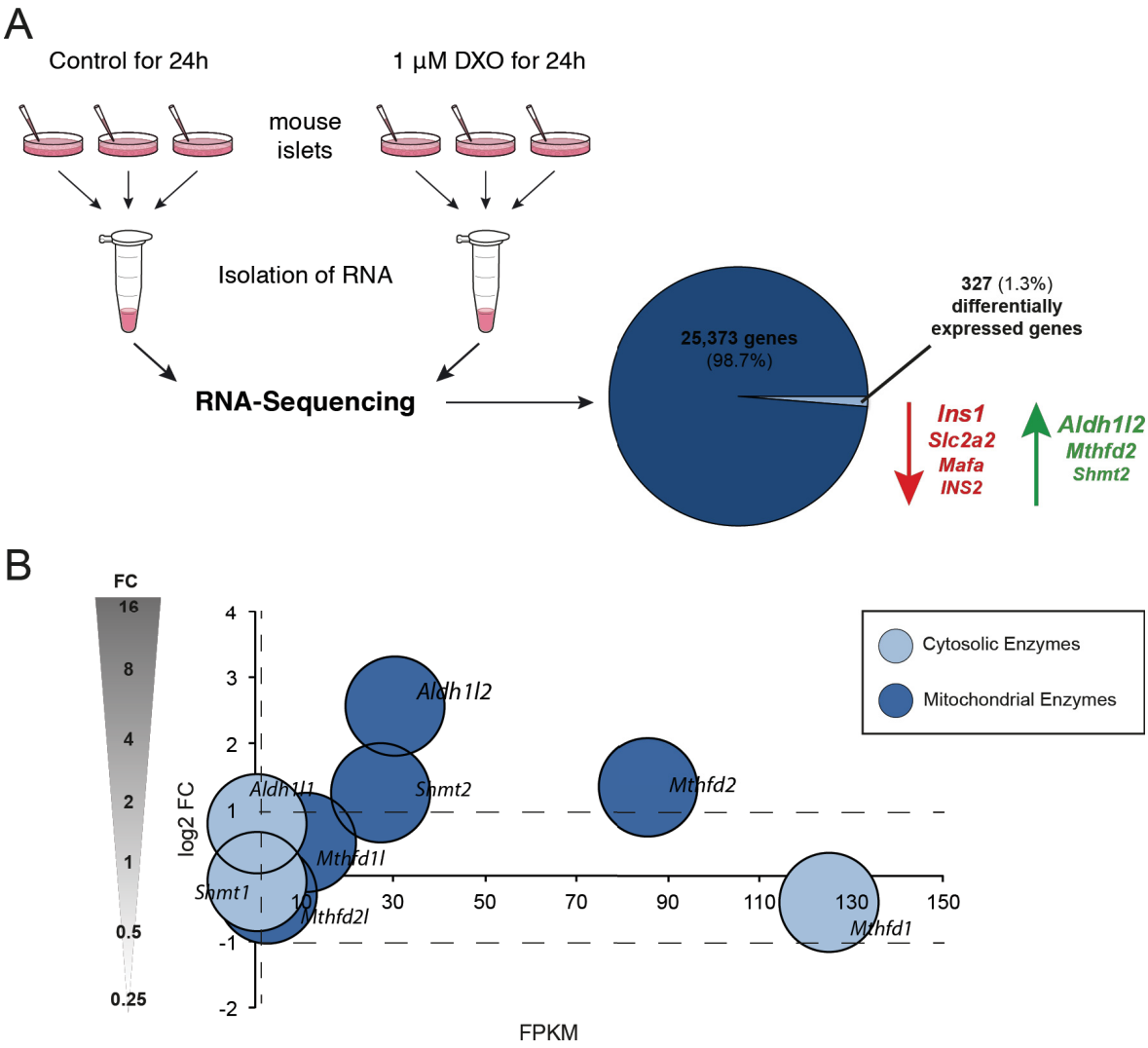

Figure 20: 1 µM DXO increases the expression of key enzymes of the mitochondrial one-carbon metabolism to a lesser extent than 10 µM DXO. A, Illustration of RNA sequencing setup. Differentially expressed genes were defined by log2 FC > 1 or < -1 and FPKM > 1. **B**. Analysis of eight genes coding for core enzymes involved in the folate-mediated one-carbon metabolism. Horizontal axes denote FPKM value and vertical axes denote log2 FC. Dashed lines indicate the restriction criteria of the log2 FC and the FPKM. Grey arrow indicates the FC.

5.5 *In vivo* treatment of *db*/*db* mice with DXM results in a slight upregulation of *Aldh1l2*

To analyze whether the one-carbon metabolism plays a role in *in vivo* conditions, *db*/*db* mice were treated with DXM via the drinking water, following the isolation of pancreatic islets and transcriptome analysis via RNA sequencing. At the age of 4 weeks, *db*/*db* mice got 3 mg/mL DXM (treatment group) or 1 mg/mL DXM (control group) orally administrated via their drinking water. Measuring the fasting blood glucose levels revealed that in contrast to the control group, the treatment group had significantly lower fasting blood glucose levels (Fig 21 A), indicating that DXM improved glucose tolerance. This effect of DXM in *db*/*db*

mice was already shown in Marquard *et al.*, 2015 [114] and could be confirmed with this experiment. Additionally, we measured the concentration of DXM in the blood plasma via Liquid chromatography-tandem mass spectrometry (LC-MS/MS). After two weeks of treatment, DXM concentrations were slightly higher in mice of the treatment group compared to control mice. The concentration in the treatment group was 1 µM on average (Fig. 21 B). Finally, two weeks after DXM treatment islets were isolated and used for further RNA sequencing analysis.

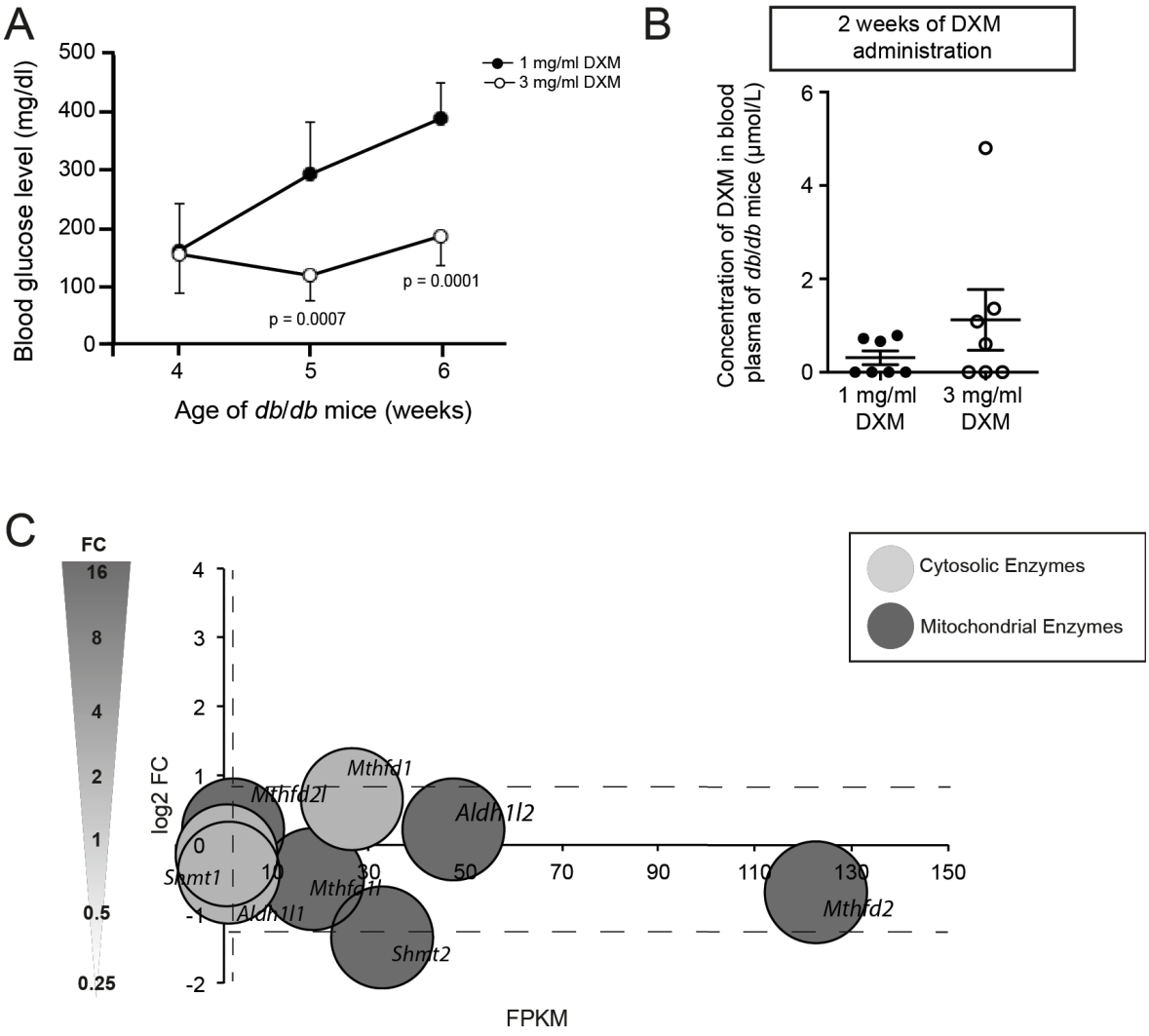

Figure 21: *In vivo* treatment of *db*/*db* mice with DXM only results in a slight upregulation of *Aldh1l2* without induction of islet dysfunction. A, Fasted blood glucose levels of *db*/*db* mice during treatment with DXM over 2 weeks. Mice got 1 mg/ml (control group) or 3 mg/ml DXM (treatment group) via drinking water (n = 7 for both groups). Data were shown as mean ± SD and *P* values were determined by Student`s *t*-test with Holm-Bonferroni correction. **B**, Concentration of DXM measured after two weeks of treatment in the blood plasma of *db*/*db* mice. Data are shown as mean ± SEM and statistical significance was determined by Student`s *t*-test. **C**, RNA sequencing was performed with islets of *db*/*db* mice after two weeks of DXM treatment. Analysis of genes coding for core enzymes of the mitochondrial one-carbon pathway and the corresponding cytosolic enzymes. The graph shows eight genes involved in one-carbon metabolism as grew circles. The vertical axis shows log2 FC, while the horizontal axis shows FPKM. Dashed lines indicate the restriction criteria of the log2 FC and the FPKM. Grey arrowhead on the left indicates the FC.

Identification of differentially expressed genes was performed between islets of *db*/*db* mice receiving a low (1 mg/ml) and a high (3 mg/ml) dosage of DXM (Fig. 21 C). We checked specific genes that were differentially expressed after DXO exposure in *in vitro* cultures. First, we had a closer look at β-cell dedifferentiation genes, which were downregulated during *in vitro* conditions (Fig. 8). Different to the *in vitro* study, the expression of β-cell differentiation markers, like *Mafa* (log2 FC = 0.82), *Slc2a2* (log2 FC = 1.67), *Ins1* (log2 FC = 1.44) and *Ins2* (log2 FC = 0.36) were increased in islets of *db*/*db* mice receiving a higher dosage of DXM (Data not shown).

Furthermore, we had a closer look at genes of one-carbon metabolism. The RNA sequencing analysis revealed that none of the genes coding for core enzymes of the mitochondrial and cytosolic one-carbon pathway showed a stong expression difference in *in vivo* conditions, except the mitochondrial localized enzyme *Shmt2* (log2 FC = -1,33) that was reduced (rather than increased) in its expression. *Aldh1l2* was slightly increased. We verified the slight effect of *Aldh1l2* on mRNA (increased by 89%) and protein levels (increased by 34%) (Fig. 22 A).

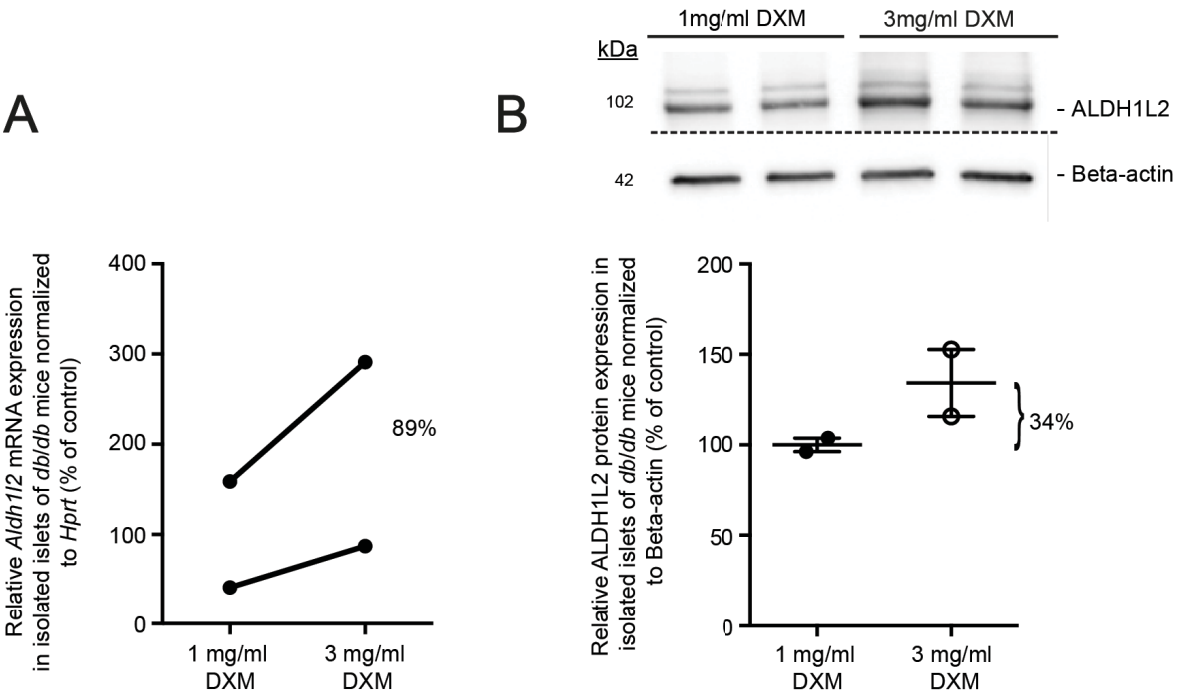

Figure 22: *In vivo* treatment of *db*/*db* mice with DXM results in a slight upregulation of ALDH1L2 on mRNA and protein level. **A**, Quantification of relative *Aldh1l2* mRNA levels in pancreatic islets of *db*/*db* mice treated with DXM in drinking water. *Aldh1l2* mRNA levels were normalized to *Hprt*. n = 2 independent experiments. **B**, Representative Western blot image from lysates of isolated pancreatic islets from *db*/*db* mice treated with DXM in drinking water. Western blot was detected for ALDH1L2 and Beta-actin. Quantification shows ALDH1L2 expression levels normalized to Beta-actin. n = 1 experiment with n = 2 technical replicates. Data in A and B are shown as mean ± SEM. Statistical significance in A was determined by two-tailed paired Student's *t*-test. Statistical significance in B was determined by Student's *t*-test.

These results suggest that genes, associated with dedifferentiation and one-carbon metabolism, are not relevant for the beneficial primary effect of DXM during *in vivo* conditions.

6 Discussion

6.1 Protective effect of DXO during cytokine-induced cell death

DXO has beneficial effects on pancreatic islets from mice and human donors under diabetogenic conditions. Therefore, one aim of this study was to further investigate the protective properties of DXO on pancreatic islets. Our findings support the hypothesis that the NMDA receptor antagonist DXO has protective effects upon inflammation. Using TUNEL assay, we showed that DXO protects pancreatic islets against cytokine-induced apoptosis. Interestingly, we figured out that a tenth of the previously used concentration (1 µM instead of 10 µM DXO) is enough to protect islets against inflammation.

Furthermore, we asked the question whether the sole blocking of the NMDA receptor is responsible for the protective effect. Therefore, islets of GluN1-KO mice as well as control mice were investigated. Treating the islets with cytokines showed that the deletion of the NMDA receptor is not sufficient to protect the cells against cytokine-induced cell death. Additionally, the protective effect of DXO in GluN1-KO islets was abolished, indicating that blocking the NMDA receptor is required for the protective effect of DXO. In line with our data, other reports provide evidence that the NMDA receptor is involved in cell viability. Indeed, *in vitro* studies in a β-cell line indicate that the sustained activation of the NMDA receptor is a novel factor of apoptotic β-cell death, induced through an impaired mitochondrial function [117]. Moreover, blocking the NMDA receptor ameliorated high-glucose-induced ER stress *in vitro* and *in vivo* [116]. Nevertheless, our results point to the possibility that the NMDA receptor is not exclusively responsible for the protective effect of DXO and that another pathway seems to be involved, which is alone not sufficient to implement the protective effect. Besides the NMDA receptor, DXM as well as DXO interact with several other receptors and transporters like the serotonin transporter, the noradrenaline transporter, and the sigma-1 receptor [148]. Various studies already show that besides blocking the NMDA receptor, neuroprotective properties can additionally be induced by the activation of sigma-1 receptor [149]. Whether DXO develops its protective effect as an agonist or antagonist of different receptors or even a combination of several receptors needs further investigation.

6.2 Effects of the insulin secretagogue DXO on pancreatic islet cell function

The second aim of this study was to analyze the long-term effect of the insulin secretagogue DXO on pancreatic islet cell function. In the present work, we found that the long-term treatment (48 hours) of mouse islets with the insulin secretagogues DXO and Glib decreased insulin content and impaired GSIS. Different from Glib, insulin secretion under low glucose conditions was not affected upon DXO treatment.

Besides DXO, multiple medications can achieve and maintain normoglycemia, but the glucose control of most oral antidiabetic agents, especially insulin secretagogues, gradually diminishes [94, 95, 99]. The molecular mechanism of this phenomenon has not been investigated yet, but it is under debate that insulin secretagogues promote β-cell exhaustion and pancreatic islet dysfunction as a consequence [107, 109]. Exhaustion seems to be induced by chronic stimulation to glucose as well as other insulin secretagogues and is defined as the physical depletion of β-cell insulin stores, leading to impaired insulin secretion [79, 109]. Our study aimed to answer the question, how does DXO, as an insulin secretagogue, induce the phenomenon of β-cell exhaustion and β-cell dysfunction as a consequence.

One possible explanation for this phenomenon could be the induction of ER stress. It is under discussion that forcing the β-cell to hypersecrete insulin is counterproductive because the increased demand of insulin biosynthesis can exceed the folding capacity of the ER and induce β-cell failure [109, 150, 151]. In response to insulin resistance, for example, the biosynthesis of proinsulin rises up to 50-fold after meal due to the increased demand of insulin [152]. As a consequence, unfolded and misfolded proteins accumulate within the ER, which triggers the activation of the UPR inducing a stress response by changing the expression of various genes [152]. The activation of ER stress genes was already measured in pancreatic islets of diabetic *db*/*db* mice and T2DM patients [85, 86], indicating that the UPR plays a role in the pathogenesis of the disease. Proinsulin is the precursor molecule for insulin. In healthy individuals only a minor amount of proinsulin is released into the circulation after food intake, whereas during insulin resistance the proportion of proinsulin is increased [153]. Interestingly, in plasma samples of T2DM patients that chronically use sulfonylureas to manage diabetes, the levels of proinsulin are elevated, indicating that the additional trigger of insulin release by insulin secretagogues exhausted islets and induce ER stress [154, 155]. It is already investigated that increased activation of the ER stressors can impair insulin biosynthesis and GSIS, whereas the mechanism is not uncovered [156-158].

Additionally, besides ER stress induction, elevated concentrations of insulin in the circulation (or medium) can affect the β-cell itself. Already published data showed that DXO significantly increased the amount of released insulin at a stimulatory concentration of 10 mM glucose [114] (Fig. 23). The continuously elevated secretion of insulin, triggered by the insulin secretagogue DXO and stimulatory glucose concentrations, can increase the autocrine action of insulin on β-cells and affects as a consequence, β-cell functionality and viability.

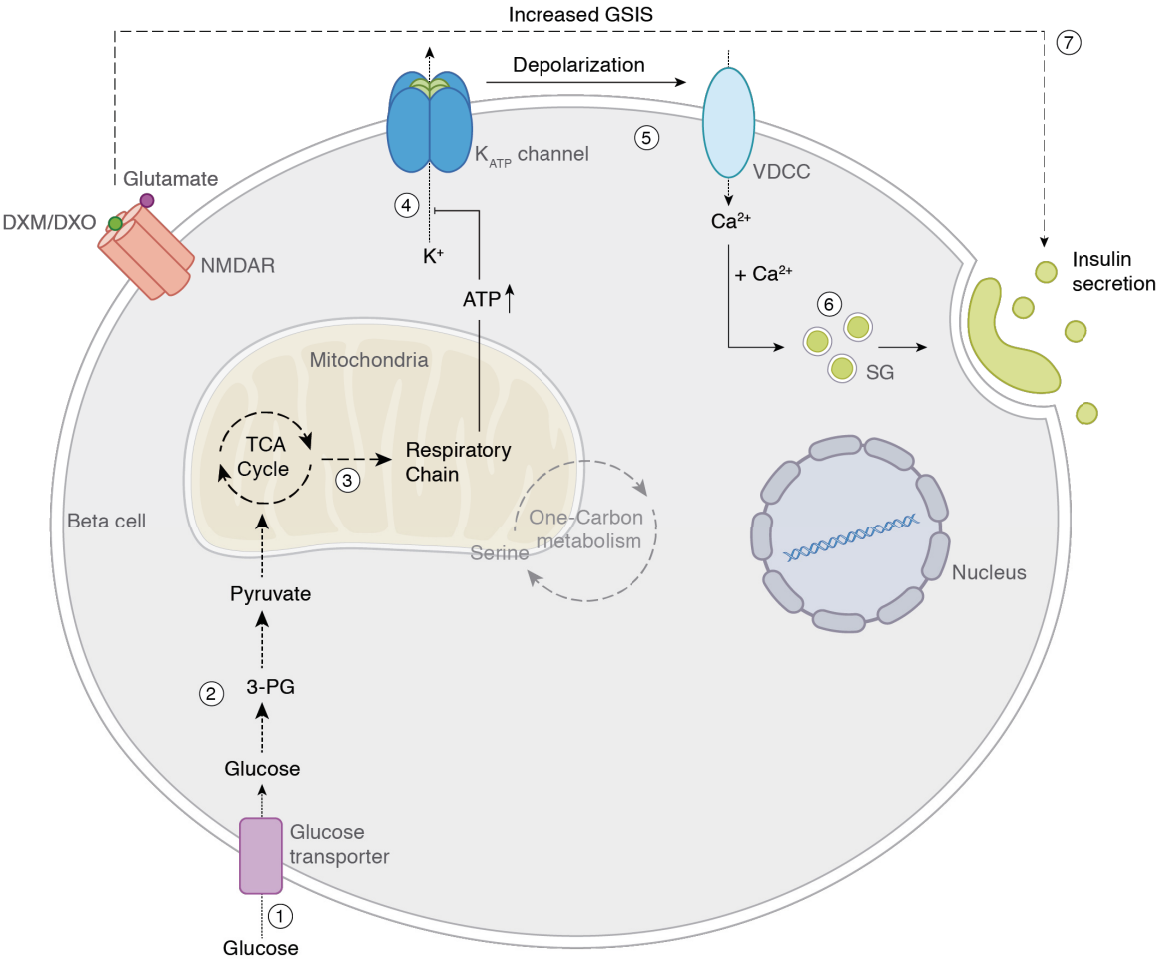

Figure 23: Current proposed mechanism of GSIS with binding of DXO on the NMDA receptor as an amplifier of insulin secretion. GSIS (Step 1-6). In brief, glucose enters the β-cell via the glucose transporter (Step 1), gets phosphorylated and enters the glycolysis. Pyruvate is during aerobe conditions the terminal product of glycolysis (Step 2). Pyruvate enters the mitochondria to produce reducing equivalents in the TCA cycle, which are subsequently oxidized in the respiratory chain to produce ATP (Step 3). Elevated ATP levels block K_{ATP} channels (Step 4), which leads to the depolarization of the cell. Depolarization induces the opening of VDCCs (Step 5), resulting in the exocytosis of insulin (Step 6). Blocking the NMDA receptor by DXM/DXO further increase GSIS (Step 7). Abbreviations: 3-PG, 3-phosphoglycerate; ATP, adenosine triphosphate; DXM, dextromethorphan; DXO, dextrorphan; GSIS, glucose-stimulated insulin secretion; K_{ATP} channels, ATP-sensitive potassium channels; NMDAR, N-methyl-D-aspartate receptor; SG, secretory granule; TCA, tricarboxylic acid cycle; VDCC, voltage-dependent Ca^{2+} channel.

However, the concept that insulin is a physiologically relevant molecule acting on β-cells is still controversially discussed [159-162]. Insulin is an anabolic hormone known to influence insulin secretion [163], proliferation [164], and viability of β-cells [165], but it is still under debate if the binding of insulin to β-cells has a negative, positive or complex (negative or positive) signaling function [165]. Insulin receptors (IRs) as well as insulin-like growth factor-1 receptors (IGF-1Rs) and the principal insulin receptor substrates (IRS), IRS-1 and IRS-2, are present on β-cells and therefore, it is speculated that autocrine insulin signaling is important for signaling events [165]. The exposure of rat islets to high concentrations of insulin for an extended period of time almost completely suppressed secretory activity [166]. Studies in human islets showed similar effects [167]. In islets of human donors, the activation of the insulin receptors by an insulin mimetic inhibits basal and GSIS [167], pointing to the possibility that insulin acts in an autocrine manner to negatively regulate its own secretion. In contrast, several other reports analyzing models with genetic deletions within parts of the insulin receptor or the receptor signaling pathway point to positive effects of this signaling pathway in islets [168, 169]. The attempt to β-cell-specifically delete the insulin receptor results in impaired insulin secretion in response to glucose, and manifests in the progressive loss of glucose tolerance [163]. However, the RIP-Cre line used for β-cell specific deletion was later shown to be strongly expressed and active in the brain, pointing to other explanations of the findings [170, 171]. Nevertheless, the deletion of IRS-1 in islets and β-cell lines showed marked insulin secretory defects in response to glucose indicating a functional link between insulin signaling and insulin secretion [169]. Furthermore, a polymorphism in the human *IRS1* gene is linked to impaired insulin secretion from the β-cells of the pancreatic islets, suggesting that IRS-1 participates in the pathway of insulin secretion [168]. The impact of glucose and insulin on the insulin receptor during GSIS was already investigated by others [172]. Notably, in β-cell lines lacking either the insulin receptor or IRS-2, the effects of glucose are abolished, indicating that glucose requires the presence of an intact insulin/IGF-I signaling pathway [172]. The beneficial effects of glucose on β-cell growth and survival are based on the activation of the insulin receptors and IRS-2, indicating a dominant role for insulin in β-cell function [172].

At the molecular level, it was shown that glucose and insulin induce the phosphorylation of eukaryotic translation initiation factor 4E-binding protein 1 (4E-BP1) [172], a protein, which maintains β-cells homeostasis during ER-stress [83]. 4E-BP1 gets activated by phosphorylation via the mechanistic target of rapamycin (mTOR), a serine/threonine kinase and a key regulator of protein synthesis. mTOR is a nutrient-responsive regulator of cell growth, which can be combined with specific proteins to different complexes, known as mTOR complex-1 (mTORC1) and mTOR complex-2 (mTORC2) [173]. mTORC1 is a signaling complex, which participate into pathways like glycolysis,

mitochondrial metabolism, protein synthesis, and lipid biosynthesis [173]. It is proposed that the activation of mTORC1 is a pathogenic hallmark in the development of diabetes [174]. mTORC1 activation can have positive or negative effects for the β-cell dependent on the duration of activation [175]. Short-term mTORC1 activation under physiological conditions improves glucose homeostasis, whereas chronic mTORC1 hyperactivation induced by hyperinsulinemia or over-nutrition often correlates with loss of pancreatic β-cell mass and GSIS [174, 176]. Islets from patients and animal models (*db*/*db* and HFD) with T2DM showed increased activity of mTORC1 [174]. Therefore, it points to the possibility that a brief increase in mTORC1 activation through the binding of insulin on the insulin receptor has beneficial effects for insulin secretion and glucose tolerance, whereas the activation over a long period of time leads to a decline in β-cell function. This prolonged activation of mTORC1 can be induced by increased release of insulin due to prolonged exposure to high concentrations of glucose in combination with insulin secretagogues.

Whether the induction of ER stress or the hyperactivation of mTORC1 or even a combination of both mechanisms participate in the functional impairment of the β-cells secretion after long-term treatment with DXO has to be further investigated.

6.3 Role of the mitochondrial one-carbon metabolism, especially ALDH1L2, in islet cell dysfunction and viability

To reveal the underlying molecular mechanism of DXO after long-term treatment leading to the protective effect against cytokines on the one hand and islet cell dysfunction on the other hand, we performed transcriptome analysis.

RNA sequencing revealed that β-cells, under long-term DXO treatment partially lost their β-cell identity indicated by the downregulation of the key β-cell genes *Mafa*, *Slc2a2*, *Ins1*, and *Ins2*. It is under discussion that dedifferentiation is one main reason for the decline in functional β-cell mass in T2DM patients [73]. The GLUT2 transporter, encoded by the gene *Slc2a2*, plays an important role in GSIS. The reduced expression of GLUT2 was detected in diabetic mice and rats and is associated with impaired GSIS [14]. MafA is also reported to be a key regulator of maintaining β-cell function [177]. Studies in *Mafa*-deficient mice showed decreased mRNA levels of *Ins1*, *Ins2*, and *Slc2a2* and identified MafA as a critical regulator in GSIS [178]. By binding to the promoter in the insulin gene, MafA is responsible for the tissue-specific activation of insulin, whereas insulin content is not significantly reduced in *Mafa*-deficient mice [178]. *Ins1* and *Ins2,* a two-gene system, code for preproinsulin in rat and mouse endocrine pancreas [179]. These four key genes influence insulin secretion as well as synthesis and have impact on β-cell dysfunction. We

hypothesize that decreased insulin content observed after long-term exposure to the insulin secretagogue DXO was induced by decreased expression of these genes, especially *Ins1* and *Ins2*. Nevertheless, these genes can also participate in the defects of insulin secretion but were not investigated further in this study.

Surprisingly, besides islet dedifferentiation, RNA sequencing revealed a group of genes that were remarkably upregulated upon DXO treatment compared to control. These genes code for core enzymes of the mitochondrial one-carbon metabolism. Especially one gene, *Aldh1l2*, was significantly overexpressed in islets treated with DXO for 24 hours. Strikingly, genes encoding enzymes of the cytoplasmic part of the one-carbon metabolism were not altered. Based on our findings, we determined *Aldh1l2* as our candidate gene and tried to figure out if this enzyme has any influence on islet function as well as viability. First, we confirmed that the expression of *Aldh1l2* is increased on mRNA and protein levels in mouse and human islets treated with high concentrations of DXO. Additionally, we verified the localization of ALDH1L2 in the mitochondria of islet cells. To our knowledge, until now nothing is known about the presence and the functionality of the one-carbon metabolism and especially ALDH1L2 in pancreatic islet cells.

6.3.1 One-carbon metabolism and ALDH1L2 – current knowledge in various cell types

The one-carbon metabolism is a metabolic pathway responsible for the transfer of one-carbon units for biosynthetic processes [180]. In eukaryotic cells, the one-carbon metabolism is compartmentalized in different organelles within the cell (Fig. 24). In the cytosol, reactions take place as the biosynthesis of purines [181] and the recovery of methionine from homocysteine [182], whereas glycine detoxification (triggered in response to high concentrations of glycine), the conversion of dimethylglycine to sarcosine and then to glycine, and the initiation step of transfer RNA (tRNA) translation for protein synthesis is localized in the mitochondria [144]. Furthermore, mitochondrial one-carbon metabolism is a source of NADPH production, indicating a role in the antioxidant defense system [183].

Folate, also known as vitamin B9, is a cofactor acting as a coenzyme in the one-carbon metabolism [184]. For the metabolic functions, the one-carbon carrier folate has to be metabolized into its active form 5,6,7,8-tetrahydrofolate (THF). THF is transported to the mitochondria via the mitochondrial folate transporter (MFT, encoded by *SCL25A32*), where it acts as a main one-carbon group carrier [184]. Serine and glycine are acting as the most important one-carbon source, donating one-carbon groups to THF [184]. The transfer of methyl groups from serine to THF is catalyzed by the mitochondrial localized enzyme SHMT2, generating glycine and 5,10-methylene-THF as main products [184]. Subsequently, the enzymes MTHFD2 or MTHFD2/L converts 5,10-methylene-THF to 10-

formyl-THF [184]. Depending on the mitochondrial requirements, formate or CO_2 are produced in the next step. The production of purines and other substances requires the formation and subsequent release of formate into the cytosol. This hydrolysis is driven by MTHFD1L and coupled to ATP production. Alternatively, ALDH1L2 can metabolize 10-formyl-THF to THF and release CO_2, with the additional reduction of $NADP^+$ to NADPH [184]. The generation of CO_2 induces the terminal release of one-carbon groups [144]. The physiologically significant mitochondrial NADPH production via ALDH1L2 and probably MTHFD2 seems to be an important part of the redox homeostasis [145].

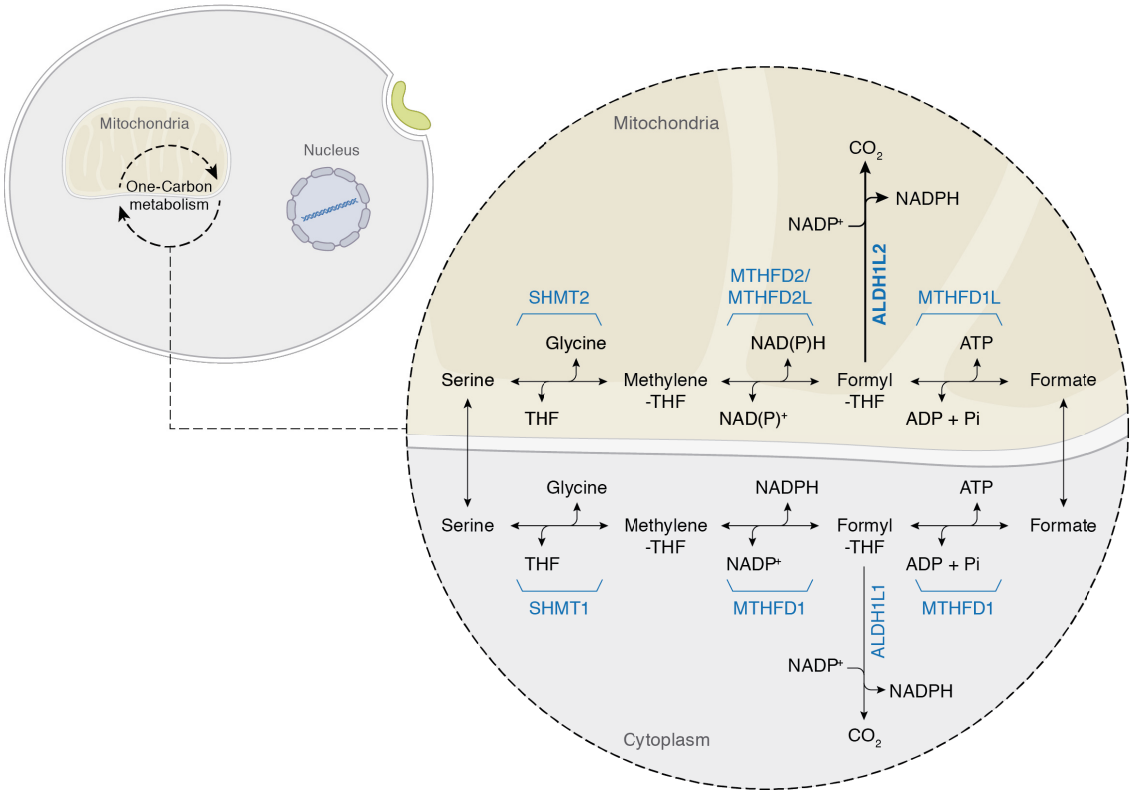

Figure 24: Schematic illustration of the one-carbon metabolism. The one-carbon metabolism is divided into the cytoplasmic and mitochondrial part. Abbreviations of the enzymes and substrates are indicated in the main text.

mRNA levels of *ALDH1L2*, also known as mtFDH, are most highly expressed in the pancreas, heart, and brain of human tissue. In addition, several human cancer cell lines express high levels of *ALDH1L2* [144]. Many cancer cells use the mitochondrial one-carbon pathway as the source of making one-carbon units. Therefore, certain genes of the mitochondrial one-carbon pathway are consistently overexpressed in cancer cells [145, 185, 186]. Additionally, primary tumors and metastasizing cells undergo genetic changes that increase their capacity to cope with oxidative stress [187]. The antifolate methotrexate, a cytotoxic chemotherapeutic agent, acts as a competitive inhibitor of dihydrofolate

reductase (DHFR), an enzyme that is responsible for the reduction of dihydrofolate to THF [180, 188]. Methotrexate decreases the amount of intracellular reduced folate pools, and thereby, induces oxidative stress [188]. In contrast, the folate-mediated elevation of NADPH levels protects cells from oxidative stress [183]. NADPH can be regenerated in the one-carbon pathway by the mitochondrial localized enzyme MTHFD2 [189] as well as ALDH1L2 [144, 145, 183]. This increase in NADPH is proposed to increase the capacity to regenerate oxidized glutathione (GSH) from reduced glutathione (GSSG) (GSH/GSSG ratio) [183], which acts as an important antioxidant in the β-cell [190]. The knockdown of *ALDH1L2* decreases the ratio of reduced to oxidized glutathione (GSH/GSSG ratio) in HEK293T cells [183]. In addition, HEK293T cells deficient for *Mthfd2* and *Aldh1l2* were vulnerable to oxidative stress in form of hydrogen peroxide (H_2O_2) [145], supporting the hypothesis that the complete oxidation of 5,10-methylene-THF plays an important role in the redox defense system. Interestingly, a recently published case report points to the possibility that ALDH1L2 deficiency in patients impairs the mitochondrial function and is likely the cause of a new neuro-ichthyotic syndrome [191]. ALDH1L2 deficiency resulted in altered mitochondrial morphology, and showed increased levels of acylcarnitine derivatives, and Krebs cycle intermediates in fibroblasts [191]. Fibroblasts of the patient show lower mitochondrial membrane potential and increased levels of ROS. Furthermore, total folate levels in fibroblasts were not different between the patient and control, whereas 10-formyl-THF, the source of the enzymatic reaction, was enriched in ALDH1L2-deficient cells. In line with recent reports, the NADPH/$NADP^+$ ratio and the amount of ATP were lower in cells lacking ALDH1L2 [191]. Studies in a human patient underline the important role of ALDH1L2 in the maintenance of mitochondrial homeostasis of the cell [191].

6.3.2 Role of ALDH1L2 in glucose homeostasis and insulin secretion

To investigate the biological function of ALDH1L2 in pancreatic islet cells we performed gain-of-function and loss-of-function experiments. By adenoviral overexpression and genetic deletion, we found that ALDH1L2 seems to be an important player in the regulation of glucose homeostasis and insulin secretion. GSIS in pseudo-islets overexpressing ALDH1L2 was impaired, whereas basal secretion of insulin was unchanged compared to control islets. Improved glycemic control was measured during an ipGTT in *Aldh1l2*-deficient mice compared to control mice. Note that after overnight fasting basal glucose levels were unchanged between *Aldh1l2*-deficient and control mice, whereas insulin levels were slightly increased. In male mice, the plasma insulin concentrations were increased 30 minutes after glucose injection. Furthermore, *Aldh1l2*-deficient islets showed increased secretion of insulin upon stimulatory glucose concentration, indicating that the enhanced glycemic control is based on the increased secretory capacity of β-cells, rather than

changes in the insulin target tissues. To our knowledge, until now nothing is known about the function of ALDH1L2 in pancreatic islet cells. Therefore, we give the first idea about the biological impact of ALDH1L2 and propose a new molecular mechanism coupling increased expression of ALDH1L2 in the development of islet cell dysfunction induced by the insulin secretagogue DXO.

As already elucidated, ALDH1L2 is part of the mitochondrial one-carbon metabolism, which is known to be responsible for the synthesis of nucleotides as well as function as antioxidant defense system [144]. Besides glycine and formate, serine acts as the main source of one-carbons in the mitochondria [192]. As a non-essential amino acid, serine is taken up by the cell or alternatively synthesized *de novo*. The *de novo* synthesis of serine through the serine synthesis pathway starts with an intermediate of glycolysis following the activation of three enzymes [193]. 3-phospho-glycerate (3-PG), the glycolytic intermediate, is catalyzed by phosphoglycerate dehydrogenase (PHGDH) to 3-phosphohydroxypyruvate (3-PHP). 3-PHP is subsequently catalyzed to 3-phosphoserine (3-PS) by phosphoserine aminotransferase 1 (PSAT1) and finally to serine by phosphoserine phosphatase (PSPH) [194] (Fig. 25, step 8-10). It has already been demonstrated that all three enzymes are increased in tumor tissue, indicating an important role during the proliferation of tumor cells [195].

Through our RNA sequencing results, increased expression of genes encoding the three enzymes of the serine synthesis pathway was measured upon DXO treatment *in vitro* (10 µM DXO vs. control: *Phgdh*, log2 FC = 2.5; *Psat1*, log2 FC = 2.4; *Psph*, log2 FC = 2.2). Synthesis of serine leads to a change in the glycolytic flux away from glycolysis and TCA to the production of serine [194]. We propose that this glycolytic flux decreases the amount of ATP and as a consequence impairs GSIS.

Interestingly, serine is an allosteric activator of pyruvate kinase isoenzyme type-M2 (PKM2), the enzyme that catalyzes the final step in glycolysis. This indicates that low levels of intracellular serine reduce the activity of PKM2, which subsequently leads to the accumulation of glycolytic intermediates, modulating the flux to feed the serine synthesis pathway [195, 196]. It is proposed that increased levels of serine could provide a feedback mechanism by activating PKM2 to restore the glycolysis rate in growing cells [195]. Elevated concentrations of serine might activate PKM2, which increase the production of pyruvate and subsequently ATP within the mitochondrion. The elevated ATP levels subsequently increase GSIS. In line with this observations, it was recently reported that dietary supplementation of L-serine to NOD mice induces improved glucose tolerance, reduces diabetes incidence and insulitis score [197].

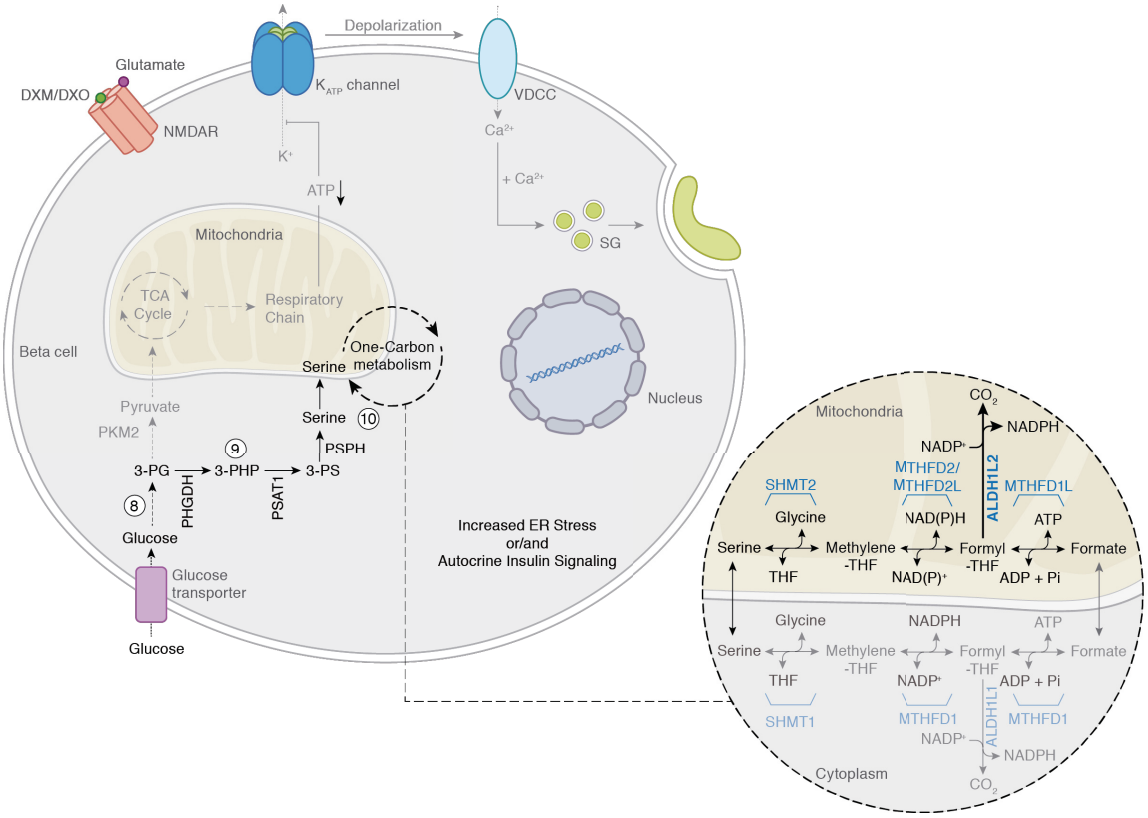

Figure 25: Proposed mechanism induced by the insulin secretagogue DXO changing the glycolytic flux from pyruvate production to the *de novo* serine synthesis pathway and one-carbon metabolism. Chronic stimulation with DXO can activate the autocrine insulin signaling pathway or/and increase ER stress which change as a consequence the glycolytic flux. Glucose enters the β-cell via the glucose transporter and gets metabolized to 3-PG in glycolysis (Step 8). PHGDH diverts glycolytic flux from pyruvate synthesis to the *de novo* serine synthesis pathway (Step 9). Serine enters the mitochondrial one-carbon pathway and gets metabolized (Step 10). Solid black line highlights the enzymes, which were upregulated in the RNA sequencing upon DXO treatment. Abbreviations: 3-PHP, 3-phosphohydroxypyruvate; 3-PG, 3-phosphoglycerate; 3-PS, 3-phosphoserine; ATP, adenosine triphosphate; DXM, dextromethorphan; DXO, dextrorphan; GSIS, glucose-stimulated insulin secretion; K_{ATP} channels, ATP-sensitive potassium channels; NMDAR, N-methyl-D-aspartate receptor; SG, secretory granule; TCA, tricarboxylic acid cycle; THF, 5,6,7,8-tetrahydrofolate; VDCC, voltage-dependent Ca^{2+} channel. Abbreviation of enzymes are in the main text.

Furthermore, at the transcriptional level, it was shown that *Phgdh*, *Psat1*, and *Psph* are targets of ATF4 [195, 198] (Fig. 26, step 11). ATF4 is a transcription factor and master regulator that modulates the expression of genes during cellular stress [199]. *Atf4*-deficient (*Atf4*$^{-/-}$) mice have significantly increased glucose tolerance and elevated levels of serum insulin compared to control mice as well as increased insulin content and enhanced expression of *Ins1* and *Ins2* in the pancreas. Additionally, *Atf4*$^{-/-}$ mice showed enhanced insulin sensitivity in liver, fat, and muscle. Yoshizawa et al. showed convincing evidence that the expression of ATF4 negatively regulates glucose homeostasis [200]. This supports our hypothesis that the increased glycolytic flux from pyruvate production towards *de novo*

serine synthesis by the elevated expression of *Phgdh*, *Pstat1*, and *Psph* upon the increased activity of ATF4 decrease GSIS.

Strikingly, ATF4 is able to increase the transcripts of the key enzymes of the serine synthesis pathway as well as key components of the mitochondrial one-carbon metabolism (Fig. 26) in response to anabolic stimuli like insulin [198]. Stimulation of mouse L cells with insulin increases the mRNA levels of *Phgdh*, *Psat1*, and *Psph* as well as *Shmt2* and *Mthfd2* by increasing ATF4 expression [198]. Adams *et al*. propose that the insulin-mediated increase of ATF4 on mRNA and protein levels is mediated by mTORC1 [198]. These results are supported by a report published by Ben-Sahra *et al*., which indicate that insulin activates mTORC1 and as a consequence increase the ATF4-dependent expression of key enzymes of the mitochondrial one-carbon metabolism as well as enzymes of the *de novo* serine synthesis pathway [201]. Surprisingly, it is proposed that mTORC does not change the expression of genes coding for enzymes of the cytosolic one-carbon metabolism [201]. This supports our data, which show that the expression of cytosolic enzymes of the one-carbon metabolism are not affected upon DXO treatment. Additionally, consistent with our data, showing that genes of the one-carbon metabolism were not affected upon short-term DXO treatment, this report also showed that short-term activation of the cells with insulin did not show changes in the ATF4 transcripts, indicating that the alternative glycolytic pathway is not activated [201].

Furthermore, it is known that the transcriptional activity of ATF4 is increased upon UPR activation [82]. Therefore, we have to consider that the induction of ER stress could also be responsible for the glycolytic flux from glycolysis and TCA to serine synthesis and one-carbon metabolism. A link between increased ER stress, activation of UPR and change in energy metabolism by increasing serine biosynthesis as well as mitochondrial one-carbon metabolism was recently given [202]. Using the potent ER stress inducer tunicamycin in cervical cancer cells, a flow of metabolism from glycolysis and TCA cycle to serine synthesis and one-carbon metabolism was detected [202]. Particularly, tunicamycin treatment increased the translation of proteins involved in the mitochondrial one-carbon metabolism (SHMT2, MTHFD2, ALDH1L2) and the serine biosynthesis (PHGDH, PSAT1, PSPH) [202]. They proposed that this alternative expression ensures NADPH production as well as glycine synthesis for GSH regeneration during ER stress [202]. During protein folding, the formation of disulfide bonds between polypeptide chains generates ROS [203]. If we take into account that the mature insulin needs the formation of three disulfide bounds for the correct folding [203], this indicates an increase in ROS generation upon increased insulin demand. Therefore, it could be speculated that ER stress leads to the glycolytic flux towards one-carbon metabolism and especially ALDH1L2 to generate NADPH, which regenerates GSH and protects the islet cells from oxidative stress. Because β-cells express

only very low levels of enzymes that neutralize ROS [87], the regeneration of glutathione upon overexpression of ALDH1L2 could be a great way to cope with ROS [202].

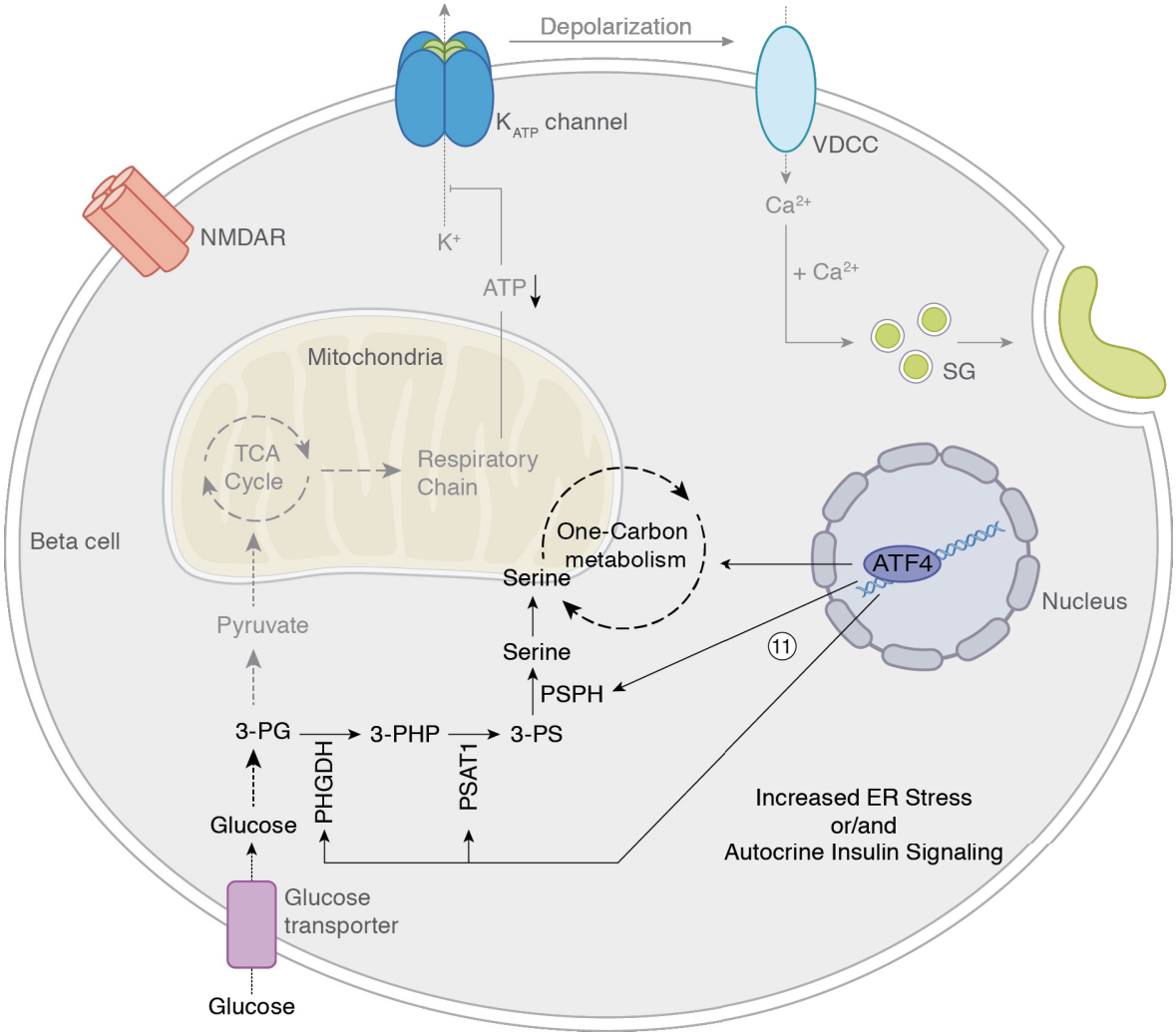

Figure 26: Proposed mechanism of β-cell dysfunction induced by the change in glycolytic flux based on increased activation of ATF4. Reduced GSIS induced by alternative glycolytic pathway. We propose that the autocrine action of insulin or/and increased ER stress enhances ATF4 activity. ATF4 regulates, as a transcription factor, the expression of genes coding for enzymes of the *de novo* serine synthesis pathway as well as genes of the mitochondrial one-carbon metabolism (Step 11). This induces a glycolytic flux from pyruvate synthesis to the *de novo* serine synthesis pathway. A decrease in pyruvate production subsequently decreases the synthesis of ATP and reduces GSIS. Abbreviations: 3-PHP, 3-phosphohydroxypyruvate; 3-PG, 3-phosphoglycerate; 3-PS, 3-phosphoserine; ATF4, activating transcription factor 4; ATP, adenosine triphosphate; GSIS, glucose-stimulated insulin secretion; K_{ATP} channels, ATP-sensitive potassium channels; NMDAR, N-methyl-D-aspartate receptor; SG, secretory granule; TCA, tricarboxylic acid cycle; THF, 5,6,7,8-tetrahydrofolate; VDCC, voltage-dependent Ca^{2+} channel. Abbreviation of enzymes are in the main text.

These findings connect the results, which were obtained during my thesis and propose the following hypothesis (Fig. 26): long-term stimulation of β-cells with insulin secretagogues increase the transcriptional activity of ATF4, which increases the expression of genes coding for enzymes of the *de novo* serine synthesis pathway as well as genes

coding for core enzymes of the mitochondrial one-carbon metabolism. The upregulation of ALDH1L2 acts as the terminal step for the release of carbon groups, pushing glycolysis towards *de novo* serine synthesis, since serine is continuously consumed. We propose that this glycolytic flux from glycolysis and TCA to serine synthesis decreases the level of ATP in the cell. As a consequence, GSIS is decreased, which could explain the phenomenon of β-cell exhaustion. In turn, the flux towards the mitochondrial one-carbon metabolism can prepare the cell additionally to withstand against oxidative stress. Whether the increase in ATF4 activity is induced via autocrine insulin signaling or increased ER stress should be part of further investigation.

6.3.3 Effect of low dose DXM on ALDH1L2 expression level, glucose homeostasis, and insulin secretion

We further evaluated the one-carbon metabolism after *in vivo* administration of DXM in *db*/*db* mice. Mice receiving a higher dosage of DXO showed reduced fasted blood glucose levels compared to control mice. Isolating the islets and analyzing the transcriptome by RNA sequencing revealed that neither genes coding for enzymes of the cytoplasmic nor the mitochondrial one-carbon metabolism were differentially expressed to a significant extent, except *Shmt2*, which is downregulated. Nevertheless, *Aldh1l2* was slightly upregulated. That was confirmed on mRNA and protein level. This leads to the hypothesis that ATF4 is not activated during *in vivo* conditions. This points to the possibility that secreted insulin, which seems to be increased by the administration of DXM, does not bind as an autocrine or paracrine signal to the β-cells itself. We hypothesize that insulin is rather directly transported through the microvascular system to mainly target other cells (such as hepatocytes) without binding to its receptor on β-cells first. Additionally, we have to take into account that the change in plasma blood glucose levels between the *db*/*db* mice due to different dosage of DXM can act as an additional trigger to modulate insulin secretion and β-cell exhaustion. In contrast to sulfonylureas, which increase insulin under glucose-stimulated as well as basal conditions, the insulin secretagogue DXM enhances insulin secretion under increased glucose concentrations without altering glucose concentrations under basal conditions [114]. Therefore, we could speculate that the decrease in plasma glucose levels do not further exhaust the β-cell, and therefore, ER stress and as a consequence ATF4 is not increased due to the higher dosage of DXM treatment.

Additionally, *in vitro* long-term treatment of islets with 1 µM DXO, instead of 10 µM DXO, decreases insulin content, but does not decrease GSIS. From previous studies we know that the increase in GSIS upon DXO treatment is dose-dependent [114], meaning that upon 1 µM DXO treatment under continuous glucose concentrations less insulin is synthesized as well as released. As a consequence, less insulin binds to the insulin

receptor. This is in line with the RNA sequencing data, indicating that upon 1 µM DXO treatment the expression of the core enzymes of the mitochondrial one-carbon metabolism were less increased compared to 10 µM DXO. These results points to the possibility that the synthesis of insulin or the concentration of insulin surrounding the β-cell must increase to a certain threshold to induce prolonged ATF4 activation, which as a consequence increases the expression of genes coding for the core enzymes of the mitochondrial one-carbon metabolism to an extent that reduces GSIS.

6.4 Role of ALDH1L2 in islet cell viability

It is known that the mitochondrial one-carbon metabolism in cancer cells is activated to withstand oxidative stress [183]. Therefore, we hypothesized that the protective mechanism against pro-inflammatory cytokines upon DXO treatment may result from the upregulation of key enzymes of the mitochondrial one-carbon metabolism, especially ALDH1L2. To figure out if ALDH1L2 protects islets during inflammatory conditions, we performed loss-of-function and gain-of-function experiments. Our experiments showed that the sole overexpression as well as loss of ALDH1L2 in pancreatic islet cells does not influence cell viability. Additionally, neither the overexpression nor the deletion of ALDH1L2 in pancreatic islet cells showed any effect during cytokine-induced cell death.

The major source of one-carbon metabolism to cope with oxidative stress is the generation of NADPH [183]. In cancer cells, it is proposed that the physiologically significant mitochondrial NADPH production via ALDH1L2 and probably MTHFD2 could be an important part of the redox homeostasis [145]. This increase in NADPH is proposed to enhance the capacity to generate GSH from GSSG (GSH/GSSG ratio) [183]. Glutathione is an important antioxidant in the β-cell. Once glutathione is oxidized by free radicals, it has to be converted in its reduced form by glutathione reductase with NADPH as a cofactor [190]. These facts lead to the hypothesis that the overexpression of ALDH1L2 protects against cytokine-induced cell death, whereas knockout of ALDH1L2 would make the cell vulnerable to oxidative stress. However, our experiments point to the possibility that ALDH1L2 does not participate in the protection of islet cells. The missing effects during ALDH1L2 overexpression could be explained by the lack of the upstream enzymes of the mitochondrial one-carbon pathway. The decreased availability of substrates for ALDH1L2 could reduce the effect of ALDH1L2 and decrease the amount of NADPH. Therefore, it is possible that overexpressing ALDH1L2 alone does not supply enough reducing power to keep a sufficient amount of NADPH to reduce GSH from GSSG. As the mitochondrial one-carbon metabolism can produce NADPH via the enzymes ALDH1L2 and MTHFD2, it points to the possibility that both or even all enzymes, which participate in the mitochondrial one-

carbon metabolism, should be overexpressed to see any effect.

7 Outlook

The concept of β-cell exhaustion during the development of T2DM is still under debate. In this work, I present a new possible mechanism leading to this process induced upon increased secretion demand. The alternative flux from glycolysis and the TCA cycle to the biosynthesis of serine and activation of the mitochondrial one-carbon metabolism as well as the increased expression of the mitochondrial localized enzyme ALDH1L2 could be one possible mechanism inducing impaired insulin secretion. It is of large interest to reveal the molecular mechanism to discover new therapeutic targets and stop the progression of diabetes. With add-on experiments, we have to gain more insight into the molecular mechanism as well as connecting the different “pieces of the puzzle” to understand the complex metabolism. Many questions still remain and have to be answered in the next months to highlight the importance of these new findings.

First, we have to figure out if β-cell dedifferentiation and the one-carbon metabolism are connected. We have to address the question whether the decreased insulin content is due to decreased transcription of *Ins1* and *Ins2* as well as the key transcription factor *Mafa* or does the highly increased release of insulin lead to empty insulin stores. Additionally, to check if the insulin secretagogue DXO induces β-cell exhaustion, we have to figure out if the phenomenon of decreased insulin secretion is reversible after rescue as it is proposed [72, 79].

Secondly, we have to evaluate if the impairment in insulin secretion is based on the alternative flux from glycolysis and the TCA cycle to serine synthesis and one-carbon metabolism. This could be tested by the pharmacologically and genetically inactivation of the enzyme PHGDH, which catalyzes the first rate-limiting step of the glucose-derived serine synthesis [204]. Due to our mechanism, we propose that blocking of this enzyme by using the pharmacological inhibitor NCT-503 [204] reduces the alternative glycolytic flux towards serine pushing the metabolism towards the TCA cycle and generation of ATP. If the inactivation of PHGDH would restore proper GSIS during long-term treatment with the insulin secretagogue DXO, we could conclude that glucose-derived serine synthesis and one-carbon metabolism attenuate GSIS. To restore glycolysis and TCA cycle by blocking PHGDH would represent a new therapeutic target.

Thirdly, we have to prove our proposed mechanisms of action. We claim that the increased activity of ATF4 on transcriptional level can be on the one hand induced by the autocrine insulin signaling and on the other hand due to increased ER stress and activation of the UPR. We can uncover these hypotheses with several molecular methods. The treatment of pancreatic islets with insulin, with subsequent expression analysis of enzymes of the *de novo* serine biosynthesis and the one-carbon metabolism, especially the expression of ALDH1L2, would give important insight into the molecular mechanism. To

check if ER stress is responsible for the metabolic flux during glycolysis rather than the autocrine action of insulin, functional assays with the ER stressors tunicamycin and thapsigargin should be performed. Additionally, ATF4 silencing with siRNA or knockout with the *CRISPR/Cas9* system would be of interest. This would provide new insights into the ATF4 signaling cascade upstream of DXO.

Fourthly, it is also important to further investigate the protective effect of ALDH1L2 as it is proposed in the literature [145, 183]. Unfortunately, we did not detect any protection in ALDH1L2-overexpressing pseudo-islets against cytokine-induced cell death. Thus, we have to improve the experimental setup using, for example, alternative stressors. Besides cytokines, oxidative stress can be induced by H_2O_2. *Aldh1l2*-deficient as well as *Mthfd2*-deficient HEK293T cells are vulnerable to cell death induced by H_2O_2 [145]. Whether this is also true in pancreatic β-cells requires further investigation. Additionally, we could improve our experimental setup by the overexpression of several genes of the one-carbon metabolism at the same time. This would better reflect the conditions, which were achieved upon DXO treatment.

With my work, I hope to contribute to the understanding of the new molecular mechanism that attenuates GSIS and decreases glucose tolerance in patients with T2DM. If further experiments support our hypothesis, ALDH1L2 could be used as a new therapeutic target in the treatment of diabetes mellitus.

8 List of Abbreviations

A

Acetyl-CoA	Acetly-coenzym A
ACTB	Beta-Actin
ADP	Adenosine diphosphate
ALDH1L1	Aldehyde dehydrogenase 1 family member L1
ALDH1L2	Aldehyde dehydrogenase 1 family member L2
AMPA	α-Amino-3-hydroxy-5-methylisoxazole-4-propionic acid
ANOVA	Analysis of variance
APC	Antigen-presenting cells
ATF4	Activating transcription factor 4
ATF6	Activating transcription factor 6
ATP	Adenosine triphosphate

B

B2M	Beta-2 microtubulin
bp	Base pair
BSA	Bovine serum albumin

C

Ca^{2+}	Calcium
cDNA	Complementary DNA
CMRL	Connaught Medical Research Laboratories medium 1066
CMV	Cytomegalovirus
COX IV	Cytochrome c oxidase IV
C_T	Cycle threshold

D

DAPI	4’,6-Diamidino-2-Phenylindole
DC	Dendritic cell
DEMEM	Dulbecco's Modified Eagle's Medium
DHFR	Dihydrofolate reductase
DMSO	Dimethyl sulfoxide
DNA	Deoxyribonucleic acid
DPBS	Dulbecco's phosphate-buffered saline
DPP-4	Dipeptidyl peptidase-4
DXM	Dextromethorphan

DXO	Dextrorphan

E

4E-BP1	Eukaryotic translation initiation factor 4E-binding protein 1
EAATs	Excitatory amino acid transporters
EDTA	Ethylenediaminetetraacetic acid
eGFP	Enhanced green fluorescent protein
ELISA	Enzyme-linked immunosorbent assay
ER	Endoplasmic reticulum

F

$FADH_2$	Flavin adenine dinucleotide
FBS	Fetal bovine serum
FC	Fold change
FDA	Food and Drug Administration
FDR	False discovery rate
FPKM	Fragments per kilobase of transcript per million mapped reads

G

G	Gastrin
GABA	γ-aminobutyric acid
GAD	Glutamic acid decarboxylase
GAPDH	Glyceraldehyde 3-phosphate dehydrogenase
Glib	Glibenclamide
GLP-1	Glucagon-like peptide 1
GLUT1-14	Gucose transporter 1-14
GSIS	Glucose-stimulated insulin secretion

H

H_2O_2	Hydrogen peroxide
HbA1c	Glycated hemoglobin
HEPES	4-(2-hydroxyethyl)-1-piperazineethanesulfonic acid
HRP	Horseradish peroxidase
HLA	Human leukocyte antigen

I

IA-2	Islet tyrosine phosphatase 2

ICA	Islet cell cytoplasmic antibodies
IFN-γ	Interferon-γ
IL	Interleukin
Ins1	Insulin 1
Ins2	Insulin 2
ipGTT	Intraperitoneal glucose tolerance test
IRE1	Inositol-requiring enzyme

K

K^+	Potassium
kDa	Kilodalton
K_{ATP}	ATP-sensitive potassium channel
KO	Knockout

L

LC-MS/MS	Liquid chromatography-tandem mass spectrometry
Log2 FC	Log2 Fold Change
LSM	Laser scan microscopy

M

M	Molar
MafA	MAF BZIP transcription factor A
MCP-1	Monocyte chemotactic protein-1
MFT	Mitochondrial folate transporter
Mg^{2+}	Magnesium
min	Minute
MOI	Multiplicity of infection
mRNA	Messenger ribonucleic acid
MFT	Mitochondrial folate transporter
MTHFD1	Methylenetetrahydrofolate dehydrogenase, cyclohydrolase and formyltetrahydrofolate synthetase 1
MTHFD2	Methylenetetrahydrofolate dehydrogenase ($NADP^+$ dependent) 2, methenyltetrahydrofolate cyclohydrolase
mTOR	Mechanistic target of rapamycin

N

Na^+	Sodium

NaCl	Sodium chloride
NaF	Sodium fluoride
NAD(H)	Nicotinamide adenine dinucleotide
NADP(H)	Nicotinamide adenine dinucleotide phosphate
NDS	Normal donkey serum
NEFA	Non-esterified fatty acid
Neurog3	Neurogenin 3
NGS	Normal goat serum
Nkx6.1	NK6 homeobox 1
NMDA	N-methyl-D-aspartate
NonT2DM	Non-diabetic donor

O

o/n	Over night
OGTT	Oral glucose tolerance test

P

3-PG	3-Phospho-glycerate
3-PHP	3-Phosphohydroxypyruvate
3-PS	3-Phosphoserine
PBS	Phosphate-buffered saline
PBS-T	PBS + 0.1% Tween-20
PCR	Polymerase chain reaction
Pdx1	Pancreatic and duodenal homeobox 1
PERK	Protein kinase RNA-like endoplasmic reticulum kinase
PFA	Paraformaldehyde
PHGDH	Phosphoglycerate dehydrogenase
PP	Pancreatic polypeptide
PSAT1	Phosphoserine aminotransferase 1
PSPH	Phosphoserine phosphatase

R

RIPA	Radioimmunoprecipitation assay
rpm	Revolutions per minute
RNA	Ribonucleic acid
ROS	Reactive oxygen species
RSV	Robus Sarcoma Virus

RT	Room temperature

S

SD	Standard deviation
SEM	Standard error of the mean
SG	Secretory granule
siRNA	Silencing interfering RNA
SGLT	Sodium/glucose cotransporter
SHMT1	Serine hydroxymethyltransferase 1
SHMT2	Serine hydroxymethyltransferase 2
SK4 channel	Ca^{2+}-activated K^{+}-channel 4
STZ	Streptozotocin

T

T1DM	Type 1 diabetes mellitus
T2DM	Type 2 diabetes mellitus
TCA	Tricarboxylic acid cycle
THF	5,6,7,8-Tetrahydrofolate
TNF-α	Tumor necrosis factor-α
tRNA	Transfer RNA
TUNEL	TdT-mediated dUTP-X nick end labeling

U

U	Unit
UPR	Unfolded protein response

V

V	Volt
VDCC	Voltage-dependent Ca^{2+} channel
Vol	Volume

Z

Zn^{2+}	Zinc
ZnT8A	Zinc transporter-8 antibodies

9 References

[1] Röder PV, Wu B, Liu Y, Han W. Pancreatic regulation of glucose homeostasis. *Experimental &Amp; Molecular Medicine*. 2016; 48: e219

[2] Langerhans PM, H. Contributions to the Microscopic Anatomy of the Pancreas ... Berlin, 1869. Reprint of the German Original with an English Translation and an Introductory Essay by H. Morrison. [With Portraits.]: Baltimore, 1937.

[3] Mandarim-de-Lacerda CA. Pancreatic islet (of Langerhans) revisited. *Histol Histopathol*. 2019: 18118

[4] Hart NJ, Powers AC. Use of human islets to understand islet biology and diabetes: progress, challenges and suggestions. *Diabetologia*. 2019; 62: 212-222

[5] Dolensek J, Rupnik MS, Stozer A. Structural similarities and differences between the human and the mouse pancreas. *Islets*. 2015; 7: e1024405

[6] Betts J.G. YKA, Wise J.A., Johnson E., Poe B., Kruse D.H., Korol O., Johnson J.E., Womble M., DeSaix P. Anatomy and Physiology Houston, Texas OpenStax 2013; Access for free at https://openstax.org/books/anatomy-and-physiology/pages/1-introduction; Section URL: https://openstax.org/books/anatomy-and-physiology/pages/17-9-the-endocrine-pancreas

[7] Eberhard D, Kragl M, Lammert E. 'Giving and taking': endothelial and beta-cells in the islets of Langerhans. *Trends Endocrinol Metab*. 2010; 21: 457-463

[8] Eberhard D, Lammert E. The pancreatic beta-cell in the islet and organ community. *Curr Opin Genet Dev*. 2009; 19: 469-475

[9] Güemes M, Rahman SA, Hussain K. What is a normal blood glucose? *Arch Dis Child*. 2016; 101: 569-574

[10] Ramnanan CJ, Edgerton DS, Kraft G, Cherrington AD. Physiologic action of glucagon on liver glucose metabolism. *Diabetes Obes Metab*. 2011; 13 Suppl 1: 118-125

[11] Hubbard SR. The insulin receptor: both a prototypical and atypical receptor tyrosine kinase. *Cold Spring Harb Perspect Biol*. 2013; 5: a008946

[12] Navale AM, Paranjape AN. Glucose transporters: physiological and pathological roles. *Biophys Rev*. 2016; 8: 5-9

[13] Augustin R. The protein family of glucose transport facilitators: It's not only about glucose after all. *IUBMB Life*. 2010; 62: 315-333

[14] Thorens B. GLUT2, glucose sensing and glucose homeostasis. *Diabetologia*. 2015; 58: 221-232

[15] McCulloch LJ, van de Bunt M, Braun M, Frayn KN, Clark A, Gloyn AL. GLUT2 (SLC2A2) is not the principal glucose transporter in human pancreatic beta cells: implications for understanding genetic association signals at this locus. *Mol Genet Metab*. 2011; 104: 648-653

[16] Vakilian M, Tahamtani Y, Ghaedi K. A review on insulin trafficking and exocytosis. *Gene*. 2019; 706: 52-61

[17] Jitrapakdee S, Wutthisathapornchai A, Wallace JC, MacDonald MJ. Regulation of insulin secretion: role of mitochondrial signalling. *Diabetologia*. 2010; 53: 1019-1032

[18] Rutter GA, Hill EV. Insulin vesicle release: walk, kiss, pause ... then run. *Physiology (Bethesda)*. 2006; 21: 189-196

[19] Nunemaker CS, Satin LS. Episodic hormone secretion: a comparison of the basis of pulsatile secretion of insulin and GnRH. *Endocrine*. 2014; 47: 49-63

[20] Matthews DR, Naylor BA, Jones RG, Ward GM, Turner RC. Pulsatile insulin has greater hypoglycemic effect than continuous delivery. *Diabetes*. 1983; 32: 617-621

[21] Satin LS, Butler PC, Ha J, Sherman AS. Pulsatile insulin secretion, impaired glucose tolerance and type 2 diabetes. *Mol Aspects Med*. 2015; 42: 61-77

[22] Ritzel RA, Veldhuis JD, Butler PC. Glucose stimulates pulsatile insulin secretion from human pancreatic islets by increasing secretory burst mass: dose-response relationships. *J Clin Endocrinol Metab*. 2003; 88: 742-747

[23] Pedersen MG, Tagliavini A, Henquin JC. Calcium signaling and secretory granule pool dynamics underlie biphasic insulin secretion and its amplification by glucose: experiments and modeling. *Am J Physiol Endocrinol Metab*. 2019; 316: E475-e486
[24] Saeedi P, Petersohn I, Salpea P*, et al.* Global and regional diabetes prevalence estimates for 2019 and projections for 2030 and 2045: Results from the International Diabetes Federation Diabetes Atlas, 9(th) edition. *Diabetes Res Clin Pract*. 2019; 157: 107843
[25] International Diabetes Federation. International Diabetes Federation, 2019:Available at: http://www.diabetesatlas.org
[26] Alberti KGMM, Zimmet Pf. Definition, diagnosis and classification of diabetes mellitus and its complications. Part 1: diagnosis and classification of diabetes mellitus. Provisional report of a WHO consultation. *Diabetic medicine*. 1998; 15: 539-553
[27] International Diabetes Federation. International Diabetes Federation, 2017:Available at: http://www.diabetesatlas.org
[28] American Diabetes Association. Diagnosis and classification of diabetes mellitus. *Diabetes care*. 2013; 36: S67-S74
[29] Saberzadeh-Ardestani B, Karamzadeh R, Basiri M*, et al.* Type 1 Diabetes Mellitus: Cellular and Molecular Pathophysiology at A Glance. *Cell J*. 2018; 20: 294-301
[30] Skyler JS, Bakris GL, Bonifacio E*, et al.* Differentiation of Diabetes by Pathophysiology, Natural History, and Prognosis. *Diabetes*. 2017; 66: 241-255
[31] Long SA, Cerosaletti K, Bollyky PL*, et al.* Defects in IL-2R signaling contribute to diminished maintenance of FOXP3 expression in CD4(+)CD25(+) regulatory T-cells of type 1 diabetic subjects. *Diabetes*. 2010; 59: 407-415
[32] Santin I, Eizirik DL. Candidate genes for type 1 diabetes modulate pancreatic islet inflammation and beta-cell apoptosis. *Diabetes Obes Metab*. 2013; 15 Suppl 3: 71-81
[33] Noble JA, Valdes AM. Genetics of the HLA region in the prediction of type 1 diabetes. *Curr Diab Rep*. 2011; 11: 533-542
[34] Xia Y, Xie Z, Huang G, Zhou Z. Incidence and trend of type 1 diabetes and the underlying environmental determinants. *Diabetes/metabolism research and reviews*. 2019; 35: e3075
[35] Zheng P, Li Z, Zhou Z. Gut microbiome in type 1 diabetes: A comprehensive review. *Diabetes Metab Res Rev*. 2018; 34: e3043
[36] American Diabetes Association. 2. Classification and Diagnosis of Diabetes: Standards of Medical Care in Diabetes-2019. *Diabetes Care*. 2019; 42: S13-s28
[37] Klöppel G, Drenck CR, Oberholzer M, Heitz PU. Morphometric evidence for a striking B-cell reduction at the clinical onset of type 1 diabetes. *Virchows Archiv A*. 1984; 403: 441-452
[38] Willcox A, Richardson SJ, Bone AJ, Foulis AK, Morgan NG. Analysis of islet inflammation in human type 1 diabetes. *Clin Exp Immunol*. 2009; 155: 173-181
[39] Nunemaker CS. Considerations for Defining Cytokine Dose, Duration, and Milieu That Are Appropriate for Modeling Chronic Low-Grade Inflammation in Type 2 Diabetes. *J Diabetes Res*. 2016; 2016: 2846570
[40] Delaney CA, Pavlovic D, Hoorens A, Pipeleers DG, Eizirik DL. Cytokines induce deoxyribonucleic acid strand breaks and apoptosis in human pancreatic islet cells. *Endocrinology*. 1997; 138: 2610-2614
[41] Pukel C, Baquerizo H, Rabinovitch A. Destruction of rat islet cell monolayers by cytokines. Synergistic interactions of interferon-gamma, tumor necrosis factor, lymphotoxin, and interleukin 1. *Diabetes*. 1988; 37: 133-136
[42] Eizirik DL, Mandrup-Poulsen T. A choice of death--the signal-transduction of immune-mediated beta-cell apoptosis. *Diabetologia*. 2001; 44: 2115-2133
[43] Gorsuch AN, Spencer KM, Lister J*, et al.* Evidence for a long prediabetic period in type I (insulin-dependent) diabetes mellitus. *Lancet*. 1981; 2: 1363-1365
[44] Knip M. Natural course of preclinical type 1 diabetes. *Horm Res*. 2002; 57 Suppl 1: 6-11

[45] Notkins AL, Lernmark A. Autoimmune type 1 diabetes: resolved and unresolved issues. *J Clin Invest*. 2001; 108: 1247-1252
[46] Palmer JP, Asplin CM, Clemons P*, et al.* Insulin antibodies in insulin-dependent diabetics before insulin treatment. *Science*. 1983; 222: 1337-1339
[47] De Aizpurua HJ, Wilson YM, Harrison LC. Glutamic acid decarboxylase autoantibodies in preclinical insulin-dependent diabetes. *Proceedings of the National Academy of Sciences of the United States of America*. 1992; 89: 9841-9845
[48] Rabin DU, Pleasic SM, Shapiro JA*, et al.* Islet cell antigen 512 is a diabetes-specific islet autoantigen related to protein tyrosine phosphatases. *J Immunol*. 1994; 152: 3183-3188
[49] Marner B, Bille G, Christy M*, et al.* Islet cell cytoplasmic antibodies (ICA) in diabetes and disorders of glucose tolerance. *Diabet Med*. 1991; 8: 812-816
[50] Wenzlau JM, Juhl K, Yu L*, et al.* The cation efflux transporter ZnT8 (Slc30A8) is a major autoantigen in human type 1 diabetes. *Proc Natl Acad Sci U S A*. 2007; 104: 17040-17045
[51] Chen C, Cohrs CM, Stertmann J, Bozsak R, Speier S. Human beta cell mass and function in diabetes: Recent advances in knowledge and technologies to understand disease pathogenesis. *Mol Metab*. 2017; 6: 943-957
[52] Koskinen MK, Helminen O, Matomäki J*, et al.* Reduced β-cell function in early preclinical type 1 diabetes. *Eur J Endocrinol*. 2016; 174: 251-259
[53] Rodriguez-Calvo T, Zapardiel-Gonzalo J, Amirian N*, et al.* Increase in Pancreatic Proinsulin and Preservation of beta-Cell Mass in Autoantibody-Positive Donors Prior to Type 1 Diabetes Onset. *Diabetes*. 2017; 66: 1334-1345
[54] Butler AE, Galasso R, Meier JJ, Basu R, Rizza RA, Butler PC. Modestly increased beta cell apoptosis but no increased beta cell replication in recent-onset type 1 diabetic patients who died of diabetic ketoacidosis. *Diabetologia*. 2007; 50: 2323-2331
[55] in't Veld P. Rodent versus human insulitis: why the huge disconnect? *Curr Opin Endocrinol Diabetes Obes*. 2015; 22: 86-90
[56] Abdul-Rasoul M, Habib H, Al-Khouly M. 'The honeymoon phase' in children with type 1 diabetes mellitus: frequency, duration, and influential factors. *Pediatr Diabetes*. 2006; 7: 101-107
[57] Ashcroft FM, Rorsman P. Diabetes mellitus and the β cell: the last ten years. *Cell*. 2012; 148: 1160-1171
[58] Welters A, Lammert E. Diabetes Mellitus. In: Lammert E, Zeeb M, eds. Metabolism of Human Diseases: Organ Physiology and Pathophysiology. Vienna: Springer Vienna, 2014:163-169
[59] Barreira E, Novo A, Vaz JA, Pereira AMG. Dietary program and physical activity impact on biochemical markers in patients with type 2 diabetes: A systematic review. *Aten Primaria*. 2018; 50: 590-610
[60] Kahn SE, Hull RL, Utzschneider KM. Mechanisms linking obesity to insulin resistance and type 2 diabetes. *Nature*. 2006; 444: 840-846
[61] Shao L, Feng B, Zhang Y, Zhou H, Ji W, Min W. The role of adipose-derived inflammatory cytokines in type 1 diabetes. *Adipocyte*. 2016; 5: 270-274
[62] Rocha VZ, Folco EJ. Inflammatory concepts of obesity. *Int J Inflam*. 2011; 2011: 529061-529061
[63] Smith U, Kahn BB. Adipose tissue regulates insulin sensitivity: role of adipogenesis, de novo lipogenesis and novel lipids. *J Intern Med*. 2016; 280: 465-475
[64] Arita Y, Kihara S, Ouchi N*, et al.* Paradoxical decrease of an adipose-specific protein, adiponectin, in obesity. *Biochem Biophys Res Commun*. 1999; 257: 79-83
[65] Tong HV, Luu NK, Son HA*, et al.* Adiponectin and pro-inflammatory cytokines are modulated in Vietnamese patients with type 2 diabetes mellitus. *J Diabetes Investig*. 2017; 8: 295-305
[66] Porte D, Jr. Clinical importance of insulin secretion and its interaction with insulin resistance in the treatment of type 2 diabetes mellitus and its complications. *Diabetes Metab Res Rev*. 2001; 17: 181-188

[67] Stumvoll M, Goldstein BJ, van Haeften TW. Type 2 diabetes: principles of pathogenesis and therapy. *Lancet*. 2005; 365: 1333-1346
[68] Prentki M, Nolan CJ. Islet beta cell failure in type 2 diabetes. *J Clin Invest*. 2006; 116: 1802-1812
[69] Olehnik SK, Fowler JL, Avramovich G, Hara M. Quantitative analysis of intra- and inter-individual variability of human beta-cell mass. *Sci Rep*. 2017; 7: 16398
[70] Rahier J, Guiot Y, Goebbels RM, Sempoux C, Henquin JC. Pancreatic beta-cell mass in European subjects with type 2 diabetes. *Diabetes Obes Metab*. 2008; 10 Suppl 4: 32-42
[71] Butler AE, Janson J, Bonner-Weir S, Ritzel R, Rizza RA, Butler PC. Beta-cell deficit and increased beta-cell apoptosis in humans with type 2 diabetes. *Diabetes*. 2003; 52: 102-110
[72] Swisa A, Glaser B, Dor Y. Metabolic Stress and Compromised Identity of Pancreatic Beta Cells. *Front Genet*. 2017; 8: 21
[73] Talchai C, Xuan S, Lin HV, Sussel L, Accili D. Pancreatic beta cell dedifferentiation as a mechanism of diabetic beta cell failure. *Cell*. 2012; 150: 1223-1234
[74] Cho J-H, Kim J-W, Shin J-A, Shin J, Yoon K-H. β-cell mass in people with type 2 diabetes. *J Diabetes Investig*. 2011; 2: 6-17
[75] Sakuraba H, Mizukami H, Yagihashi N, Wada R, Hanyu C, Yagihashi S. Reduced beta-cell mass and expression of oxidative stress-related DNA damage in the islet of Japanese Type II diabetic patients. *Diabetologia*. 2002; 45: 85-96
[76] Yoon KH, Ko SH, Cho JH*, et al.* Selective beta-cell loss and alpha-cell expansion in patients with type 2 diabetes mellitus in Korea. *J Clin Endocrinol Metab*. 2003; 88: 2300-2308
[77] Marchetti P, Del Guerra S, Marselli L*, et al.* Pancreatic islets from type 2 diabetic patients have functional defects and increased apoptosis that are ameliorated by metformin. *J Clin Endocrinol Metab*. 2004; 89: 5535-5541
[78] Leibowitz G, Kaiser N, Cerasi E. beta-Cell failure in type 2 diabetes. *J Diabetes Investig*. 2011; 2: 82-91
[79] Robertson RP, Harmon J, Tran PO, Tanaka Y, Takahashi H. Glucose toxicity in β-cells: type 2 diabetes, good radicals gone bad, and the glutathione connection. *Diabetes*. 2003; 52: 581-587
[80] Fonseca SG, Gromada J, Urano F. Endoplasmic reticulum stress and pancreatic β-cell death. *Trends Endocrinol Metab*. 2011; 22: 266-274
[81] Scheuner D, Kaufman RJ. The unfolded protein response: a pathway that links insulin demand with beta-cell failure and diabetes. *Endocr Rev*. 2008; 29: 317-333
[82] Eizirik DL, Miani M, Cardozo AK. Signalling danger: endoplasmic reticulum stress and the unfolded protein response in pancreatic islet inflammation. *Diabetologia*. 2013; 56: 234-241
[83] Yamaguchi S, Ishihara H, Yamada T*, et al.* ATF4-mediated induction of 4E-BP1 contributes to pancreatic beta cell survival under endoplasmic reticulum stress. *Cell Metab*. 2008; 7: 269-276
[84] Izumi T, Yokota-Hashimoto H, Zhao S, Wang J, Halban PA, Takeuchi T. Dominant Negative Pathogenesis by Mutant Proinsulin in the Akita Diabetic Mouse. *Diabetes*. 2003; 52: 409-416
[85] Cnop M, Ladriere L, Igoillo-Esteve M, Moura RF, Cunha DA. Causes and cures for endoplasmic reticulum stress in lipotoxic beta-cell dysfunction. *Diabetes Obes Metab*. 2010; 12 Suppl 2: 76-82
[86] Laybutt DR, Preston AM, Akerfeldt MC*, et al.* Endoplasmic reticulum stress contributes to beta cell apoptosis in type 2 diabetes. *Diabetologia*. 2007; 50: 752-763
[87] Wang J, Wang H. Oxidative Stress in Pancreatic Beta Cell Regeneration. *Oxid Med Cell Longev*. 2017; 2017: 1930261-1930261
[88] Cinti F, Bouchi R, Kim-Muller JY*, et al.* Evidence of β-Cell Dedifferentiation in Human Type 2 Diabetes. *The Journal of Clinical Endocrinology & Metabolism*. 2016; 101: 1044-1054

[89] Wang Z, York NW, Nichols CG, Remedi MS. Pancreatic beta cell dedifferentiation in diabetes and redifferentiation following insulin therapy. *Cell Metab*. 2014; 19: 872-882
[90] International Expert Committee. International Expert Committee report on the role of the A1C assay in the diagnosis of diabetes. *Diabetes care*. 2009; 32: 1327-1334
[91] Bonadonna RC, Borghi C, Consoli A, Volpe M. Novel antidiabetic drugs and cardiovascular risk: Primum non nocere. *Nutr Metab Cardiovasc Dis*. 2016; 26: 759-766
[92] American Diabetes Association. 8. Pharmacologic Approaches to Glycemic Treatment: Standards of Medical Care in Diabetes-2018. *Diabetes Care*. 2018; 41: S73-s85
[93] Krentz AJ, Bailey CJ. Oral antidiabetic agents: current role in type 2 diabetes mellitus. *Drugs*. 2005; 65: 385-411
[94] Nakatsuma A, Kiriyama Y, Kino K, Ninomiya M. Diabetes drugs that protect pancreatic β cells. *Integrative Molecular Medicine*. 2016; 3:
[95] Welters A, Kluppel C, Mrugala J*, et al.* NMDAR antagonists for the treatment of diabetes mellitus-Current status and future directions. *Diabetes Obes Metab*. 2017; 19 Suppl 1: 95-106
[96] Tuomilehto J, Lindstrom J, Eriksson JG*, et al.* Prevention of type 2 diabetes mellitus by changes in lifestyle among subjects with impaired glucose tolerance. *N Engl J Med*. 2001; 344: 1343-1350
[97] Knowler WC, Barrett-Connor E, Fowler SE*, et al.* Reduction in the incidence of type 2 diabetes with lifestyle intervention or metformin. *N Engl J Med*. 2002; 346: 393-403
[98] Hunter RW, Hughey CC, Lantier L*, et al.* Metformin reduces liver glucose production by inhibition of fructose-1-6-bisphosphatase. *Nat Med*. 2018; 24: 1395-1406
[99] Kahn SE, Haffner SM, Heise MA*, et al.* Glycemic Durability of Rosiglitazone, Metformin, or Glyburide Monotherapy. *New England Journal of Medicine*. 2006; 355: 2427-2443
[100] Turner RC, Cull CA, Frighi V, Holman RR. Glycemic control with diet, sulfonylurea, metformin, or insulin in patients with type 2 diabetes mellitus: progressive requirement for multiple therapies (UKPDS 49). UK Prospective Diabetes Study (UKPDS) Group. *Jama*. 1999; 281: 2005-2012
[101] Cook MN, Girman CJ, Stein PP, Alexander CM. Initial monotherapy with either metformin or sulphonylureas often fails to achieve or maintain current glycaemic goals in patients with Type 2 diabetes in UK primary care. *Diabet Med*. 2007; 24: 350-358
[102] Nauck M, Frid A, Hermansen K*, et al.* Long-term efficacy and safety comparison of liraglutide, glimepiride and placebo, all in combination with metformin in type 2 diabetes: 2-year results from the LEAD-2 study. *Diabetes Obes Metab*. 2013; 15: 204-212
[103] Bennett WL, Maruthur NM, Singh S*, et al.* Comparative effectiveness and safety of medications for type 2 diabetes: an update including new drugs and 2-drug combinations. *Ann Intern Med*. 2011; 154: 602-613
[104] Phung OJ, Scholle JM, Talwar M, Coleman CI. Effect of Noninsulin Antidiabetic Drugs Added to Metformin Therapy on Glycemic Control, Weight Gain, and Hypoglycemia in Type 2 Diabetes. *JAMA*. 2010; 303: 1410-1418
[105] Nauck MA, Hompesch M, Filipczak R, Le TD, Zdravkovic M, Gumprecht J. Five weeks of treatment with the GLP-1 analogue liraglutide improves glycaemic control and lowers body weight in subjects with type 2 diabetes. *Exp Clin Endocrinol Diabetes*. 2006; 114: 417-423
[106] Davies MJ. Insulin secretagogues. *Curr Med Res Opin*. 2002; 18 Suppl 1: s22-30
[107] Abdulreda MH, Rodriguez-Diaz R, Caicedo A, Berggren PO. Liraglutide Compromises Pancreatic beta Cell Function in a Humanized Mouse Model. *Cell Metab*. 2016; 23: 541-546

[108] Baggio LL, Drucker DJ. Biology of incretins: GLP-1 and GIP. *Gastroenterology*. 2007; 132: 2131-2157
[109] Aston-Mourney K, Proietto J, Morahan G, Andrikopoulos S. Too much of a good thing: why it is bad to stimulate the beta cell to secrete insulin. *Diabetologia*. 2008; 51: 540-545
[110] Tentolouris A, Vlachakis P, Tzeravini E, Eleftheriadou I, Tentolouris N. SGLT2 Inhibitors: A Review of Their Antidiabetic and Cardioprotective Effects. *Int J Environ Res Public Health*. 2019; 16:
[111] Birkeland KI, Jorgensen ME, Carstensen B*, et al.* Cardiovascular mortality and morbidity in patients with type 2 diabetes following initiation of sodium-glucose co-transporter-2 inhibitors versus other glucose-lowering drugs (CVD-REAL Nordic): a multinational observational analysis. *Lancet Diabetes Endocrinol*. 2017; 5: 709-717
[112] Kosiborod M, Cavender MA, Fu AZ*, et al.* Lower Risk of Heart Failure and Death in Patients Initiated on Sodium-Glucose Cotransporter-2 Inhibitors Versus Other Glucose-Lowering Drugs: The CVD-REAL Study (Comparative Effectiveness of Cardiovascular Outcomes in New Users of Sodium-Glucose Cotransporter-2 Inhibitors). *Circulation*. 2017; 136: 249-259
[113] Del Prato S, Nauck M, Duran-Garcia S*, et al.* Long-term glycaemic response and tolerability of dapagliflozin versus a sulphonylurea as add-on therapy to metformin in patients with type 2 diabetes: 4-year data. *Diabetes Obes Metab*. 2015; 17: 581-590
[114] Marquard J, Otter S, Welters A*, et al.* Characterization of pancreatic NMDA receptors as possible drug targets for diabetes treatment. *Nat Med*. 2015; 21: 363-372
[115] Huang XT, Li C, Peng XP*, et al.* An excessive increase in glutamate contributes to glucose-toxicity in β-cells via activation of pancreatic NMDA receptors in rodent diabetes. *Scientific Reports*. 2017; 7: 44120
[116] Huang XT, Liu W, Zhou Y*, et al.* Endoplasmic reticulum stress contributes to NMDA-induced pancreatic beta-cell dysfunction in a CHOP-dependent manner. *Life Sci*. 2019; 232: 116612
[117] Huang XT, Yue SJ, Li C*, et al.* A Sustained Activation of Pancreatic NMDARs Is a Novel Factor of beta-Cell Apoptosis and Dysfunction. *Endocrinology*. 2017; 158: 3900-3913
[118] Kalia LV, Kalia SK, Salter MW. NMDA receptors in clinical neurology: excitatory times ahead. *Lancet Neurol*. 2008; 7: 742-755
[119] Yashiro K, Philpot BD. Regulation of NMDA receptor subunit expression and its implications for LTD, LTP, and metaplasticity. *Neuropharmacology*. 2008; 55: 1081-1094
[120] Zhou Y, Danbolt NC. Glutamate as a neurotransmitter in the healthy brain. *J Neural Transm (Vienna)*. 2014; 121: 799-817
[121] Otter S, Lammert E. Exciting Times for Pancreatic Islets: Glutamate Signaling in Endocrine Cells. *Trends Endocrinol Metab*. 2015:
[122] Papouin T, Ladepeche L, Ruel J*, et al.* Synaptic and extrasynaptic NMDA receptors are gated by different endogenous coagonists. *Cell*. 2012; 150: 633-646
[123] Kreutzwiser D, Tawfic QA. Expanding Role of NMDA Receptor Antagonists in the Management of Pain. *CNS Drugs*. 2019; 33: 347-374
[124] Bem JL, Peck R. Dextromethorphan. An overview of safety issues. *Drug Saf*. 1992; 7: 190-199
[125] Dicpinigaitis PV. Clinical perspective - cough: an unmet need. *Curr Opin Pharmacol*. 2015; 22: 24-28
[126] Pu B, Xue Y, Wang Q, Hua C, Li X. Dextromethorphan provides neuroprotection via anti-inflammatory and anti-excitotoxicity effects in the cortex following traumatic brain injury. *Mol Med Rep*. 2015; 12: 3704-3710
[127] Franklin PH, Murray TF. High affinity [3H]dextrorphan binding in rat brain is localized to a noncompetitive antagonist site of the activated N-methyl-D-aspartate receptor-cation channel. *Mol Pharmacol*. 1992; 41: 134-146

[128] LePage KT, Ishmael JE, Low CM, Traynelis SF, Murray TF. Differential binding properties of [3H]dextrorphan and [3H]MK-801 in heterologously expressed NMDA receptors. *Neuropharmacology*. 2005; 49: 1-16
[129] Bozic M, Valdivielso JM. The potential of targeting NMDA receptors outside the CNS. *Expert Opin Ther Targets*. 2015; 19: 399-413
[130] Marquard J, Stirban A, Schliess F*, et al.* Effects of dextromethorphan as add-on to sitagliptin on blood glucose and serum insulin concentrations in individuals with type 2 diabetes mellitus: a randomized, placebo-controlled, double-blinded, multiple crossover, single-dose clinical trial. *Diabetes Obesity & Metabolism*. 2016; 18: 100-103
[131] Gu G, Dubauskaite J, Melton DA. Direct evidence for the pancreatic lineage: NGN3+ cells are islet progenitors and are distinct from duct progenitors. *Development*. 2002; 129: 2447-2457
[132] Yesil P, Michel M, Chwalek K*, et al.* A new collagenase blend increases the number of islets isolated from mouse pancreas. *Islets*. 2009; 1: 185-190
[133] Chomczynski P, Sacchi N. Single-step method of RNA isolation by acid guanidinium thiocyanate-phenol-chloroform extraction. *Anal Biochem*. 1987; 162: 156-159
[134] Livak KJ, Schmittgen TD. Analysis of relative gene expression data using real-time quantitative PCR and the 2(-Delta Delta C(T)) Method. *Methods*. 2001; 25: 402-408
[135] Schmittgen TD, Livak KJ. Analyzing real-time PCR data by the comparative C(T) method. *Nat Protoc*. 2008; 3: 1101-1108
[136] Dobin A, Davis CA, Schlesinger F*, et al.* STAR: ultrafast universal RNA-seq aligner. *Bioinformatics*. 2013; 29: 15-21
[137] Liao Y, Smyth GK, Shi W. The Subread aligner: fast, accurate and scalable read mapping by seed-and-vote. *Nucleic Acids Res*. 2013; 41: e108
[138] Robinson MD, McCarthy DJ, Smyth GK. edgeR: a Bioconductor package for differential expression analysis of digital gene expression data. *Bioinformatics*. 2010; 26: 139-140
[139] Hatakeyama M, Opitz L, Russo G, Qi W, Schlapbach R, Rehrauer H. SUSHI: an exquisite recipe for fully documented, reproducible and reusable NGS data analysis. *BMC Bioinformatics*. 2016; 17: 228
[140] Anderson RD, Haskell RE, Xia H, Roessler BJ, Davidson BL. A simple method for the rapid generation of recombinant adenovirus vectors. *Gene Ther*. 2000; 7: 1034-1038
[141] Cavallari G, Zuellig RA, Lehmann R, Weber M, Moritz W. Rat pancreatic islet size standardization by the "hanging drop" technique. *Transplant Proc*. 2007; 39: 2018-2020
[142] Rehrauer H, Wu L, Blum W*, et al.* How asbestos drives the tissue towards tumors: YAP activation, macrophage and mesothelial precursor recruitment, RNA editing, and somatic mutations. *Oncogene*. 2018; 37: 2645-2659
[143] Nguyen L, Thomas KL, Lucke-Wold BP, Cavendish JZ, Crowe MS, Matsumoto RR. Dextromethorphan: An update on its utility for neurological and neuropsychiatric disorders. *Pharmacol Ther*. 2016; 159: 1-22
[144] Krupenko NI, Dubard ME, Strickland KC, Moxley KM, Oleinik NV, Krupenko SA. ALDH1L2 is the mitochondrial homolog of 10-formyltetrahydrofolate dehydrogenase. *J Biol Chem*. 2010; 285: 23056-23063
[145] Ducker GS, Chen L, Morscher RJ*, et al.* Reversal of Cytosolic One-Carbon Flux Compensates for Loss of the Mitochondrial Folate Pathway. *Cell Metab*. 2016; 23: 1140-1153
[146] Shabram P, Aguilar-Cordova E. Multiplicity of infection/multiplicity of confusion. *Mol Ther*. 2000; 2: 420-421
[147] Mauvais-Jarvis F. Gender differences in glucose homeostasis and diabetes. *Physiol Behav*. 2018; 187: 20-23
[148] Taylor CP, Traynelis SF, Siffert J, Pope LE, Matsumoto RR. Pharmacology of dextromethorphan: Relevance to dextromethorphan/quinidine (Nuedexta(R)) clinical use. *Pharmacol Ther*. 2016; 164: 170-182

[149] Nguyen L, Lucke-Wold BP, Mookerjee S, Kaushal N, Matsumoto RR. Sigma-1 Receptors and Neurodegenerative Diseases: Towards a Hypothesis of Sigma-1 Receptors as Amplifiers of Neurodegeneration and Neuroprotection. *Adv Exp Med Biol*. 2017; 964: 133-152
[150] Meier JJ. Beta cell mass in diabetes: a realistic therapeutic target? *Diabetologia*. 2008; 51: 703-713
[151] Qian L, Zhang S, Xu L, Peng Y. Endoplasmic reticulum stress in beta cells: latent mechanism of secondary sulfonylurea failure in type 2 diabetes? *Med Hypotheses*. 2008; 71: 889-891
[152] Sun J, Cui J, He Q, Chen Z, Arvan P, Liu M. Proinsulin misfolding and endoplasmic reticulum stress during the development and progression of diabetes. *Mol Aspects Med*. 2015; 42: 105-118
[153] Pfützner A, Forst T. Elevated intact proinsulin levels are indicative of Beta-cell dysfunction, insulin resistance, and cardiovascular risk: impact of the antidiabetic agent pioglitazone. *J Diabetes Sci Technol*. 2011; 5: 784-793
[154] Dworacka M, Abramczyk M, Winiarska H, Kuczynski S, Borowska M, Szczawinska K. Disproportionately elevated proinsulin levels in type 2 diabetic patients treated with sulfonylurea. *Int J Clin Pharmacol Ther*. 2006; 44: 14-21
[155] Inoguchi T, Umeda F, Kakimoto M*, et al.* Chronic sulfonylurea treatment and hyperglycemia aggravate disproportionately elevated plasma proinsulin levels in patients with type 2 diabetes. *Endocr J*. 2000; 47: 763-770
[156] Kim MJ, Min SH, Shin SY*, et al.* Attenuation of PERK enhances glucose-stimulated insulin secretion in islets. *J Endocrinol*. 2018; 236: 125-136
[157] Lipson KL, Fonseca SG, Ishigaki S*, et al.* Regulation of insulin biosynthesis in pancreatic beta cells by an endoplasmic reticulum-resident protein kinase IRE1. *Cell Metabolism*. 2006; 4: 245-254
[158] Tran K, Li Y, Duan H, Arora D, Lim H-Y, Wang W. Identification of small molecules that protect pancreatic β cells against endoplasmic reticulum stress-induced cell death. *ACS Chem Biol*. 2014; 9: 2796-2806
[159] Harbeck MC, Louie DC, Howland J, Wolf BA, Rothenberg PL. Expression of insulin receptor mRNA and insulin receptor substrate 1 in pancreatic islet beta-cells. *Diabetes*. 1996; 45: 711-717
[160] Martinez SC, Cras-Meneur C, Bernal-Mizrachi E, Permutt MA. Glucose regulates Foxo1 through insulin receptor signaling in the pancreatic islet beta-cell. *Diabetes*. 2006; 55: 1581-1591
[161] Zawalich WS, Zawalich KC. Effects of glucose, exogenous insulin, and carbachol on C-peptide and insulin secretion from isolated perifused rat islets. *J Biol Chem*. 2002; 277: 26233-26237
[162] Marincola F, Frank W, Clark W, Douglas M, Merrell R. The independence of insulin release and ambient insulin in vitro. *Diabetes*. 1983; 32: 1162-1167
[163] Kulkarni RN, Brüning JC, Winnay JN, Postic C, Magnuson MA, Kahn CR. Tissue-specific knockout of the insulin receptor in pancreatic beta cells creates an insulin secretory defect similar to that in type 2 diabetes. *Cell*. 1999; 96: 329-339
[164] Duvillie B, Currie C, Chrones T*, et al.* Increased islet cell proliferation, decreased apoptosis, and greater vascularization leading to beta-cell hyperplasia in mutant mice lacking insulin. *Endocrinology*. 2002; 143: 1530-1537
[165] Leibiger IB, Leibiger B, Berggren PO. Insulin signaling in the pancreatic beta-cell. *Annu Rev Nutr*. 2008; 28: 233-251
[166] Loreti L, Dunbar JC, Chen S, Foa PP. The autoregulation of insulin secretion in the isolated pancreatic islets of lean (obOb) and obese-hyperglycemic (obob) mice. *Diabetologia*. 1974; 10: 309-315
[167] Persaud SJ, Asare-Anane H, Jones PM. Insulin receptor activation inhibits insulin secretion from human islets of Langerhans. *FEBS Lett*. 2002; 510: 225-228
[168] Porzio O, Federici M, Hribal ML*, et al.* The Gly972-->Arg amino acid polymorphism in IRS-1 impairs insulin secretion in pancreatic beta cells. *J Clin Invest*. 1999; 104: 357-364

[169] Kulkarni RN, Winnay JN, Daniels M*, et al.* Altered function of insulin receptor substrate-1-deficient mouse islets and cultured beta-cell lines. *J Clin Invest*. 1999; 104: R69-75
[170] Lee JY, Ristow M, Lin X, White MF, Magnuson MA, Hennighausen L. RIP-Cre revisited, evidence for impairments of pancreatic beta-cell function. *J Biol Chem*. 2006; 281: 2649-2653
[171] Song J, Xu Y, Hu X, Choi B, Tong Q. Brain expression of Cre recombinase driven by pancreas-specific promoters. *Genesis*. 2010; 48: 628-634
[172] Assmann A, Ueki K, Winnay JN, Kadowaki T, Kulkarni RN. Glucose effects on beta-cell growth and survival require activation of insulin receptors and insulin receptor substrate 2. *Mol Cell Biol*. 2009; 29: 3219-3228
[173] Saxton RA, Sabatini DM. mTOR Signaling in Growth, Metabolism, and Disease. *Cell*. 2017; 168: 960-976
[174] Yuan T, Rafizadeh S, Gorrepati KDD*, et al.* Reciprocal regulation of mTOR complexes in pancreatic islets from humans with type 2 diabetes. *Diabetologia*. 2017; 60: 668-678
[175] Bartolome A, Kimura-Koyanagi M, Asahara S*, et al.* Pancreatic beta-cell failure mediated by mTORC1 hyperactivity and autophagic impairment. *Diabetes*. 2014; 63: 2996-3008
[176] Ardestani A, Lupse B, Kido Y, Leibowitz G, Maedler K. mTORC1 Signaling: A Double-Edged Sword in Diabetic beta Cells. *Cell Metab*. 2018; 27: 314-331
[177] El Khattabi I, Sharma A. Proper activation of MafA is required for optimal differentiation and maturation of pancreatic beta-cells. *Best Pract Res Clin Endocrinol Metab*. 2015; 29: 821-831
[178] Zhang C, Moriguchi T, Kajihara M*, et al.* MafA is a key regulator of glucose-stimulated insulin secretion. *Mol Cell Biol*. 2005; 25: 4969-4976
[179] Shiao M-S, Liao B-Y, Long M, Yu H-T. Adaptive evolution of the insulin two-gene system in mouse. *Genetics*. 2008; 178: 1683-1691
[180] Ducker GS, Rabinowitz JD. One-Carbon Metabolism in Health and Disease. *Cell Metab*. 2017; 25: 27-42
[181] Baggott JE, Tamura T. Folate-Dependent Purine Nucleotide Biosynthesis in Humans. *Adv Nutr*. 2015; 6: 564-571
[182] Blom HJ, Smulders Y. Overview of homocysteine and folate metabolism. With special references to cardiovascular disease and neural tube defects. *J Inherit Metab Dis*. 2011; 34: 75-81
[183] Fan J, Ye J, Kamphorst JJ, Shlomi T, Thompson CB, Rabinowitz JD. Quantitative flux analysis reveals folate-dependent NADPH production. *Nature*. 2014; 510: 298-302
[184] Ormazabal A, Casado M, Molero-Luis M*, et al.* Can folic acid have a role in mitochondrial disorders? *Drug Discov Today*. 2015; 20: 1349-1354
[185] Liu F, Liu Y, He C*, et al.* Increased MTHFD2 expression is associated with poor prognosis in breast cancer. *Tumour Biol*. 2014; 35: 8685-8690
[186] Noguchi K, Konno M, Koseki J*, et al.* The mitochondrial one-carbon metabolic pathway is associated with patient survival in pancreatic cancer. *Oncol Lett*. 2018; 16: 1827-1834
[187] Piskounova E, Agathocleous M, Murphy MM*, et al.* Oxidative stress inhibits distant metastasis by human melanoma cells. *Nature*. 2015; 527: 186-191
[188] Ayromlou H, Hajipour B, Hossenian MM, Khodadadi A, Vatankhah AM. Oxidative effect of methotrexate administration in spinal cord of rabbits. *J Pak Med Assoc*. 2011; 61: 1096-1099
[189] Shin M, Momb J, Appling DR. Human mitochondrial MTHFD2 is a dual redox cofactor-specific methylenetetrahydrofolate dehydrogenase/methenyltetrahydrofolate cyclohydrolase. *Cancer Metab*. 2017; 5: 11
[190] Jezek P, Dlaskova A, Plecita-Hlavata L. Redox homeostasis in pancreatic beta cells. *Oxid Med Cell Longev*. 2012; 2012: 932838

[191] Sarret C, Ashkavand Z, Paules E*, et al.* Deleterious mutations in ALDH1L2 suggest a novel cause for neuro-ichthyotic syndrome. *NPJ Genom Med*. 2019; 4: 17
[192] Tibbetts AS, Appling DR. Compartmentalization of Mammalian folate-mediated one-carbon metabolism. *Annu Rev Nutr*. 2010; 30: 57-81
[193] Yang M, Vousden KH. Serine and one-carbon metabolism in cancer. *Nat Rev Cancer*. 2016; 16: 650-662
[194] Amelio I, Cutruzzolá F, Antonov A, Agostini M, Melino G. Serine and glycine metabolism in cancer. *Trends in biochemical sciences*. 2014; 39: 191-198
[195] Ye J, Mancuso A, Tong X*, et al.* Pyruvate kinase M2 promotes de novo serine synthesis to sustain mTORC1 activity and cell proliferation. *Proc Natl Acad Sci U S A*. 2012; 109: 6904-6909
[196] Chaneton B, Hillmann P, Zheng L*, et al.* Serine is a natural ligand and allosteric activator of pyruvate kinase M2. *Nature*. 2012; 491: 458-462
[197] Holm LJ, Haupt-Jorgensen M, Larsen J, Giacobini JD, Bilgin M, Buschard K. L-serine supplementation lowers diabetes incidence and improves blood glucose homeostasis in NOD mice. *PLoS One*. 2018; 13: e0194414
[198] Adams CM. Role of the transcription factor ATF4 in the anabolic actions of insulin and the anti-anabolic actions of glucocorticoids. *J Biol Chem*. 2007; 282: 16744-16753
[199] Wortel IMN, van der Meer LT, Kilberg MS, van Leeuwen FN. Surviving Stress: Modulation of ATF4-Mediated Stress Responses in Normal and Malignant Cells. *Trends Endocrinol Metab*. 2017; 28: 794-806
[200] Yoshizawa T, Hinoi E, Jung DY*, et al.* The transcription factor ATF4 regulates glucose metabolism in mice through its expression in osteoblasts. *J Clin Invest*. 2009; 119: 2807-2817
[201] Ben-Sahra I, Hoxhaj G, Ricoult SJH, Asara JM, Manning BD. mTORC1 induces purine synthesis through control of the mitochondrial tetrahydrofolate cycle. *Science*. 2016; 351: 728-733
[202] Rendleman J, Cheng Z, Maity S*, et al.* New insights into the cellular temporal response to proteostatic stress. *eLife*. 2018; 7: e39054
[203] Shimizu Y, Hendershot LM. Oxidative folding: cellular strategies for dealing with the resultant equimolar production of reactive oxygen species. *Antioxid Redox Signal*. 2009; 11: 2317-2331
[204] Pacold ME, Brimacombe KR, Chan SH*, et al.* A PHGDH inhibitor reveals coordination of serine synthesis and one-carbon unit fate. *Nat Chem Biol*. 2016; 12: 452-458

10 Supplementary Information

10.1 Fiji/ImageJ macro scripts

Following Fiji/ImageJ macro scripts were used for quantification of cell viability (Cell Viability Assay – 4.3.2.)

Syntax highlighting was performed with http://www.planetb.ca/syntax-highlight-word.

Marco script 1

```
run("Z Project...", "projection=[Max Intensity]");
Stack.setDisplayMode("composite");
```

Marco script 2

```
run("Set Measurements...", "area limit redirect=None decimal=3");
setSlice(1); // select the DAPI channel
// Gaussian blur ? run("Gaussian blur...", "sigma=2");
setAutoThreshold("Otsu dark");
run("Measure");
setSlice(3); // select the EtBr channel
// Gaussian blur ?
// setAutoThreshold("RenyiEntropy dark");
setThreshold(55, 255);

run("Measure");
```

10.2 Differentially expressed genes

Supplementary Table 1 to Figure 8: List of differentially expressed genes

Long-term exposure of pancreatic islets to 10 µM DXO compared to untreated control

gene_id	gene_name	log2 Ratio	pValue	fdr	Control.24h [FPKM]	DXO.24h [FPKM]
ENSMUSG00000030717	Nupr1	4.94	9.29E-11	2.55E-07	31.26	1083.00
ENSMUSG00000015652	Steap1	4.15	3.05E-08	3.79E-05	3.08	61.55
ENSMUSG00000038742	Angptl6	3.77	2.00E-07	0.0001303	6.62	102.00
ENSMUSG00000054136	Adm2	3.66	7.52E-07	0.0004121	2.06	29.39
ENSMUSG00000032715	Trib3	3.55	6.88E-07	0.0003927	20.93	276.70
ENSMUSG00000031957	Ctrb1	3.49	4.73E-06	0.001544	1.07	13.63
ENSMUSG00000064065	Ipcef1	3.38	3.69E-06	0.001489	1.31	15.37
ENSMUSG00000028179	Cth	3.32	1.02E-05	0.002862	1.11	12.47
ENSMUSG00000026483	Fam129a	3.27	3.93E-06	0.001511	5.24	56.76
ENSMUSG00000025408	Ddit3	3.24	4.20E-06	0.001514	50.87	542.80
ENSMUSG00000020256	Aldh1l2	3.19	5.57E-06	0.001735	14.01	144.30
ENSMUSG00000009092	Derl3	3.13	9.27E-06	0.002703	6.61	65.34
ENSMUSG00000036699	Zcchc12	3.12	9.80E-06	0.002798	4.92	48.13
ENSMUSG00000026456	Cyb5r1	2.95	2.24E-05	0.00539	22.02	192.30
ENSMUSG00000039158	Akna	2.95	2.70E-05	0.006022	1.24	10.84
ENSMUSG00000031574	Star	2.93	3.75E-05	0.007664	1.38	11.80
ENSMUSG00000047963	Stbd1	2.92	3.70E-05	0.007664	2.29	19.47
ENSMUSG00000037278	Tmem97	2.84	4.38E-05	0.008691	11.46	92.60
ENSMUSG00000017446	C1qtnf1	2.81	9.63E-05	0.01691	1.39	11.07
ENSMUSG00000018821	Avpi1	2.73	0.0001119	0.01893	4.54	33.88
ENSMUSG00000031271	Serpina7	2.65	0.0001223	0.02043	13.71	96.78
ENSMUSG00000048078	Tenm4	2.60	0.0001565	0.02523	2.79	19.09
ENSMUSG00000025140	Pycr1	2.60	0.0001517	0.02475	26.84	183.60
ENSMUSG00000011171	Vipr2	2.50	0.0004272	0.05226	1.25	7.97
ENSMUSG00000053398	Phgdh	2.50	0.0002617	0.03623	28.06	178.70
ENSMUSG00000089809	A930011G23Rik	2.48	0.0004244	0.05226	1.12	7.04
ENSMUSG00000032816	Igdcc4	2.45	0.0003893	0.04986	1.75	10.72
ENSMUSG00000056666	Retsat	2.44	0.000415	0.05226	4.55	27.75
ENSMUSG00000038508	Gdf15	2.43	0.0005875	0.06654	1.81	10.95
ENSMUSG00000024640	Psat1	2.40	0.0004394	0.05328	20.40	121.00
ENSMUSG00000013089	Etv5	2.38	0.0004781	0.05696	10.47	61.47
ENSMUSG00000040435	Ppp1r15a	2.35	0.0005542	0.06328	20.44	117.00
ENSMUSG00000025068	Gsto1	2.33	0.0006343	0.07064	19.87	112.50
ENSMUSG00000046027	Stard5	2.30	0.0007252	0.07764	15.79	87.36
ENSMUSG00000003355	Fkbp11	2.29	0.0007577	0.07926	23.61	130.30
ENSMUSG00000063975	Slco1a5	2.29	0.001057	0.1035	1.41	7.78
ENSMUSG00000031490	Eif4ebp1	2.27	0.000824	0.08516	25.93	140.90
ENSMUSG00000031530	Dusp4	2.27	0.0009254	0.09393	3.08	16.69
ENSMUSG00000028542	Slc6a9	2.24	0.001007	0.09929	7.79	41.39
ENSMUSG00000030785	Cox6a2	2.22	0.00108	0.1036	28.20	147.80
ENSMUSG00000029446	Psph	2.21	0.001179	0.1102	8.55	44.51
ENSMUSG00000026628	Atf3	2.20	0.001473	0.131	2.00	10.39
ENSMUSG00000038550	Ciart	2.19	0.001437	0.1287	6.65	34.06

ENSMUSG00000031762	Mt2	2.17	0.00131	0.1205	155.80	788.20
ENSMUSG00000027313	Chac1	2.16	0.001342	0.1226	31.50	159.00
ENSMUSG00000029378	Areg	2.11	0.003199	0.2307	1.41	6.88
ENSMUSG00000029161	Cgref1	2.11	0.001943	0.1654	7.32	35.53
ENSMUSG00000015085	Entpd2	2.10	0.002156	0.1758	3.30	15.91
ENSMUSG00000023272	Creld2	2.09	0.001896	0.1624	49.76	238.60
ENSMUSG00000029304	Spp1	2.06	0.002118	0.1738	84.87	399.90
ENSMUSG00000031391	L1cam	2.06	0.00242	0.193	4.65	21.91
ENSMUSG00000039552	Rsph4a	2.06	0.002786	0.2064	1.22	5.74
ENSMUSG00000055725	Paqr3	2.05	0.002785	0.2064	2.97	13.84
ENSMUSG00000005413	Hmox1	2.01	0.002779	0.2064	31.22	141.80
ENSMUSG00000024164	C3	2.00	0.003732	0.2557	1.87	8.43
ENSMUSG00000027249	F2	1.96	0.005263	0.3163	1.16	5.08
ENSMUSG00000023883	Phf10	1.95	0.003668	0.2539	30.16	131.00
ENSMUSG00000022769	Sdf2l1	1.94	0.003724	0.2557	84.89	367.10
ENSMUSG00000044447	Dock5	1.92	0.004269	0.278	1.41	6.02
ENSMUSG00000031700	Gpt2	1.92	0.004422	0.2859	5.75	24.45
ENSMUSG00000042942	Greb1l	1.90	0.005457	0.3223	1.19	5.03
ENSMUSG00000032281	Acsbg1	1.90	0.007656	0.3959	1.77	7.46
ENSMUSG00000010830	Kdelr3	1.89	0.005083	0.3096	9.28	38.62
ENSMUSG00000029413	Naaa	1.88	0.005182	0.3142	9.57	39.65
ENSMUSG00000031765	Mt1	1.87	0.004988	0.3051	305.80	1262.00
ENSMUSG00000049422	Chchd10	1.86	0.00538	0.3205	43.45	177.70
ENSMUSG00000041168	Lonp1	1.85	0.005504	0.3237	34.56	140.50
ENSMUSG00000034472	Rasd2	1.85	0.005968	0.3436	7.74	31.35
ENSMUSG00000023034	Nr4a1	1.84	0.006622	0.3688	2.48	10.03
ENSMUSG00000025190	Got1	1.83	0.006048	0.3439	25.52	102.50
ENSMUSG00000044894	Uqcrq	1.79	0.007198	0.3838	59.48	232.00
ENSMUSG00000040618	Pck2	1.78	0.007523	0.3935	31.43	121.50
ENSMUSG00000056501	Cebpb	1.72	0.00999	0.4722	9.98	37.15
ENSMUSG00000041313	Slc7a1	1.72	0.009856	0.4706	24.82	91.77
ENSMUSG00000027737	Slc7a11	1.71	0.01097	0.4954	2.29	8.45
ENSMUSG00000020680	Taf15	1.69	0.01087	0.4947	38.45	140.00
ENSMUSG00000026864	Hspa5	1.67	0.01179	0.5153	1089.00	3900.00
ENSMUSG00000041028	Ghitm	1.67	0.01189	0.5161	60.40	216.10
ENSMUSG00000024261	Syt4	1.66	0.01225	0.5215	39.96	142.30
ENSMUSG00000037722	Gnpnat1	1.66	0.01272	0.5332	15.69	55.66
ENSMUSG00000041920	Slc16a6	1.65	0.01426	0.5666	4.09	14.48
ENSMUSG00000030659	Nucb2	1.64	0.01308	0.5452	99.42	350.10
ENSMUSG00000002274	Metrn	1.64	0.02152	0.7127	1.36	4.78
ENSMUSG00000044424	Gm9493	1.64	0.03019	0.8391	1.43	5.11
ENSMUSG00000023827	Agpat4	1.63	0.0161	0.6118	5.59	19.50
ENSMUSG00000052062	Pard3b	1.63	0.01477	0.5821	2.42	8.43
ENSMUSG00000028266	Lmo4	1.60	0.01766	0.6401	5.33	18.22
ENSMUSG00000034667	Xpot	1.60	0.01569	0.6057	22.35	76.25
ENSMUSG00000029591	Ung	1.60	0.02052	0.6965	1.79	6.11
ENSMUSG00000026615	Eprs	1.59	0.01633	0.618	84.21	285.20
ENSMUSG00000024359	Hspa9	1.58	0.01674	0.6251	257.50	868.10
ENSMUSG00000005667	Mthfd2	1.58	0.01703	0.6291	39.20	131.90
ENSMUSG00000001670	Tat	1.58	0.01725	0.6352	23.37	78.66
ENSMUSG00000031770	Herpud1	1.57	0.01745	0.6361	211.10	706.50

ENSMUSG00000030839	Sergef	1.57	0.02132	0.7127	4.51	15.05
ENSMUSG00000078622	Ccdc47	1.56	0.01823	0.6443	64.41	214.10
ENSMUSG00000036330	Slc18a1	1.55	0.01976	0.6808	10.47	34.46
ENSMUSG00000021263	Degs2	1.55	0.02212	0.7236	2.57	8.46
ENSMUSG00000006611	Hfe	1.54	0.02054	0.6965	20.57	67.20
ENSMUSG00000017204	Gsdma	1.54	0.02102	0.7077	6.09	19.89
ENSMUSG00000052298	Cdc42se2	1.53	0.02059	0.6965	57.75	187.80
ENSMUSG00000048007	Timm8a1	1.52	0.02643	0.7924	2.49	8.06
ENSMUSG00000023067	Cdkn1a	1.50	0.02369	0.763	33.80	107.40
ENSMUSG00000025198	Erlin1	1.50	0.024	0.763	17.36	55.14
ENSMUSG00000025403	Shmt2	1.49	0.02408	0.7638	16.77	53.14
ENSMUSG00000020547	Bzw2	1.49	0.02509	0.7804	10.40	32.85
ENSMUSG00000029752	Asns	1.48	0.02487	0.7779	121.40	381.30
ENSMUSG00000068523	Gng5	1.48	0.02517	0.7804	39.30	123.50
ENSMUSG00000042406	Atf4	1.48	0.02504	0.7804	203.40	637.70
ENSMUSG00000019689	1110001J03Rik	1.47	0.02965	0.8321	9.79	30.65
ENSMUSG00000033813	Tcea1	1.47	0.02592	0.7906	43.72	136.30
ENSMUSG00000026755	Arpc5l	1.46	0.02669	0.7953	38.56	119.80
ENSMUSG00000020142	Slc1a4	1.46	0.02702	0.7996	8.11	25.18
ENSMUSG00000007594	Hapln4	1.46	0.0267	0.7953	38.07	118.10
ENSMUSG00000032526	Deb1	1.46	0.02824	0.823	38.10	117.70
ENSMUSG00000027944	Hax1	1.45	0.02802	0.8186	81.77	251.60
ENSMUSG00000041654	Slc39a11	1.45	0.02919	0.8268	10.93	33.61
ENSMUSG00000023393	Slc17a9	1.43	0.03102	0.849	20.13	60.96
ENSMUSG00000028893	Sesn2	1.42	0.0311	0.849	36.74	110.70
ENSMUSG00000011179	Odc1	1.42	0.03123	0.849	34.81	104.90
ENSMUSG00000038323	1700066M21Rik	1.40	0.03584	0.901	2.69	8.01
ENSMUSG00000036111	Lmo1	1.40	0.04427	0.9672	2.28	6.77
ENSMUSG00000029521	Chek2	1.40	0.05102	0.9998	1.27	3.79
ENSMUSG00000058440	Nrf1	1.40	0.03483	0.8901	12.68	37.57
ENSMUSG00000070713	Gm10282	1.39	0.05267	0.9998	1.22	3.57
ENSMUSG00000042747	Krtcap2	1.39	0.03471	0.89	80.82	238.80
ENSMUSG00000031781	Ciapin1	1.39	0.03633	0.9045	13.11	38.62
ENSMUSG00000023122	Sult1c2	1.38	0.03702	0.9106	8.35	24.53
ENSMUSG00000040111	Gramd1b	1.38	0.03629	0.9045	10.75	31.57
ENSMUSG00000045455	Gm9797	1.37	0.05434	0.9998	1.39	4.05
ENSMUSG00000044080	S100a1	1.36	0.03873	0.9346	60.29	174.70
ENSMUSG00000000278	Scpep1	1.36	0.03827	0.9298	36.72	106.40
ENSMUSG00000020964	Sel1l	1.36	0.03874	0.9346	75.69	218.60
ENSMUSG00000033307	Mif	1.36	0.0399	0.9483	60.40	174.10
ENSMUSG00000072568	Fam84b	1.35	0.04037	0.9483	8.08	23.22
ENSMUSG00000026142	Rhbdd1	1.35	0.04066	0.9483	13.49	38.70
ENSMUSG00000036067	Slc2a6	1.34	0.04681	0.9998	3.25	9.31
ENSMUSG00000028139	Riiad1	1.34	0.05734	0.9998	2.85	8.16
ENSMUSG00000027999	Pla2g12a	1.34	0.04251	0.9549	29.53	84.00
ENSMUSG00000028059	Arhgef2	1.33	0.04333	0.9665	49.62	140.40
ENSMUSG00000024587	Nars	1.32	0.04373	0.9665	79.20	223.40
ENSMUSG00000021696	Elovl7	1.32	0.04875	0.9998	1.20	3.36
ENSMUSG00000024493	Lars	1.32	0.04447	0.9672	33.21	93.43
ENSMUSG00000030738	Eif3c	1.32	0.04458	0.968	80.37	225.80
ENSMUSG00000003402	Prkcsh	1.31	0.04555	0.983	57.01	159.60

ENSMUSG00000022790	Igsf11	1.31	0.04821	0.9998	4.53	12.67
ENSMUSG00000023952	Gtpbp2	1.30	0.04749	0.9998	67.53	187.60
ENSMUSG00000024436	Mrps18b	1.29	0.04979	0.9998	33.68	93.03
ENSMUSG00000031513	Leprotl1	1.29	0.04912	0.9998	24.08	66.46
ENSMUSG00000064307	Lrrc51	1.29	0.06707	0.9998	2.18	6.02
ENSMUSG00000031202	Rab39b	1.29	0.04962	0.9998	15.29	42.16
ENSMUSG00000060950	Trmt61a	1.29	0.05229	0.9998	5.14	14.13
ENSMUSG00000032353	Tmed3	1.29	0.04971	0.9998	153.50	422.20
ENSMUSG00000028780	Sema3c	1.29	0.05453	0.9998	2.58	7.10
ENSMUSG00000025007	Aldh18a1	1.28	0.05053	0.9998	87.34	239.50
ENSMUSG00000028773	Fabp3	1.28	0.05399	0.9998	11.21	30.74
ENSMUSG00000041112	Elmo1	1.28	0.05179	0.9998	7.66	21.01
ENSMUSG00000020601	Trib2	1.28	0.05428	0.9998	2.16	5.92
ENSMUSG00000046997	Spsb4	1.28	0.05867	0.9998	1.50	4.10
ENSMUSG00000006057	Atp5g1	1.27	0.05283	0.9998	26.23	71.35
ENSMUSG00000042507	Elmsan1	1.27	0.05338	0.9998	5.31	14.45
ENSMUSG00000030104	Edem1	1.27	0.05285	0.9998	23.50	63.85
ENSMUSG00000029596	Sdsl	1.27	0.0693	0.9998	2.00	5.45
ENSMUSG00000021185	9030617O03Rik	1.27	0.05831	0.9998	2.95	8.01
ENSMUSG00000016487	Ppfibp1	1.27	0.05368	0.9998	30.81	83.51
ENSMUSG00000029167	Ppargc1a	1.26	0.06196	0.9998	1.43	3.86
ENSMUSG00000091228	Gm20390	1.26	0.05599	0.9998	57.72	155.20
ENSMUSG00000036632	Alg5	1.26	0.05675	0.9998	16.46	44.27
ENSMUSG00000028538	St3gal3	1.25	0.05699	0.9998	20.32	54.53
ENSMUSG00000028145	Them4	1.25	0.06169	0.9998	3.97	10.64
ENSMUSG00000006442	Srm	1.25	0.05707	0.9998	45.59	122.20
ENSMUSG00000001627	Ifrd1	1.25	0.05775	0.9998	41.09	109.90
ENSMUSG00000025277	Abhd6	1.25	0.05927	0.9998	10.53	28.13
ENSMUSG00000053519	Kcnip1	1.24	0.05827	0.9998	31.74	84.65
ENSMUSG00000034990	Otoa	1.24	0.05959	0.9998	12.11	32.31
ENSMUSG00000039208	Metrnl	1.24	0.09004	0.9998	1.09	2.92
ENSMUSG00000030588	Yif1b	1.24	0.05987	0.9998	34.15	90.73
ENSMUSG00000043091	Tuba1c	1.23	0.06234	0.9998	8.02	21.23
ENSMUSG00000070284	Gmppb	1.23	0.06085	0.9998	35.75	94.50
ENSMUSG00000025823	Pdia4	1.23	0.06085	0.9998	83.48	220.30
ENSMUSG00000021094	Dhrs7	1.23	0.06206	0.9998	26.80	70.65
ENSMUSG00000068739	Sars	1.22	0.06164	0.9998	122.20	321.70
ENSMUSG00000048483	Zdhhc22	1.22	0.06775	0.9998	8.25	21.70
ENSMUSG00000036534	Slc38a7	1.22	0.06324	0.9998	23.16	60.83
ENSMUSG00000040690	Col16a1	1.22	0.06869	0.9998	2.71	7.11
ENSMUSG00000020099	Unc5b	1.22	0.06395	0.9998	6.65	17.41
ENSMUSG00000021203	Otub2	1.22	0.06551	0.9998	6.99	18.28
ENSMUSG00000008892	Vdac3	1.21	0.06417	0.9998	44.88	117.30
ENSMUSG00000022346	Myc	1.21	0.06859	0.9998	4.52	11.80
ENSMUSG00000061360	Phf5a	1.21	0.06603	0.9998	23.15	60.41
ENSMUSG00000018672	Copz2	1.21	0.0665	0.9998	44.55	115.80
ENSMUSG00000028466	Creb3	1.21	0.06619	0.9998	83.72	217.40
ENSMUSG00000054612	Mgmt	1.20	0.08985	0.9998	2.07	5.38
ENSMUSG00000040010	Slc7a5	1.20	0.06666	0.9998	105.20	272.30
ENSMUSG00000021831	Ero1l	1.20	0.0668	0.9998	25.61	66.32
ENSMUSG00000080115	Mettl21b	1.20	0.07087	0.9998	4.37	11.27

ENSMUSG00000023010	Tmbim6	1.20	0.06795	0.9998	383.10	987.80
ENSMUSG00000048978	Nrsn1	1.19	0.07226	0.9998	5.80	14.91
ENSMUSG00000063659	Zbtb18	1.18	0.07178	0.9998	21.84	55.83
ENSMUSG00000010048	Ifrd2	1.18	0.07511	0.9998	9.64	24.62
ENSMUSG00000049233	Apoo-ps	1.18	0.1095	0.9998	1.24	3.11
ENSMUSG00000045312	Lhfpl2	1.18	0.07642	0.9998	3.44	8.77
ENSMUSG00000010095	Slc3a2	1.17	0.07269	0.9998	89.64	227.90
ENSMUSG00000027397	Slc20a1	1.17	0.07375	0.9998	22.51	57.23
ENSMUSG00000015943	Bola1	1.17	0.07839	0.9998	9.60	24.39
ENSMUSG00000040945	Rcc2	1.17	0.07359	0.9998	31.44	79.81
ENSMUSG00000034557	Zfyve9	1.17	0.07429	0.9998	6.75	17.13
ENSMUSG00000048216	Gpr85	1.17	0.07719	0.9998	4.28	10.85
ENSMUSG00000028811	Yars	1.17	0.07444	0.9998	61.16	154.80
ENSMUSG00000004069	Dnaja3	1.17	0.0747	0.9998	33.30	84.28
ENSMUSG00000029534	St7	1.16	0.08188	0.9998	2.92	7.38
ENSMUSG00000096145	Vkorc1	1.16	0.07655	0.9998	82.40	207.60
ENSMUSG00000050854	Tmem125	1.16	0.1141	0.9998	1.11	2.80
ENSMUSG00000003814	Calr	1.16	0.07647	0.9998	705.40	1774.00
ENSMUSG00000032026	Rexo2	1.16	0.0776	0.9998	40.73	102.40
ENSMUSG00000045917	6330416G13Rik	1.16	0.07917	0.9998	7.75	19.47
ENSMUSG00000049690	Nckap5	1.16	0.08893	0.9998	1.09	2.74
ENSMUSG00000015837	Sqstm1	1.15	0.07753	0.9998	488.40	1224.00
ENSMUSG00000037601	Nme1	1.15	0.07921	0.9998	41.28	103.20
ENSMUSG00000027195	Hsd17b12	1.15	0.07913	0.9998	39.83	99.56
ENSMUSG00000022241	Tars	1.15	0.07911	0.9998	32.18	80.44
ENSMUSG00000025381	Cnpy2	1.15	0.08051	0.9998	69.78	173.80
ENSMUSG00000036781	Rps27l	1.14	0.08157	0.9998	68.79	171.30
ENSMUSG00000022364	Tbc1d31	1.14	0.08366	0.9998	5.21	12.96
ENSMUSG00000022881	Rfc4	1.14	0.09809	0.9998	2.95	7.34
ENSMUSG00000032849	Abcc4	1.14	0.08128	0.9998	8.63	21.47
ENSMUSG00000031382	Asb11	1.14	0.08665	0.9998	4.78	11.88
ENSMUSG00000030824	Nucb1	1.14	0.08104	0.9998	246.50	612.30
ENSMUSG00000001424	Snd1	1.14	0.08105	0.9998	110.70	275.00
ENSMUSG00000035443	Thyn1	1.14	0.08445	0.9998	12.90	32.05
ENSMUSG00000071451	Psmg4	1.14	0.09546	0.9998	6.50	16.13
ENSMUSG00000020857	Nme2	1.14	0.08247	0.9998	92.36	228.80
ENSMUSG00000035504	Reep6	1.14	0.08263	0.9998	71.97	178.10
ENSMUSG00000020869	Lrrc59	1.13	0.08377	0.9998	87.59	216.10
ENSMUSG00000031813	Mvb12a	1.13	0.08483	0.9998	30.82	76.04
ENSMUSG00000037851	Iars	1.13	0.08417	0.9998	56.15	138.40
ENSMUSG00000021684	Pde8b	1.13	0.1036	0.9998	1.07	2.64
ENSMUSG00000026663	Atf6	1.13	0.08475	0.9998	49.16	120.90
ENSMUSG00000040354	Mars	1.13	0.0855	0.9998	48.91	120.20
ENSMUSG00000057054	Inca1	1.12	0.1229	0.9998	1.06	2.60
ENSMUSG00000018171	Vmp1	1.12	0.0881	0.9998	29.29	71.59
ENSMUSG00000036800	Fam135b	1.12	0.09386	0.9998	1.68	4.11
ENSMUSG00000032383	Ppib	1.11	0.08852	0.9998	90.13	219.80
ENSMUSG00000055013	Agap1	1.11	0.08893	0.9998	14.86	36.19
ENSMUSG00000024150	Mcfd2	1.11	0.08935	0.9998	76.08	185.20
ENSMUSG00000020571	Pdia6	1.11	0.08986	0.9998	240.70	584.50
ENSMUSG00000051319	1500011K16Rik	1.11	0.09594	0.9998	10.47	25.42

ENSMUSG00000040269	Mrps28	1.10	0.09483	0.9998	18.28	44.22
ENSMUSG00000064016	Gm648	1.10	0.1331	0.9998	1.15	2.78
ENSMUSG00000028860	Sytl1	1.10	0.09501	0.9998	14.79	35.63
ENSMUSG00000034636	Zyg11b	1.10	0.09395	0.9998	9.93	23.91
ENSMUSG00000038954	Supt3	1.09	0.1035	0.9998	3.98	9.58
ENSMUSG00000002279	Lmf1	1.09	0.09697	0.9998	7.79	18.72
ENSMUSG00000039236	Isg20	1.09	0.09521	0.9998	82.71	198.60
ENSMUSG00000029198	Grpel1	1.09	0.09637	0.9998	11.99	28.73
ENSMUSG00000055976	Cldn23	1.09	0.1128	0.9998	1.54	3.69
ENSMUSG00000022365	Derl1	1.09	0.0958	0.9998	52.04	124.70
ENSMUSG00000031278	Acsl4	1.09	0.09663	0.9998	11.12	26.61
ENSMUSG00000044748	Defb1	1.09	0.09674	0.9998	77.15	184.60
ENSMUSG00000028708	Mknk1	1.09	0.0972	0.9998	38.66	92.47
ENSMUSG00000038213	Tapbpl	1.09	0.09722	0.9998	22.10	52.83
ENSMUSG00000028680	Plk3	1.09	0.09801	0.9998	12.83	30.69
ENSMUSG00000001751	Naglu	1.08	0.09794	0.9998	15.86	37.88
ENSMUSG00000020224	Llph	1.08	0.1007	0.9998	19.13	45.57
ENSMUSG00000103897	Pcdhga8	1.08	0.1028	0.9998	2.29	5.45
ENSMUSG00000061126	Cyp4f39	1.08	0.1019	0.9998	9.20	21.90
ENSMUSG00000031960	Aars	1.08	0.09975	0.9998	106.20	252.00
ENSMUSG00000038776	Ephx1	1.08	0.1018	0.9998	19.16	45.48
ENSMUSG00000056216	Cebpg	1.07	0.1007	0.9998	34.38	81.48
ENSMUSG00000040451	Sgms1	1.07	0.1017	0.9998	14.00	33.18
ENSMUSG00000039252	Lgi2	1.07	0.1018	0.9998	4.93	11.68
ENSMUSG00000033809	Alg3	1.07	0.1044	0.9998	11.00	26.03
ENSMUSG00000042289	Hsd3b7	1.07	0.103	0.9998	19.42	45.95
ENSMUSG00000029544	Cabp1	1.07	0.105	0.9998	12.94	30.58
ENSMUSG00000054196	Cthrc1	1.07	0.1201	0.9998	2.69	6.36
ENSMUSG00000037447	Arid5a	1.07	0.1128	0.9998	2.10	4.94
ENSMUSG00000032575	Manf	1.07	0.1027	0.9998	296.00	697.90
ENSMUSG00000011257	Pabpc4	1.07	0.1032	0.9998	34.97	82.41
ENSMUSG00000024841	Eif1ad	1.07	0.1047	0.9998	10.91	25.71
ENSMUSG00000024875	Yif1a	1.06	0.1042	0.9998	35.64	83.89
ENSMUSG00000024924	Vldlr	1.06	0.1059	0.9998	32.44	75.98
ENSMUSG00000030876	Mettl9	1.05	0.1076	0.9998	43.36	101.30
ENSMUSG00000027357	Crls1	1.05	0.1098	0.9998	15.70	36.64
ENSMUSG00000022748	Cmss1	1.05	0.1284	0.9998	2.68	6.27
ENSMUSG00000009108	Gnat2	1.05	0.1103	0.9998	13.59	31.70
ENSMUSG00000036390	Gadd45a	1.04	0.1146	0.9998	13.52	31.41
ENSMUSG00000036678	Aaas	1.04	0.1161	0.9998	6.15	14.24
ENSMUSG00000028825	Rhd	1.03	0.131	0.9998	2.93	6.74
ENSMUSG00000078898	Gm4723	1.03	0.1274	0.9998	3.64	8.41
ENSMUSG00000031919	Tmed6	1.03	0.1201	0.9998	11.44	26.31
ENSMUSG00000057058	Skap1	1.03	0.116	0.9998	42.39	97.36
ENSMUSG00000054484	Tmem62	1.03	0.1177	0.9998	11.19	25.71
ENSMUSG00000021610	Clptm1l	1.03	0.1154	0.9998	77.24	177.30
ENSMUSG00000035595	1600002K03Rik	1.03	0.1256	0.9998	8.61	19.74
ENSMUSG00000072582	Ptrh2	1.02	0.1203	0.9998	5.48	12.54
ENSMUSG00000032115	Hyou1	1.02	0.1174	0.9998	318.70	728.60
ENSMUSG00000037613	Tnfrsf23	1.02	0.1206	0.9998	9.33	21.32
ENSMUSG00000031570	Ppapdc1b	1.02	0.119	0.9998	73.31	167.20

ENSMUSG00000058013	Sep 11	1.02	0.1196	0.9998	10.14	23.12
ENSMUSG00000062619	2310039H08Rik	1.02	0.122	0.9998	22.71	51.78
ENSMUSG00000078348	Sf3b5	1.02	0.1235	0.9998	3.69	8.40
ENSMUSG00000037772	Mrpl23	1.01	0.1242	0.9998	22.62	51.39
ENSMUSG00000040511	Pvr	1.01	0.1312	0.9998	3.18	7.22
ENSMUSG00000037966	Ninj1	1.01	0.1228	0.9998	61.08	138.40
ENSMUSG00000019158	Tmem160	1.01	0.1274	0.9998	13.30	30.13
ENSMUSG00000043284	Tmem11	1.01	0.1262	0.9998	13.13	29.71
ENSMUSG00000055799	Tcf7l1	1.01	0.132	0.9998	3.72	8.41
ENSMUSG00000042750	Bex2	1.00	0.1241	0.9998	180.50	407.60
ENSMUSG00000043008	Klhl6	1.00	0.1422	0.9998	2.95	6.65
ENSMUSG00000062070	Pgk1	1.00	0.1249	0.9998	80.37	181.30
ENSMUSG00000001020	S100a4	1.00	0.1313	0.9998	21.17	47.71
ENSMUSG00000036856	Wnt4	-1.00	0.1252	0.9998	59.04	33.25
ENSMUSG00000024968	Rcor2	-1.00	0.1402	0.9998	4.74	2.67
ENSMUSG00000050555	Hyls1	-1.00	0.1428	0.9998	1.92	1.08
ENSMUSG00000044468	Fam46c	-1.00	0.1251	0.9998	23.34	13.14
ENSMUSG00000052364	B630019K06Rik	-1.00	0.1271	0.9998	16.89	9.51
ENSMUSG00000025492	Ifitm3	-1.00	0.1468	0.9998	6.91	3.88
ENSMUSG00000022952	Runx1	-1.01	0.1403	0.9998	2.21	1.24
ENSMUSG00000026463	Atp2b4	-1.01	0.1229	0.9998	15.47	8.66
ENSMUSG00000049148	Plcxd3	-1.01	0.1318	0.9998	3.54	1.98
ENSMUSG00000020427	Igfbp3	-1.01	0.1235	0.9998	24.10	13.49
ENSMUSG00000020122	Egfr	-1.01	0.1273	0.9998	3.91	2.19
ENSMUSG00000026034	Clk1	-1.01	0.1214	0.9998	92.44	51.66
ENSMUSG00000028541	B4galt2	-1.01	0.1277	0.9998	7.78	4.33
ENSMUSG00000043323	Fbrsl1	-1.01	0.1211	0.9998	39.25	21.91
ENSMUSG00000054675	Tmem119	-1.01	0.1489	0.9998	2.82	1.57
ENSMUSG00000047712	Ust	-1.02	0.1272	0.9998	3.20	1.78
ENSMUSG00000028339	Col15a1	-1.02	0.1222	0.9998	11.66	6.50
ENSMUSG00000024538	Ppic	-1.02	0.1443	0.9998	3.26	1.81
ENSMUSG00000030247	Kcnj8	-1.02	0.1443	0.9998	1.92	1.07
ENSMUSG00000022091	Sorbs3	-1.02	0.1282	0.9998	3.78	2.10
ENSMUSG00000000753	Serpinf1	-1.02	0.1447	0.9998	4.70	2.61
ENSMUSG00000026208	Des	-1.02	0.1379	0.9998	3.32	1.84
ENSMUSG00000018899	Irf1	-1.02	0.1188	0.9998	41.88	23.22
ENSMUSG00000022324	Matn2	-1.02	0.1196	0.9998	8.50	4.71
ENSMUSG00000047344	Lancl3	-1.03	0.1256	0.9998	2.74	1.52
ENSMUSG00000047146	Tet1	-1.03	0.1247	0.9998	1.98	1.10
ENSMUSG00000006519	Cyba	-1.03	0.1317	0.9998	8.55	4.73
ENSMUSG00000002603	Tgfb1	-1.03	0.1195	0.9998	22.11	12.22
ENSMUSG00000025743	Sdc3	-1.03	0.1162	0.9998	48.58	26.84
ENSMUSG00000031355	Arhgap6	-1.03	0.1228	0.9998	2.99	1.64
ENSMUSG00000037579	Kcnh3	-1.03	0.1285	0.9998	1.99	1.10
ENSMUSG00000032852	Rspo4	-1.03	0.1157	0.9998	18.32	10.09
ENSMUSG00000029420	Rimbp2	-1.03	0.113	0.9998	109.50	60.24
ENSMUSG00000030302	Atp2b2	-1.03	0.1148	0.9998	8.84	4.86
ENSMUSG00000027603	Ggt7	-1.04	0.1147	0.9998	36.48	20.04
ENSMUSG00000040972	Igsf21	-1.04	0.1376	0.9998	2.07	1.13
ENSMUSG00000028957	Per3	-1.04	0.1141	0.9998	9.77	5.36
ENSMUSG00000026312	Cdh7	-1.04	0.1174	0.9998	5.37	2.94

ENSMUSG00000002910	Arrdc2	-1.04	0.1208	0.9998	4.37	2.39
ENSMUSG00000021221	Dpf3	-1.04	0.1346	0.9998	2.65	1.45
ENSMUSG00000052135	Foxo6	-1.04	0.1141	0.9998	9.84	5.38
ENSMUSG00000062960	Kdr	-1.04	0.1119	0.9998	10.71	5.86
ENSMUSG00000038456	Dennd2a	-1.04	0.1207	0.9998	4.29	2.34
ENSMUSG00000032035	Ets1	-1.05	0.114	0.9998	9.41	5.14
ENSMUSG00000052613	Pcdh15	-1.05	0.113	0.9998	4.20	2.29
ENSMUSG00000002020	Ltbp2	-1.05	0.1168	0.9998	3.23	1.76
ENSMUSG00000023505	Cdca3	-1.05	0.1547	0.9998	1.86	1.01
ENSMUSG00000040732	Erg	-1.05	0.1226	0.9998	3.48	1.89
ENSMUSG00000072966	Gprasp2	-1.05	0.1084	0.9998	51.16	27.83
ENSMUSG00000003948	Mmd	-1.05	0.1146	0.9998	6.06	3.29
ENSMUSG00000019900	Rfx6	-1.05	0.1072	0.9998	46.81	25.41
ENSMUSG00000021388	Aspn	-1.05	0.1209	0.9998	3.03	1.64
ENSMUSG00000029720	Gm20605	-1.05	0.1096	0.9998	6.40	3.47
ENSMUSG00000035578	Iqcg	-1.06	0.1285	0.9998	2.98	1.61
ENSMUSG00000027947	Il6ra	-1.06	0.1058	0.9998	31.42	17.01
ENSMUSG00000058297	Spock2	-1.06	0.1049	0.9998	313.60	169.70
ENSMUSG00000034255	Arhgap27	-1.06	0.1208	0.9998	3.53	1.91
ENSMUSG00000035246	Pcyt1b	-1.06	0.1059	0.9998	8.60	4.64
ENSMUSG00000054074	Skida1	-1.06	0.1241	0.9998	2.29	1.23
ENSMUSG00000057530	Ece1	-1.06	0.1033	0.9998	283.40	152.80
ENSMUSG00000026489	Adck3	-1.06	0.1061	0.9998	34.82	18.77
ENSMUSG00000019987	Arg1	-1.06	0.107	0.9998	16.18	8.72
ENSMUSG00000040543	Pitpnm3	-1.07	0.1035	0.9998	22.34	12.03
ENSMUSG00000056888	Glipr1	-1.07	0.1417	0.9998	2.73	1.47
ENSMUSG00000022211	Lrrc16b	-1.07	0.1028	0.9998	25.72	13.83
ENSMUSG00000000142	Axin2	-1.07	0.1087	0.9998	8.44	4.54
ENSMUSG00000074743	Thbd	-1.07	0.1116	0.9998	2.83	1.52
ENSMUSG00000025375	Aatk	-1.07	0.1029	0.9998	12.21	6.56
ENSMUSG00000025221	Kcnip2	-1.07	0.1181	0.9998	4.83	2.59
ENSMUSG00000001566	Mnx1	-1.07	0.1054	0.9998	9.08	4.86
ENSMUSG00000028072	Ntrk1	-1.07	0.1195	0.9998	1.97	1.05
ENSMUSG00000030218	Mgp	-1.07	0.1028	0.9998	58.55	31.33
ENSMUSG00000001552	Jup	-1.07	0.1004	0.9998	50.77	27.17
ENSMUSG00000021733	Slc4a7	-1.07	0.1	0.9998	36.20	19.36
ENSMUSG00000029287	Tgfbr3	-1.07	0.1031	0.9998	10.53	5.63
ENSMUSG00000084128	Esrp2	-1.08	0.1047	0.9998	16.35	8.74
ENSMUSG00000068551	Zfp467	-1.08	0.1047	0.9998	10.78	5.76
ENSMUSG00000022899	Slc15a2	-1.08	0.1221	0.9998	3.43	1.83
ENSMUSG00000055692	Tmem191c	-1.08	0.1063	0.9998	13.09	6.99
ENSMUSG00000045282	Tmem86b	-1.08	0.119	0.9998	4.05	2.16
ENSMUSG00000042757	Tmem108	-1.08	0.1042	0.9998	6.18	3.29
ENSMUSG00000003070	Efna2	-1.08	0.1141	0.9998	2.86	1.52
ENSMUSG00000005131	4930550C14Rik	-1.08	0.1321	0.9998	2.30	1.22
ENSMUSG00000018126	Baiap2l2	-1.08	0.1259	0.9998	1.93	1.03
ENSMUSG00000032782	Cntrob	-1.08	0.09898	0.9998	41.41	22.03
ENSMUSG00000027765	P2ry1	-1.08	0.09907	0.9998	14.26	7.58
ENSMUSG00000070604	Vsig10l	-1.08	0.1068	0.9998	2.70	1.44
ENSMUSG00000034687	Fras1	-1.09	0.09909	0.9998	4.76	2.52
ENSMUSG00000052783	Grk4	-1.09	0.1135	0.9998	2.73	1.45

ENSMUSG00000026072	Il1r1	-1.09	0.0949	0.9998	131.20	69.43
ENSMUSG00000028995	Fam126a	-1.09	0.105	0.9998	3.17	1.68
ENSMUSG00000029162	Khk	-1.09	0.1	0.9998	15.58	8.23
ENSMUSG00000025498	Irf7	-1.09	0.122	0.9998	2.75	1.45
ENSMUSG00000042428	Mgat3	-1.10	0.0944	0.9998	24.41	12.87
ENSMUSG00000038058	Nod1	-1.10	0.09583	0.9998	10.28	5.42
ENSMUSG00000021493	Pdlim7	-1.10	0.09701	0.9998	17.53	9.23
ENSMUSG00000054690	Emcn	-1.10	0.09595	0.9998	14.67	7.72
ENSMUSG00000053693	Mast1	-1.10	0.09555	0.9998	14.13	7.43
ENSMUSG00000099032	Tcf24	-1.10	0.0947	0.9998	12.09	6.36
ENSMUSG00000022129	Dct	-1.10	0.1141	0.9998	1.96	1.03
ENSMUSG00000010021	Kif19a	-1.10	0.09439	0.9998	27.69	14.56
ENSMUSG00000020182	Ddc	-1.10	0.09198	0.9998	206.90	108.60
ENSMUSG00000027166	Dnajc24	-1.10	0.09542	0.9998	27.12	14.23
ENSMUSG00000018920	Cxcl16	-1.10	0.09618	0.9998	10.31	5.41
ENSMUSG00000028634	Hivep3	-1.10	0.09519	0.9998	3.30	1.73
ENSMUSG00000021127	Zfp36l1	-1.10	0.1023	0.9998	3.39	1.77
ENSMUSG00000031375	Bgn	-1.11	0.0918	0.9998	38.47	20.14
ENSMUSG00000025735	Rhbdl1	-1.11	0.1266	0.9998	2.18	1.14
ENSMUSG00000028763	Hspg2	-1.11	0.09381	0.9998	1.92	1.01
ENSMUSG00000039809	Gabbr2	-1.11	0.09126	0.9998	12.62	6.60
ENSMUSG00000001166	Oas1c	-1.11	0.1204	0.9998	2.70	1.41
ENSMUSG00000059921	Unc5c	-1.11	0.09437	0.9998	4.17	2.18
ENSMUSG00000074457	S100a16	-1.11	0.1076	0.9998	6.19	3.23
ENSMUSG00000043924	Ncmap	-1.11	0.1043	0.9998	4.86	2.53
ENSMUSG00000034845	Plvap	-1.11	0.09012	0.9998	24.78	12.90
ENSMUSG00000041773	Enc1	-1.11	0.09118	0.9998	6.65	3.46
ENSMUSG00000031596	Slc7a2	-1.12	0.08809	0.9998	74.64	38.83
ENSMUSG00000056481	Cd248	-1.12	0.1067	0.9998	1.95	1.01
ENSMUSG00000045382	Cxcr4	-1.12	0.09052	0.9998	20.34	10.56
ENSMUSG00000040613	Apobec1	-1.12	0.09015	0.9998	15.52	8.05
ENSMUSG00000011751	Sptbn4	-1.12	0.0869	0.9998	31.51	16.33
ENSMUSG00000027796	Smad9	-1.12	0.09456	0.9998	2.13	1.10
ENSMUSG00000029581	Fscn1	-1.12	0.09082	0.9998	12.86	6.66
ENSMUSG00000024679	Ms4a6d	-1.12	0.1106	0.9998	4.51	2.33
ENSMUSG00000026452	Syt2	-1.12	0.09153	0.9998	4.61	2.38
ENSMUSG00000044197	Gpr146	-1.12	0.09421	0.9998	4.35	2.25
ENSMUSG00000021760	Gpx8	-1.12	0.1293	0.9998	2.06	1.06
ENSMUSG00000038930	Rccd1	-1.13	0.09195	0.9998	8.60	4.44
ENSMUSG00000014599	Csf1	-1.13	0.08803	0.9998	14.97	7.73
ENSMUSG00000005986	Ankrd13d	-1.13	0.09313	0.9998	10.04	5.17
ENSMUSG00000047735	Samd9l	-1.13	0.08715	0.9998	5.85	3.02
ENSMUSG00000056895	Hist3h2ba	-1.13	0.1111	0.9998	5.61	2.88
ENSMUSG00000024232	Bambi	-1.13	0.08604	0.9998	9.21	4.75
ENSMUSG00000068522	Aard	-1.13	0.1129	0.9998	2.37	1.22
ENSMUSG00000049313	Sorl1	-1.13	0.08525	0.9998	14.22	7.32
ENSMUSG00000026806	Ddx31	-1.13	0.08593	0.9998	12.90	6.64
ENSMUSG00000030873	Scnn1b	-1.13	0.08335	0.9998	85.62	43.98
ENSMUSG00000053964	Lgals4	-1.13	0.09132	0.9998	12.98	6.66
ENSMUSG00000066456	Hmgn3	-1.14	0.08289	0.9998	230.90	118.40
ENSMUSG00000009545	Kcnq1	-1.14	0.1084	0.9998	4.13	2.11

ENSMUSG00000048376	F2r	-1.14	0.09327	0.9998	2.47	1.27
ENSMUSG00000032578	Cish	-1.14	0.08505	0.9998	14.03	7.19
ENSMUSG00000022421	Nptxr	-1.14	0.08155	0.9998	33.21	16.98
ENSMUSG00000026678	Rgs5	-1.14	0.08406	0.9998	12.27	6.27
ENSMUSG00000025608	Podxl	-1.14	0.0849	0.9998	4.37	2.23
ENSMUSG00000020917	Acly	-1.14	0.08084	0.9998	644.10	329.00
ENSMUSG00000000579	Dynlt1c	-1.14	0.08335	0.9998	19.51	9.95
ENSMUSG00000019846	Lama4	-1.14	0.08523	0.9998	7.89	4.03
ENSMUSG00000021071	Trim9	-1.14	0.08362	0.9998	6.35	3.24
ENSMUSG00000074272	Ceacam1	-1.14	0.08751	0.9998	3.78	1.92
ENSMUSG00000031374	Zfp92	-1.14	0.08188	0.9998	15.01	7.66
ENSMUSG00000031024	St5	-1.14	0.08091	0.9998	24.60	12.54
ENSMUSG00000018822	Sfrp5	-1.15	0.0816	0.9998	26.85	13.68
ENSMUSG00000029027	Dffb	-1.15	0.08695	0.9998	10.29	5.22
ENSMUSG00000034947	Tmem106a	-1.15	0.09447	0.9998	3.68	1.87
ENSMUSG00000039377	Hlx	-1.15	0.1005	0.9998	2.74	1.39
ENSMUSG00000087651	1500009L16Rik	-1.15	0.08589	0.9998	9.99	5.07
ENSMUSG00000038178	Slc43a2	-1.15	0.07811	0.9998	101.30	51.33
ENSMUSG00000021806	Nid2	-1.16	0.08208	0.9998	3.43	1.73
ENSMUSG00000020743	Mif4gd	-1.16	0.07999	0.9998	19.31	9.73
ENSMUSG00000009292	Trpm2	-1.16	0.08037	0.9998	5.82	2.93
ENSMUSG00000053166	Cdh22	-1.16	0.07951	0.9998	7.55	3.80
ENSMUSG00000090877	Hspa1b	-1.16	0.08223	0.9998	4.33	2.16
ENSMUSG00000033032	Afap1l1	-1.16	0.086	0.9998	2.62	1.32
ENSMUSG00000029475	Kdm2b	-1.17	0.07535	0.9998	45.27	22.74
ENSMUSG00000030220	Arhgdib	-1.17	0.0853	0.9998	8.81	4.42
ENSMUSG00000017692	Rhbdl3	-1.17	0.08162	0.9998	7.38	3.70
ENSMUSG00000027435	Cd93	-1.17	0.0768	0.9998	5.05	2.53
ENSMUSG00000001029	Icam2	-1.17	0.1134	0.9998	3.18	1.59
ENSMUSG00000078161	Erich3	-1.17	0.07595	0.9998	9.70	4.86
ENSMUSG00000002227	Mov10	-1.17	0.07945	0.9998	5.71	2.86
ENSMUSG00000022490	Ppp1r1a	-1.17	0.07364	0.9998	229.90	115.00
ENSMUSG00000024338	Psmb8	-1.17	0.08154	0.9998	7.33	3.66
ENSMUSG00000074892	B3galt5	-1.17	0.07456	0.9998	12.25	6.13
ENSMUSG00000058258	Idi1	-1.17	0.07509	0.9998	33.42	16.69
ENSMUSG00000052336	Cx3cr1	-1.17	0.07925	0.9998	3.80	1.89
ENSMUSG00000020810	Cygb	-1.17	0.0866	0.9998	2.67	1.33
ENSMUSG00000019970	Sgk1	-1.18	0.07793	0.9998	10.28	5.12
ENSMUSG00000042269	Fam92b	-1.18	0.08399	0.9998	10.50	5.22
ENSMUSG00000032012	Pvrl1	-1.18	0.0742	0.9998	6.71	3.34
ENSMUSG00000098112	Bin2	-1.18	0.09703	0.9998	2.69	1.34
ENSMUSG00000038024	Dennd4c	-1.18	0.07134	0.9998	50.81	25.26
ENSMUSG00000026043	Col3a1	-1.18	0.07261	0.9998	27.01	13.42
ENSMUSG00000052117	D630039A03Rik	-1.18	0.0736	0.9998	11.91	5.92
ENSMUSG00000021678	F2rl1	-1.18	0.07563	0.9998	5.98	2.96
ENSMUSG00000034771	Tle2	-1.18	0.07181	0.9998	36.34	18.02
ENSMUSG00000044164	Rnf182	-1.19	0.0751	0.9998	8.63	4.27
ENSMUSG00000055862	Izumo4	-1.19	0.07482	0.9998	18.50	9.16
ENSMUSG00000020241	Col6a2	-1.19	0.07295	0.9998	5.66	2.80
ENSMUSG00000019320	Noxo1	-1.19	0.07878	0.9998	5.82	2.87
ENSMUSG00000054728	Phactr1	-1.19	0.06874	0.9998	118.20	58.30

ENSMUSG00000036572	Upf3b	-1.19	0.06945	0.9998	44.09	21.73
ENSMUSG00000022315	Slc30a8	-1.20	0.06773	0.9998	360.20	177.10
ENSMUSG00000022098	Bmp1	-1.20	0.06807	0.9998	31.87	15.66
ENSMUSG00000060206	Zfp462	-1.20	0.07007	0.9998	5.97	2.93
ENSMUSG00000032125	Robo4	-1.20	0.07172	0.9998	4.92	2.42
ENSMUSG00000007035	Msh5	-1.20	0.07616	0.9998	5.15	2.52
ENSMUSG00000020205	Phlda1	-1.20	0.07673	0.9998	4.12	2.02
ENSMUSG00000067215	Usp51	-1.20	0.07289	0.9998	5.57	2.72
ENSMUSG00000001911	Nfix	-1.21	0.06851	0.9998	13.22	6.46
ENSMUSG00000000216	Scnn1g	-1.21	0.0727	0.9998	3.90	1.91
ENSMUSG00000052595	A1cf	-1.22	0.06641	0.9998	6.72	3.26
ENSMUSG00000025993	Slc40a1	-1.22	0.06393	0.9998	44.07	21.35
ENSMUSG00000022805	Maats1	-1.22	0.07464	0.9998	2.71	1.31
ENSMUSG00000049502	Dtx3l	-1.22	0.06631	0.9998	5.63	2.72
ENSMUSG00000026278	Bok	-1.22	0.07807	0.9998	5.15	2.49
ENSMUSG00000027544	Nfatc2	-1.22	0.06374	0.9998	14.30	6.91
ENSMUSG00000027074	Slc43a3	-1.22	0.08279	0.9998	2.87	1.38
ENSMUSG00000081058	Hist2h3c2	-1.22	0.09806	0.9998	2.19	1.06
ENSMUSG00000030102	Itpr1	-1.22	0.06209	0.9998	14.51	7.00
ENSMUSG00000042655	Fam159b	-1.23	0.06447	0.9998	18.62	8.96
ENSMUSG00000046688	Tifa	-1.23	0.07397	0.9998	3.15	1.52
ENSMUSG00000002265	Peg3	-1.23	0.06027	0.9998	532.70	255.80
ENSMUSG00000040181	Fmo1	-1.23	0.06544	0.9998	9.68	4.65
ENSMUSG00000048126	Col6a3	-1.23	0.06188	0.9998	6.89	3.30
ENSMUSG00000092035	Peg10	-1.23	0.06695	0.9998	2.17	1.04
ENSMUSG00000021676	Iqgap2	-1.24	0.06446	0.9998	2.71	1.29
ENSMUSG00000061751	Kalrn	-1.24	0.06159	0.9998	4.07	1.94
ENSMUSG00000028073	Pear1	-1.25	0.06881	0.9998	2.46	1.16
ENSMUSG00000003411	Rab3b	-1.25	0.05795	0.9998	27.60	13.08
ENSMUSG00000044770	Scml4	-1.25	0.0594	0.9998	12.55	5.95
ENSMUSG00000041245	Wnk3	-1.25	0.05909	0.9998	3.81	1.80
ENSMUSG00000026986	Hnmt	-1.26	0.0728	0.9998	3.15	1.48
ENSMUSG00000072688	Gm10399	-1.26	0.1201	0.9998	2.40	1.13
ENSMUSG00000031227	Magee1	-1.27	0.05437	0.9998	11.93	5.57
ENSMUSG00000064288	Hist1h4k	-1.27	0.1514	0.9998	2.37	1.10
ENSMUSG00000021679	S100z	-1.27	0.1067	0.9998	4.66	2.16
ENSMUSG00000038630	Zkscan16	-1.27	0.05441	0.9998	10.58	4.93
ENSMUSG00000029644	Pdx1	-1.28	0.05069	0.9998	53.71	24.87
ENSMUSG00000029309	Sparcl1	-1.28	0.05171	0.9998	28.52	13.20
ENSMUSG00000031613	Hpgd	-1.29	0.06243	0.9998	3.22	1.48
ENSMUSG00000051790	Nlgn2	-1.29	0.04929	0.9998	46.71	21.49
ENSMUSG00000067219	Nipal1	-1.29	0.04923	0.9998	71.64	32.94
ENSMUSG00000024659	Anxa1	-1.29	0.0596	0.9998	9.29	4.26
ENSMUSG00000040998	Npnt	-1.30	0.04957	0.9998	17.60	8.08
ENSMUSG00000032193	Ldlr	-1.30	0.04811	0.9998	78.89	36.16
ENSMUSG00000079419	Ms4a6c	-1.30	0.06894	0.9998	2.83	1.29
ENSMUSG00000020407	Upp1	-1.30	0.05049	0.9998	33.15	15.18
ENSMUSG00000063558	Aox1	-1.30	0.04995	0.9998	5.73	2.63
ENSMUSG00000001240	Ramp2	-1.30	0.05705	0.9998	8.39	3.83
ENSMUSG00000034656	Cacna1a	-1.30	0.04759	0.9998	26.80	12.22
ENSMUSG00000003228	Grk5	-1.31	0.04737	0.9998	16.53	7.52

ENSMUSG00000098306	Gm28040	-1.32	0.0746	0.9998	2.64	1.20
ENSMUSG00000046593	Tmem215	-1.32	0.04469	0.969	61.83	27.92
ENSMUSG00000076431	Sox4	-1.32	0.04647	0.9982	7.00	3.16
ENSMUSG00000045658	Pid1	-1.32	0.04804	0.9998	10.66	4.79
ENSMUSG00000062593	Lilrb4	-1.32	0.0571	0.9998	3.74	1.68
ENSMUSG00000021803	Cdhr1	-1.33	0.04409	0.9672	28.73	12.92
ENSMUSG00000056724	Nbeal2	-1.33	0.04366	0.9665	29.95	13.44
ENSMUSG00000040875	Osbpl10	-1.33	0.04728	0.9998	9.03	4.05
ENSMUSG00000024378	Stard4	-1.33	0.04419	0.9672	24.33	10.90
ENSMUSG00000041329	Atp1b2	-1.33	0.04424	0.9672	20.52	9.19
ENSMUSG00000064177	Ghrl	-1.34	0.05991	0.9998	7.00	3.11
ENSMUSG00000030409	Dmpk	-1.34	0.04172	0.9483	73.44	32.68
ENSMUSG00000041930	Fam222a	-1.35	0.04162	0.9483	15.05	6.66
ENSMUSG00000029718	Pcolce	-1.35	0.06553	0.9998	2.45	1.08
ENSMUSG00000056222	Spock1	-1.35	0.04046	0.9483	23.67	10.44
ENSMUSG00000031216	Stard8	-1.36	0.04445	0.9672	4.28	1.88
ENSMUSG00000008318	Relt	-1.36	0.04033	0.9483	35.21	15.48
ENSMUSG00000078444	Gm10941	-1.37	0.04815	0.9998	8.52	3.73
ENSMUSG00000022941	Ripply3	-1.37	0.03912	0.9405	19.47	8.49
ENSMUSG00000042116	Vwa1	-1.37	0.04355	0.9665	2.60	1.13
ENSMUSG00000025316	Banp	-1.37	0.03854	0.9346	28.56	12.43
ENSMUSG00000034926	Dhcr24	-1.38	0.0381	0.9272	8.54	3.71
ENSMUSG00000007039	Ddah2	-1.38	0.05339	0.9998	4.03	1.75
ENSMUSG00000044949	Ubtd2	-1.38	0.041	0.9483	11.83	5.12
ENSMUSG00000020614	Fam20a	-1.38	0.03704	0.9106	22.10	9.56
ENSMUSG00000029153	Ociad2	-1.39	0.03547	0.895	72.37	31.22
ENSMUSG00000029561	Oasl2	-1.39	0.04332	0.9665	5.46	2.34
ENSMUSG00000056144	Trim34a	-1.39	0.04366	0.9665	3.06	1.32
ENSMUSG00000036887	C1qa	-1.39	0.03511	0.8901	62.48	26.82
ENSMUSG00000000317	Bcl6b	-1.39	0.03564	0.8977	26.34	11.30
ENSMUSG00000037617	Spag1	-1.39	0.0402	0.9483	2.83	1.21
ENSMUSG00000029923	Rab19	-1.40	0.04077	0.9483	5.45	2.33
ENSMUSG00000036834	Plch1	-1.40	0.03639	0.9045	4.93	2.11
ENSMUSG00000071551	Akr1c19	-1.40	0.0353	0.8925	23.02	9.83
ENSMUSG00000039058	Ak5	-1.40	0.04294	0.9629	4.02	1.71
ENSMUSG00000048644	Ctxn1	-1.40	0.04345	0.9665	4.56	1.94
ENSMUSG00000060639	Hist1h4i	-1.41	0.04373	0.9665	7.39	3.13
ENSMUSG00000025092	Hspa12a	-1.41	0.03362	0.8776	8.54	3.63
ENSMUSG00000009418	Nav1	-1.41	0.03257	0.8645	20.19	8.56
ENSMUSG00000036502	Tmem255a	-1.41	0.03475	0.89	7.35	3.12
ENSMUSG00000026637	Traf5	-1.41	0.04045	0.9483	5.13	2.17
ENSMUSG00000047747	Rnf150	-1.41	0.03391	0.8799	3.28	1.39
ENSMUSG00000040495	Chrm4	-1.41	0.04052	0.9483	4.81	2.04
ENSMUSG00000047040	Prr15l	-1.41	0.03504	0.8901	10.46	4.43
ENSMUSG00000084950	Gm5577	-1.41	0.04096	0.9483	5.68	2.40
ENSMUSG00000025422	Agap2	-1.42	0.03495	0.8901	2.92	1.23
ENSMUSG00000090236	Car15	-1.42	0.03209	0.8635	52.49	22.15
ENSMUSG00000029273	Sult1d1	-1.42	0.03274	0.8662	14.14	5.96
ENSMUSG00000049721	Gal3st1	-1.42	0.03488	0.8901	8.70	3.67
ENSMUSG00000032908	Sgpp2	-1.42	0.03105	0.849	21.46	9.01
ENSMUSG00000038167	Plekhg6	-1.43	0.03262	0.8645	7.30	3.06

ENSMUSG00000078451	Ppil6	-1.43	0.04998	0.9998	2.81	1.18
ENSMUSG00000029385	Ccng2	-1.43	0.0316	0.857	11.39	4.76
ENSMUSG00000057069	Ero1lb	-1.43	0.02974	0.8321	372.90	155.90
ENSMUSG00000020262	Adarb1	-1.43	0.03032	0.8411	22.44	9.38
ENSMUSG00000020151	Ptprr	-1.44	0.03101	0.849	8.33	3.46
ENSMUSG00000034282	Evpl	-1.44	0.03165	0.857	2.85	1.18
ENSMUSG00000037843	Vstm2l	-1.44	0.02888	0.8268	84.60	35.07
ENSMUSG00000046470	Sox18	-1.44	0.0364	0.9045	4.25	1.76
ENSMUSG00000021947	Cryl1	-1.45	0.02926	0.8268	30.74	12.71
ENSMUSG00000032377	Plscr4	-1.45	0.03644	0.9045	2.69	1.11
ENSMUSG00000063704	Mapk15	-1.45	0.02892	0.8268	23.44	9.67
ENSMUSG00000068220	Lgals1	-1.45	0.02981	0.8321	26.37	10.85
ENSMUSG00000040428	Plekha4	-1.45	0.03328	0.8754	4.50	1.85
ENSMUSG00000089837	Npcd	-1.45	0.04163	0.9483	2.91	1.19
ENSMUSG00000055116	Arntl	-1.46	0.02934	0.8272	6.22	2.54
ENSMUSG00000017868	Sgk2	-1.46	0.02978	0.8321	7.34	3.00
ENSMUSG00000037071	Scd1	-1.48	0.02841	0.823	2.98	1.21
ENSMUSG00000034427	Myo15b	-1.48	0.02541	0.7834	14.37	5.79
ENSMUSG00000034422	Parp14	-1.48	0.02629	0.7924	6.47	2.61
ENSMUSG00000054320	Lrrc36	-1.49	0.03067	0.8473	3.40	1.37
ENSMUSG00000031161	Hdac6	-1.49	0.02375	0.763	154.10	61.72
ENSMUSG00000020990	Cdkl1	-1.50	0.02558	0.7834	11.72	4.68
ENSMUSG00000020734	Grin2c	-1.50	0.02471	0.775	6.53	2.61
ENSMUSG00000025582	Nptx1	-1.51	0.02399	0.763	5.47	2.17
ENSMUSG00000078439	Smim24	-1.51	0.03438	0.8873	4.26	1.68
ENSMUSG00000043079	Synpo	-1.52	0.02254	0.7337	9.75	3.84
ENSMUSG00000040147	Maob	-1.52	0.02146	0.7127	145.80	57.29
ENSMUSG00000054263	Lifr	-1.52	0.02126	0.7127	19.37	7.58
ENSMUSG00000034871	Fam151a	-1.53	0.02041	0.6956	118.60	46.18
ENSMUSG00000021999	Cpb2	-1.53	0.02961	0.8321	3.32	1.29
ENSMUSG00000037921	Ddx60	-1.53	0.02551	0.7834	3.60	1.40
ENSMUSG00000067279	Ppp1r3c	-1.54	0.02602	0.7906	2.62	1.02
ENSMUSG00000028328	Tmod1	-1.55	0.01977	0.6808	28.15	10.83
ENSMUSG00000034205	Loxl2	-1.56	0.01889	0.6638	16.77	6.42
ENSMUSG00000038393	Txnip	-1.57	0.01811	0.6443	87.40	33.28
ENSMUSG00000015944	Gatsl2	-1.57	0.01738	0.6361	84.20	31.89
ENSMUSG00000070880	Gad1	-1.57	0.01739	0.6361	106.80	40.41
ENSMUSG00000074793	Hspa12b	-1.58	0.02416	0.764	2.89	1.09
ENSMUSG00000016494	Cd34	-1.58	0.01915	0.6693	7.94	2.99
ENSMUSG00000026443	Lrrn2	-1.58	0.01933	0.6739	4.74	1.79
ENSMUSG00000015829	Tnr	-1.58	0.01703	0.6291	41.68	15.71
ENSMUSG00000091971	Hspa1a	-1.58	0.01991	0.682	4.10	1.55
ENSMUSG00000039131	Gipc2	-1.59	0.02898	0.8268	3.51	1.31
ENSMUSG00000020732	Rab37	-1.59	0.01612	0.6118	74.73	27.88
ENSMUSG00000026827	Gpd2	-1.61	0.01539	0.5986	24.63	9.11
ENSMUSG00000050914	Ankrd37	-1.61	0.01938	0.674	10.13	3.74
ENSMUSG00000046157	Tmem229b	-1.62	0.01443	0.5716	45.63	16.70
ENSMUSG00000026303	Mlph	-1.63	0.01542	0.5986	12.25	4.47
ENSMUSG00000091898	Tnnc1	-1.63	0.02996	0.8345	3.81	1.38
ENSMUSG00000067455	Hist1h4j	-1.64	0.02746	0.8076	3.40	1.24
ENSMUSG00000026989	Dapl1	-1.65	0.01557	0.6028	22.19	7.99

ENSMUSG00000041633	Kctd12b	-1.65	0.01347	0.546	13.25	4.77
ENSMUSG00000031255	Sytl4	-1.68	0.01136	0.5056	140.90	49.59
ENSMUSG00000022026	Olfm4	-1.68	0.01248	0.5293	14.54	5.11
ENSMUSG00000033174	Mgll	-1.69	0.01391	0.5572	3.54	1.24
ENSMUSG00000078588	Ccdc24	-1.70	0.0139	0.5572	6.47	2.23
ENSMUSG00000032221	Mns1	-1.71	0.01056	0.4842	18.82	6.48
ENSMUSG00000042607	Asb4	-1.73	0.01333	0.5452	3.15	1.07
ENSMUSG00000024027	Glp1r	-1.74	0.008975	0.4456	180.40	60.97
ENSMUSG00000090019	Gimap1	-1.74	0.02138	0.7127	3.10	1.04
ENSMUSG00000038855	Itpkb	-1.76	0.007988	0.41	59.97	19.89
ENSMUSG00000051209	Gpr119	-1.78	0.00828	0.4171	10.75	3.52
ENSMUSG00000094893	Gm4791	-1.78	0.01161	0.5116	18.40	6.01
ENSMUSG00000074240	Cib3	-1.81	0.00764	0.3959	27.72	8.89
ENSMUSG00000037106	Fer1l6	-1.82	0.00681	0.3733	9.52	3.04
ENSMUSG00000020814	Mxra7	-1.82	0.008202	0.4156	9.35	2.98
ENSMUSG00000049892	Rasd1	-1.83	0.006237	0.3532	35.01	11.07
ENSMUSG00000094370	Gm3373	-1.84	0.01129	0.5039	3.24	1.03
ENSMUSG00000027931	Npr1	-1.85	0.006024	0.3439	24.72	7.74
ENSMUSG00000029352	Crybb3	-1.87	0.01198	0.5161	4.13	1.27
ENSMUSG00000045871	Slitrk6	-1.88	0.004912	0.3032	20.25	6.18
ENSMUSG00000044453	Ffar1	-1.89	0.004662	0.2931	41.25	12.52
ENSMUSG00000020635	Fkbp1b	-1.90	0.004624	0.2931	112.60	34.09
ENSMUSG00000026834	Acvr1c	-1.90	0.005424	0.3218	5.08	1.53
ENSMUSG00000040350	Trim7	-1.96	0.004487	0.2887	6.48	1.88
ENSMUSG00000002266	Zim1	-1.96	0.003523	0.245	19.56	5.65
ENSMUSG00000003379	Cd79a	-1.98	0.004237	0.278	8.18	2.34
ENSMUSG00000037762	Slc16a9	-2.00	0.003329	0.2352	8.97	2.53
ENSMUSG00000009075	Cabp7	-2.02	0.0026	0.1972	60.86	16.87
ENSMUSG00000028965	Tnfrsf9	-2.08	0.004046	0.2705	3.78	1.01
ENSMUSG00000047507	Baiap3	-2.08	0.001971	0.1657	91.71	24.41
ENSMUSG00000043719	Col6a6	-2.08	0.001964	0.1657	22.42	5.96
ENSMUSG00000079165	Sap25	-2.10	0.005211	0.3146	5.02	1.29
ENSMUSG00000009246	Trpm5	-2.13	0.001671	0.1449	31.33	8.09
ENSMUSG00000079620	Muc4	-2.20	0.001173	0.1102	17.68	4.32
ENSMUSG00000030406	Gipr	-2.25	0.0009104	0.0931	51.51	12.19
ENSMUSG00000034614	Pik3ip1	-2.33	0.0009874	0.09804	8.87	1.99
ENSMUSG00000000215	Ins2	-2.34	0.0005508	0.06328	256500.00	57030.00
ENSMUSG00000005373	Mlxipl	-2.50	0.0002494	0.03488	248.20	49.45
ENSMUSG00000067786	Nnat	-2.55	0.0004211	0.05226	9.06	1.73
ENSMUSG00000019429	Ffar3	-3.00	3.92E-05	0.007899	7.95	1.12
ENSMUSG00000035804	Ins1	-3.22	4.66E-06	0.001544	47000.00	5688.00
ENSMUSG00000027690	Slc2a2	-3.23	4.44E-06	0.001527	272.30	32.71
ENSMUSG00000047591	Mafa	-4.26	9.24E-09	1.58E-05	149.70	8.80

Supplementary Table 2 to Figure 10: List of differentially expressed genes

Short-term exposure of pancreatic islets to 10 µM DXO compared to untreated control

gene_id	gene_name	log2 Ratio	pValue	fdr	Control.1h [FPKM]	DXO.1h [FPKM]
ENSMUSG00000023034	Nr4a1	3.90	8.33E-08	0.0002266	10.68	174.80
ENSMUSG00000021250	Fos	3.12	9.95E-06	0.009017	3.75	35.99
ENSMUSG00000069306	Hist1h4m	2.95	0.0001714	0.1059	1.46	12.57
ENSMUSG00000069305	Hist1h4n	2.90	0.0002171	0.118	1.40	11.38
ENSMUSG00000098132	Rassf10	2.55	0.0002208	0.118	2.39	15.42
ENSMUSG00000052565	Hist1h1d	2.52	0.0003324	0.1674	4.36	27.54
ENSMUSG00000047990	C2cd4a	2.46	0.0005647	0.2076	1.53	9.24
ENSMUSG00000025408	Ddit3	2.41	0.0003919	0.1838	62.32	365.30
ENSMUSG00000064317	Gm10146	2.40	0.002009	0.6211	1.40	8.33
ENSMUSG00000027313	Chac1	2.38	0.0004643	0.2029	22.26	127.70
ENSMUSG00000024042	Sik1	2.38	0.000486	0.2029	4.15	23.76
ENSMUSG00000038418	Egr1	2.27	0.0008337	0.2907	5.04	26.77
ENSMUSG00000032515	Csrnp1	2.23	0.001034	0.3346	4.30	22.23
ENSMUSG00000091956	C2cd4b	2.15	0.001481	0.4684	26.27	127.80
ENSMUSG00000086965	Gm16314	2.00	0.005963	1	1.48	6.49
ENSMUSG00000038894	Irs2	1.98	0.003149	0.8565	8.51	36.97
ENSMUSG00000029135	Fosl2	1.95	0.003578	0.9542	6.78	28.86
ENSMUSG00000051627	Hist1h1e	1.94	0.007133	1	1.82	7.82
ENSMUSG00000056313	1810011O10Rik	1.91	0.004898	1	4.35	17.95
ENSMUSG00000028214	Gem	1.89	0.005049	1	6.46	26.28
ENSMUSG00000031770	Herpud1	1.86	0.005231	1	193.30	772.60
ENSMUSG00000060639	Hist1h4i	1.85	0.006515	1	7.81	31.12
ENSMUSG00000052837	Junb	1.81	0.006579	1	24.40	94.27
ENSMUSG00000031381	Piga	1.80	0.00736	1	3.55	13.63
ENSMUSG00000026826	Nr4a2	1.78	0.00775	1	6.83	25.80
ENSMUSG00000095562	Gm21887	1.75	0.01543	1	2.80	10.45
ENSMUSG00000056749	Nfil3	1.73	0.009613	1	8.90	32.47
ENSMUSG00000020893	Per1	1.73	0.009388	1	17.25	62.83
ENSMUSG00000032265	Fam46a	1.66	0.01223	1	13.85	48.20
ENSMUSG00000067455	Hist1h4j	1.66	0.01611	1	4.08	14.11
ENSMUSG00000078901	Gm14440	1.62	0.01813	1	1.84	6.24
ENSMUSG00000073448	Gm10509	1.57	0.03815	1	3.15	10.45
ENSMUSG00000005148	Klf5	1.54	0.02106	1	5.48	17.57
ENSMUSG00000083695	Rnf138rt1	1.49	0.02687	1	5.49	16.93
ENSMUSG00000053560	Ier2	1.48	0.02735	1	5.78	17.67
ENSMUSG00000063245	Gm13248	1.47	0.04729	1	1.24	3.78
ENSMUSG00000052684	Jun	1.44	0.02906	1	22.30	66.51
ENSMUSG00000032501	Trib1	1.43	0.03016	1	16.76	49.67
ENSMUSG00000039910	Cited2	1.36	0.03892	1	17.05	48.19
ENSMUSG00000002732	Fkbp7	1.34	0.06215	1	1.79	4.99
ENSMUSG00000034936	Arl4d	1.34	0.05549	1	1.46	4.07
ENSMUSG00000038550	Ciart	1.33	0.04828	1	6.08	16.78
ENSMUSG00000019850	Tnfaip3	1.31	0.04924	1	3.11	8.49
ENSMUSG00000021453	Gadd45g	1.29	0.04899	1	57.24	154.40
ENSMUSG00000031530	Dusp4	1.29	0.0507	1	9.39	25.23

ENSMUSG00000032715	Trib3	1.28	0.05272	1	27.06	72.02
ENSMUSG00000020420	Zfp607	1.27	0.0634	1	1.51	3.98
ENSMUSG00000093769	Hist2h3c1	1.26	0.05692	1	6.51	17.17
ENSMUSG00000038451	Spsb2	1.26	0.05641	1	15.79	41.61
ENSMUSG00000027397	Slc20a1	1.26	0.05567	1	20.32	53.48
ENSMUSG00000060981	Hist1h4h	1.25	0.06799	1	6.91	17.93
ENSMUSG00000071083	Gm10311	1.25	0.1448	1	1.02	2.67
ENSMUSG00000070360	Amy2a1	1.24	0.095	1	1.09	2.89
ENSMUSG00000037465	Klf10	1.23	0.0609	1	8.87	22.95
ENSMUSG00000010067	Rassf1	1.23	0.06182	1	11.47	29.66
ENSMUSG00000020812	1810032O08Rik	1.21	0.07655	1	3.52	8.98
ENSMUSG00000009772	Nuak2	1.20	0.06921	1	8.02	20.23
ENSMUSG00000024190	Dusp1	1.19	0.0717	1	11.78	29.48
ENSMUSG00000096718	Zfp781	1.17	0.09048	1	3.49	8.61
ENSMUSG00000056501	Cebpb	1.17	0.07606	1	16.56	40.88
ENSMUSG00000064288	Hist1h4k	1.16	0.1055	1	4.61	11.31
ENSMUSG00000036432	Siah2	1.16	0.07695	1	20.54	50.45
ENSMUSG00000034460	Six4	1.15	0.07923	1	3.69	9.04
ENSMUSG00000026475	Rgs16	1.13	0.08656	1	13.38	32.08
ENSMUSG00000027438	Napb	1.12	0.09122	1	3.29	7.85
ENSMUSG00000000301	Pemt	1.12	0.1251	1	1.64	3.91
ENSMUSG00000057895	Zfp105	1.11	0.1029	1	2.45	5.83
ENSMUSG00000069270	Hist1h2ac	1.11	0.165	1	1.28	2.91
ENSMUSG00000037573	Tob1	1.10	0.09171	1	33.27	78.61
ENSMUSG00000003545	Fosb	1.10	0.09763	1	2.21	5.22
ENSMUSG00000006720	Zfp184	1.09	0.1043	1	2.29	5.38
ENSMUSG00000015312	Gadd45b	1.09	0.1002	1	6.91	16.19
ENSMUSG00000057924	Gm10033	1.09	0.1353	1	1.81	4.23
ENSMUSG00000039810	Zc3h10	1.07	0.1024	1	9.66	22.31
ENSMUSG00000073771	Btbd19	1.07	0.1515	1	1.09	2.51
ENSMUSG00000039531	Zufsp	1.07	0.1072	1	4.16	9.58
ENSMUSG00000046962	Zbtb21	1.06	0.1049	1	5.85	13.43
ENSMUSG00000024807	Syvn1	1.06	0.1058	1	39.08	89.38
ENSMUSG00000032593	Amigo3	1.05	0.1131	1	4.11	9.36
ENSMUSG00000004500	Zfp324	1.04	0.1119	1	6.41	14.52
ENSMUSG00000026628	Atf3	1.04	0.1164	1	4.80	10.86
ENSMUSG00000072568	Fam84b	1.03	0.1149	1	8.09	18.19
ENSMUSG00000040435	Ppp1r15a	1.03	0.1155	1	25.43	57.03
ENSMUSG00000052253	Zfp622	1.02	0.1173	1	17.05	38.14
ENSMUSG00000030469	Zfp719	1.01	0.1231	1	7.68	17.01
ENSMUSG00000054648	Zfp869	1.01	0.1238	1	19.79	43.79
ENSMUSG00000032718	Mansc1	-1.03	0.1232	1	4.47	2.40
ENSMUSG00000047379	B4gat1	-1.04	0.1161	1	8.93	4.77
ENSMUSG00000001999	Blvra	-1.06	0.1167	1	8.78	4.64
ENSMUSG00000025950	Idh1	-1.06	0.1045	1	62.19	32.72
ENSMUSG00000008307	1700109H08Rik	-1.13	0.1325	1	2.08	1.04
ENSMUSG00000068923	Syt11	-1.15	0.07893	1	21.23	10.50
ENSMUSG00000026904	Slc4a10	-1.16	0.07696	1	9.36	4.59
ENSMUSG00000030707	Coro1a	-1.17	0.08939	1	6.36	3.11
ENSMUSG00000032554	Trf	-1.19	0.08894	1	3.85	1.85
ENSMUSG00000030110	Ret	-1.22	0.06333	1	31.91	15.09

ENSMUSG00000032014	Oaf	-1.24	0.06399	1	7.08	3.31
ENSMUSG00000000876	Pxmp4	-1.25	0.06219	1	8.48	3.93
ENSMUSG00000017802	Fam134c	-1.30	0.04889	1	30.80	13.79
ENSMUSG00000090247	Bloc1s1	-1.35	0.04751	1	18.01	7.75
ENSMUSG00000029632	Ndufa4	-1.35	0.04079	1	152.10	65.67
ENSMUSG00000106106	Rn18s-rs5	-1.49	0.0254	1	14.29	5.59
ENSMUSG00000048087	Gm4737	-1.50	0.02958	1	3.33	1.29
ENSMUSG00000103565	Sgsm3	-1.58	0.02088	1	4.52	1.67
ENSMUSG00000035215	Lsm7	-1.94	0.006562	1	11.47	3.24

Supplementary Table 3 to Figure 20: List of differentially expressed genes

Long-term exposure of pancreatic islets to 1 µM DXO compared to untreated control

gene_id	gene_name	log2 Ratio	pValue	fdr	Control.24h [FPKM]	DXO. 24h [FPKM]
ENSMUSG00000009092	Derl3	4.52	1.19E-09	1.59E-06	6.732	167.8
ENSMUSG00000038742	Angptl6	4.18	1.09E-08	1.14E-05	4.028	78.84
ENSMUSG00000030717	Nupr1	4.08	2.40E-08	2.20E-05	54.96	970.5
ENSMUSG00000032715	Trib3	3.76	1.68E-07	0.0001296	15.66	224
ENSMUSG00000015652	Steap1	3.40	9.80E-07	0.0005991	1.633	20.39
ENSMUSG00000054136	Adm2	3.29	1.79E-06	0.001009	1.237	14.63
ENSMUSG00000025408	Ddit3	3.18	5.86E-06	0.002424	37.55	355.4
ENSMUSG00000022769	Sdf2l1	3.01	1.53E-05	0.005615	46.78	393.5
ENSMUSG00000027313	Chac1	2.82	4.35E-05	0.01301	14.57	107.9
ENSMUSG00000017446	C1qtnf1	2.74	4.83E-05	0.01417	1.314	10.1
ENSMUSG00000026483	Fam129a	2.70	8.27E-05	0.02247	4.492	30.76
ENSMUSG00000039158	Akna	2.64	0.0001015	0.02707	1.474	9.986
ENSMUSG00000003355	Fkbp11	2.63	0.0001225	0.031	21.29	138.4
ENSMUSG00000020256	Aldh1l2	2.58	0.0001642	0.03887	30.42	189.3
ENSMUSG00000046229	Scand1	2.53	0.0001173	0.03018	1.311	9.419
ENSMUSG00000023272	Creld2	2.52	0.0002156	0.04721	40.33	242.1
ENSMUSG00000030785	Cox6a2	2.49	0.0002451	0.05212	17	101.1
ENSMUSG00000078901	Gm14440	2.40	0.0003451	0.06842	1.682	9.812
ENSMUSG00000036067	Slc2a6	2.39	0.0003281	0.06593	1.215	7.231
ENSMUSG00000025140	Pycr1	2.38	0.0004488	0.08442	27.07	147.3
ENSMUSG00000047963	Stbd1	2.29	0.0006278	0.1096	3.865	20.39
ENSMUSG00000024164	C3	2.28	0.0006475	0.1118	2.048	10.88
ENSMUSG00000056501	Cebpb	2.24	0.0007448	0.1214	1.698	8.927
ENSMUSG00000037278	Tmem97	2.23	0.0009222	0.1487	8.955	44.29
ENSMUSG00000018821	Avpi1	2.16	0.001089	0.1718	3.254	16.18
ENSMUSG00000053398	Phgdh	2.11	0.001624	0.2406	21.59	98.08
ENSMUSG00000031770	Herpud1	2.10	0.001811	0.2598	222.5	990
ENSMUSG00000031490	Eif4ebp1	2.09	0.001824	0.2598	11.06	49.44
ENSMUSG00000026456	Cyb5r1	2.07	0.002034	0.2688	26.42	115.9
ENSMUSG00000008461	Fut1	2.03	0.001946	0.2633	1.653	7.588
ENSMUSG00000010830	Kdelr3	2.02	0.002372	0.3026	5.514	23.85
ENSMUSG00000044894	Uqcrq	1.99	0.002842	0.3447	27.72	115.8
ENSMUSG00000048078	Tenm4	1.92	0.003974	0.458	5.656	22.42
ENSMUSG00000080115	Eef1akmt3	1.91	0.003994	0.458	3.079	12.26
ENSMUSG00000095742	CAAA01147332.1	1.90	0.001464	0.2214	1.438	8.342
ENSMUSG00000026864	Hspa5	1.87	0.005143	0.5513	1073	4068
ENSMUSG00000024640	Psat1	1.86	0.005101	0.5513	15.69	59.83
ENSMUSG00000023393	Slc17a9	1.86	0.005149	0.5513	14.92	56.88
ENSMUSG00000028542	Slc6a9	1.85	0.005259	0.5591	5.136	19.63
ENSMUSG00000029163	Emilin1	1.80	0.006717	0.6463	37.19	135.2
ENSMUSG00000036699	Zcchc12	1.80	0.006593	0.6463	6.399	23.46
ENSMUSG00000020598	Nrcam	1.80	0.006352	0.6332	2.429	9.04
ENSMUSG00000038550	Ciart	1.79	0.006322	0.6332	4.549	17.03
ENSMUSG00000030588	Yif1b	1.79	0.006915	0.6503	17.64	64.05
ENSMUSG00000029161	Cgref1	1.79	0.006796	0.6463	8.271	30.31

ENSMUSG00000055725	Paqr3	1.78	0.006717	0.6463	2.58	9.553
ENSMUSG00000042737	Dpm3	1.76	0.007564	0.7001	18.19	65.36
ENSMUSG00000046027	Stard5	1.75	0.008099	0.738	17.6	62.21
ENSMUSG00000030659	Nucb2	1.75	0.008517	0.7684	115.9	405.1
ENSMUSG00000028044	Cks1b	1.71	0.009028	0.7918	8.254	29.02
ENSMUSG00000015943	Bola1	1.71	0.008697	0.7733	4.307	15.37
ENSMUSG00000044447	Dock5	1.70	0.01026	0.8652	2.866	9.762
ENSMUSG00000020964	Sel1l	1.67	0.01159	0.9494	84.41	280.1
ENSMUSG00000007594	Hapln4	1.67	0.01165	0.9494	68.05	225.7
ENSMUSG00000032575	Manf	1.64	0.01334	0.9999	227.1	735.7
ENSMUSG00000025823	Pdia4	1.63	0.01397	0.9999	157.6	506.6
ENSMUSG00000006611	Hfe	1.61	0.01486	0.9999	14.96	47.71
ENSMUSG00000032115	Hyou1	1.60	0.01559	0.9999	296.5	934.6
ENSMUSG00000028860	Sytl1	1.60	0.01534	0.9999	10.62	33.73
ENSMUSG00000003872	Lin7b	1.60	0.0111	0.9255	2.256	8.118
ENSMUSG00000040794	C1qtnf4	1.59	0.01315	0.9999	1.626	5.491
ENSMUSG00000041168	Lonp1	1.58	0.01665	0.9999	31.54	98.36
ENSMUSG00000035202	Lars2	1.57	0.0177	0.9999	75.01	231.4
ENSMUSG00000054196	Cthrc1	1.56	0.01524	0.9999	2.482	8.186
ENSMUSG00000029446	Psph	1.55	0.01787	0.9999	9.115	28.31
ENSMUSG00000019158	Tmem160	1.55	0.01745	0.9999	7.707	24.16
ENSMUSG00000040690	Col16a1	1.55	0.01688	0.9999	1.819	5.783
ENSMUSG00000032997	Chpf	1.55	0.01912	0.9999	28.94	88.1
ENSMUSG00000006442	Srm	1.51	0.02187	0.9999	40.63	120.9
ENSMUSG00000028671	Gale	1.51	0.02188	0.9999	22.85	68.06
ENSMUSG00000042406	Atf4	1.49	0.0239	0.9999	156.6	457.6
ENSMUSG00000103865	Gm37416	1.48	0.01646	0.9999	2.639	9.004
ENSMUSG00000062619	2310039H08Rik	1.47	0.02452	0.9999	9.878	29.02
ENSMUSG00000020571	Pdia6	1.47	0.02583	0.9999	368.3	1061
ENSMUSG00000040618	Pck2	1.47	0.0257	0.9999	56.6	163.2
ENSMUSG00000058579	Cela2a	1.46	0.01913	0.9999	1.457	4.753
ENSMUSG00000029591	Ung	1.46	0.02266	0.9999	1.371	4.18
ENSMUSG00000031765	Mt1	1.46	0.02703	0.9999	162.8	465
ENSMUSG00000027737	Slc7a11	1.46	0.02556	0.9999	1.791	5.226
ENSMUSG00000017204	Gsdma	1.45	0.0268	0.9999	3.264	9.419
ENSMUSG00000033307	Mif	1.44	0.02767	0.9999	30.03	85.78
ENSMUSG00000042747	Krtcap2	1.44	0.02862	0.9999	63.4	179.4
ENSMUSG00000115018	AL732309.1	1.44	0.025	0.9999	1.155	3.468
ENSMUSG00000028893	Sesn2	1.43	0.02925	0.9999	23.85	67.17
ENSMUSG00000045948	Mrps12	1.43	0.02965	0.9999	34.47	97.08
ENSMUSG00000063954	Hist2h2aa2	1.43	0.02881	0.9999	14.63	41.66
ENSMUSG00000023952	Gtpbp2	1.42	0.03047	0.9999	60.42	168.9
ENSMUSG00000031574	Star	1.42	0.02898	0.9999	2.286	6.539
ENSMUSG00000070284	Gmppb	1.41	0.03231	0.9999	37.64	104.1
ENSMUSG00000020857	Nme2	1.40	0.03253	0.9999	70.67	195.2
ENSMUSG00000003814	Calr	1.40	0.03366	0.9999	721.3	1976
ENSMUSG00000026615	Eprs	1.39	0.03474	0.9999	82.67	225.2
ENSMUSG00000024807	Syvn1	1.38	0.03504	0.9999	31.52	85.77
ENSMUSG00000036111	Lmo1	1.38	0.02975	0.9999	2.012	5.864
ENSMUSG00000031700	Gpt2	1.38	0.03449	0.9999	7.902	21.67
ENSMUSG00000053317	Sec61b	1.37	0.0374	0.9999	144.9	389.4

ENSMUSG00000002043	Trappc6a	1.36	0.03685	0.9999	9.363	25.52
ENSMUSG00000042942	Greb1l	1.35	0.03557	0.9999	1.044	2.907
ENSMUSG00000005667	Mthfd2	1.34	0.04081	0.9999	85.8	226.7
ENSMUSG00000029596	Sdsl	1.34	0.03333	0.9999	1.491	4.293
ENSMUSG00000038539	Atf5	1.33	0.04224	0.9999	121.8	319.5
ENSMUSG00000032383	Ppib	1.32	0.0444	0.9999	37.08	96.36
ENSMUSG00000031762	Mt2	1.31	0.04561	0.9999	175	452.5
ENSMUSG00000022136	Dnajc3	1.31	0.0458	0.9999	87.84	226.7
ENSMUSG00000020940	1700023F06Rik	1.31	0.04042	0.9999	2.817	7.681
ENSMUSG00000047617	Paxx	1.31	0.0449	0.9999	15.73	41.01
ENSMUSG00000003380	Rabac1	1.31	0.04616	0.9999	121	312
ENSMUSG00000055799	Tcf7l1	1.31	0.04395	0.9999	4.849	12.77
ENSMUSG00000028919	Arhgef19	1.30	0.04518	0.9999	8.061	21.03
ENSMUSG00000030036	Mogs	1.30	0.04697	0.9999	39.07	100.4
ENSMUSG00000032353	Tmed3	1.30	0.04741	0.9999	161.6	414.2
ENSMUSG00000052271	Bhlha15	1.30	0.04726	0.9999	22.13	56.81
ENSMUSG00000024856	Cdk2ap2	1.30	0.04775	0.9999	35.63	91.43
ENSMUSG00000015363	Trabd	1.29	0.04952	0.9999	61.78	157.1
ENSMUSG00000061306	Slc38a10	1.29	0.04984	0.9999	220	558.5
ENSMUSG00000040010	Slc7a5	1.28	0.05021	0.9999	118.3	300
ENSMUSG00000015085	Entpd2	1.28	0.04837	0.9999	4.669	12.05
ENSMUSG00000049422	Chchd10	1.28	0.05057	0.9999	21.99	55.83
ENSMUSG00000040435	Ppp1r15a	1.27	0.05183	0.9999	26.71	67.35
ENSMUSG00000009108	Gnat2	1.27	0.05161	0.9999	13.76	34.81
ENSMUSG00000034667	Xpot	1.27	0.05311	0.9999	48.24	120.9
ENSMUSG00000028825	Rhd	1.27	0.04849	0.9999	2.863	7.475
ENSMUSG00000012017	Scarf2	1.26	0.05059	0.9999	1.449	3.723
ENSMUSG00000069633	Pex11g	1.26	0.05244	0.9999	6.445	16.31
ENSMUSG00000032593	Amigo3	1.26	0.05202	0.9999	2.41	6.137
ENSMUSG00000025403	Shmt2	1.26	0.05474	0.9999	27.26	68.03
ENSMUSG00000022346	Myc	1.26	0.05222	0.9999	3.079	7.849
ENSMUSG00000055976	Cldn23	1.26	0.04715	0.9999	1.784	4.758
ENSMUSG00000050138	Kcnk12	1.25	0.04967	0.9999	1.208	3.164
ENSMUSG00000038522	Mfsd4b1	1.25	0.04834	0.9999	1.183	3.161
ENSMUSG00000075702	Selenom	1.25	0.05678	0.9999	56.63	140.1
ENSMUSG00000002014	Ssr4	1.24	0.05753	0.9999	148.9	367.2
ENSMUSG00000033467	Crlf2	1.24	0.05153	0.9999	2.005	5.209
ENSMUSG00000039236	Isg20	1.24	0.05842	0.9999	78.92	194.1
ENSMUSG00000020308	Tpgs1	1.23	0.05602	0.9999	8.521	21.42
ENSMUSG00000063975	Slco1a5	1.23	0.05233	0.9999	1.102	2.846
ENSMUSG00000028780	Sema3c	1.23	0.05691	0.9999	2.144	5.366
ENSMUSG00000011171	Vipr2	1.22	0.05528	0.9999	2.269	5.785
ENSMUSG00000096145	Vkorc1	1.22	0.06177	0.9999	74.06	180.1
ENSMUSG00000026189	Pecr	1.22	0.06088	0.9999	15.34	37.55
ENSMUSG00000020471	Pold2	1.22	0.06176	0.9999	18.67	45.56
ENSMUSG00000032816	Igdcc4	1.22	0.06115	0.9999	2.733	6.696
ENSMUSG00000042419	Nfkbil1	1.22	0.06059	0.9999	6.173	15.22
ENSMUSG00000005413	Hmox1	1.21	0.0628	0.9999	21.22	51.52
ENSMUSG00000050854	Tmem125	1.21	0.04725	0.9999	1.053	2.914
ENSMUSG00000023067	Cdkn1a	1.21	0.06349	0.9999	25.39	61.48
ENSMUSG00000028334	Nans	1.21	0.06425	0.9999	28.06	67.73

ENSMUSG00000030826	Bcat2	1.21	0.06382	0.9999	14.56	35.26
ENSMUSG00000031919	Tmed6	1.20	0.06357	0.9999	9.877	24.05
ENSMUSG00000026544	Dusp23	1.20	0.06459	0.9999	9.019	21.83
ENSMUSG00000028641	P3h1	1.20	0.06585	0.9999	18.28	43.92
ENSMUSG00000004460	Dnajb11	1.20	0.06698	0.9999	72.96	174.4
ENSMUSG00000001105	Ift20	1.20	0.06737	0.9999	56.69	135.4
ENSMUSG00000041263	Rusc1	1.19	0.06808	0.9999	29	69.11
ENSMUSG00000035845	Alg12	1.19	0.06802	0.9999	10.91	26.07
ENSMUSG00000042275	Pelo	1.19	0.06836	0.9999	7.507	17.97
ENSMUSG00000078348	Sf3b5	1.19	0.06781	0.9999	2.359	5.663
ENSMUSG00000051703	Tmem198	1.18	0.06939	0.9999	8.871	21.15
ENSMUSG00000025130	P4hb	1.18	0.07173	0.9999	757.5	1784
ENSMUSG00000020660	Pomc	1.17	0.05902	0.9999	1.558	4.036
ENSMUSG00000025318	Jph3	1.17	0.07347	0.9999	9.384	22.05
ENSMUSG00000089901	Gm8113	1.16	0.0716	0.9999	2.134	5.086
ENSMUSG00000003402	Prkcsh	1.16	0.07542	0.9999	57.71	134.5
ENSMUSG00000056629	Fkbp2	1.16	0.07562	0.9999	98.47	229.5
ENSMUSG00000007892	Rplp1	1.16	0.0762	0.9999	352.2	818.9
ENSMUSG00000041313	Slc7a1	1.16	0.07632	0.9999	25.41	59.12
ENSMUSG00000005983	1700037C18Rik	1.15	0.07371	0.9999	5.044	11.97
ENSMUSG00000057163	Prss2	1.15	0.07197	0.9999	4.189	10.06
ENSMUSG00000039278	Pcsk1n	1.15	0.07809	0.9999	54.15	125.3
ENSMUSG00000010048	Ifrd2	1.15	0.07609	0.9999	7.577	17.77
ENSMUSG00000067847	Romo1	1.15	0.07738	0.9999	24.46	57
ENSMUSG00000021610	Clptm1l	1.14	0.07974	0.9999	147.6	339.8
ENSMUSG00000058833	Rex1bd	1.14	0.07837	0.9999	14.3	33.26
ENSMUSG00000030824	Nucb1	1.14	0.08088	0.9999	218.8	502.3
ENSMUSG00000054716	Zfp771	1.14	0.06901	0.9999	2.235	5.524
ENSMUSG00000015337	Endog	1.14	0.07815	0.9999	6.171	14.41
ENSMUSG00000020873	Slc35b1	1.14	0.08204	0.9999	111.7	255.8
ENSMUSG00000038213	Tapbpl	1.14	0.08184	0.9999	18.37	42.11
ENSMUSG00000050737	Ptges	1.13	0.07942	0.9999	5.236	12.18
ENSMUSG00000006057	Atp5g1	1.13	0.08267	0.9999	22.77	52.06
ENSMUSG00000020048	Hsp90b1	1.13	0.08341	0.9999	901.3	2054
ENSMUSG00000042293	Gm5617	1.13	0.07961	0.9999	9.873	23.03
ENSMUSG00000031760	Mt3	1.13	0.06551	0.9999	2.11	5.401
ENSMUSG00000024359	Hspa9	1.13	0.08414	0.9999	245.4	558.4
ENSMUSG00000064220	Hist2h2aa1	1.13	0.07367	0.9999	3.416	8.237
ENSMUSG00000089704	Galnt2	1.13	0.08069	0.9999	4	9.287
ENSMUSG00000031570	Plpp5	1.12	0.08534	0.9999	61.96	140.6
ENSMUSG00000025508	Rplp2	1.12	0.08554	0.9999	184	417.5
ENSMUSG00000040945	Rcc2	1.12	0.08549	0.9999	38.97	88.45
ENSMUSG00000027248	Pdia3	1.12	0.08641	0.9999	975.9	2208
ENSMUSG00000089847	Timm10b	1.12	0.08612	0.9999	16.39	37.28
ENSMUSG00000075227	Znhit2	1.11	0.08582	0.9999	7.241	16.52
ENSMUSG00000023043	Krt18	1.11	0.08924	0.9999	76.95	172.9
ENSMUSG00000024150	Mcfd2	1.11	0.08973	0.9999	86.03	193.2
ENSMUSG00000038181	Chpf2	1.10	0.09039	0.9999	26.12	58.59
ENSMUSG00000063897	CAAA01118383.1	1.10	0.08587	0.9999	1.918	4.414
ENSMUSG00000020163	Uqcr11	1.10	0.09095	0.9999	51.74	116
ENSMUSG00000031813	Mvb12a	1.10	0.09107	0.9999	31.72	71.1

ENSMUSG00000020703	5530401A14Rik	1.10	0.08542	0.9999	1.157	2.678
ENSMUSG00000057863	Rpl36	1.09	0.09329	0.9999	116.1	258.6
ENSMUSG00000055681	Cope	1.09	0.09407	0.9999	110.3	244.9
ENSMUSG00000028059	Arhgef2	1.09	0.09482	0.9999	51.54	114.3
ENSMUSG00000018672	Copz2	1.09	0.09449	0.9999	44.68	99.31
ENSMUSG00000049086	Bmyc	1.09	0.09263	0.9999	9.19	20.62
ENSMUSG00000053334	Ficd	1.09	0.09518	0.9999	25.02	55.46
ENSMUSG00000031391	L1cam	1.09	0.09335	0.9999	5.218	11.69
ENSMUSG00000035032	Nek11	1.08	0.08588	0.9999	1.149	2.687
ENSMUSG00000025007	Aldh18a1	1.08	0.09721	0.9999	86.99	191.8
ENSMUSG00000068523	Gng5	1.08	0.09704	0.9999	35.7	78.83
ENSMUSG00000020131	Pcsk4	1.08	0.09743	0.9999	10.25	22.65
ENSMUSG00000030104	Edem1	1.08	0.09907	0.9999	51.2	112.4
ENSMUSG00000058440	Nrf1	1.08	0.09828	0.9999	13.6	29.98
ENSMUSG00000031271	Serpina7	1.08	0.0983	0.9999	12.86	28.36
ENSMUSG00000074063	Osgin1	1.07	0.09853	0.9999	15.75	34.73
ENSMUSG00000048385	Scrt1	1.07	0.09852	0.9999	4.998	11.02
ENSMUSG00000020444	Guk1	1.07	0.09962	0.9999	123.7	271.4
ENSMUSG00000027944	Hax1	1.07	0.09957	0.9999	84.11	184.6
ENSMUSG00000002083	Bbc3	1.07	0.09403	0.9999	4.44	10.02
ENSMUSG00000002279	Lmf1	1.07	0.09884	0.9999	8.035	17.71
ENSMUSG00000038422	Hdhd3	1.07	0.09223	0.9999	3.793	8.65
ENSMUSG00000091228	Gm20390	1.07	0.1003	0.9999	40.34	88.45
ENSMUSG00000024516	Sec11c	1.07	0.1013	0.9999	86.43	188.9
ENSMUSG00000040462	Os9	1.07	0.1019	0.9999	126.3	275.6
ENSMUSG00000041654	Slc39a11	1.06	0.1018	0.9999	10.99	24.07
ENSMUSG00000032182	Yipf2	1.06	0.1046	0.9999	51.8	112.4
ENSMUSG00000001082	Mfsd10	1.06	0.1033	0.9999	16.52	36.08
ENSMUSG00000004931	Apba3	1.05	0.1042	0.9999	15.76	34.35
ENSMUSG00000019579	Mydgf	1.05	0.1059	0.9999	73.58	159.2
ENSMUSG00000036372	Tmem258	1.05	0.107	0.9999	62.35	134.7
ENSMUSG00000040904	Gm21988	1.05	0.1028	0.9999	3.472	7.653
ENSMUSG00000034974	Dapk3	1.05	0.1067	0.9999	17.9	38.76
ENSMUSG00000110234	Gm45799	1.05	0.1031	0.9999	4.295	9.486
ENSMUSG00000041028	Ghitm	1.04	0.1093	0.9999	113.9	244.4
ENSMUSG00000001751	Naglu	1.04	0.1087	0.9999	24.01	51.71
ENSMUSG00000019066	Rab3d	1.04	0.1097	0.9999	99.47	213.4
ENSMUSG00000112449	Srp54a	1.04	0.1089	0.9999	20.22	43.53
ENSMUSG00000028062	Lamtor2	1.04	0.109	0.9999	47.81	102.9
ENSMUSG00000041774	Ydjc	1.04	0.105	0.9999	2.725	5.98
ENSMUSG00000047721	Bola2	1.04	0.1077	0.9999	5.568	12.09
ENSMUSG00000026755	Arpc5l	1.04	0.1117	0.9999	38.63	82.6
ENSMUSG00000070360	Amy2a1	1.04	0.09731	0.9999	1.868	4.284
ENSMUSG00000067274	Rplp0	1.03	0.1135	0.9999	538.8	1147
ENSMUSG00000014504	Srp19	1.03	0.112	0.9999	17.57	37.61
ENSMUSG00000023707	Ogfod2	1.03	0.1139	0.9999	41.52	88.42
ENSMUSG00000044339	Alkbh2	1.03	0.1059	0.9999	3.832	8.461
ENSMUSG00000017664	Slc35c2	1.03	0.1142	0.9999	36.09	76.81
ENSMUSG00000015092	Edf1	1.03	0.1145	0.9999	56.88	121
ENSMUSG00000060950	Trmt61a	1.03	0.1122	0.9999	6.513	14.01
ENSMUSG00000059654	Reg1	1.03	0.08936	0.9999	1.091	2.627

ENSMUSG00000079111	Kdelr2	1.03	0.1154	0.9999	89.31	189.4
ENSMUSG00000029752	Asns	1.02	0.1159	0.9999	142.3	301.4
ENSMUSG00000059824	Dbp	1.02	0.1165	0.9999	27.36	57.97
ENSMUSG00000055013	Agap1	1.02	0.1168	0.9999	19.58	41.41
ENSMUSG00000035637	Grhpr	1.02	0.1153	0.9999	17.97	38.28
ENSMUSG00000038900	Rpl12	1.02	0.1177	0.9999	160.9	339.8
ENSMUSG00000078570	1110065P20Rik	1.02	0.1162	0.9999	19.02	40.39
ENSMUSG00000063838	Cdc42ep5	1.02	0.09736	0.9999	1.963	4.557
ENSMUSG00000031957	Ctrb1	1.02	0.116	0.9999	14.21	30.24
ENSMUSG00000041355	Ssr2	1.02	0.1184	0.9999	235	495.3
ENSMUSG00000031960	Aars	1.02	0.1187	0.9999	100.5	211.7
ENSMUSG00000037349	Nudt22	1.02	0.1139	0.9999	6.269	13.48
ENSMUSG00000029725	Ppp1r35	1.02	0.1088	0.9999	4.594	10.11
ENSMUSG00000002660	Clpp	1.01	0.1185	0.9999	19.89	42.02
ENSMUSG00000058441	Panx2	1.01	0.1157	0.9999	3.447	7.37
ENSMUSG00000028923	Necap2	1.01	0.1181	0.9999	13.96	29.58
ENSMUSG00000012117	Dhdds	1.01	0.1203	0.9999	57.48	120.8
ENSMUSG00000058569	Tmed9	1.01	0.1206	0.9999	143.3	300.8
ENSMUSG00000020680	Taf15	1.01	0.1209	0.9999	47.36	99.43
ENSMUSG00000037722	Gnpnat1	1.01	0.1208	0.9999	33.78	71.01
ENSMUSG00000074884	Serf2	1.01	0.1218	0.9999	112.4	235.4
ENSMUSG00000089809	Rasgef1b	1.01	0.1196	0.9999	4.804	10.16
ENSMUSG00000020869	Lrrc59	1.01	0.1225	0.9999	70.17	146.8
ENSMUSG00000050299	Gm9843	1.01	0.1228	0.9999	195.4	408.6
ENSMUSG00000028708	Mknk1	1.00	0.1228	0.9999	38.72	81.03
ENSMUSG00000024875	Yif1a	1.00	0.1232	0.9999	30.41	63.59
ENSMUSG00000020087	Tysnd1	1.00	0.1218	0.9999	14.68	30.88
ENSMUSG00000024327	Slc39a7	1.00	0.1245	0.9999	168.2	350.5
ENSMUSG00000005373	Mlxipl	-1.00	0.1243	0.9999	189.8	98.67
ENSMUSG00000070823	Gm1043	-1.00	0.1113	0.9999	2.483	1.228
ENSMUSG00000000215	Ins2	-1.01	0.1229	0.9999	269800	139900
ENSMUSG00000047246	Hist1h2be	-1.01	0.1135	0.9999	3.5	1.757
ENSMUSG00000112148	Lilrb4a	-1.02	0.1033	0.9999	2.218	1.072
ENSMUSG00000045871	Slitrk6	-1.03	0.1132	0.9999	23.97	12.18
ENSMUSG00000028804	Csmd2	-1.03	0.1085	0.9999	2.502	1.248
ENSMUSG00000005232	G6pc2	-1.04	0.1124	0.9999	1734	880.6
ENSMUSG00000041633	Kctd12b	-1.05	0.1084	0.9999	16.15	8.121
ENSMUSG00000103182	Gm37091	-1.05	0.09597	0.9999	2.383	1.142
ENSMUSG00000037279	Ovol2	-1.05	0.09207	0.9999	3.33	1.566
ENSMUSG00000029273	Sult1d1	-1.06	0.1017	0.9999	29.74	14.73
ENSMUSG00000015533	Itga2	-1.06	0.09807	0.9999	3.09	1.505
ENSMUSG00000015829	Tnr	-1.07	0.1004	0.9999	43.52	21.53
ENSMUSG00000027931	Npr1	-1.07	0.0989	0.9999	28.71	14.12
ENSMUSG00000054320	Lrrc36	-1.09	0.08594	0.9999	2.936	1.372
ENSMUSG00000096847	Tmem151b	-1.09	0.09098	0.9999	2.383	1.141
ENSMUSG00000103560	Gm38070	-1.14	0.08121	0.9999	13.75	6.488
ENSMUSG00000044716	Dok7	-1.14	0.07187	0.9999	2.517	1.128
ENSMUSG00000040147	Maob	-1.16	0.07505	0.9999	166.9	77.49
ENSMUSG00000044453	Ffar1	-1.17	0.07353	0.9999	41.37	19.12
ENSMUSG00000036353	P2ry12	-1.17	0.0649	0.9999	3.066	1.346
ENSMUSG00000028989	Angptl7	-1.18	0.06533	0.9999	3.54	1.566

ENSMUSG00000078451	Ppil6	-1.19	0.054	0.9999	4.424	1.824
ENSMUSG00000030865	Chp2	-1.19	0.05286	0.9999	3.278	1.341
ENSMUSG00000019933	Mrln	-1.19	0.06595	0.9999	51.58	23.14
ENSMUSG00000070880	Gad1	-1.22	0.06262	0.9999	102.3	45.71
ENSMUSG00000030406	Gipr	-1.22	0.06226	0.9999	54.38	24.26
ENSMUSG00000047230	Cldn2	-1.23	0.04929	0.9999	2.821	1.151
ENSMUSG00000021947	Cryl1	-1.25	0.05562	0.9999	55.26	24.05
ENSMUSG00000003379	Cd79a	-1.25	0.05249	0.9999	9.3	3.964
ENSMUSG00000031255	Sytl4	-1.26	0.05508	0.9999	204.4	88.99
ENSMUSG00000034947	Tmem106a	-1.29	0.04388	0.9999	5.335	2.17
ENSMUSG00000026989	Dapl1	-1.29	0.04479	0.9999	16.05	6.595
ENSMUSG00000074240	Cib3	-1.30	0.04685	0.9999	29.59	12.42
ENSMUSG00000028965	Tnfrsf9	-1.30	0.03888	0.9999	3.564	1.391
ENSMUSG00000040170	Fmo2	-1.33	0.03579	0.9999	2.872	1.109
ENSMUSG00000047591	Mafa	-1.41	0.03139	0.9999	36.07	14.02
ENSMUSG00000067455	Hist1h4j	-1.45	0.01757	0.9999	3.396	1.086
ENSMUSG00000110195	Pde2a	-1.47	0.02299	0.9999	5.602	2.03
ENSMUSG00000067786	Nnat	-1.49	0.01919	0.9999	6.598	2.263
ENSMUSG00000032377	Plscr4	-1.51	0.01875	0.9999	3.007	1.036
ENSMUSG00000037106	Fer1l6	-1.62	0.0139	0.9999	11.97	4.007
ENSMUSG00000046593	Tmem215	-1.65	0.01246	0.9999	66.58	21.99
ENSMUSG00000027690	Slc2a2	-1.67	0.01175	0.9524	295.7	96.75
ENSMUSG00000019429	Ffar3	-1.70	0.008907	0.7872	7.596	2.317
ENSMUSG00000035804	Ins1	-1.73	0.009068	0.7918	52060	16310
ENSMUSG00000054459	Vsnl1	-1.81	0.005309	0.5603	5.553	1.549
ENSMUSG00000009246	Trpm5	-1.87	0.004884	0.5387	27.57	7.781
ENSMUSG00000078889	Gm14288	-2.51	0.0001569	0.03806	6.405	1.063

10.3 Western Blots

Fully unedited gel images used for representative Western blot images in this thesis:

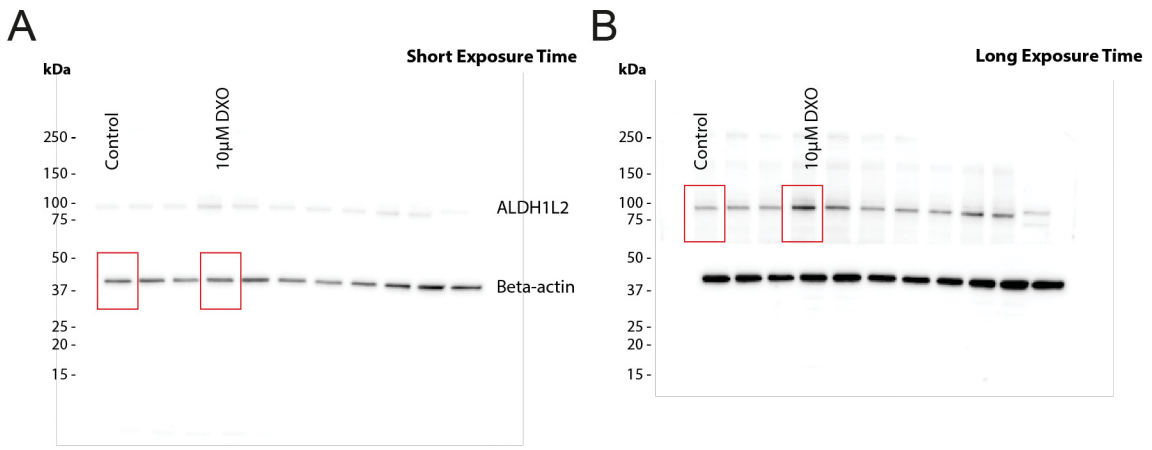

Supplementary Figure 1 to Figure 11 B: Western blot scan with size marker indications (molecular weights in kilodalton (kDa)). Cropped regions in red-rimmed boxes were used for the representative image.

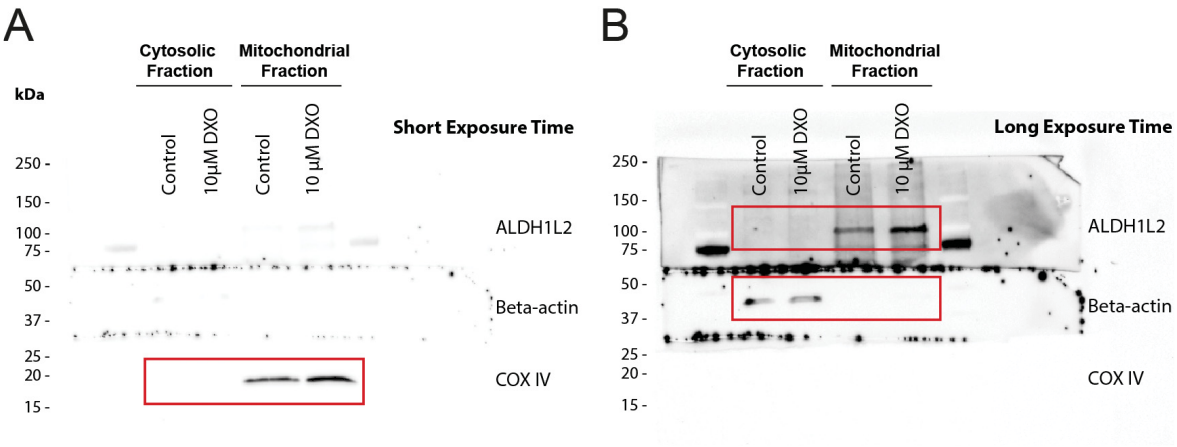

Supplementary Figure 2 to Figure 11 C: Western blot scan with size marker indications (molecular weights in kDa). Cropped regions in red-rimmed boxes were used for the representative image. **A**, Image after short exposure time. **B**, Image after long exposure time.

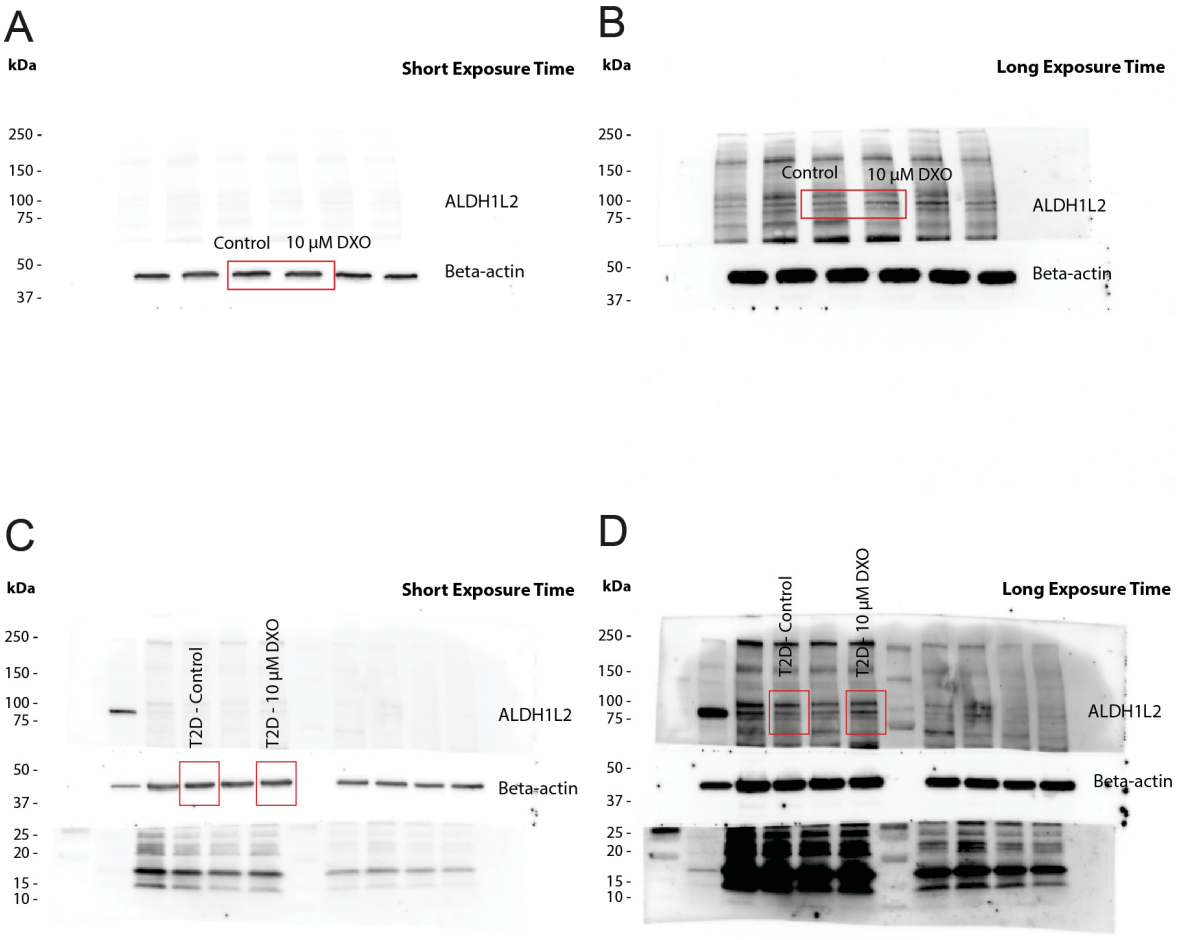

Supplementary Figure 3 to Figure 12 B: Western blot scan with size marker indications (molecular weights in kDa). Cropped regions in red-rimmed boxes were used for the representative images. **A**, Lysates from NonT2DM 1 donor. Image after short exposure time. **B**, Lysates from NonT2DM donor 1. Image after long exposure time. **C**, Lysates from T2DM donor. Image after short exposure time. **D**, Lysates from T2DM donor. Image after long exposure time.

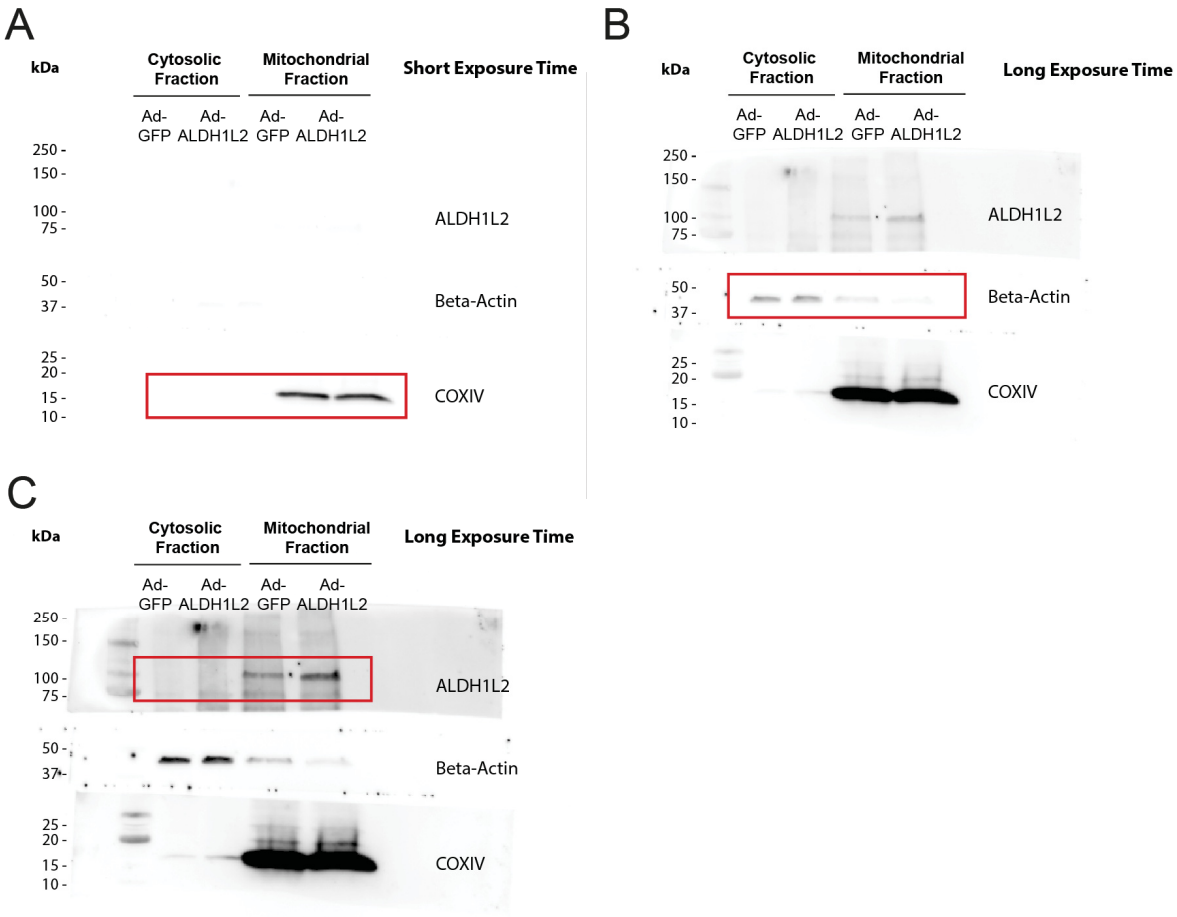

Supplementary Figure 4 to Figure 14 A: Western blot scan with size marker indications (molecular weights in kDa). Cropped regions in red-rimmed boxes were used for the representative image. **A**, Image after short exposure time to detect Cox IV. **B**, Image after long exposure time to detect Beta-actin. **C**, Image after long exposure time to detect ALDH1L2.

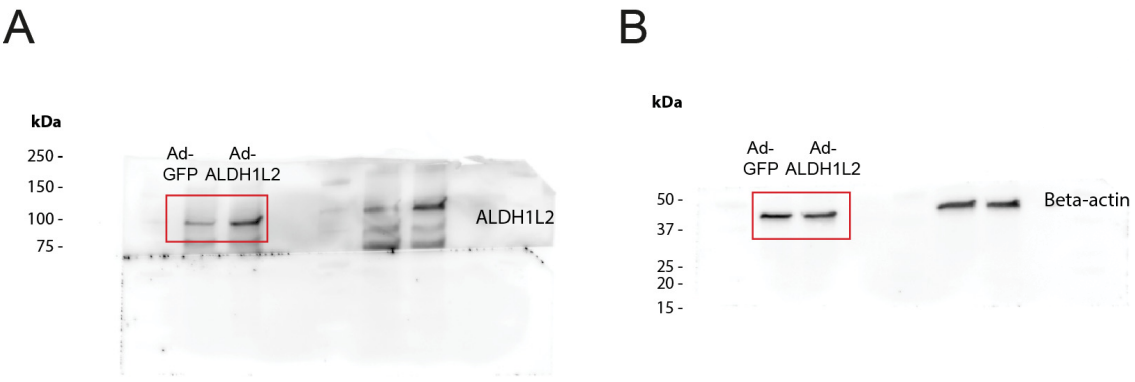

Supplementary Figure 5 to Figure 14 B: Western blot scan with size marker indications (molecular weights in kDa). Cropped regions in red-rimmed boxes were used for the representative image. **A**, Detected for ALDH1L2. **B**, Detected for Beta-actin.

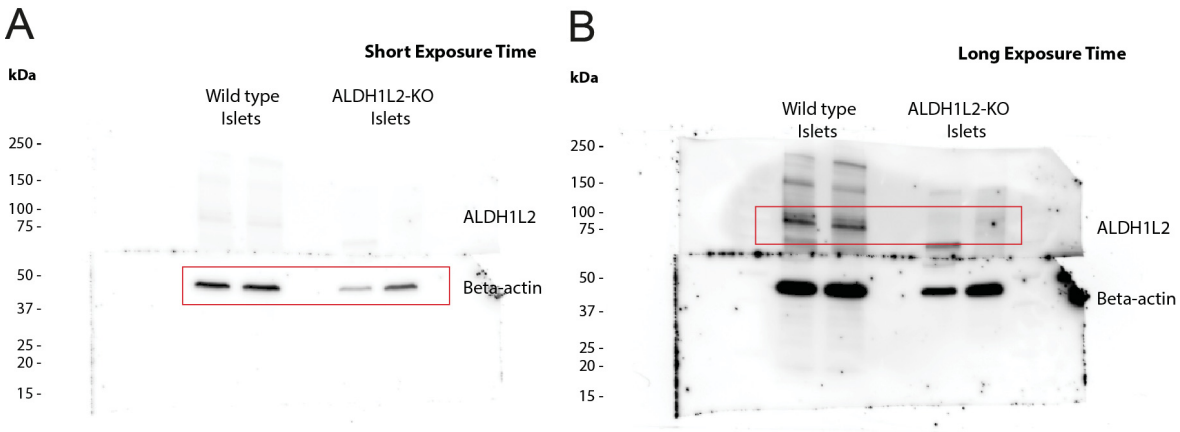

Supplementary Figure 6 to Figure 16 A: Western blot scan with size marker indications (molecular weights in kDa). Cropped regions in red-rimmed boxes were used for the representative image. **A**, Image after short exposure time. **B**, Image after long exposure time.

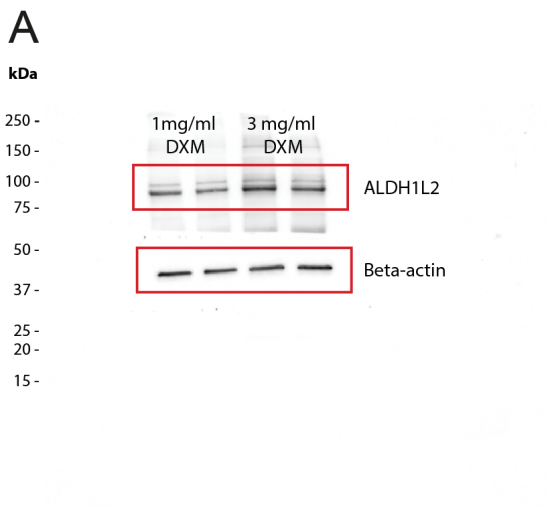

Supplementary Figure 7 to Figure 22 B: Western blot scan with size marker indications (molecular weights in kDa). Cropped regions in red-rimmed boxes were used for the representative image.

11 Eidesstattliche Erklärung

Ich versichere an Eides Statt, dass die Dissertation „Molecular investigations into the effects of the insulin secretagogue dextrorphan on pancreatic islet cell function and viability" von mir selbstständig und ohne unzulässige fremde Hilfe unter Beachtung der „Grundsätze zur Sicherung guter wissenschaftlicher Praxis an der Heinrich-Heine-Universität Düsseldorf" erstellt worden ist. Ich habe keine anderen, als die angegebenen Quellen verwendet. Aussagen, in denen ich Bezug zu der Arbeit Anderer nehme, wurden als solches kenntlich gemacht.

Ich versichere, dass ich die Dissertation weder in dieser vorgelegten noch in einer ähnlichen Form von mir bei einem anderen Institut eingereicht wurde. Bisher wurden von mir keine Promotionsversuche unternommen.

Düsseldorf, den

_____

Jessica Mrugala

12 Danksagung

Danke sagen möchte ich meinem Doktorvater Ecki. Danke, dass du mir die Möglichkeit gegeben hast meine Doktorarbeit in deinem Institut zu absolvieren. Danke für die wissenschaftliche Unterstützung während meiner jahrelangen Arbeit in deinem Team.

Außerdem möchte ich mich bei meinem Mentor und Zweitgutachter Prof. Dr. Thomas Meissner bedanken. Dank für die Unterstützung während meiner Zeit als Doktorandin.

Ich möchte mich bei Daniel bedanken. Danke, für zahlreiche wissenschaftliche Diskussionen und hilfreiche Vorschläge.

Ich danke Bengt für seine wissenschaftliche Unterstützung. Ein Dank geht außerdem an die gesamte AG Belgardt für eure stätige Hilfsbereitschaft!

Ein sehr großer Dank geht an alle Mitarbeiter des LammertLabs. Danke an Okka Scholz, Laura Wörmeyer und Haiko Karsjens für die wundervolle Zeit, in aber vor allem außerhalb des Labors. Danke für eure Freundschaft! Ein besonders großes Danke geht an Barbara Bartosinska für die tatkräftige Unterstützung während meiner gesamten Zeit. Danke für die tolle Hilfe im Labor und das offene Ohr zu jeder Zeit. Von ganzem Herzen danken möchte ich auch Angela Pelligra und Dominik Gebel für die tolle und produktive Zusammenarbeit! Danke für die Unterstützung im Team „ALDH1L2“! Danke an Laura Hilger, Silke Otter, Linda Lorenz, Anna Brandopolski, Carina Henning, Paula Follert, Silke Jakob, Andrea Krause, Esther Hedderich und Fatma Demir! Es war mir jeden Tag ein Vergnügen mit euch zu Arbeiten! Danke für tolle Karnevals- und legendäre Weihnachtsfeiern!

Bedanken möchte ich mich auch bei den ehemaligen Labormitgliedern Jan Eglinger, Alena Welters, Martin Kragl und Tobias Buschmann. Ein besonderer Dank geht an Sofia Urner für ihre zahlreichen wissenschaftlichen und persönlichen Gespräche während ihrer Zeit im Labor. Danke, dass du immer für mich da warst.

Ein ganz besonderer Dank gilt meinen Freunden. Danke, dass ihr mich über die ganzen Jahre unterstützt habt und mich vor allem immer wieder auf andere Gedanken bringen konntet. Ein großer Dank geht an Anna, Lisa, Marianna, Stabi und Jonny! Danke, dass ihr mich immer verstanden und mir zugehört habt! Ein besonderer Dank geht außerdem an Lena! Danke für die unvergessliche Zeit in Düsseldorf! Ohne dich wäre es bei weitem nicht so toll gewesen! Danke, dass du immer für mich da warst!

Von tiefstem Herzen möchte ich mich bei meinem Freund Christian, meiner Mutter Renate, meinem Vater Heinrich und meiner Schwerster Kami bedanken. Danke für eure bedingungslose Unterstützung und Liebe während der gesamten Zeit. Danke für das Verständnis, auch wenn es häufig schwierig war! Ohne euch wäre das Projekt „Doktorarbeit“ niemals möglich gewesen! Ihr habt einen sehr großen Teil zu dieser Arbeit beigetragen!